



Study of environmentally friendly working mixtures containing ionic liquids for absorption heat transformers

El Shaimaa Talaat Yussef Abumandour

► To cite this version:

El Shaimaa Talaat Yussef Abumandour. Study of environmentally friendly working mixtures containing ionic liquids for absorption heat transformers. Food and Nutrition. Université de Lorraine, 2015. English. NNT : 2015LORR0070 . tel-01751700

HAL Id: tel-01751700

<https://hal.univ-lorraine.fr/tel-01751700>

Submitted on 29 Mar 2018

HAL is a multi-disciplinary open access archive for the deposit and dissemination of scientific research documents, whether they are published or not. The documents may come from teaching and research institutions in France or abroad, or from public or private research centers.

L'archive ouverte pluridisciplinaire **HAL**, est destinée au dépôt et à la diffusion de documents scientifiques de niveau recherche, publiés ou non, émanant des établissements d'enseignement et de recherche français ou étrangers, des laboratoires publics ou privés.



AVERTISSEMENT

Ce document est le fruit d'un long travail approuvé par le jury de soutenance et mis à disposition de l'ensemble de la communauté universitaire élargie.

Il est soumis à la propriété intellectuelle de l'auteur. Ceci implique une obligation de citation et de référencement lors de l'utilisation de ce document.

D'autre part, toute contrefaçon, plagiat, reproduction illicite encourt une poursuite pénale.

Contact : ddoc-theses-contact@univ-lorraine.fr

LIENS

Code de la Propriété Intellectuelle. articles L 122. 4

Code de la Propriété Intellectuelle. articles L 335.2- L 335.10

http://www.cfcopies.com/V2/leg/leg_droi.php

<http://www.culture.gouv.fr/culture/infos-pratiques/droits/protection.htm>

UNIVERSITÉ DE LORRAINE

Ecole Doctorale RP2E : Ressources, Procédés, Produits, Environnement
Laboratoire Réactions et Génie des Procédés – UMR 7274 CNRS – ENSIC

THÈSE

Présentée

El Shaimaa Talaat Yussef ABUMANDOUR

Pour l'obtention du grade de

Docteur en Science de l'Université de Lorraine

Spécialité : Génie des Procédés et des Produits

**STUDY OF ENVIRONMENTALLY FRIENDLY WORKING
MIXTURES CONTAINING IONIC LIQUIDS FOR
ABSORPTION HEAT TRANSFORMERS**

Thèse soutenue publiquement le 2 Juillet 2015

devant la commission d'examen :

Rapporteurs:

Prof. Christophe COQUELET
Prof. Jean-Philippe PASSARELLO

Examineurs :

Prof. Viviane RENAUDIN
Dr. Christophe NICOLAS
Dr. Fabrice MUTELET
Dr. Dominique ALONSO

ACKNOWLEDGMENTS

First of all, I am grateful to **Almighty God** for giving me the strength to fulfill this work.

I would like to express my sincere gratitude to my Supervisor, **Dr. Fabrice MUTELET**. I am thankful for his support, aspiring guidance, invaluable constructive criticism and friendly advices during my PhD. I am sincerely grateful to him for sharing his truthful and illuminating views on a number of issues related to the study.

I would like to express my deepest gratitude to my Co-advisor, **Dr. Dominique ALONSO**, for his excellent guidance, caring, patience, and providing me with excellent ideas, explanations and suggestions throughout my study. I am extremely grateful for his assistance and support. I owe you an enormous debt of gratitude for your help, time and consideration.

I attribute the level of my PhD degree to Fabrice and Dominique encouragement and effort without them this thesis, would not have been completed or written. The enjoyment and passion they have for scientific research was infectious and motivational for me, even during tough periods in the Ph.D. quest. One simply could not wish for a better or friendlier supervision.

I would like to thank the Université de Lorraine and Erasmus mundus for giving me the opportunity to fulfill my PhD.

A very special thanks goes out to Laboratoire Réactions et Génie des Procédés (LRGP-UMR 7274 CNRS) in Nancy, where this work was accomplished. I would first like to thank **Mr. Gabriel WILD**, (former director of LRGP) and **Laurent FALK** (current director), for hosting me in this laboratory.

I would also like to thank **Mr. Mohamed Bourokba** for his help and precious conversations.

Special thanks and gratitude goes to **Prof. Christophe COQUELET** and **Prof Jean-Philippe PASSARELLO** for accepting the task of judging this work. I assure my deep gratitude to **Prof. Viviane RENAUDIN** and **Dr. Christophe NICOLAS**. Their presence in the jury honors me.

I would like to express my appreciation to all the staff members of ThermE: **Jean-Noël JAUBERT** (Responsible of the team), **Jean-Charles MOÏSE**, **Romain PRIVAT**, **Michel DIRAND**, **Nathalie HUBERT** and **Roland SOLIMANDO**.

I would like to thank **Mr. Patrick carre** for his availability and help.

Additionally, I would also like to thank all my colleagues who have made these three years an enjoyable and rewarding experience: **El Sayed R. HASSAN**, **Armél GONDA**, **Niramol JUNTARACHAT**, **Imane HADDADOU**, **Amal AYAD**, **Chen YUSHU**, **Zehor BENSAID**, **Afef ATTIA**, **Lais TEDESCO**, **Mohamed ALJUBURY**, **Joël MALLICK**, **Vincent PLEE**, **Laëtitia CESARI** and **Silvia LASALA**.

Most of all, I am fully indebted to my “**Mother**”, my elder **Sister** and my younger **Brothers** for their unconditional love, understating, wisdom, patience, encouragement and for pushing me farther than I thought I could go.

Table of contents

Nomenclature and symbols	xi
Résumé	1
INTRODUCTION	9
CHAPTER ONE: STATE OF THE ART	13
I.1. Introduction	13
I.2. Ionic Liquids	13
I.3. History and progress of ionic liquids	15
I.4. Classes of ionic liquids	17
I.5. Physico-chemical properties of Ionic liquids	18
I.5.1. vapor pressure	18
I.5.2. Activity coefficient for ionic liquids	18
I.5.3. Density	20
I.5.4. Viscosity	20
I.5.5. Surface tension	21
I.5.6. Miscibility with water	21
I.5.7. Melting point	22
I.5.8. Thermal stability	23
I.5.9. Flammability and corrosion	24
I.5.10. Toxicity and human health	25
I.6. Potential Applications of Ionic Liquids	26
I.7. General information about Absorption cycles	32
I.8. Classification of Absorption cycles	34
I.8.1. Absorption refrigerators (Chillers) (AC)	37
I.8.2. Absorption heat pumps (AHP)	37
I.8.3. Absorption heat transformers (AHT)	38

I.9. Working fluids containing {water + ILs} for absorption cycles	39
I.9.1. {H ₂ O + Ionic liquids} binary systems in literature	39
I.10. Thermodynamic properties of {H ₂ O + IL}	41
I.10.1. Thermodynamic model for the representation of binary system {H ₂ O + IL} ..	41
I.10.2. Experimental thermodynamic data of {H ₂ O + IL}	43
I.10.2.1. Vapor liquid equilibrium (VLE)	43
I.10.2.2. Heat capacity	48
I.10.2.3. Excess Enthalpy (H ^E)	50
I.10.2.4. Density.....	52
I.10.2.5. Viscosity	57
I.10.2.6. Thermal decomposition.....	58
References	60
CHAPTER TWO: THERMODYNAMIC OF BINARY SYSTEMS COMPOSED OF {WATER + IONIC LIQUID}.....	69
II.1. Experimental section	69
II.1.1. Materials	69
II.1.2. Vapor Liquid Equilibrium (VLE)	70
II.1.2.1. Isobaric VLE apparatus.....	72
II.1.2.2. Isothermal VLE measurement	73
II.1.3. Heat capacity (C _p)	75
II.1.4. Density (ρ)	76
II.1.5. Excess enthalpy (H ^E)	78
II.2. Results and discussion	80
II.2.1. Vapor Liquid Equilibrium (VLE)	80
II.2.2. Heat capacity (C _p).....	90

II.2.3. Density (ρ)	97
II.2.3.1. Excess molar volume V^E	101
II.2.4. Excess molar Enthalpy (H^E)	106
References	110
CHAPTER THREE: PERFORMANCE SIMULATION (COP)	115
III.1. Simulation of the AHT cycle performance	118
III.2. COP definition for an Absorption refrigeration cycle	124
III.3. Absorption heat transformer	125
References	139
CONCLUSIONS AND PERSPECTIVES	141
References	144
Annexes	145

List of Tables

Tableau 1: Liquides ioniques étudiés	5
Table I.1: Common ILs cations and anions	14
Table I.2: Melting point data for different ionic liquids [6, 7]	23
Table I.3: LC ₅₀ values for certain solvents [34]	26
Table I.4: Overview of industrial applications of ILs (Commercial/pilot plants) [6, 7]	31
Table I.5: NRTL parameters of binary systems {H ₂ O + ILs}	47
Table I.6: Mass heat capacity parameters of binary systems {H ₂ O + ILs}	49
Table I.7: Excess enthalpy H ^E parameters of binary systems {H ₂ O (1) + ILs (2)}	51
Table I.8: Density parameters of binary systems {H ₂ O (1)+ ILs (2)}	53
Table I.9: Decomposition temperature for miscible ILs	59
Table II.1: Physical properties of studied ionic liquids	71
Table II.2: Comparison of the saturated vapor pressure of pure water (P ^{exp.}) measured in this work and those published (P ^{lit.}) in the literature [11]	80
Table II.3: Summary of VLE measurements for the studied binary systems {H ₂ O (1) + ILs (2)}	81
Table II.4: NRTL parameters of the VLE data for {H ₂ O (1) + IL (2)}	85
Table II.5: Mass heat capacity comparison of ultrapure water [4]	90
Table II.6: Parameters for the correlation of Eq. (II.11)	91
Table II.7: Parameters for the correlation of Eq. (II.13)	92
Table II.8: Parameters for the correlation of Eq. (II.15)	97
Table II.9: Redlich Kister parameters for V ^E for {H ₂ O (1) + ILs (2)} binary systems	103
Table II.10: Redlich-kister parameters for H ^E for {H ₂ O (1) + ILs (2)}	108
Table III.1: Binary systems investigated in this work and their Thermodynamic properties	116
Table III.2: COP of {H ₂ O + absorbent} binary systems for absorption refrigeration cycle found in literature	125

Table III.3: Calculated COP of {H ₂ O + ILs} binary systems for absorption heat transformer cycle compared to data found in literature ^{*,**}	128
Table III.4: The available heat output per unit mass of refrigerant (q) for AHT cycle	135

List of Figures

Figure 1: Cations des liquides ioniques	3
Figure 2: Influence de la structure du liquide ionique sur le coefficient de performance	6
Figure I.1: Growth rate of ionic liquid publications, 1999-2013 [SciFinder, 2014]	17
Figure I.2: Commonly used anions and their miscibility with water	22
Figure I.3: Ignition test of 1 g of protonated [1-Bu-3H-IM][NO ₃] [26]	24
Figure I.4: Possible applications of ILs	27
Figure I.5: The BASIL TM process [16]	28
Figure I.6: Process scheme integrating Dimersol and Difasol [16]	29
Figure I.7: A spray nozzle for aqueous solutions of sodium chloride (left) and a hydrophilic ionic liquid (right), each after 10 h of operation (©IoLiTec 2007) [16]	30
Figure I.8: Absorption cycles	35
Figure I.9: Schematic diagram of an absorption refrigeration cycle; A-absorber, C-condenser, E-evaporator, G-generator, SHE-heat exchanger	36
Figure I.10: Schematic diagram of an absorption heat transformer; A-absorber, C-condenser, E-evaporator, G-generator, SHE-heat exchanger, P1, P2-pump, v-valve	38
Figure I.11: Water activity coefficients, γ^w , as function of the water mole fraction in binary solutions of {water (1) + IL (2)}: (a) ● [BMIM][Br], ● [BMIM][C1SO ₃], ● [BMIM][SCN]; (b) : ● [EMIM][(CF ₃ SO ₂) ₂ N], ● [BMIM][(CF ₃ SO ₂) ₂ N], ● [EMIM][BF ₄]	45
Figure I.12: Excess enthalpy, H^E for the binary mixtures {water (1) + ionic liquid (2)} at T = 298.15 K. Ionic liquids ● [EMIM][EtSO ₄], ● [BMIM][MeSO ₄], ● [EMIM][Triflate], ● [BMIM][Triflate], ● [BMPy][BF ₄] [84]	51
Figure I.13: Excess molar volumes, V^E for the binary mixtures {water (1) + ionic liquid (2)} at T = 298.15 K. Ionic liquids: (a) ● [BMIM][DCA], ● [EEPyr][EtSO ₄], ● [BMIM][TFO]; (b) ● [BMPy][DCA], ● [BMPyr][TFO], ● [BMPy][TFO]; (c) ● [HMIM][DCA], ● [MPy][MeSO ₄] [87]	56
Figure I.14: Viscosity for the binary mixtures {water (1) + [EMIM][DMP] (2)} at different temperatures and mole fractions of IL ● $x_2 = 0.2$; ● $x_2 = 0.4$; ● $x_2 = 0.6$; ● $x_2 = 0.8$; ● $x_2 = 1$ with solid lines to guide the eye [60]	58
Figure II.1: Schematic diagram of isobaric VLE apparatus. 1. Temperature transmitter; 2. Pressure transducer (Druck-PMP4010); 3. Condenser; 4. Refrigerator; 5. Temperature sensor (T900 series); 6. Equilibrium vessel; 7. Thermostatic bath; 8. Magnetic stirrer; 9. Pressure buffer; 10. Vacuum control valve; 11. Vacuum pump	73

Figure II.2: Schematic representation of the VLE apparatus: VP: Vacuum Pump; VT: Vacuum Trap; A: Magnetic Stirrer; C: Equilibrium Cell; PT: Platinum resistance Thermometer (PT-100); T: Temperature Indicator; M: Calibrated Pressure Sensor, P: Digital Pressure Indicator and TB: Thermostatic Bath	74
Figure II.3: Setaram microDSCIII Calorimeter	75
Figure II.4: MicroDSC III Hastelloy pans	75
Figure II.5: DMA 512P measuring vibrating cell [7]	77
Figure II.6: Schematic diagram of C80 reversal mixing cell. 1. body of the stacked cell .2. vessel stopper .3. stainless steel stopper .4. Teflon O-ring .5. lid .6. Teflon O-ring .7. bottom chamber .8. bottom compartments of the cell	79
Figure II.7: Experimental γ_1 values for the binary systems $\{H_2O (1) + ILs (2)\}$ as a function of mole fraction of water (●) [DMIM][MPh]; (●) [EMIM][MPh]; (●) [EMIM][EPh]; (●) [DMIM][MeSO ₄]; (●) [BMIM][DCA]; —, calculated by NRTL equation	82
Figure II.8: The reduction trend of the activity coefficients and vapor pressure with respect to the anion type	83
Figure II.9: Experimental VLE data for the investigated binary systems $\{H_2O (1) + IL (2)\}$ symbols are experimental data for different mole fractions of ILs and —, calculated by NRTL equation: (a) [DMIM][MPh] (●) $x_2=0.1$; (●) $x_2=0.19$; (●) $x_2=0.3$; (●) $x_2=0.4$, (b) [EMIM][MPh] (●) $x_2=0.1$; (●) $x_2=0.2$; (●) $x_2=0.29$; (●) $x_2=0.4$, (c) [EMIM][EPh] : (●) $x_2=0.1$; (●) $x_2=0.23$; (●) $x_2=0.31$; (●) $x_2=0.4$	86
Figure II.10: Experimental VLE data for the investigated binary systems $\{H_2O (1) + [DMIM][MeSO_4] (2)\}$: (a) Isobaric VLE data symbols are experimental data at different mole fractions of [DMIM][MeSO ₄]: (●) $x_2=0.1$; (●) $x_2=0.2$; (●) $x_2=0.25$; —, calculated by NRTL equation, (b) Isothermal VLE for: (●) T= 298.15 K; (●) T= 303.15 K; (●) T= 308.15 K; (●) T= 313.15 K; (●) T= 318.15 K; —, calculated by NRTL	87
Figure II.11: Experimental VLE data for the investigated binary systems $\{H_2O (1) + [EMIM][MeSO_4] (2)\}$: (a) symbols are experimental data for different mole fractions of [EMIM][MeSO ₄]: (●) $x_2=0.15$; (●) $x_2=0.25$; (●) $x_2=0.35$; —, calculated by NRTL equation, (b) Isothermal VLE for: (●) T= 293.15 K; (●) T= 298.15 K; (●) T= 303.15; (●) T= 308.15; (●) T= 313.15K; —, calculated by NRTL	88
Figure II.12: Experimental VLE data for the investigated binary systems $\{H_2O (1) + IL (2)\}$ symbols are experimental data at different mole fractions of ILs and —, calculated by NRTL equation: (a) [BMIM][DCA]: (●) $x_2=0.1$; (●) $x_2=0.2$; (●) $x_2=0.3$, (b) [BMIM][Ac]: (●) $x_2=0.1$; (●) $x_2=0.2$; (●) $x_2=0.3$	89

Figure II.13: Heat capacities of $\{H_2O (1) + ILs (2)\}$ versus temperature at different mole fractions of IL: (a) $\{H_2O (1) + [EMIM][EPH] (2)\}$ (●) $x_2=1$; (●) $x_2=0.1$; (●) $x_2=0.2$; (●) $x_2=0.3$; (●) $x_2=0.48$; (●) $x_2=0.87$; —, calculated by polynomial equation (II.11) 92

Figure II.14: Heat capacities of $\{H_2O (1) + ILs (2)\}$ versus temperature at different mole fractions of IL: (a) $\{H_2O (1) + [DMIM][MeSO_4] (2)\}$ (●) $x_2=1$; (●) $x_2=0.1$; (●) $x_2=0.2$; (●) $x_2=0.3$; (●) $x_2=0.4$; (●) $x_2=0.5$; (●) $x_2=0.6$; (●) $x_2=0.7$, (b) $\{H_2O (1) + [EMIM][MeSO_4] (2)\}$ (●) $x_2=1$; (●) $x_2=0.1$; (●) $x_2=0.2$; (●) $x_2=0.3$; (●) $x_2=0.4$; (●) $x_2=0.5$; (●) $x_2=0.6$; (●) $x_2=0.8$; —, calculated by polynomial equation (II.11) 93

Figure II.15: Heat capacities of $\{H_2O (1) + [BMIM][DCA] (2)\}$ versus temperature at different mole fractions of the IL: (●) $x_2=1$; (●) $x_2=0.1$; (●) $x_2=0.2$; (●) $x_2=0.3$; (●) $x_2=0.4$; (●) $x_2=0.5$; (●) $x_2=0.6$; (●) $x_2=0.7$; (●) $x_2=0.86$; —, calculated by polynomial equation (II.11) 94

Figure II.16: Excess heat capacities of $\{H_2O (1) + ILs (2)\}$ versus x_2 of the IL at different temperatures: (a) $\{H_2O (1) + [EMIM][EPH] (2)\}$ (●) $T=301.15K$; (●) $T=303.15K$; (●) $T=321.15K$; —, calculated by Redlich–Kister equation 94

Figure II.17: Excess heat capacities of $\{H_2O (1) + ILs (2)\}$ versus x_2 of the IL at different temperatures: (a) $\{H_2O (1) + [DMIM][MeSO_4] (2)\}$ (●) $T=301.15K$; (●) $T=318.15K$; (●) $T=337.15K$, (b) $\{H_2O (1) + [EMIM][MeSO_4] (2)\}$ (●) $T=301.15K$; (●) $T=318.15K$; (●) $T=337.15K$; —, calculated by Redlich–Kister equation 95

Figure II.18: Excess heat capacities of $\{H_2O (1) + [BMIM][DCA] (2)\}$ versus x_2 of the IL at different temperatures: (●) $T=301.15K$; (●) $T=303.15K$; (●) $T=321.15K$; —, calculated by Redlich–Kister equation 96

Figure II.19: Trend of density of the investigated binary systems (●) $[DMIM][MPh]$; (●) $[EMIM][MPh]$; (●) $[EMIM][EPH]$; (●) $[BMIM][DCA]$; (●) $[DMIM][MeSO_4]$; (●) $[EMIM][MeSO_4]$; —, calculated by polynomial equation (II.15) 98

Figure II.20: Density of $\{H_2O (1) + IL (2)\}$ versus temperature at different molar fractions of IL: (a) $\{H_2O (1) + [DMIM][MPh] (2)\}$ (●) $x_2=1$; (●) $x_2=0.1$; (●) $x_2=0.2$; (●) $x_2=0.3$; (●) $x_2=0.4$; (●) $x_2=0.5$, (b) $\{H_2O (1) + [EMIM][MPh] (2)\}$ (●) $x_2=1$; (●) $x_2=0.1$; (●) $x_2=0.2$; (●) $x_2=0.3$, (c) $\{H_2O (1) + [EMIM][EPH] (2)\}$ (●) $x_2=1$; (●) $x_2=0.1$; (●) $x_2=0.2$; (●) $x_2=0.3$; —, calculated by polynomial equation (II.15) 99

Figure II.21: Density of $\{H_2O (1) + IL (2)\}$ versus temperature at different molar fractions of IL: (a) $\{H_2O (1) + [DMIM][MeSO_4] (2)\}$ (●) $x_2=1$; (●) $x_2=0.1$; (●) $x_2=0.2$; (●) $x_2=0.3$; (●) $x_2=0.4$; (●) $x_2=0.5$; (●) $x_2=0.6$, (b) $\{H_2O (1) + [EMIM][MeSO_4] (2)\}$ (●) $x_2=1$; (●) $x_2=0.1$; (●) 99

) $x_2=0.2$; (●) $x_2=0.3$; (●) $x_2=0.4$; (●) $x_2=0.5$; (●) $x_2=0.6$; (●) $x_2=0.7$; —, calculated by polynomial equation (II.15) 100

Figure II.22: Density of {H₂O (1) + [BMIM][DCA] (2)} versus temperature at different molar fractions of [BMIM][DCA]: (●) $x_2=1$; (●) $x_2=0.1$; (●) $x_2=0.3$; (●) $x_2=0.5$; (●) $x_2=0.7$; —, calculated by polynomial equation (II.15) 101

Figure II.23: Experimental excess molar volume, V^E against mole fraction of IL at different temperatures, (a) [DMIM][MPh]T: (●) T=293.15 K; (●) T = 303.15 K; (●) T = 313.15 K; (●) T = 313.15 K, (b) [EMIM][MPh] T: (●) T=293.15 K; (●) T = 303.15 K; (●) T = 313.15 K; (●) T = 313.15 K, (c) [EMIM][EPh] T: (●) T=293.15 K; (●) T = 303.15 K; (●) T = 313.15 K; (●) T = 313.15 K; —, correlated by Redlich-kister equation 104

Figure II.24: Experimental excess molar volume, V^E against mole fraction of IL at different temperatures, (a) [DMIM][MeSO₄] T: (●) T=293.15 K; (●) T = 313.15 K; (●) T = 323.15 K, (b) [EMIM][MeSO₄] T: (●) T=293.15 K; (●) T = 303.15 K; (●) T = 313.15 K; (●) T = 323.15 K; —, correlated by Redlich-kister equation 105

Figure II.25: Experimental excess molar volume, V^E against mole fraction of [BMIM][DCA] at different temperature T: (●) T=293.15 K; (●) T = 303.15 K; (●) T = 313.15 K; (●) T = 323.15 K; —, correlated by Redlich-kister equation 106

Figure II.26: Experimental excess molar enthalpy, H^E against different mole fraction x_2 of: (●) [DMIM][MPh], (●) [EMIM][MPh], (b) (●) [DMIM][MeSO₄], (●) [EMIM][MeSO₄] at 312.92 K (b) ; —, correlated by Redlich-kister equation 107

Figure II.27: Experimental excess molar enthalpy, H^E against different mole fraction x_2 of: (●) [DMIM][MeSO₄], (●) [DMIM][MPh] at 312.92 K; —, correlated by Redlich-kister equation 109

Figure II.28: Experimental excess molar enthalpy, H^E against different mole fraction x_2 of: (●) [EMIM][MPh], (●) [EMIM][EPh], (●) [EMIM][MeSO₄] at 312.92 K (b) ; —, correlated by Redlich-kister equation 109

Figure III.1: Schematic diagram of an absorption heat transformer; T_M-medium temperature, T_L-low temperature, T_H-high temperature, SHE-solution heat exchanger 118

Figure III.2: Thermodynamic cycle in absorption heat transformer (AHT) 126

Figure III.3: Flow chart for COP simulation 127

Figure III.4: COP of binary systems {water + ILs} versus T_L for single effect absorption heat transformer cycle 131

Figure III.5: COP of binary systems {water + ILs} versus T_M for single effect absorption heat transformer cycle 132

Figure III.6: COP of binary systems {water + ILs} versus T_H for single effect absorption heat transformer cycle	134
Figure III.7: Effect of T_H on (x_w^m) weak solution concentration	135
Figure III.8: Simulation trend for the investigated binary systems Group I (■) and II (■)	137

Nomenclature and symbols

Abbreviations

AHP	Absorption heat pump
AHT	Absorption heat transformers
AC	Absorption chillers (refrigeration)
ARD	Average relative deviation
COP	Coefficient of performance
COSMO-RS	Conductor like screening model for real solvents
CHF ₃	Fluoroform
E181	Tetraethylene glycol dimethyl ether
EOS	Equation of state
f	Circulation ratio
GWP	Global warming potential
HFCs	Hydrofluorocarbons
IL	Ionic liquids
LLE	Liquid-liquid equilibrium (T (K), P (kPa))
NRTL	Nonrandom two-liquid model
ODP	Ozone depletion potential
PC-SAFT	Perturbed-chain statistical associating fluid theory equation of state

TGA	Thermogravimetric analysis
TFE	2, 2, 2-trifluoroethanol
UNIQUAC	Universal quasi chemical model
UNIFAC	Universal functional activity coefficient
VLE	Vapor liquid equilibrium (T (K), P (kPa))
VLLE	Vapor-liquid-liquid equilibrium (T (K), P (kPa))

Symbols

A_i and B_i	Adjustable parameters
a_i and b_i	Adjustable parameters
C_p	Molar heat capacity ($\text{J}\cdot\text{mol}^{-1}\cdot\text{K}^{-1}$)
C_p^E	Molar excess heat capacity ($\text{J}\cdot\text{mol}^{-1}\cdot\text{K}^{-1}$)
g_{ij}	Energy of interaction between species i and j
h_i	Enthalpy of stream ($i=1, 2, \dots, 10$) ($\text{kJ}\cdot\text{kg}^{-1}$)
H^E	Molar excess enthalpy ($\text{J}\cdot\text{mol}^{-1}$)
$\Delta_{\text{mix}}h$	Mixing enthalpy of the system (kJ kg^{-1})
$i=1$	Water (refrigerant)
$i=2$	Ionic liquids (absorbent)
\dot{m}_i	Mass flow rate of stream ($i=1, 2, \dots, 10$) ($\text{kg}\cdot\text{s}^{-1}$)
p	System pressure (kPa)
p^s	Saturated vapor pressure of the refrigerant species (kPa)

Q	Heat load (kJ.s^{-1})
T_H, T_M, T_L	High, moderate and low temperature level (K, °C)
T_C, T_E, T_G, T_A	Condenser, Evaporator, Generator and Absorber temperatures (K, °C)
T	System temperature (K)
Δt	Gross temperature lift (K, °C)
V^E	Excess molar volum ($\text{cm}^3. \text{mol}^{-1}$)
x_i^m	Mass fraction of species i where $i = 1,2$
x_s^m	Mass fraction of ILs in the strong solution
x_w^m	Mass fraction of ILs in the weak solution
x	Mole fraction
Δx^m	Difference of mass fraction between strong and weak solutions

Subscripts

A	Absorber
C	Condenser
E	Evaporator
G	Generator
SHE	Solution heat exchanger
ss	Strong solution
ws	Weak solution

Greek letters

α	Non-random parameter of NRTL model
ρ	Density (g.cm ⁻³)
γ_i	Activity coefficient of species i (dimensionless), $i=1, 2$, (1 = refrigerant, 2 = absorbant)

Ionic liquids

[DMIM][Cl]	1,3-dimethylimidazolium chloride
[DMIM][MPh]	1,3-dimethylimidazolium methyl-phosphonate
[DMIM][BF ₄]	1,3-dimethylimidazolium tetrafluoroborate
[DMIM][DMP]	1,3-dimethylimidazolium dimethylphosphate
[HOEtMIM][Cl]	1-(2-hydroxyethyl)-3-methylimidazolium chloride
[HOEtMIM][BF ₄]	1-(2-hydroxyethyl)-3-methylimidazolium tetrafluoroborate
[HOEtMIM][TFA]	1-(2-hydroxyethyl)-3-methylimidazolium trifluoroacetate
[EMIM][BF ₄]	1-ethyl-3-methylimidazolium tetrafluoroborate
[EMIM][DMP]	1-ethyl-3-methylimidazolium dimethylphosphate
[EMIM][I]	1-ethyl-3-methylimidazolium iodide
[EMIM][Tf ₂ N] or [(CF ₃ SO ₂) ₂ N]	1-ethyl-3-methylimidazolium bis-(trifluoromethyl sulfonyl) imide
[EMIM][Ac]	1-ethyl-3-methylimidazolium acetate
[EMIM][HSO ₄]	1-ethyl-3-methylimidazolium hydrogen sulfate
[EMIM][EtSO ₄]	1-ethyl-3-methylimidazolium ethyl sulfate
[EMIM][DEP]	1-ethyl-3-methylimidazolium diethyl phosphate

[EMIM][TFO] or [Triflate] 1-ethyl-3-methylimidazolium trifluoromethane sulfonate

[EMIM][TFA] 1-ethyl-3-methylimidazolium trifluoroacetat

[EMIM][SCN] 1-ethyl-3-methylimidazolium thiocyanate

[EMIM][MeSO₃] 1-ethyl-3-methylimidazolium methanesulfonate

[EMIM][TOS] 1-ethyl-3-methylimidazolium tosylate

[BMIM][DMP] 1-butyl-3-methylimidazolium dimethylphosphate

[BMIM][BF₄] 1-butyl-3-methylimidazolium tetrafluoroborate

[BMIM][CF₃SO₃] or [TFO] or [triflate] 1-butyl-3-methylimidazolium trifluoromethane sulfonate

[BMIM][C₁SO₃] 1-butyl-3-methylimidazolium methane sulfonate

[BMIM][Cl] 1-butyl-3-methylimidazolium chloride

[BMIM][Br] 1-butyl-3-methylimidazolium bromide

[BMIM][Ac] 1-butyl-3-methylimidazolium acetate

[BMIM][CF₃CO₂] 1-butyl-3-methylimidazolium trifluoroacetate

[BMIM][I] 1-butyl-3-methylimidazolium iodide

[BMIM][SCN] 1-butyl-3-methylimidazolium thiocyanate

[BMIM][TOS] 1-butyl-3-methylimidazolium tosylate

[BMIM][N(CN)₂] 1-butyl-3-methylimidazolium dicyanamide

[BMIM][C(CN)₃] 1-butyl-3-methylimidazolium tricyanomethane

[BMIM][Tf₂N] 1-butyl-3-methylimidazolium bis(trifluoromethylsulfonyl)imide

[BMIM][MeSO₄] 1-butyl-3-methylimidazoliumMethylsulfate

[HMIM][BF₄] 1-hexyl-3-methylimidazolium tetrafluoroborate

[HMIM][DCA] 1-hexyl-3-methylimidazolium dicyanamide

[BDMIM][BF₄] 1-butyl-2,3-dimethylimidazolium tetrafluoroborat

[EEIM][DEP] 1-ethyl-3-ethylimidazolium diethyl phosphate
[DEMA][OMs] diethylmethyllummonium methane sulfonate
[BMPYR][DCA] 1-butyl-1-methylpyrrolidinium dicyanamide
[BMPy][TFO] 1-butyl-3-methylpyridinium trifluoromethanesulfonate
[BMPyr][TFO] 1-butyl-1-methylpyrrolidinium trifluoromethanesulfonate
[BMPIP][DCA] 1-butyl-1-methylpiperidinium dicyanamide
[BMPy][BF₄] 1-butyl-3-methylpyridinium tetrafluoroborate
[BPy][BF₄] N-butyl-pyridinium tetrafluoroborate
[BPy][PF₆] N-butyl-pyridinium hexafluorophosphate
[BPy][Ac] N-butyl-pyridinium acetate
[BPy][Br] N-butyl-pyridinium bromide
[Choline][MeSO₃] choline methanesulfonate
[Choline][Gly] choline glycolate
[Choline][Lac] choline lactate
[EEPy][EtSO₄] 1,2-diethylpyridinium ethylsulfate
[MPy][MeSO₄] 1-methylpyridinium methylsulfate
[P₆₆₆₁₄][Br] trihexyl(tetradecyl)phosphonium bromide
[C6iQuin][SCN] 1-hexylisoquinolinium thiocyanate
[C8iQuin][SCN] 1-octylisoquinolinium thiocyanate

Résumé

Ces dernières années, les activités domestiques et industrielles ont entraîné un besoin croissant en ressources fossiles alors que les réserves mondiales s'épuisent. De plus, les problèmes environnementaux liés à l'effet de serre deviennent prégnants. Par conséquent, l'efficacité énergétique, la conservation et le développement de sources d'énergie alternatives comme l'énergie solaire connaissent un intérêt croissant. À l'heure actuelle, la communauté scientifique s'intéresse au développement d'équipements qui facilitent la récupération et l'utilisation rationnelle de l'énergie. Ainsi, la réutilisation des flux thermiques des chaleurs résiduelles provenant des activités industrielles, telles que les centrales électriques, constitue une alternative prometteuse. En effet, d'énormes quantités de chaleur à basse température (de 60 à 100°C) sont libérées dans l'atmosphère par de nombreuses installations [1].

Les pompes à chaleur à absorption sont particulièrement appropriées pour utiliser les chaleurs fatales. Elles peuvent être utilisées aussi bien pour le chauffage que pour le refroidissement (air conditionné ou la réfrigération). De plus, il est possible de produire de la chaleur à haute température (120 - 150°C) à partir d'une source de chaleur à température moyenne (typiquement 60 - 80°C) en utilisant un type particulier de pompe à chaleur à absorption : le thermo-transformateur de chaleur à absorption.

Malheureusement, des limitations techniques empêchent un plus grand développement de cette technologie. Le mélange de travail utilisé dans le cycle est généralement constitué d'eau et de bromure de lithium et impose l'utilisation de matériaux spécifiques afin d'éviter tout problème de corrosion. L'éventuelle cristallisation du bromure de lithium limite aussi les conditions de fonctionnement. Le mélange eau/ammoniac peut aussi être utilisé, mais exige de travailler sous haute pression. Ce système est toxique et peu respectueux de l'environnement. La volatilité relative de ce mélange significativement supérieure à l'unité implique la présence d'une étape de rectification dans le cycle réduisant ainsi l'efficacité énergétique du procédé.

La recherche de mélanges de travail alternatifs pour les pompes à chaleur à absorption a connu de nombreux développements ces dernières décennies. L'utilisation de mélanges binaires constitués d'un liquide ionique et d'un solvant semble être prometteuse en remplacement des fluides de travail conventionnels ($\{H_2O + LiBr\}$ ou $\{NH_3 + H_2O\}$) [2-5].

I/ Cycles à absorption

Les cycles à absorption ont été développés au cours du XIX^{ème} siècle et ont reçu une attention importante ces dernières décennies. Parmi les technologies récentes, on trouve les réfrigérateurs à absorption ou refroidisseurs, les pompes à chaleur à absorption et les thermo-transformateurs de chaleur à absorption. Les cycles à absorption permettent l'échange de chaleur avec au minimum trois sources **à trois niveaux de température différents** : faible, intermédiaire et élevé. Quand un système à absorption est exploité comme un réfrigérateur ou une pompe à chaleur, la chaleur motrice provient de la source haute température. Dans le cas du réfrigérateur, le froid utile est produit à un niveau de température faible et de la chaleur est rejetée à un niveau de température intermédiaire. L'environnement est ainsi utilisé en tant que réservoir à température intermédiaire. Dans le cas de la pompe à chaleur, la chaleur utile produite est à un niveau de température intermédiaire et l'environnement est alors utilisé comme un réservoir à basse température. Le thermo-transformateur de chaleur à absorption reçoit quant à lui une chaleur issue d'un réservoir à température intermédiaire et rejette de la chaleur à un niveau de température faible (l'environnement). La sortie utile est obtenue à un niveau de température plus élevé.

Malgré leur intérêt évident, les thermo-transformateurs de chaleur à absorption sont rarement utilisés dans la pratique car leurs performances restent faibles (seulement 30 à 50% de la chaleur résiduaire est revalorisée). De plus, il existe des limitations techniques liées à la corrosion et au risque de cristallisation, notamment lorsque le mélange $\{H_2O + LiBr\}$ est utilisé [6-7].

Qu'il s'agisse de réfrigérateur, de pompe à chaleur ou de thermo-transformateur, le mélange de travail est constitué d'un composé léger : le réfrigérant (l'eau dans cette étude) et d'un composé moins volatil : l'absorbant (un liquide ionique dans cette étude). Le cycle à absorption est schématiquement réalisé par l'association d'une étape de séparation et d'une étape de mélange réalisées à différentes pressions. On compte cinq composants principaux dans ce cycle : l'évaporateur, le condenseur, le générateur (ou désorbeur), l'absorbeur ainsi que l'échangeur de chaleur (ou économiseur).

II/ Les liquides ioniques

Les liquides ioniques (LIs) sont des sels liquides se différenciant de l'ensemble des sels fondus classiques par une température de fusion inférieure à 100°C. La plupart d'entre eux sont liquides

à température ambiante [1]. Les LIs sont constitués d'un cation le plus souvent organique, associé à un anion organique ou inorganique. De plus, les combinaisons possibles entre cation et anion sont très nombreuses ($>10^6$). Les cations rencontrés sont généralement volumineux et dissymétriques. Les plus classiques sont des ammoniums, imidazoliums, pyridiniums, pyrrolidiniums, phosphoniums et sulphoniums (Figure 1). Les plus étudiés sont les sels d'imidazoliums substitués sur les atomes d'azote et de carbone. Les chaînes R1 et R2 sont le plus souvent des chaînes alkyles, cependant, il existe également des structures de liquides ioniques sur lesquelles nous pouvons introduire des groupes fonctionnels particuliers tels que des groupements amines [8], alcools [9-10], acides carboxyliques [11], thiols [12] et alcynes [13] afin de définir des liquides ioniques à tâche spécifique ou des liquides ioniques fonctionnalisés. La plupart des anions mis en œuvre peuvent être inorganiques comme le Fluor, le Chlore, l'Iode et le Brome ou organiques comme le tétrafluoroborate $[BF_4]^-$, le hexafluorophosphate $[PF_6]^-$ ou bien les alkylphosphonates et les alkylsulphates.

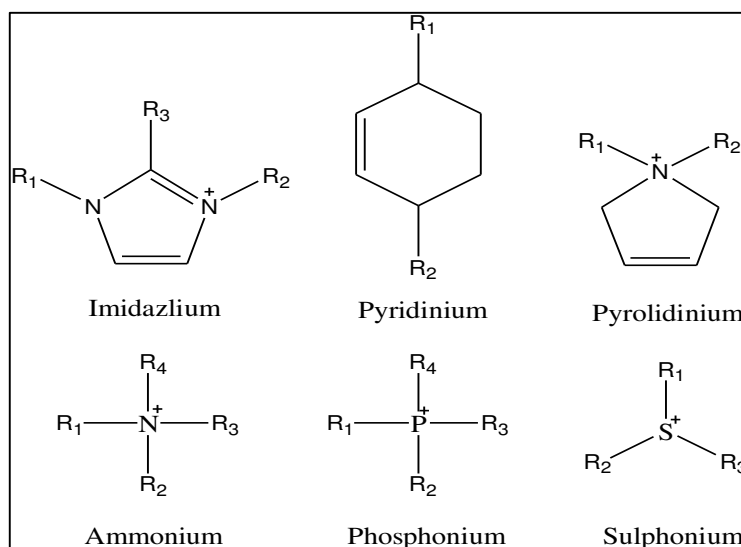


Figure 1: Cations des liquides ioniques.

Les LIs présentent de nombreuses propriétés physico-chimiques intéressantes qui en font une classe de solvants verts très prometteurs pour de nombreuses applications [14,15]. Notamment, leur très faible pression de vapeur saturante en font de bons candidats comme absorbants pour les pompes à chaleur à absorption. Leurs caractéristiques physico-chimiques peuvent être

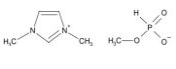
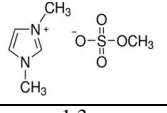
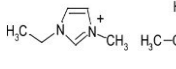
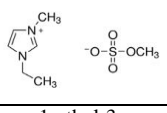
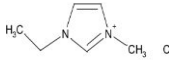
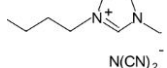
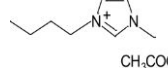
ajustées en jouant sur le choix de l'anion et/ou du cation mais également en modifiant les substituants sur le cation. La pureté du liquide ionique est aussi un facteur pouvant influencer leurs propriétés de manière significative [16].

L'objectif de cette thèse est d'évaluer les performances de thermo-transformateurs de chaleur d'absorption à l'aide de nouveaux fluides de travail $\{H_2O + ILs\}$ à l'aide de propriétés thermodynamiques mesurées expérimentalement.

Dans un premier temps, nous nous sommes intéressés à la présentation des cycles à absorption et des liquides ioniques en insistant sur leurs définitions, leurs propriétés physico-chimiques et leurs applications. Ensuite, une synthèse bibliographique sur les données thermodynamiques de systèmes binaires constitués de liquides ioniques et d'eau en insistant tout particulièrement sur les équilibres liquide-vapeur, densité, capacité calorifique et les enthalpies d'excès est présentée. Une liste de 35 mélanges potentiels issue de la littérature est alors proposée.

Après cette synthèse bibliographique, une étude expérimentale sur les propriétés thermodynamiques de 7 systèmes binaires $\{H_2O + LI\}$ est effectuée. La liste des systèmes étudiés est donnée dans le tableau 1. Plus concrètement, les objectifs concernent la détermination des équilibres liquide-vapeur, des densités, des capacités calorifiques et des enthalpies d'excès de tels systèmes. Les équilibres liquide-vapeur (ELV) des systèmes ont été mesurés à l'aide de deux dispositifs statiques isotherme et isobare. Les capacités calorifiques et les enthalpies d'excès ont été déterminées à l'aide de deux calorimètres et les masses volumiques ont été obtenues à l'aide d'un densimètre à tube vibrant. L'ensemble des résultats expérimentaux ont été corrélés à l'aide de modèles adaptés. Plus précisément, les ELV des systèmes binaires sont représentés à l'aide du modèle thermodynamique NRTL. Les enthalpies d'excès sont modélisées à l'aide d'un modèle de type Redlich-Kister. Les densités ainsi que les capacités calorifiques sont représentés à l'aide de modèles polynomiaux.

Tableau 1: Liquides ioniques étudiés.

Propriétés	[DMIM][MPh]	[DMIM][MeSO ₄]	[EMIM][MPh]	[EMIM][MeSO ₄]
Structure				
Nom	1,3-diméthylimidazolium méthylphosphonate	1,3-diméthylimidazolium méthyl sulfate	1-éthyl-3-méthylimidazolium méthyl phosphonate	1-éthyl-3-méthylimidazolium méthyl sulfate
Formule brute	C ₆ H ₁₃ N ₂ PO ₃	C ₆ H ₁₂ N ₂ SO ₄	C ₇ H ₁₃ N ₂ PO ₃	C ₇ H ₁₄ N ₂ SO ₄
Pureté (%)	> 98	97	> 98	98
Source	Solvionic	Sigma-Aldrich	Solvionic	Sigma-Aldrich
Propriétés	[EMIM][EPh]	[BMIM][DCA]	[BMIM][Ac]	
Structure				
Nom	1-éthyl-3-méthylimidazolium éthyl phosphonate	1-butyl-3-méthylimidazolium dicyanamide	1-butyl-3-méthylimidazolium acetate	
Formule brute	C ₈ H ₁₇ N ₂ PO ₃	C ₁₀ H ₁₅ N ₅	C ₁₀ H ₁₈ N ₂ O ₂	
Pureté (%)	> 98	99.5	> 98	
Source	Solvionic	Solvionic	Solvionic	

La dernière partie de cette étude est consacrée aux calculs de performances des divers systèmes binaires envisagés dont les propriétés physico-chimiques proviennent de la littérature et/ou de l'expérience. Les simulations numériques réalisées consistent en la résolution des bilans de matière et d'énergie au sein des différents appareils constituant un thermo-transformateur à absorption simple-effet en régime permanent. Elles donnent accès à la connaissance des propriétés du mélange en tout point du cycle et des flux de chaleur échangés. Les niveaux de températures considérées sont de 20°C pour la source basse température, 80°C pour la chaleur résiduaire et 130°C pour la chaleur revalorisée. Les critères de performance retenue sont le coefficient de performance (COP) qui représente le pourcentage de la chaleur résiduaire effectivement revalorisée et le saut thermique maximal qui représente l'élévation maximale de température qu'il est possible d'obtenir. Les résultats de simulation montrent que les performances des fluides de travail constitués de liquide ionique et d'eau sont proches de celles du fluide de travail {H₂O + LiBr}. On constate que les liquides ioniques constitués d'une chaîne alkyle courte conduisent à des COP plus élevés. Ces résultats sont en cohérence avec le fait que la solubilité de l'eau diminue lorsque la chaîne alkyle greffée sur le cation (ou l'anion) augmente (voir figure 2).

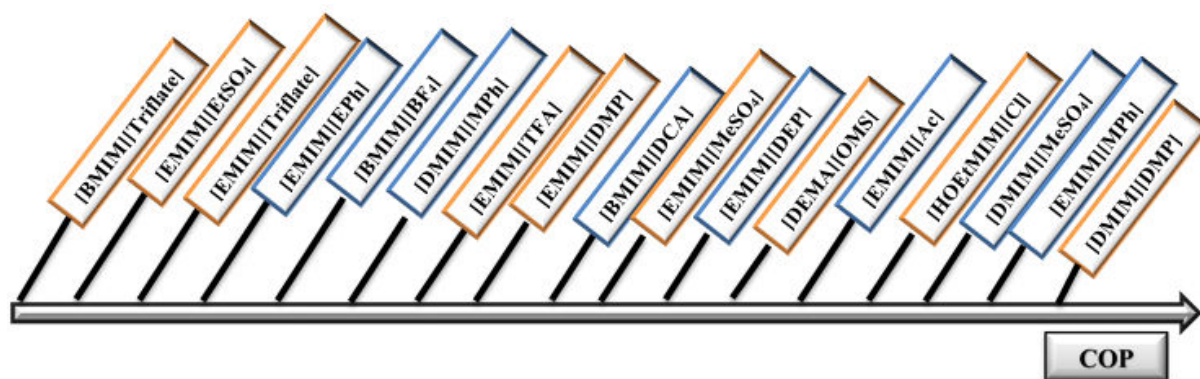


Figure 2: Influence de la structure du liquide ionique sur le coefficient de performance.

References

- [1] J. Ren, Z. Zhao, X. Zhang, Vapor pressures, excess enthalpies, and specific heat capacities of the binary working pairs containing the ionic liquid 1-ethyl-3-methylimidazolium dimethylphosphate, *J. of Chem. Thermodynamics*, 43 (2011) 576-583.
- [2] X. Zhang, D. Hu., Performance analysis of the single-stage absorption heat transformer using a new working pair composed of ionic liquid and water, *Applied Thermal Engineering*, 37 (2012) 129–135.
- [3] L. Dong , D. Zheng, N. Nie, Y. Li, Performance prediction of absorption refrigeration cycle based on the measurements of vapor pressure and heat capacity of {H₂O + [DMIM][DMP]} system, *Applied Energy*, 98 (2012) 326–332.
- [4] Y.J. Kim, S. Kim, Y.K. Joshi, A.G. Fedorov, P.A. Kohl, Thermodynamic analysis of an absorption refrigeration system with ionic-liquid/refrigerant mixture as a working fluid, *Energy*, 44 (2012) 1005–1016.
- [5] M. Krolikowska, K. Paduszyn, M. Krolikowska, J. Antonowicz, Vapor – Liquid phase equilibria and excess thermal properties of binary mixtures of ethylsulfate-based ionic liquids with water : new experimental data, correlations, and predictions, *Ind. Eng. Chem. Res.*, 53(2014) 18316–25.

- [6] D. Alonso, T. Cachot, J.M. Hornut, Experimental study of an innovative absorption heat transformer using partially miscible working mixtures, *International Journal of Thermal Sciences*, 42 (2003) 631–638.
- [7] D. Alonso, T. Cachot, J.M. Hornut, Performance simulation of an absorption heat transformer operating with partially miscible mixtures, *Applied Energy*, 72 (2002) 583–597.
- [8] E.D. Bates, R.D. Mayton, I. Ntai, J.H. Davis, Jr., CO₂ capture by a task-specific ionic liquid, *J. Am. Chem. Soc.*, 124 (2002) 926–927.
- [9] L.C. Branco, J.N. Rosa, J.J.M. Ramos, C.A.M. Afonso, Preparation and characterization of new room temperature ionic liquids, *Chem. Eur. J.*, 8 (2002) 3671–3677.
- [10] H.S. Schrekker, M.P. Stracke, C.M.L. Schrekker, J. Dupont, Ether-functionalized imidazolium hexafluorophosphate ionic liquids for improved water miscibilities, *Ind. Eng. Chem. Res.*, 46 (2007) 7389–7392.
- [11] Z.F. Fei, W.H. Ang, T.J. Geldbach, R. Scopelliti, P.J. Dyson, Ionic solid-state dimers and polymers derived from imidazolium dicarboxylic acids, *Chem. Eur. J.*, 12 (2006) 4014–4020.
- [12] H. Itoh, K. Naka, Y. Chujo, Synthesis of gold nanoparticles modified with ionic liquid based on the imidazolium cation, *J. Am. Chem. Soc.*, 126 (2004) 3026–3027.
- [13] Z.F. Fei, D. Zhao, R. Scopelliti, P.J. Dyson, Organometallic complexes derived from alkyne-functionalized imidazolium salts, *Organometallics*, 23 (2004) 1622–1628.
- [14] P. Bonhôte, A.P. Dias, N. Papageorgiou, K. Kalyanasundaram, M. Grätzel, Hydrophobic, highly conductive ambient-temperature molten salts, *Inorg. Chem.*, 35 (1996) 1168–1178.
- [15] J.G. Huddleston, A.E. Visser, W.M. Reichert, H.D. Willauer, G.A. Broker, R.D. Rogers, Characterization and comparison of hydrophilic and hydrophobic room temperature ionic liquids incorporating the imidazolium cation, *Green Chem.*, 3 (2001) 156–164.
- [16] K.R. Seddon, A. Stark, M.J. Torres, Influence of chloride, water, and organic solvents on the physical properties of ionic liquids, *Pure Appl. Chem.*, 72 (2000) 2275–2287.

INTRODUCTION

In recent years, industrial and domestic activities increased oil and fossil fuel demand while fossil fuel supplies of the world are limited and the fuel reserves are getting depleted. Moreover, environmental problems represented by the greenhouse effect and increasing CO₂ emissions have been rapidly thrust upon us. Therefore, we are observing a growing interest in energy efficiency, increasing general interest in energy conservation and development of alternative energy sources such as solar energy. At the present time, researchers are interested in developing equipment that facilitate the recovery and efficient use of energy. Reusing thermal waste heat streams from industrial activities, such as power stations, instead of discharging them as thermal pollutant to air and water, receives considerable attention.

Recently, researchers have shown an increased interest in absorption heat pumps, which are considered as a suitable solution for a rational use of waste heat. One of the most promising devices for energy savings, which consume negligible amount of primary energy, is the absorption heat transformer (AHT). In this field of application, absorption heat transformers can use low temperature level heat (waste heat) to produce useful thermal energy at higher temperature level to be recycled in industrial and domestic applications [1, 2, 3, 4].

Absorption cycles were first developed in the nineteenth century and have received much attention in the last few decades. Among current absorption cycle technologies are absorption refrigerators or chillers (AC), absorption heat pumps (AHP) and absorption heat transformers (AHT). This last cycle is attractive because of its high primary energy efficiency compared to other technologies, its ability to use environmentally benign refrigerants and since it allows to decrease the amount of primary energy (i.e. fossil fuels) consumed. Nonetheless, AHT are rarely used in practice. Their performances remain low (only 30 to 50% of the driving waste heat is effectively upgraded to an interesting temperature level [4]). The commonly used working fluids in AHT are {water + LiBr} and {ammonia + water}. However, these working fluids have technical drawbacks such as corrosion and crystallization, while ammonia is toxic. Those technical limitations lead to long payback periods. However, these problems can be avoided if these working pairs are replaced with new alternatives. Essential efforts to propose new working fluids or multistage structures have still not allowed to widespread this technology [4].

Following an idea suggested by several authors [5], mainly for absorption chillers [6, 7, 8], we propose to use alternative working fluids composed of {water + ILs} as working fluids for the absorption heat transformers (AHT). Few experimental works have been realized on this type of absorption cycle. Consequently, the aim of this study is to build a database of new binary systems {water + ILs} in order to evaluate their performance as working fluids in AHT.

Ionic liquids are salts in the liquid state having melting point below some arbitrary temperature, such as 100°C (373 K). These solvents consist of an asymmetric, bulky organic cation and a weakly coordinating organic or inorganic anion. A large number of possible combinations enhance the ability to ‘fine tune’ the solvent properties for a specific purpose [9]. The attractive physical and chemical properties of ionic liquids are influenced by the nature of the cation and the nature of cation substituents as well as the polarity and the size of the anion.

ILs have unique properties such as negligible vapor pressure, non-flammability, nontoxicity, good thermal stability, low melting points, wide range of liquid state from room temperature up to 200 or 300 °C, and good solubility for many organic or inorganic chemicals. These features infer to ILs numerous applications, in organic synthesis, separation processes and electrochemistry [10]. For instance, many ILs are completely miscible with water, which nominate them to be investigated as alternatives working fluids in absorption cycle. The use of ionic liquids as absorbents in absorption cycle will enhance absorption of large amount of refrigerant under low temperature conditions and hence, yield to high coefficient of performance [11].

In order to optimize the use of ILs and design the desirable ILs, knowledge of their thermodynamic and physical properties is of great importance. Physical properties such as density and viscosity are related to the mechanical and engineering components associated with a process. For academic research, thermodynamic and chemical properties are also essential to validate the theoretical models.

The main aim of this thesis is to provide a data base of thermodynamic and physical properties for binary systems composed of {water + ILs} by experimentally investigating new ILs and through collecting data from literature for already published ILs properties. Based on the database, the thermodynamic properties of ILs and the variations of properties with the change of cations and anions are studied. Models with good correlation of thermodynamic data for all

ILs are developed. Drawing upon these data, simulation of the performance of absorption heat transformers using these binary systems $\{\text{H}_2\text{O} + \text{ILs}\}$ as working fluids is achieved. Simulation results are compared to the already used working fluids in order to evaluate these binary systems $\{\text{H}_2\text{O} + \text{ILs}\}$ for future use in absorption heat transformers. The present purpose is to examine the feasibility of using water and ILs in an absorption heat transformer cycle and to show some promising results for this application.

Outline of thesis chapters

Chapter one begins by laying out a full description of ionic liquids, history, their thermodynamic properties and their industrial applications. In addition, the second part is devoted to define the principle of absorption heat transformers. The final part is concerned with presenting a review of thermodynamic properties of binary systems consisting of $\{\text{water} + \text{ILs}\}$ used in absorption cycle in particular absorption refrigeration cycle.

Chapter two presents in details the materials, the experimental methods and equipment used for all measurements in this research. Additionally, a brief discussion on thermodynamic theories and models including non-random two liquid (NRTL) model is described. Finally, the third section presents experimental results for the selected binary systems.

Chapter three is devoted to simulate the performance of absorption heat transformers using the new investigated binary systems based on the experimentally and literature thermodynamics properties mentioned in both chapter one and two. In addition, evaluation of the simulation results for all the systems investigated is provided. Finally, the conclusion gives a brief summary and critique of the findings as it discuss recommendations for future work.

References

[1] A. Huicochea, W. Rivera, H. Martínez, J. Siqueiros, E. Cadenas, Analysis of the behavior of an experimental absorption heat transformer for water purification for different mass flux rates in the generator, *Applied Thermal Engineering*, 52 (2013) 38–45.

- [2] M. Meza, A. Márquez-Nolasco, A. Huicochea, D. Juárez-Romero, J. Siqueiros, Experimental study of an absorption heat transformer with heat recycling to the generator, *Experimental Thermal and Fluid Science*, 53 (2014) 171–178.
- [3] D. Alonso, T. Cachot, J.M. Hornut, Performance simulation of an absorption heat transformer operating with partially miscible mixtures, *Applied Energy*, 72 (2002) 583–597.
- [4] D. Alonso, T. Cachot, J.M. Hornut, Experimental study of an innovative absorption heat transformer using partially miscible working mixtures, *International Journal of Thermal Sciences*, 42 (2003) 631–638.
- [5] X. Zhang, D. Hu., Performance analysis of the single-stage absorption heat transformer using a new working pair composed of ionic liquid and water, *Applied Thermal Engineering*, 37 (2012) 129–135.
- [6] A. Yokozeki, M.B. Shiflett, Water solubility in ionic liquids and application to absorption cycles, *Ind. Eng. Chem. Res.*, 49 (2010) 9496–9503.
- [7] L. Dong , D. Zheng, N. Nie, Y. Li, Performance prediction of absorption refrigeration cycle based on the measurements of vapor pressure and heat capacity of {H₂O + [DMIM][DMP]} system, *Applied Energy*, 98 (2012) 326–332.
- [8] X. Zhang, D. Hu, Performance simulation of the absorption chiller using water and ionic liquid 1-ethyl-3-methylimidazolium dimethylphosphate as the working pair, *Applied Thermal Engineering*, 31 (2011) 3316–21.
- [9] A.L. Revelli, F. Mutelet, J.N. Jaubert, Partition coefficients of organic compounds in new imidazolium based ionic liquids using inverse gas chromatography, *Journal of Chromatography A*, 1216 (2009) 4775–4786.
- [10] L.K. Chellappan, Synthesis of ionic liquids based on new cationic cores. PhD thesis, Department of Chemistry, Faculty of Science, Katholieke Universiteit, Heverlee (Leuven), Belgium; May 2012.
- [11] M. Krolikowska, M. Zawadzki, M. Krolikowski, Physicochemical and thermodynamic study on aqueous solutions of dicyanamide – based ionic liquids, *The Journal of Chemical Thermodynamics*, 70 (2014) 127–137.

CHAPTER ONE

STATE OF THE ART

I.1. Introduction

This first part of this chapter gives a full description of ionic liquids, their thermodynamic properties and industrial applications. After, the second part describes the principle of absorption cycle and absorption heat transformer. The last part is devoted to present a review of thermodynamic properties of working fluids containing {ionic liquids + water}.

I.2. Ionic Liquids

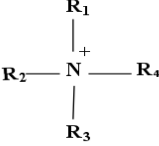
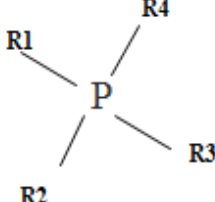
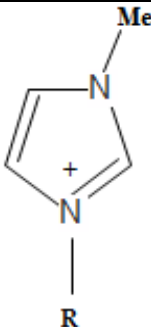
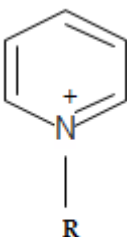
One of the objectives of green chemistry is the design of new chemicals and methods in order to reduce or eliminate the use of hazardous substances. Ionic liquids (ILs) are a new type of environmentally-friendly solvents, which can be defined as the liquids which exclusively consisting of ions (cations and anions), and have low melting point (below 100 °C). Ionic liquids have attracted considerable attention due to their unique properties which distinguish ionic liquids from conventional organic solvents. These are negligible vapor pressure, non-flammability, good thermal stability, low melting points, wide range of liquid state from room temperature up to 200 or 300° C and good solubility for many organic or inorganic chemicals. Therefore, ILs have been proposed as effective substitute for common volatile organic compounds (VOCs) for “green processing” which would inhibit a major source of environmental pollution [1].

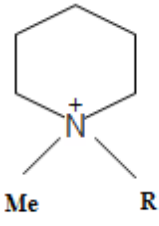
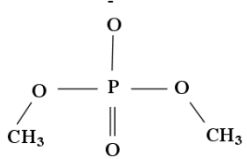
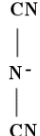
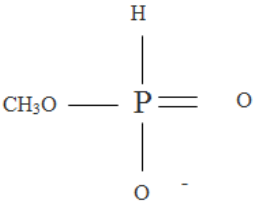
In the literature, ionic liquids sometimes are called liquid organic salts, fused or molten salts, ionic melts, NAILs (nonaqueous ionic liquids), room-temperature molten salts, OILs (organic ionic liquids) and ionic fluids [2]. Generally, ionic liquids are composed of a large bulky and asymmetric organic cations and organic or inorganic anions. Asymmetry of the cation is assumed to be the reason of the low melting points of ionic liquids, while the type of the anion is believed to be responsible for many of the physical properties of ionic liquids such as their miscibility with different solvents and hygroscopicity [3].

A major advantage of these solvents is that their physical properties (such as melting point, viscosity, density, and hydrophobicity) can be tuned to design different ionic liquids, to be applied in different applications by selection of different cation, anion, and substituents. Hence,

ILs constitute a huge family of chemicals due to the infinite combinations of different cations and anions [4]. Some commonly used ionic liquids (cations and anions) are listed in Table I.1.

Table I.1: Common ILs cations and anions.

Cation	Abbreviation	Name
	Amm	Tetra-alkyl ammonium
	Ph	Tetra-alkyl phosphonium
	C _n MIM	1-alkyl -3- methyl Imidazolium
	Py	N-Pyridinium

	PIP	N-alkyl-N-methylpiperidinium
Anion	Abbreviation	Name
	DMP	dimethylphosphate
	DCA	dicyanamide
	MPh	methylphosphonate

I.3. History and progress of ionic liquids

In 1914, Paul Walden [5, 6, 7] had synthesized the first low melting point ionic liquid “ethylammonium nitrate ($[\text{EtNH}_3]^+[\text{NO}_3]^-$)”, with melting point of 12 °C. Nevertheless, their wide spread use as solvents in chemical and industrial processes for synthesis, separation processes and catalysis has become lately significant. In 1940s, aluminium chloride based molten salts were used for high temperature electroplating. Hurley and coworkers in 1951 [8] synthesized an ionic liquid by warming a mixture of 1-ethylpyridinium chloride with aluminium chloride for low-temperature electroplating of aluminium. During 1970s and 1980s,

a thorough investigation on room temperature organic chloride-aluminium chloride was done by Robinson *et al.* [9] and Hussey *et al.* [10, 11, 12]. These solvents were used for electrochemical applications in nuclear warheads batteries.

In the early 1970s, Wilkes [13] tried to develop better batteries for nuclear warheads and space probes which required molten salts to operate. These molten salts were hot enough to damage the nearby materials. Therefore, the chemists searched for salts which remain liquid at lower temperatures and eventually they identified one which is liquid at room temperature. Wilkes and his colleagues continued to improve their ILs for use as battery electrolytes and then a small community of researchers began to make ILs and test their properties [14].

During the mid of 1980s, low melting point ionic liquids were used as solvents for organic synthesis. The first major review about ionic liquids was written by Hussey in 1983 [10]. Afterwards, ionic liquids became one of the most promising chemicals as solvents. Generally, ionic liquids such as organo-aluminate, have limited range of applications because they were unstable to air and water. Moreover, these ILs were not inert towards different organic compounds. In 1992, the first reports appeared about the synthesis and applications of water and air stable ILs based on 1-ethyl-3-methylimidazolium cation [EMIM]⁺ and different anions such as tetrafluoroborate [BF₄]⁻ and hexafluorophosphate [PF₆]⁻ [7]. Few years later, Davis *et al.* [15] prepared a new class of ionic liquids called "functional ionic liquids" based on cations derived from the antifungal drug miconazole.

There are literally billions of different structures that may form an IL. The composition and the specific properties of these liquids depend on the type of cation and anion in the IL structure. By combining various kinds of cation and anion structures, it is estimated that 10¹⁸ ILs can be designed [16]. Recently, interest in ionic liquids has been grown significantly in the scientific community (both in academia and industry) with over than 8000 papers have been published in the last decade. This growth can be observed in Figure I.1 (number of publications per year), where the number of publications and patents are increasing rapidly.

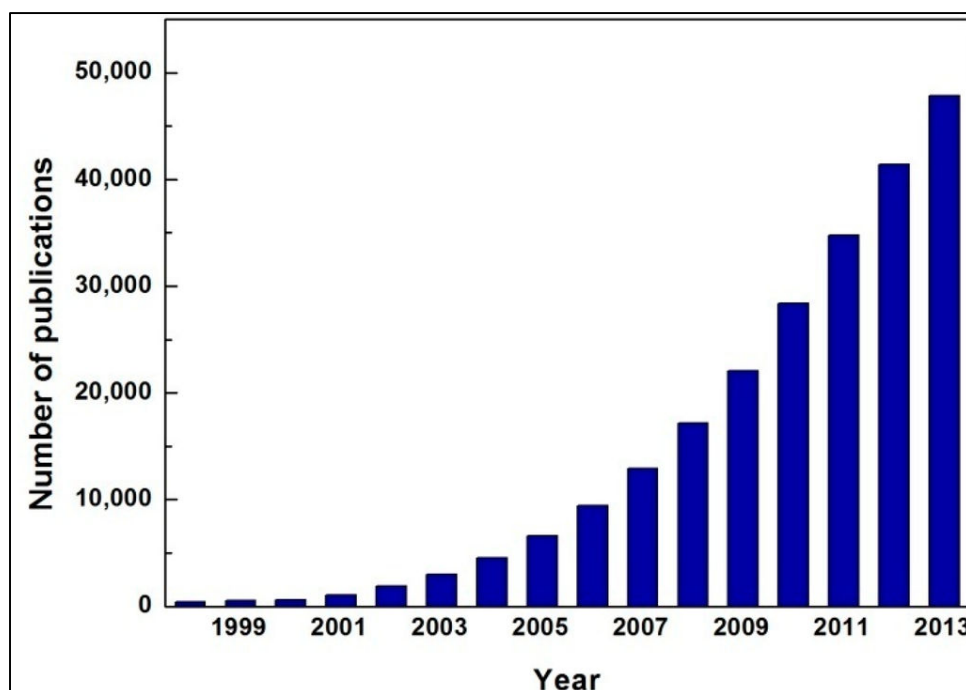


Figure I.1: Growth rate of ionic liquid publications, 1999-2013 [SciFinder, 2014].

I.4. Classes of ionic liquids

Ionic liquids can be classified into three categories: First, second and third-generation ionic liquids [6]. The first-generation of ionic liquids has been widely studied and is mainly composed of bulky cations like 1, 3-dialkylimidazolium (or N, N'- dialkylimidazolium) or 1-alkylpyridinium (or N-alkylpyridinium), and anions based mostly on haloaluminate (III). The interesting property of these ionic liquids is their tunable Lewis acidity. Nevertheless, this generation of ILs is sensitive towards water and it forms hydroxoaluminate (III) species with the aluminium (III) chloride and hence the ionic liquid decomposes. The second-generation ionic liquids are generally air and water stable and can be used on the bench-top. Nevertheless, water-stability does not mean that there is no interaction with water at all. Second-generation ionic liquids are usually hygroscopic and gradually absorb water from the atmosphere. The third generation of ionic liquids has a functional group covalently attached to the cation or to the anion or both. The advantage of introducing a functional group into ionic liquids is the fine-tuning of their properties for a particular application [6, 7].

I.5. Physico-chemical properties of Ionic liquids

I.5.1. vapor pressure

Ionic liquids have a negligible vapor pressure even at high temperature due to their ionic nature. Thus, ILs tend not to give off vapors in contrast to traditional organic solvents such as benzene, acetone, and toluene. Kabo *et al.* [17] evaluated the vapor pressure of [BMIM][PF₆] at 298.15 K around 10^{-11} Pa [16]. Hence, the impact on the environment and the process operation personnel is minimal. Additional, advantage is that volatile products, and even products with conventionally low vapor pressures, can be easily isolated from ionic liquids by distillation.

I.5.2. Activity coefficient for ionic liquids

Activity coefficients give information concerning the interaction between solute and IL. This parameter describes also the degree of non-ideality for a species *i* in a mixture. The large dataset of activity coefficients at infinite dilution published in the literature may be used to present a general behaviour of solutes with ionic liquids [6, 7].

The values of activity coefficients at infinite dilution γ^∞ for n-alkanes increase with an increase in carbon number. In most ionic liquids, the high γ^∞ values observed with n-alkanes indicate their low solubility in ionic liquids. γ^∞ values of n-alkanes are higher than the values obtained with cyclohexane, alkenes, alkynes and aromatics. Introduction of a double or triple bond in the n-alkanes decreases the γ^∞ values.

Cyclization of the alkane skeleton reduces the value of γ^∞ in comparison to that of the corresponding linear alkanes. Aromatics with their π -delocalized electrons have smaller γ^∞ values, presumably because of the interaction with the cation species. Using computer simulation, Lynden-Bell *et al.* [18] showed that the cations are found to interact predominantly with the ring of the benzene while the anions interact with the ring hydrogens to a first approximation.

In the series of chloromethanes, it is usually observed that γ^∞ values strongly increase from dichloromethane to tetrachloromethane. This behavior observed with all types of ionic liquids

indicates that polar compounds have better solubility in the ILs when attractive interaction between polar molecules and the charged ions of the solvent is possible. The γ^∞ values for the alcohols are relatively small (ranging between 1.2 and 4.6). The lone pair of electrons on the oxygen atom could interact with the ionic liquid cation, and the acidic proton is attracted by oxygen atoms in the cation. γ^∞ values of branched alkanol skeleton are smaller than γ^∞ values of the corresponding linear alcohol. γ^∞ values of n-alkanols increase with increasing chain length. γ^∞ values of ethers and amine are higher in comparison with those of the alcohols. For most solutes, their solubility increase when the alkyl chain length grafted on the ionic liquid increase. The behavior of solutes with ionic liquids is also strongly affected by the nature of the chain grafted on the ionic liquids. For example, grafting a polar chain on the cation of dicyanamide based ionic liquid increases strongly the interactions. Replacing the 1-ethyl-3-methylimidazolium cation by 1-(3-cyanopropyl)-3-methylimidazolium in dicyanamide based ionic liquids, the activity coefficients values of n-hexane are divided by two (241 to 111).

The alkoxymethyl-group grafted on the imidazolium cation makes the ionic liquid more polar and with possible anti-microbial activities [19]. Domanska and Marciniak [20] studied the interaction between organic compounds and 1-hexyloxymethyl-3-methyl-imidazolium bis(trifluoromethylsulfonyl)-imide and 1,3-dihexyloxymethyl-imidazolium bis(trifluoromethylsulfonyl)-imide. The authors found that ILs with two alkoxymethyl groups in the cation reveals stronger interactions with solutes, e.g. additional interaction of the IL with n-alkanes, alkenes and alkynes (i.e. Van der Waals interaction between alkane chains of the solute and the cation), and also stronger interaction with aromatic hydrocarbons, thiophene and alcohols (hydrogen bonding, n- π , or π - π interactions).

Revelli *et al.* [21] measured activity coefficients at infinite dilution of organic compounds in the ionic liquid trihexyl(tetradecyl) phosphonium bis(trifluoromethylsulfonyl)imide. As observed with imidazolium-based ionic liquids, cations with a long alkyl chain tend to increase the solubility of most organic compounds in IL. The activity coefficients of 39 organic compounds in this IL are below unity apart from the alkanes and alcohols indicating a strong affinity of the solutes for the ionic liquid. The introduction of a cyanoalkyl chain dramatically decreases the solubility of a polar compounds in ILs. Aromatics, alkenes and alkynes have lower interactions with cyanoalkylimidazolium based ILs than dialkylimidazolium. There is a lack of information concerning piperidinium based ionic liquids. In their recent study, Domanska and Paduszynski, [22] demonstrate that 1-propyl-1-methylpiperidinium

bis(trifluoromethyl)sulfonyl)imide behaves like the other measured ionic liquids based on different cations.

I.5.3. Density

Ionic liquids are denser than water with values ranging from 1-1.6 g.cm⁻³ and their densities decrease with increase in the length of the alkyl chain in the cation. For instance, imidazolium based ionic liquids coupled with [CF₃SO₃]⁻ anion, the density has the following behavior [EMIM]⁺ > [EEIM]⁺ > [BMIM]⁺ > [BEIM]⁺ with values 1.39 g.cm⁻³, 1.33 g.cm⁻³, 1.29 g.cm⁻³, 1.27 g.cm⁻³, respectively. This can be explained by the ability of the shorter alkyl chain to close-packing and therefore achieve a higher density, whereas the bulkiness of the longer chain derivatives leads to less efficient close-packing. The densities of ionic liquids are also affected by the identity of anions. For example, the densities of [BMIM]⁺ ionic liquid with different anions, such as BF₄⁻, PF₆⁻, TFA⁻ and Tf₂N⁻ are 1.12 g.cm⁻³, 1.21 g.cm⁻³, 1.36 g.cm⁻³ and 1.43 g.cm⁻³, respectively. Recently, it has been observed that phosphonium-based ionic liquids possess very low densities: at 30° C, the density of trihexyl tetradecylphosphonium chloride ([P₆₆₆₁₄][Cl]) is 0.88 g.cm⁻³, while that of the corresponding [BF₄]⁻ was found to be 0.93 g.cm⁻³ [6, 7].

I.5.4. Viscosity

Knowledge of the viscosity of ionic liquids is of great importance because it plays a key role in stirring, mixing and pumping processes. In addition, viscosity affects other transport properties such as diffusion and thermal conductivity as it affects heat and mass transfer. In general, ionic liquids are more viscous than common molecular solvents and their viscosities are ranging from 10 mPa.s to about 500 mPa.s at room temperature. The viscosity of ionic liquids mainly depends on van der Waals forces and hydrogen bondings. Both anions and cations have a strong influence on the viscosity of ILs. Toduka *et al.* [23] and Chellappan [7] found that the alkyl chain length and the nature of the anion have an important influence on the viscosity of ionic liquids. The fluorinated anions such as [BF₄]⁻ and [PF₆]⁻ form viscous ionic liquids because of the formation of complexes with hydrogen bonding donors. It was also found that the viscosity of ionic liquids depends on the alkyl chain length of the cations. It is obvious that alkyl groups

with short chain lengths have low viscosity. An increase of alkyl chains will increase the viscosity due to the increased possibility of van der Waals forces which in turn increase the energy needed for the molecular motions.

Impurities and moisture play a significant role on physicochemical properties of ILs. Seddon *et al.* [24] have shown that the presence of even low concentration of halide (chloride) can increase the viscosity significantly. The high viscosity of ILs reduces considerably their applications in industry. One of the solutions is the addition of solvents in ILs in order to reduce the viscosity.

I.5.5. Surface tension

There is a lack of data for the surface tension of ionic liquids in literature. Values of surface tension differs according to the ionic liquid (i.e. 33.8 N.m⁻¹ for [OMIM][Cl], 49.8 N.m⁻¹ for [BMIM][PF₆] and 54.7 N.m⁻¹ for [BMIM][I]). The surface tension of ionic liquids were found to be higher than that of conventional organic solvents such as methanol 22.07 N.m⁻¹, acetone 23.5 N.m⁻¹ and those of n-alkanes (i.e. pentane 16.0 N.m⁻¹, dodecane 25.6 N.m⁻¹, while it is lower than that of water (71.98 N.m⁻¹)) at 20° C. Freire *et al.* [25] investigated the effect of cations, anions, water and temperature on the surface tension of ionic liquids. They stated that both the cations and anions have an influence on the surface tension. In the case of imidazolium based ionic liquids, the increase in the cation alkyl chain length decreases the surface tension values. Additionally, an increase of the size of the anion leads to a decrease in the surface tension. They referred this behavior to the fact that an increase of the anion size decreases its ability to form hydrogen bonds. The water content in the ionic liquids has little or no influence on the surface tension values. Surface tension decreases linearly with an increase in temperature.

I.5.6. Miscibility with water

Solubility of water in ionic liquids mainly depends on their structure and especially on the nature of the anion. At room temperature, ILs based on [PF₆]⁻, [Tf₂N]⁻ and [CF₃SO₂)₂N]⁻ anions are insoluble in water (Figure I.2). Most of the ionic liquids based on anions such as ethanoate, trifluoroacetate, nitrate, acetate, halides are fully miscible with water. Nevertheless, the water

solubility in $[\text{BF}_4]^-$ and $[\text{CF}_3\text{SO}_3]^-$ based ILs depends on the alkyl chain length grafted on the cation. For instance, $[\text{EMIM}][\text{BF}_4]$ and $[\text{BMIM}][\text{BF}_4]$ are fully water miscible. However, $[\text{C}_n\text{MIM}][\text{BF}_4]$ ionic liquids with alkyl chain length higher than four ($n > 4$) are immiscible with water. Hence, the anion has a key role on water miscibility and the cation a secondary effect. It is well known that ionic liquids based on $[\text{PF}_6]^-$ and $[\text{Tf}_2\text{N}]^-$ are hygroscopic. However, this is not in agreement with the literature results which shows that water saturation of hydrophobic ionic liquids such as $[\text{C}_{4-8}\text{MIM}][\text{BF}_4]$ and $[\text{C}_{6-10}\text{MIM}][\text{PF}_6]$ is a function of both alkyl chain and the anion. Chellapan [7] stated that $[\text{PF}_6]^-$ based ionic liquids dissolve less water in comparison to the $[\text{BF}_4]^-$ based ionic liquids and the water intake decreases as the chain length of the alkyl group increases. Seddon *et al.* [24] reported that the so-called hydrophobic ionic liquids are in fact hygroscopic. They investigated the extent of hygroscopicity of $[\text{OMIM}][\text{Cl}]$, $[\text{OMIM}][\text{NO}_3]$, $[\text{BMIM}][\text{BF}_4]$, and $[\text{BMIM}][\text{PF}_6]$. Although the fully water-soluble chloride and nitrate ionic liquids absorb much more water than the corresponding hexafluorophosphate, an uptake of 1% w/w (0.16 mole fraction of water) over 3 hour is significant.

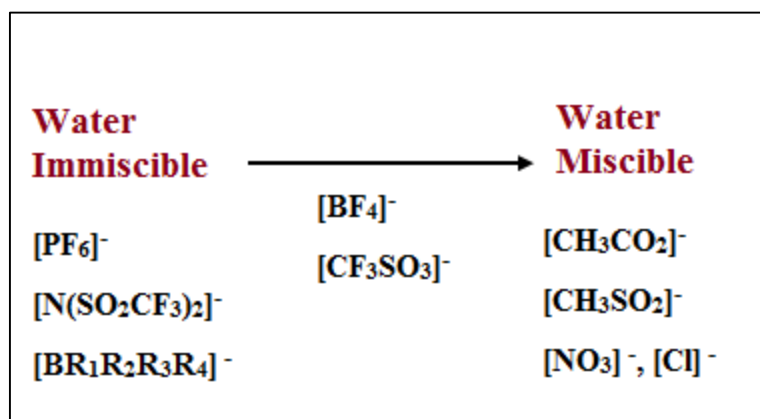


Figure I.2: Commonly used anions and their miscibility with water.

I.5.7. Melting point

Both cations and anions have an impact on the low melting points of ionic liquids. The increase in anion size leads to a decrease in melting point [6, 7]. For example, the melting points of 1-ethyl-3-methylimidazolium type ionic liquids with different anions, such as $[\text{BF}_4]^-$, $[\text{Tf}_2\text{N}]^-$ and $[\text{C}_2\text{H}_5\text{SO}_4]^-$ are 15 °C, -3 °C and -20 °C, respectively. Melting points of some of the ionic liquids is tabulated in Table I.2. The cation size and symmetry also play an important role on

the melting point of ionic liquids. Large cations and increased asymmetric substitution results in a melting point reduction.

Table I.2: Melting point data for different ionic liquids [6, 7].

Ionic liquids	Melting point	Ionic liquids	Melting point
[EMIM][NO ₃]	38	[PMIM][PF ₆]	40
[EMIM][NO ₂]	55	[BMIM][Cl]	41
[EMIM][TA]	-14	[BMIM][I]	-72
[EMIM][CH ₃ CO ₂]	45	[BMIM][BF ₄]	-81
[EMIM][PF ₆]	58-60	[BMIM][PF ₆]	10
[EMIM][TfO]	-9	[BMIM][TfO]	16
[EMIM][NfO]	28	[BMIM][NfO]	20
[EMIM][Tf ₂ N]	-3	[BMIM][Tf ₂ N]	-4
		[HMIM][PF ₆]	-61

I.5.8. Thermal stability

Thermal stability of ionic liquids is one of the most important properties because it defines their applications in processes. Low thermal stability may limit and decrease the performance in the industrial application. Numerous studies [6, 7] have concluded that the thermal stability of ionic liquids strongly depends on the nature of the anions. Ionic liquids containing nucleophilic and coordinating anions such as halides [Cl][−] decompose at low temperature. Ionic liquids with poor proton abstracting anions such as bis(trifluoromethylsulfonyl)amide [Tf₂N][−] are more stable to high-temperature decomposition. Types of cations also have an influence on the decomposition temperature of ionic liquids. Chellappan [7] stated that ammonium-based ionic liquids have lower stability if compared to imidazolium-based ionic liquids, whereas the thermal stability of phosphonium based ionic liquids is better than of the ammonium-based ionic liquids. Moreover, it was found that imidazolium based ionic liquids are thermally more stable than pyridinium and tetra-alkyl ammonium-based ionic liquids. Chellappan [7] referred this to the presence of methyl substitution on the C (2) of the imidazolium cation, which increases the thermal stability due to the replacement of the acidic hydrogen. Then, it was observed that the chain length of the alkyl group on the cation has low influence on the thermal stability of the ionic liquids.

I.5.9. Flammability and corrosion

A large number of ionic liquids are combustible because of their positive heats of formation, oxygen content and decomposition products. A study on the flammability of twenty ionic liquids has shown that the rate of combustion depends on the nitrogen and oxygen content. [26] Some of the ionic liquids burned for a short period of time and went out, others, after first ignition, burned quickly to complete or nearly complete combustion (Figure I.3).

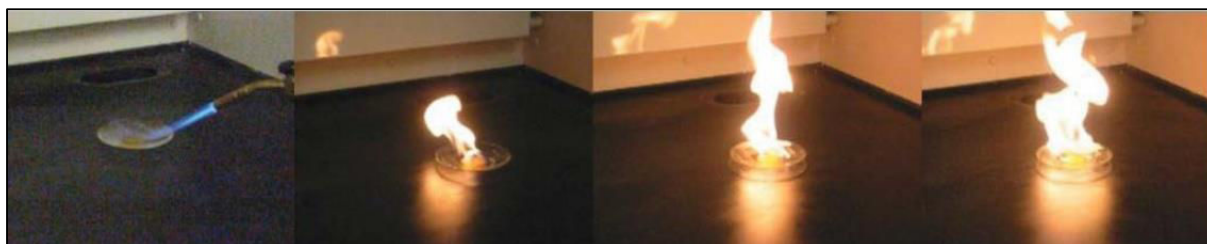


Figure I.3: Ignition test of 1 g of protonated [1-Bu-3H-IM][NO₃] [26].

In the literature, many publications describe the design of ionic liquids as energetic materials. These ionic liquids are mainly prepared by the inclusion of energetic functional groups such as NO₂, CN, N₃ [7].

The corrosivity of ionic liquids for a given metal is mainly depending on the chemical structure of the IL cation and the nature of the anion. Strong corrosion were observed with ILs containing tosylate [TOS][−] and dimethylphosphate [DMP][−] anions. Many researchers [27] referred this to presence of water which could lead to hydrolysis of many anions used in ILs and then produce acids (i.e. HF, HCl, H₂SO₄ or H₃PO₄). Furthermore, residual halide impurities from the synthesis of the ionic liquid may corrode metal vessels. Perissi *et al.* [28] investigated the corrosion behavior of several metals and metal alloys (copper, nickel, AISI 1018 steel, brass, Inconel 600) exposed to 1-butyl-3-methyl-imidazolium bis-(trifluoromethanesulfonyl) imide, ([BMIM][Tf₂N]), by electrochemical and weight-loss methods. Low corrosion current densities (0.1–1.2 μA/cm²) are observed with all the metals and alloys investigated. It was also demonstrated that the corrosion current dramatically increased show with an increase of temperature.

I.5.10. Toxicity and human health

Due to their low vapor pressure, the risk of air pollution by ionic liquids is minimal and so, they have low impact on the environment and human health. It should be noticed that an ideal green solvent should also be non-toxic and not persist in the environment. Even if ionic liquids can be used in large-scale in industrial applications, their entry to the aquatic environment through accidental spills or as effluents is the most possible pathway for their contributing to environmental hazards. Consequently, aqueous toxicology investigations are the most important topic of interest concerning ionic liquids environmental safety. However, their toxicology data have been very limited until now. Several authors [29-31] already mentioned this lack of toxicological data in the literature. The eco-toxicological studies performed to understand the effects of different ILs on enzymatic activities, cells and microorganisms mainly use LC_{50} levels (lethal concentration). Decreasing LC_{50} values indicate higher toxicities according to the toxicity classes of Hodge and Sterner scale [32]. This scale indicates that the LC_{50} value (in terms of mg/l) of 10 or less shows that the chemical is extremely toxic, LC_{50} value between 10 and 100 shows that chemical is highly toxic, LC_{50} value between 100 and 1000 shows that chemical is slightly toxic, and finally LC_{50} value between 1000 and 10,000 means that chemical is practically nontoxic.

Early studies suggested that quaternary ammonium and pyridinium ILs have significant toxic effects on a variety of bacteria and fungi [7]. Bernot *et al.* [33] studied the toxicity of imidazolium and pyridinium ionic liquids using fresh water snails. The toxicity was tested by the LC_{50} method. They observed that the alkyl chain length of the cation has a great impact on the toxicity of the ionic liquids. The ionic liquids with a longer carbon chain (C_8) were found to be more toxic than the alkyl chains with C_4 and C_6 . Maginn [34] presented the LC_{50} levels for two imidazolium-based ionic liquids with *Daphnia magna*. *Daphnia* are common fresh water crustaceans (a large group of Phylum Arthropoda). The LC_{50} values obtained for [BMIM]⁺ cations with [PF₆]⁻ and [BF₄]⁻ anions illustrated that these two ionic liquids are about as toxic to *Daphnia* as benzene and are far more toxic than acetone (Table I.3).

Mikkola *et al.* [35] investigated the toxicity of some promising amidinium, imidazolium, and phosphonium based ILs toward two different cell lines, human corneal epithelial cells and *Escherichia coli* bacterial cells. They found that the toxicity of the phosphonium ILs was highly dependent on the longest linear chain of the IL as mentioned above. They referred this to the

increasing hydrophobicity, with the long-chain phosphonium ILs which leads to toxicity. While the shorter-chain versions were significantly less toxic or not toxic at all. Amidinium and imidazolium ILs showed no significant effect on the cells, within the concentration range used.

Table I.3: LC₅₀ values for *Daphnia* for certain solvents [34].

Compound	LC ₅₀ (mg/l)
[BMIM][PF ₆]	250–300
[BMIM][BF ₄]	225–275
Acetone	30,642
Dichloromethane	310
Toluene	60–313
Benzene	203
Chlorobenzene	5–86
Phenol	5
Ammonia	0.53–4.94
Chlorine	0.028

I.6. Potential Applications of Ionic Liquids

Nowadays, ionic liquids have been investigated for a wide variety of potential applications such as organic chemistry, biorefinery, supercritical fluid, desulfurization of petroleum oil but also in solar cells, as lubricants, for heat storage, as working fluids in absorption cycles etc. Since the interest in ionic liquids has only increased after 1999, the development of ionic liquids is still mostly in the research phase. Therefore, only few processes have reached commercialization to date. [6, 7, 16]. However, there is a large field of potentially interesting applications (Figure I.4).

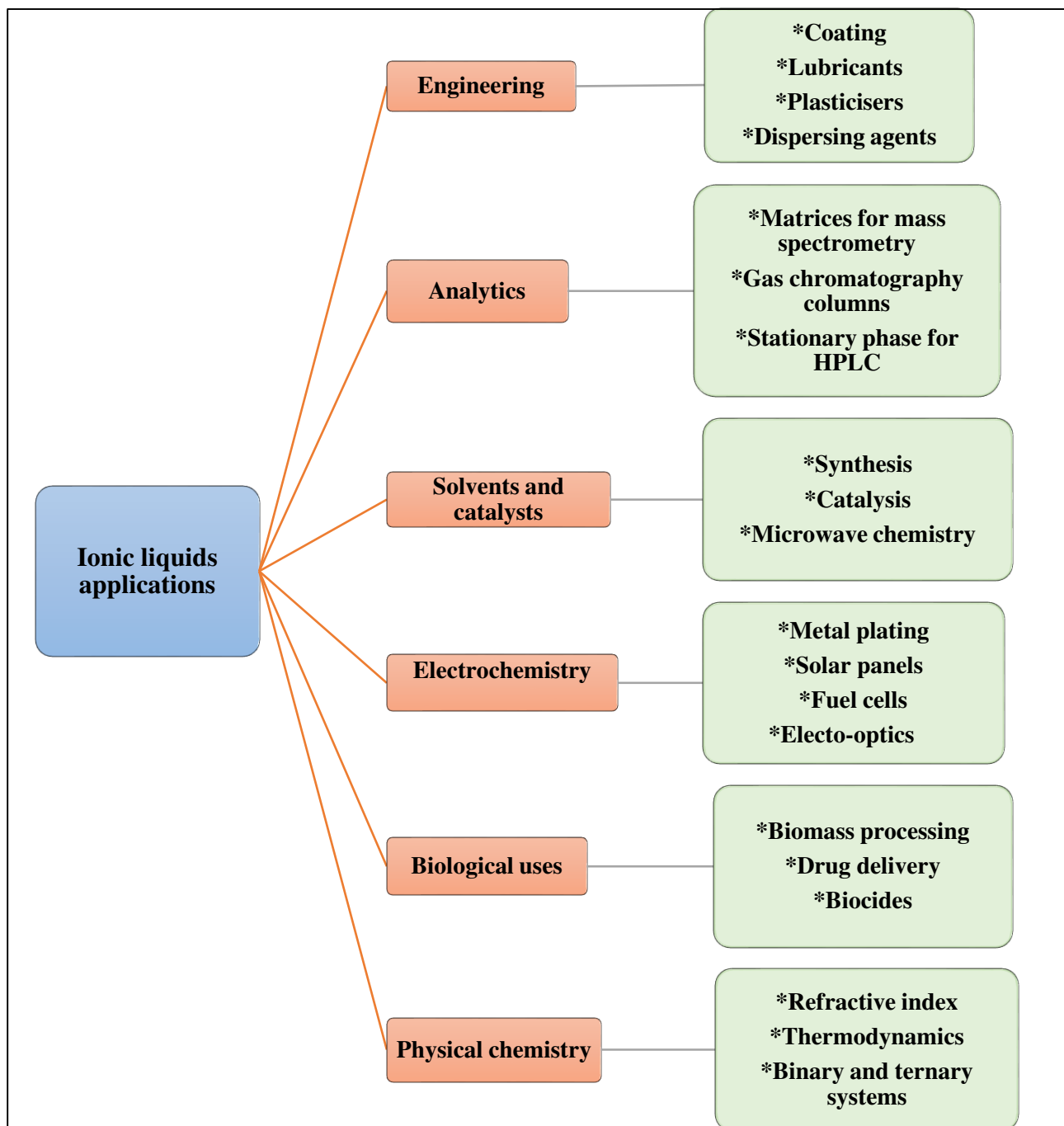


Figure I.4: Possible applications of ILs.

The BASIL™ process: The first most successful commercial application of ionic liquids recently is called the BASIL™ (Biphasic Acid Scavenging utilizing Ionic Liquids) process [6, 7]. The BASIL process is a general solution for all kinds of acid removal problems. The BASIL process is used in a plant producing diethoxyphenyl phosphine, a photo initiator intermediate prepared by the reaction of dichlorophenyl phosphine with ethanol. The reaction generates HCl as a byproduct, which must be removed to prohibit an unwanted side reaction. Originally in this process, triethylamine was used to remove the acid but a byproduct formed of a dense triethylammonium chloride, makes it difficult to handle the reaction. Thus, in order to solve this problem BASF recently, adds 1-methylimidazole, which forms ionic liquid 1-methylimidazolium chloride. Afterwards, two phases are formed which can be easily separated. The upper phase is the pure product and the lower phase is the pure ionic liquid. The ionic liquid formed can be reused after deprotonation (Figure I.5). The BASIL process uses a much smaller reactor than the initial process and the space–time yield for the formation of the product was increased from $8 \text{ kg m}^{-3}\text{h}^{-1}$ to $690,000 \text{ kg m}^{-3}\text{h}^{-1}$. The yield increased from 50 % to 98 %. The reaction is now carried out at a multi-ton scale, proving that handling large quantities of ionic liquids is practical. Its success was almost immediately recognized: the process won the ECN Innovation Award in 2004 [16].

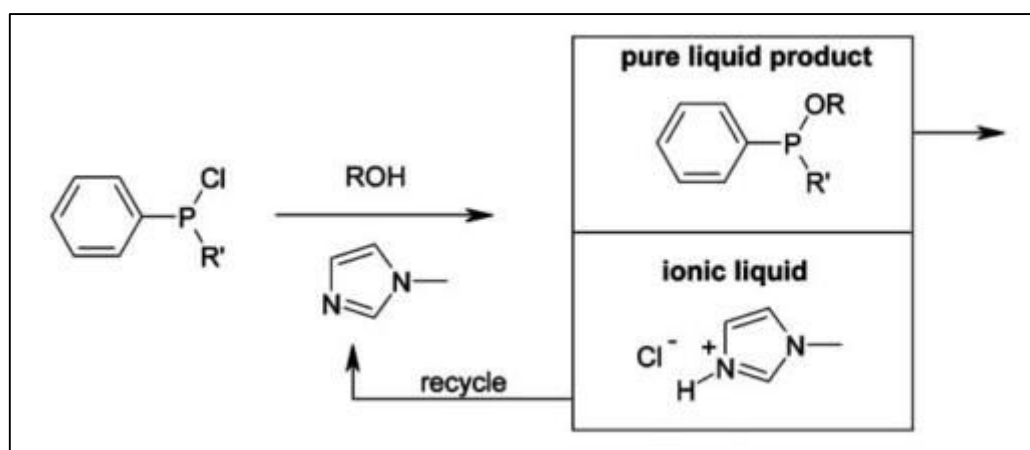


Figure I.5: The BASIL™ process [16].

Breaking azeotropes. Ionic liquids as entrainers, or separation enhancers, have been used to break common azeotropes, such as water–ethanol and water–tetrahydrofuran. The costs of separation and recycling of the entrainer are significantly reduced [16].

IFP (Institut Francais du Pétrole) Axens: IFP was the first to run an ionic liquid pilot plant described in Figure I.6. The Dimersol process, based on traditional technology, consists of the dimerisation of alkenes, typically propene (Dimersol-G) and butenes (Dimersol-X) to the more valuable branched hexenes and octenes. The longer-chain olefins produced in the dimerisation process are usually hydroformylated to alcohols (e.g. isononanols): isononanols are then converted into dialkyl phthalates, which are used as poly (vinyl chloride) plasticisers. The dimerisation reaction is catalysed by a cationic nickel complex of the general form $[\text{LNiCH}_2\text{R}_9][\text{AlCl}_4](\text{L} = \text{PR}_3)$ and is commonly operated without solvent. However, it has been found that the catalyst shows greater activity when it is dissolved in undesirable aromatic or halogenated hydrocarbons. The use of chloroaluminate (III) ionic liquids as solvents for these nickel-catalyzed dimerisation reactions has been developed and pioneered at IFP (France), especially by Nobel laureate Yves Chauvin and Helene Olivier-Bourbigou.

When the Difasol reactor, which involves the use of an ionic liquid, was added to the existing Dimersol reactor, the process became much more efficient. The process uses a biphasic mixture which results in a much better use of the catalyst, and therefore a reduced catalyst disposal cost, and a better dimer selectivity. A higher yield into dimers can be achieved in a single step, even with a low-concentration alkene feed, and from an engineering point of view, the reactor size is much smaller than in the homogeneous system. Moreover, this new process can be possibly extended to higher, less reactive olefins [16].

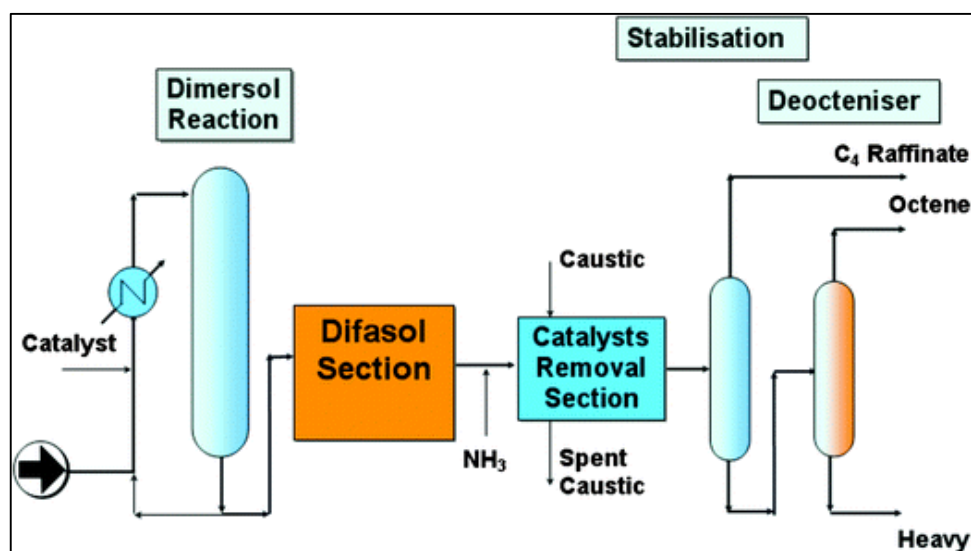


Figure I.6: Process scheme integrating Dimersol and Difasol [16].

Lithium-ion batteries: Degussa, has been investigating the use of ionic liquids in lithium batteries as alternatives for volatile and flammable mixtures of organic solvents, i.e. ethylene carbonate and dialkyl carbonates. This is a pre-commercial study, and results look promising [16].

Air products: At the first International Congress on Ionic Liquids (COIL-1) in Salzburg, Dan Tempel [16, 36] revealed a new Air Products technology which is based around entrainment by the complexing of reactive gases in ionic liquids. It produces at least twice the performance of the main rival process, which relies on the physical adsorption of gases on solids, and provides a method to deliver these reactive and hazardous gases in a safe, effective, more easily handled way, reducing both the risks and hazards in the work place – a true green chemistry success. The gases can be stored and transported at sub-atmospheric pressure instead of the normal pressurized cylinders, adding dramatically to safety.

IoLiTec: (Ionic Liquids Technologies) is an interesting new company specializing in marketing ionic liquids. They have developed a practical and efficient technology to clean high value and sensitive surfaces, using ionic liquids as antistatic cleaning agents. Conventionally, dilute aqueous sodium chloride solutions have been used as the wetting agent, but the effect of replacing this with an ionic liquid is dramatically demonstrated in Figure I.7. IoLiTec has also interests in the application of ionic liquids in medicine (coated implants), food analytics, sensors, and heat pumps, and is currently involved in the development of various green applications based on ionic liquids, e.g. electrolytes for dye-sensitized solar cells (Gratzel cells or DSSCs) and phase change materials (PCMs) for the storage of solar energy and for sorption cooling media for “solar cooling”. Pilot installations for both DSSC and PCM applications are currently being constructed [16].

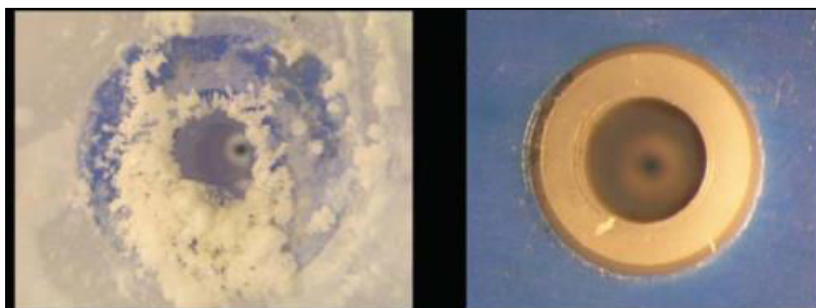


Figure I.7: A spray nozzle for aqueous solutions of sodium chloride (left) and a hydrophilic ionic liquid (right), each after 10 h of operation (©IoLiTec 2007) [16].

Table I.4: Overview of industrial applications of ILs (Commercial/pilot plants) [6, 7].

Company	Process	Ionic liquids used	Scale
Air products	Storage of gases (Phosphine (PH ₃), arsine (AsH ₃) and boron trifluoride (BF ₃)) Gas compression	Liquid support ([BMIM][Cu ₂ Cl ₃] for PH ₃ and [BMIM][BF ₄] for BF ₃)	Pilot
Arkema	Fluorination	Solvent	Pilot
BASF	BASIL TM (Biphasic Acid Scavenging utilizing Ionic Liquids)	Auxiliary	Commercial
BASF	Chlorination	Solvent	Commercial
BASF	Extractive distillation (breaking water-ethanol and water-tetrahydrofuran azeotropes)	Extractant	Pilot
BP	Aromatic alkylation	Catalyst (Chloroaluminate ILs)	Confidential
BP	Ethylbenzene production	Catalyst ([C _n MIM][Cl-AlCl ₃] (n=2,4 or 8))	Confidential
Central Glass Company	Sonogashira coupling reaction (to produce pharmaceutical intermediates)	Catalyst ([P ₄₄₄ 16][Br] / tetraalkylphosphonium cation based ILs)	Commercial
Chevron Phillips	Olefin oligomerization	Catalyst	Pilot
Degussa	Hydrosilylation	Solvent	Pilot
Degussa	Compatibilizer	Performance additive	Commercial
Eastman Chemical	Production of 2,5-dihydrofuran	Catalyst [P ₈₈₈ 18][I]	Commercial until 2004
Eli Lilly	Cleavage of ethers	Catalyst/reagent [Pyr][HCl]	Pilot
IFP (Axens)	Olefin dimerization (Dimersol process)	Solvent (Chloroaluminate (III) ILs)	Pilot
Iolitec	Cleaning fluid	Performance additive	Commercial
Linde	Gas compression	Liquid piston	Pilot
PetroChina	Alkylation	Catalyst (Aluminium(III) chloride based ILs)	Pilot
SASOL	Metathesis and Olefin trimerisation	Solvent ([C _n DMIM][NTf ₂])	Pilot
Scionix	Electroplating (Cr)	Electrolyte (Choline-chromium(III) derived ILs)	Pilot
University of Twente	Extraction	Extractant	Pilot

Absorption Heat Transformer: Numerous articles [1, 37, 38] published in the literature demonstrated that working fluids containing ILs may be used in Absorption Heat Transformer. It was found that the performance of some binary systems is close to the classical working fluids used in the industry.

I.7. General information about Absorption cycles

Most of industrial activities use a lot of thermal energy by burning fossil fuel to produce steam or heat. After being used and degraded, heat is rejected to the surrounding as low grade waste heat. Huge quantities of low temperature waste heat are released from many industrial plants to the atmosphere at temperatures ranging from 60 to 100 °C on daily basis [39]. Amongst heat driven devices are the absorption cycles which include absorption heat pump (AHP), absorption chiller (AC), and absorption heat transformer (AHT). Absorption heat cycles become of great interest since electrical energy is replaced with low grade or waste heat resulting in decreasing the consumption of primary energy and increasing the energy efficiency [37]. Moreover, absorption cycles preserve the atmospheric conditions by reducing the emissions of carbon dioxide and the implementation of environmentally friendly working pair will reduce the negative impact on the environment [39].

Absorption cycle early development dates back to the 1700's. In 1810, ice was made from water in a vessel, which was connected to another vessel containing sulfuric acid. As the acid absorbed water vapor, causing a decrease of temperature, layers of ice were formed on the water surface. The main problems of this system were corrosion and leakage of air into the vacuum vessel. A real breakthrough was achieved in 1859 by Ferdinand Carre [40, 41] who introduced a novel apparatus using {H₂O + ammonia} as working fluids, which took out a US, patent in 1860. In 1852, Lord Kelvin [42] published a paper about absorption cycle (heat pump). He illustrated that a heat pump could be used for heating and cooling. In spite of Kelvin's early work, the use of heat pumps for heating water or air was not seriously examined until the 1920s and 30s. In 1922, Morley renovated Kelvin's work [42, 43].

One of the key points of the performance of an absorption cycle is the working fluid used. Nowadays, the most used binary systems in absorption heat cycle are {water + lithium bromide (H₂O + LiBr)} and {ammonium + water (NH₃+H₂O)}. The commercial applications of the {H₂O + LiBr} absorption cycle have obtained great success and widely spread all over the world [42-45]. Nevertheless, LiBr aqueous solution has some main drawbacks:

- Absorption heat pumps (AHP) cannot operate at an evaporation temperature below 0 °C because of the use of water as refrigerant, which make it unusable for subfreezing refrigeration or heating/domestic hot water (DHW) supplementation in cold regions.
- Crystallization of {H₂O + LiBr} at high concentrations is a common problem.

- High vacuum conditions should be preserved in the system for proper operation of the $\{\text{H}_2\text{O} + \text{LiBr}\}$ system; otherwise, the performance of the absorption cycle would be greatly degraded [43].
- $\{\text{H}_2\text{O} + \text{LiBr}\}$ is corrosive to metals [1, 37].

The working fluid $\{\text{NH}_3 + \text{H}_2\text{O}\}$ requires high working pressure and ammonia is toxic. Owing to these disadvantages which have not been solved properly, the development and application of $\{\text{H}_2\text{O} + \text{LiBr}\}$ absorption cycles were limited for a long time [1, 37, 46]. Therefore, heat pump and absorption chiller technologies suffer from lack of suitable working pairs. Hence, searching for new beneficial and reliable binary systems with excellent thermal stability, no corrosion, no crystallization and environmentally friendly has become of great importance in recent years.

Limited numbers of critical reviews have been published in the literature on the subject of absorption technologies. In 2001, Srihirin *et al.* [43] reviewed various types of absorption refrigeration cycles and working fluids. Performance improvement and enhancement of absorption cycles were discussed. They concluded that double-effect absorption systems using $\{\text{H}_2\text{O} + \text{LiBr}\}$ seem to be the only high performance system available commercially. Multi-effect cycles show considerable promise for further application. A combined ejector-absorption system is another possible option. This system can provide coefficient of performance (COP) as high as a double-effect system with little increase in system complexity. A diffusion absorption refrigeration system is the only true heat-operated refrigeration cycle. This system has been widely used as a domestic refrigerator. However, it is only available with small cooling capacity and its COP is low (0.1 to 0.2).

In 2012, Sun *et al.* [38] have shown that $\{\text{H}_2\text{O} + \text{LiBr}\}$ and $\{\text{NH}_3 + \text{H}_2\text{O}\}$ mixtures with different additives would play a much more important role for absorption cycles. However, working fluids containing HFCs are more promising when absorption cycles will be employed in special cases such as solar energy, ground heat and low grade heat in industrials.

ILs could be used as alternatives for most used toxic working fluids such as $\{\text{NH}_3 + \text{water}\}$ in absorption cycles. Meanwhile, the ionic liquids have melting points below the lowest solution temperature in the absorption system. They also remove the crystallization and metal-compatibility problems of $\{\text{water} + \text{LiBr}\}$ system [38]. Since many of ILs are highly hygroscopic and miscible with water, this enhances analysis of binary systems composed of $\{\text{ILs} + \text{water}\}$ for this application [47, 48].

Few ionic liquids have been investigated as potential absorbent for AHP. The different working fluids containing ILs are divided into five series according to the nature of the refrigerant: NH_3 series, H_2O series, alcohol series, halogenated hydrocarbon series and other refrigerants. Although many working fluids are proposed in the literature, there is not a complete review with comparison of their properties and performances. Researchers focused on evaluating $\{\text{H}_2\text{O} + \text{IL}\}$ systems for their potential use in absorption heat cycles.

The review of Khamooshi *et al.* 2013 [37] is focused on the performance of working pairs containing ionic liquids in absorption cycles. The authors compared different working fluids containing IL and different types of refrigerants in order to define the most suitable binary system. The simulation of binary systems composed of $\{\text{H}_2\text{O} + \text{ILs}\}$ for absorption cooling cycle shows their COP value is lower than $\{\text{H}_2\text{O} + \text{LiBr}\}$ by 7% but still higher than 0.7.

In 2014, Zheng *et al.* [47] present a compilation of thermodynamic properties of binary systems containing $\{\text{NH}_3$ or HFCs or alcohols + ILs $\}$. The simulation of IL working fluids for single effect absorption cooling cycles shows that several binary systems have a real potential.

The researches on the development of working fluids and absorption cycles literature have mainly focused on air conditioning and refrigeration. No previous review has comprehensively summarized the studies and applications of absorption heat transformers using $\{\text{H}_2\text{O} + \text{ILs}\}$ as working fluid.

This work is mainly focused on the study of binary systems $\{\text{H}_2\text{O} + \text{ILs}\}$ in absorption heat transformers (AHT). The first part of the work shortly describes the absorption cycle. Then, the thermodynamic and physical properties of the binary systems $\{\text{H}_2\text{O} + \text{IL}\}$ such as vapor pressure, heat capacity, excess enthalpy, density, viscosity and thermal decomposition will be summarized. In this section, the performance of the working fluids $\{\text{H}_2\text{O} + \text{IL}\}$ in absorption heat cycle found in literature are also presented.

I.8. Classification of Absorption cycles

Absorption cycles exchange heat with three external reservoirs at low, intermediate, and high temperature levels as shown in Figure I.8. When an absorption system is operated as a refrigerator or a heat pump, the driving heat is supplied from the high temperature reservoir. Refrigeration effect is produced at a low temperature level and heat is rejected at an intermediate temperature level. For a refrigerator, the useful heat transfer is at a low

temperature. For the heat pump, the useful heat transfer is at an intermediate temperature. Normally, the surroundings are used as a low temperature reservoir for a heat pump or as an intermediate temperature reservoir for the refrigerator.

Another type of absorption cycle is known as “an absorption heat transformer”. This system is driven by heat from an intermediate temperature reservoir and rejects heat out at a low temperature level (normally to the surroundings). The useful output is obtained at the highest temperature level.

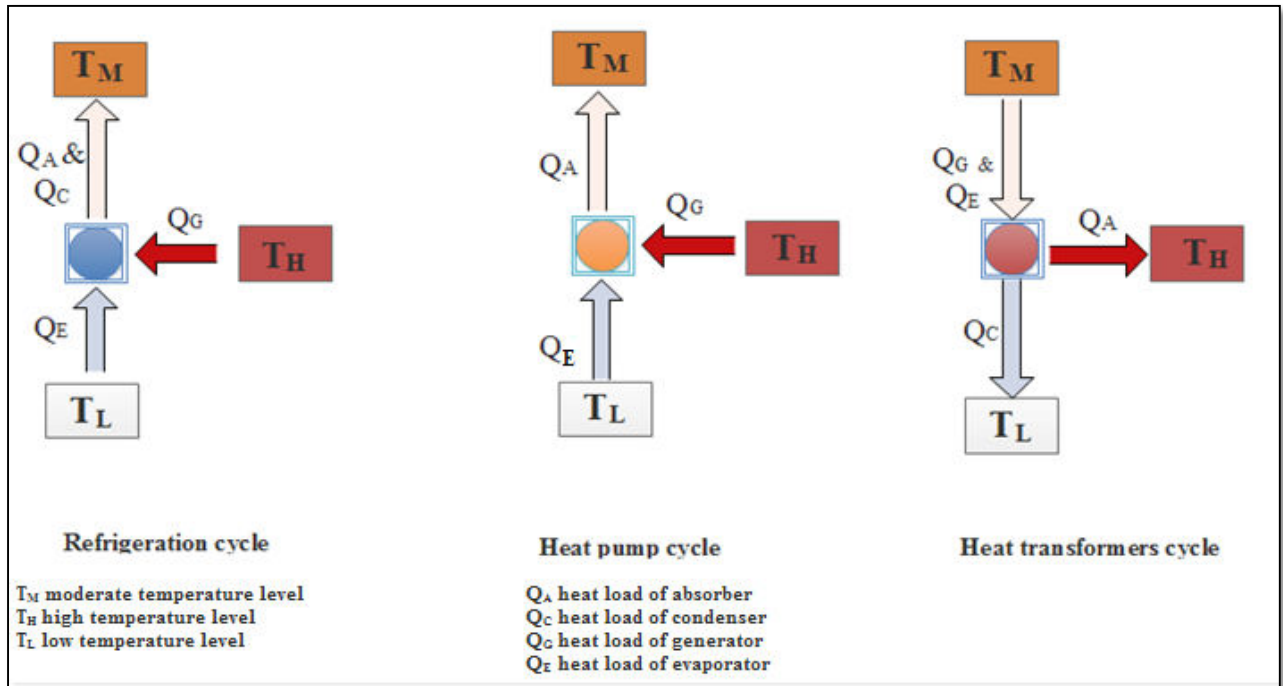


Figure I.8: Absorption cycles.

The absorption cycles have five main components evaporator, condenser, generator, absorber and solution heat exchanger (economizer). Figure I.9 shows a schematic diagram of the cycle. The basic principle of an absorption cycle is when high pressure liquid refrigerant from the condenser entering the evaporator through an expansion valve which reduces the pressure of the refrigerant to the low pressure level of the evaporator. The liquid refrigerant vaporizes in the evaporator by absorbing heat from the reservoir needing to be cooled and the resulting low-pressure vapor is circulated to the absorber, where the vapor is absorbed by the solution coming from the generator (strong solution). The resulting low concentration solution (weak solution) is pumped to the generator, where the refrigerant is boiled off. The strong solution flows back to the absorber and, thus, completes the cycle [49].

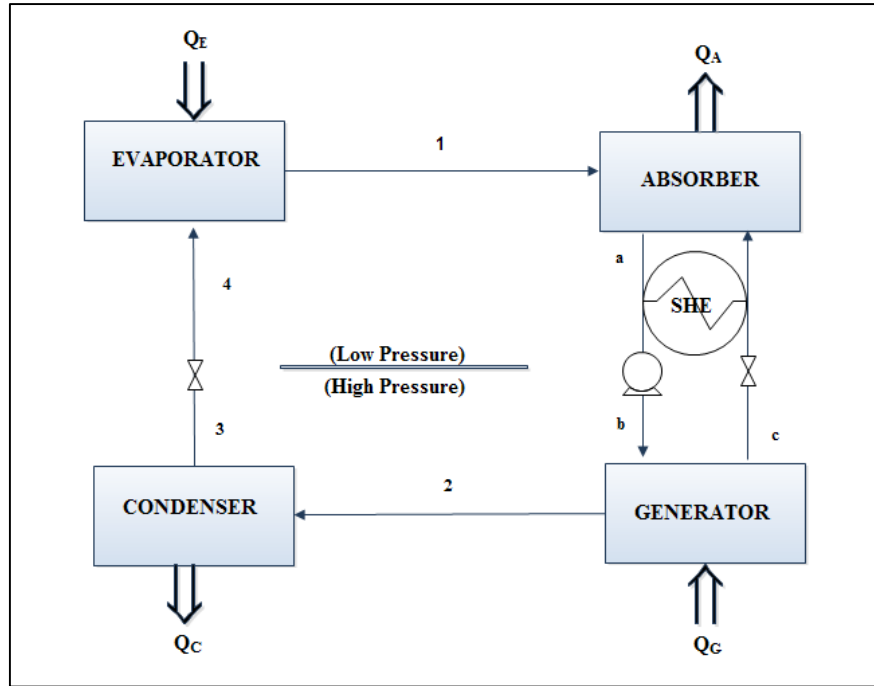


Figure I.9: Schematic diagram of an absorption refrigeration cycle; A-absorber, C-condenser, E-evaporator, G-generator, SHE-heat exchanger.

The performance of an absorption cycle mainly depends on the thermodynamic properties of the binary system used. The most important requirements of these binary systems are [38]:

1. Binary system should have large boiling-temperature elevation and/or vapor pressure depression than the pure refrigerant at the same pressure.
2. Refrigerant should have high latent heat and high concentration within the absorbent in order to have low circulation ratio between the generator and the absorber.
3. Transport properties that affect heat and mass transfer such as viscosity, thermal conductivity, and diffusion coefficient, should be the lowest as possible.
4. Additionally, both refrigerant and absorbent should be non-corrosive and have low cost. Furthermore, working fluids should be environmentally friendly, have low global warming potential (GWP) and zero ozone depletion potential (ODP).

The coefficient of performance (COP) describing the efficiency of the cycle is a measure of a cycle's capability to transfer heat between different temperature levels [39]. The COP can be defined according to the type of the Absorption cycle. Thus, COP for the absorption refrigeration cycle is defined as the cooling capacity (Q_E) divided by the energy input (Q_G) [49]:

$$\text{COP} = \frac{\text{cooling capacity obtained at evaporator (QE)}}{\text{heat input for the generator (QG) + work input for the pump (W)}} \quad (\text{I.1})$$

I.8.1. Absorption refrigerators (Chillers) (AC)

Any absorption refrigeration cycle exchanges heat with three external reservoirs: low, intermediate, and high temperature levels (Figure I.8). The driving heat is supplied from high temperature reservoir, while refrigeration effect is produced at a low temperature level and rejects heat out at an intermediate temperature level. As mentioned above, absorber, generator, condenser and evaporator are the main components of the absorption refrigeration cycle. The majority of studies on absorption technologies have focused on cooling and refrigeration cycle.

I.8.2. Absorption heat pumps (AHP)

Recently, absorption heat pump (AHP) has attracted considerable attention due to its ability to use sustainable energy systems giving a high primary energy efficiency and low environmental impact [42]. The driving heat source for AHP is various, such as hydrocarbon fuels, solar energy, geothermal energy, district heating network or waste heat. Heated by the high-grade driving source supplied to the generator the AHP can extract low-grade heat in the evaporator side from low temperature sources, such as the ambient air, underground soil, surface water or waste heat. Then, medium temperature hot water is produced in the condenser and absorber. Because the heat supplied to the generator and evaporator is converted into the supplied hot water, the heat quantity is increased [49].

The operating sequence of the basic AHP is explained as follows: refrigerant vapor is produced in the evaporator which is heated by a low-medium grade heat source. The refrigerant vapor is absorbed in the strong solution that enters the absorber and the resulting weak solution returns back to generator. In the generator some refrigerant vapor is separated from the weak solution to be sent to the condenser and therefore the strong solution from the generator is returned back to the absorber. The vaporized refrigerant is condensed in the condenser then it is pumped to a higher pressure level as it enters the evaporator. The waste heat given to the evaporator causes its vaporization. Once again, the absorber absorbs the refrigerant vapor at a higher temperature.

Hence, the absorption heat pump has the ability of raising the temperature of the solution above the temperature of the waste heat source [37, 39].

I.8.3. Absorption heat transformers (AHT)

A different category of absorption cycle is known as “absorption heat transformer” or “reverse absorption heat pump”. AHT operates in a cycle that is the reverse of the AHP. The basic AHT, shown schematically in Figure I.10, has similar components as a single-effect absorption cycle. The difference is the inversion of pressure levels between generator/condenser and evaporator/absorber. AHT also uses heat from an intermediate temperature reservoir as the driving heat (generally an industrial waste heat) (Figure I.8). The system rejects heat out at a low temperature level (normally to the surroundings). The useful output is obtained at the highest temperature level. The use of AHTs allow any waste heat to be upgraded to a higher temperature level without any other heat input except some work required to circulation pumps.

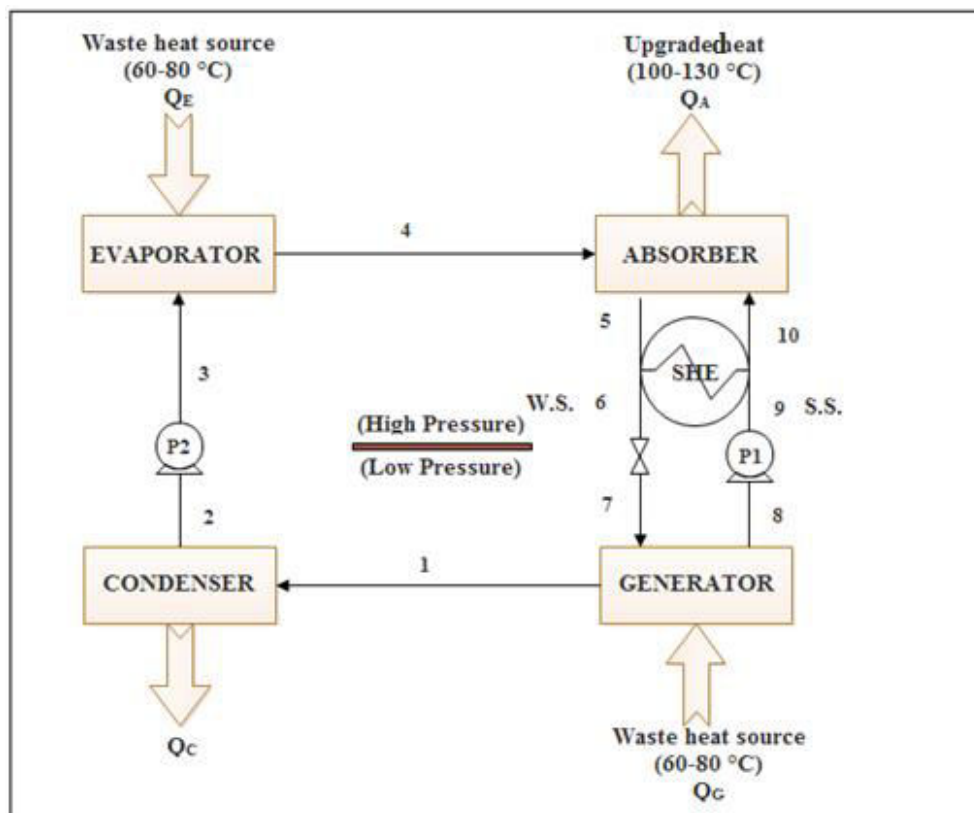


Figure I.10: Schematic diagram of an absorption heat transformer; A-absorber, C-condenser, E-evaporator, G-generator, SHE-heat exchanger, P1, P2-pump, v-valve.

The generator is supplied with a relatively moderate temperature waste heat for refrigerant separation as the usual method. Liquid refrigerant from the condenser is then pumped to the evaporator operating at a higher pressure. In the evaporator, it is vaporized by using the same moderate temperature waste heat used to drive the generator (absorption heat transformers are usually operated so that the generator and evaporator temperatures are equal). The refrigerant vapor is then absorbed into solution in the absorber, which rejects the useful heat out at a high temperature level. The low-grade heat as solar energy [50] or industrial waste heat [51, 52, 53] can be upgraded using AHT. Performance of an AHT with various working fluids such as {water + LiBr} and {TFE + E181} were studied [1].

COP definition for absorption heat transformers is defined as the ratio of available heat output of the absorber (Q_A) to the total heat inputs of the system heat input of the generator (Q_G) and evaporator (Q_E).

$$COP = \frac{Q_A}{Q_G + Q_E} \quad (I.2)$$

This point will be discussed later herein.

I.9. Working fluids containing {water + ILs} for absorption cycles

Water can be considered as a green refrigerant, nontoxic, having high latent heat and excellent thermal characteristics. If {H₂O + ILs} are selected as the working fluids, the ILs selected should be very hygroscopic and water stable.

It is well established that many ILs are completely miscible with water, especially imidazolium-based ILs. Nevertheless, there is still a lack of thermodynamic data for IL and water systems.

I.9.1. {H₂O + Ionic liquids} binary systems in literature

Recently, many research groups have investigated {H₂O + IL} as alternatives binary systems in absorption cycle [49]. Numerous articles present thermodynamic studies of binary systems containing water and IL. Annex I lists the most studied ILs in the literature and the thermo

physical properties available. Alkylsulfate and alkylphosphaste based ILs are well known and their performance as working fluids $\{H_2O + IL\}$ were evaluated in different absorption cycle [46, 49, 54- 57].

Among others, the binary systems $\{H_2O + [DMIM][DMP]\}$ [46] was extensively studied by different research groups. Kato and Gmehling [58] have measured the vapor-liquid equilibria (VLE) of the $\{H_2O + [DMIM][DMP]\}$ system with a computer-driven static apparatus. He *et al.* [57] measured the thermodynamic properties including VLE, density, viscosity, heat capacity and excess enthalpy of this system. Wang *et al.* [59] measured VLE for the same binary system using a quasi-static ebulliometric method, while Dong *et al.* [46] simulated the performance of absorption refrigeration cycle based on the measured data of VLE and heat capacity of the same binary mixture. The simulation results show that the cycle performance of $\{H_2O + [DMIM][DMP]\}$ is close to that of conventional working pair $\{H_2O + LiBr\}$. Nevertheless, using the $\{H_2O + [DMIM][DMP]\}$ system increases the operating temperature range and stops crystallization and corrosion caused by $\{H_2O + LiBr\}$.

Zhang and Hu [55]; Gong *et al.* [60]; Ren *et al.* [54]; and Wang *et al.* [61] have studied the binary system $\{H_2O + 1\text{-Ethyl-3-methylimidazolium dimethyl phosphate } [EMIM][DMP]\}$ using different techniques. Zhang and Hu [55] simulated the performance of the working pairs $\{H_2O + [EMIM][DMP]\}$ in an absorption refrigeration cycle. The results of the simulation show that the coefficient of performance (COP) of $\{H_2O + [EMIM][DMP]\}$ is lower than $\{H_2O + LiBr\}$ but still higher than 0.7, while the generation temperature was lower than that for $\{H_2O + LiBr\}$. Ren and his coworkers [54] stated that the binary system $\{H_2O + [EMIM][DMP]\}$ can meet the basic requirements for working pairs and has potential to be new working pair for absorption heat pump or absorption refrigeration.

The binary system $\{H_2O + [EMIM][EtSO_4]\}$ was proposed by Ficke [49] and Zuo *et al.* [56] as a working fluid in (AHP). They determined the basic thermodynamic properties such as VLE, heat capacity and density of the binary system in a large range of temperature and concentration. Their results indicate that this binary system can be considered as a potential working fluid in AHP. Yokozeki and Shiflet [62] also examined the feasibility of this system in an absorption cooling cycle and they found out that this system shows a promising result. Romich *et al.* [63] measured the vapor liquid equilibrium, density, heat capacity and viscosity of $\{H_2O + 1\text{-ethyl-3-methylimidazolium acetate } [EMIM][Ac]\}$. The viscosity of this system was also measured by Fendt *et al.* [64]. Nie *et al.* [65] studied the binary system $\{H_2O + 1\text{-(2-}$

hydroxyethyl)-3-methylimidazolium chloride [HOEtMIM][Cl]} as a replaceable working pair for AHP cycle. The VLE of the system show strong negative deviation from the Raoult's law which is a basic characteristic for the absorption working pairs. They found that density and heat capacity data of the investigated system are quite low, which are beneficial to decrease power consumption and improve the COP of the absorption heat pump cycle.

I.10. Thermodynamic properties of {H₂O + IL}

The knowledge of thermodynamic properties, phase behavior, and safety/environmental hazards of {H₂O + IL} is required for the evaluation of this system in an AHT. The following section presents the behavior of ILs in presence of water and the influence of their structure on thermodynamic properties.

I.10.1. Thermodynamic model for the representation of binary system {H₂O + IL}

Owing to the large number of possible combinations of binary mixtures {H₂O + IL}, the experimental evaluation of all of these systems is an important effort. Hence, several research groups started to present modeling results characterizing the VLE of several {water + IL} systems. A large number of thermodynamic models have been used to modelize the VLE properties of binary solutions, such as NRTL equation, UNIQUAC equation and UNIFAC equation, among others. Some groups show that NRTL model can be successfully used to represent thermodynamic properties of systems containing ILs [57]. Zhao *et al.* [66] correlated the vapor pressure data of the binary system {water + [DMIM] [DMP]} by the non-electrolyte NRTL equation. The calculated values are significantly consistent with the experimental data. They found that the experimental activity coefficients are well correlated by the NRTL model and the average relative deviations of the activity coefficients is lower than 2 %. For the work of Dong [46] and his research group whom analyzed the same binary system {water + [DMIM] [DMP]} their results were consistent with the data reported by Zhao *et al.* [66] and Wang *et al.* [61], but have deviation with the data reported by He *et al.* [57]. Their vapor pressure data have been well correlated using the NRTL model, the average relative deviations for the vapor pressure between experimental and calculated values are 1.44%. Zhang and Hu [55] used the same approach for correlating VLE data of the binary mixture containing {H₂O +

[EMIM][DMP]}. Ren *et al.* [54] represent the VLE of $\{\text{H}_2\text{O} + [\text{EMIM}][\text{DMP}]\}$ using NRTL model with the average relative deviation of 2% and show that this system can be predicted by traditional non-electrolyte solution model. VLE of binary systems $\{\text{H}_2\text{O} + [\text{EMIM}][\text{Ac}]\}$ and $\{\text{H}_2\text{O} + [\text{DEMA}][\text{OMs}]\}$ were correlated by Romich *et al.* [63] using activity coefficient models. They correlated VLE data using NRTL model which showed consistency.

Alevizou *et al.* [67] also used the UNIFAC model to describe the phase equilibria of solvent/ionic liquid systems. While the ionic liquids were based on an imidazolium cation and a hexafluorophosphate anion, water was regarded as refrigerant. Two new main groups, the imidazolium and the hexafluorophosphate groups, were introduced in UNIFAC.

Passos *et al.* [68] evaluate the PC-SAFT equation of state for the description of the pure-IL density, water activity coefficients at 298.15 K, and the VLE the binary mixtures $\{\text{water} + \text{IL}\}$. The PC-SAFT pure-component parameters and the independent temperature binary interaction parameter were determined by a simultaneous fitting to the pure-IL densities, vapor-liquid equilibria data and water activity coefficients. It was found that PC-SAFT equation allowed for quantitative modeling the thermodynamic properties of $\{\text{water} + \text{IL}\}$ systems. Moreover, PC-SAFT is capable to satisfactorily predict water activity coefficients at infinite dilution for systems where model parameters were adjusted to water activity coefficients at low IL molalities. Chen *et al.* [69] measured the experimental VLE data of two binary mixtures $\{\text{H}_2\text{O} + [\text{EMIM}][\text{SCN}]\}$ and $\{\text{H}_2\text{O} + [\text{DMIM}][\text{MPh}]\}$ at temperatures ranging from 283.15 to 298.15 K and the authors show that the PC-SAFT EOS were able to correlate with good accuracy these data. Nann *et al.* [70] studied the ternary systems $\{1\text{-butanol} + \text{water} + \text{IL}\}$. In this work, the binary interaction parameters were determined by fitting to the binary LLE data in $\{1\text{-butanol} + \text{water}\}$ and $\{\text{water} + \text{IL}\}$ mixtures. Without the introduction of any additional parameters or the refitting of the existing PC-SAFT parameter sets, the LLE data of the ternary systems and the 1-butanol distribution coefficients and selectivities over water were predicted in very good agreement with the experimental data. This confirms the ability of PC-SAFT to model the extraction behavior of IL systems based on limited experimental data for pure components and binary systems. Llovel *et al.* [71] have shown that the soft-SAFT can be used to predict with good accuracy the vapor-liquid equilibrium of water with dialkylimidazolium bis(trifluoromethylsulfonyl) imide. Concerning liquid-liquid equilibria calculations, the prediction without using binary parameters gives only qualitative agreement. Two adjustable binary parameters are necessary to quantitatively reproduce this equilibrium.

Cubic equations of state such as Peng-Robinson (PR), Soave-Redlich-Kwong are used mainly to predict systems containing ionic liquids and gases (CO_2 , NH_3 , H_2S). Yokozeki and Shiflett [62] apply a modified Redlich-Kwong equation of state to predict the water solubility in various ionic liquids ([BMIM][BF_4], [EMIM][BF_4], [DMIM][DMP], [EMIM][DMP], [EEIM][DEP], [EMIM][DEP], [BMIM][DBP], [EMIM][EtSO_4], [Choline][Gly], [Choline][Lac], [Choline][MeSO_3], [BMIM][I], and [EMIM][TF_2N]. Results indicate that this (EOS) can correlate the VLE data successfully. Excess functions (Gibbs, enthalpy, and entropy) calculated using the EOS are negative indicating that there exist some chemical complex formation between water and IL molecules.

Shariati and Peters [72] have shown that PR EOS is capable to satisfactorily describe the experimental bubble point data of the system {fluoroform + IL} and to qualitatively predict the solubility of the ionic liquid in supercritical CHF_3 . Carvalho *et al.* [73-75] propose to use a thermodynamic model based on the Peng–Robinson EOS with the Wong–Sandler/UNIQUAC mixing rule. This approach was used with success in the correlation of the CO_2 solubility in ILs. The model provides a good description of the experimental data and the estimation of the Henry's constants for these systems. Ren and Scurto [76] have measured the phase equilibria of 1, 1, 1, 2-tetrafluoroethane (R134a) with dialkylimidazolium based ILs. These systems are Type V according to the classification scheme of Scott and van Konynenburg. In this case, regions of multiphase equilibria exist at the higher temperatures (VLE, LLE and VLLE). The authors propose to correlate experimental data with the Peng–Robinson equation of state. The bubble-point data demonstrates excellent agreement with the model. However, the predicted compositions of the VLLE transition to LLE are only satisfactorily predicted for all systems using the interaction parameters regressed from the VLE data alone. The mixture critical point pressure systematically under-predicted, however, close to the experimental value.

I.10.2. Experimental thermodynamic data of { H_2O + IL}

I.10.2.1. Vapor liquid equilibrium (VLE)

The experimental techniques used for VLE measurements are boiling point technique [46, 56, 57], static apparatus [58] or quasi static ebulliometer method [59]. In the case of binary mixtures

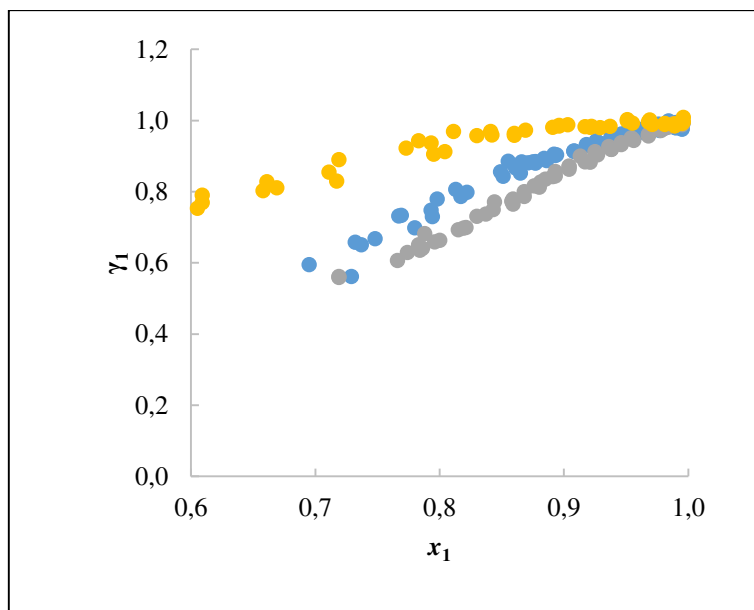
containing IL, the most widely used technique is the boiling point. Most of the articles related to VLE measurements concerning the binary systems $\{H_2O + IL\}$ are listed in Annex I.

Activity coefficient can be calculated from VLE data. This parameter illustrating the deviation from ideality of the mixture can be used to investigate the interaction between H_2O and ILs.

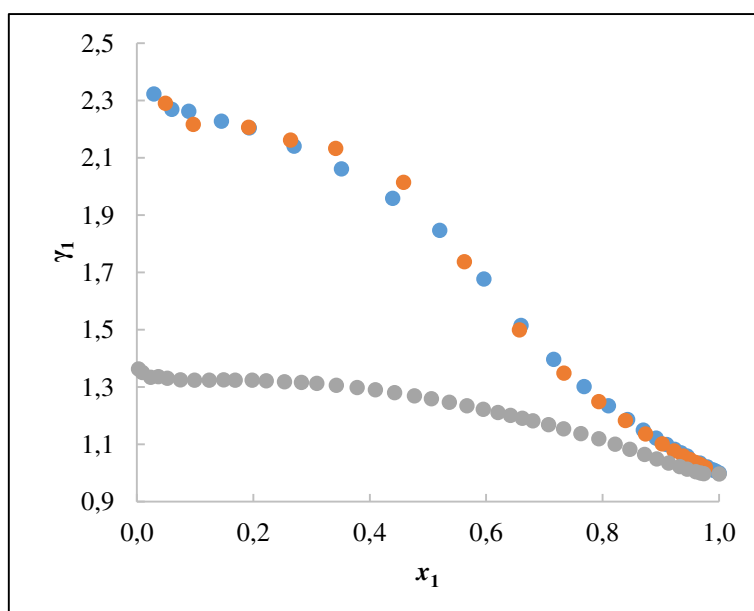
Ficke [49] and Passos *et al.* [68] stated that the activity coefficient may be also related to the hydrophilicity of the IL. Most of the ILs studied for absorption cycle are considered hydrophilic since they are completely water-soluble but their hydrophilicity is not the same.

Morrissey and O'Donnell [77] have shown that working pairs with highly negative deviation from Raoult's law produce the best results. The solvent vapor pressure decreases because the solvent molecules in the liquid phase have strong affinity to the solute molecules. Negative deviation to the ideal behavior (leading to activity coefficient values lower than unity) results from the stronger IL–water interactions than the water–water. These stronger interaction forces keep water molecules in the liquid phase, and higher potential is required to transfer water molecules into the vapor phase. Therefore, the water boiling temperature will increase as observed in the VLE experimental data. Moreover, this effect is stronger for the ILs with higher interactions with water (higher hydrogen-bond basicity). Lungwitz *et al.* [78] have found a relationship between IL's ability to increase the water boiling temperature and their hydrogen-bond basicity values determined by solvatochromic probes. ILs with higher hydrogen-bond basicity values interact strongly with water and stronger IL-water interactions prevent the evaporation of water molecules leading to higher boiling-point elevations and vapor-pressure depressions.

It is noted that the activity coefficients of most of the investigated binary systems $\{water + ILs\}$ are lower than unity (Figure I.11 (a)), exhibiting a negative deviation from the ideal solution behavior. The higher IL content is, the larger the deviation from the Raoult's law, which is indicated by the decreasing activity coefficients of solvent [57]. Ficke [49] stated that with respect to the anion, the activity coefficients decrease as follows: $[(CF_3SO_2)_2N]^- > [BF_4]^- > [EtSO_4]^- > [lactate]^- > [CH_3SO_4]^- > [glycolate]^- > [(CH_3)_2PO_4]^-$.



(a)



(b)

Figure I.11: Water activity coefficients, γ^w , as function of the water mole fraction in binary solutions of {water (1) + IL (2)}: (a) ● [BMIM][Br], ● [BMIM][C1SO₃], ● [BMIM][SCN]; (b) ● [EMIM][(CF₃SO₂)₂N], ● [BMIM][(CF₃SO₂)₂N], ● [EMIM][BF₄].

On the other hand, Kato and Gmehling [58] observed the presence of miscibility gap with $\{H_2O + [EMIM][(CF_3SO_2)_2N]\}$ and $\{H_2O + [BMIM][(CF_3SO_2)_2N]\}$. Thus, these two ionic liquids exhibit positive deviation from Raoult's law and activity coefficient higher than unity (Figure I.11 (b)).

The investigation of water sorption by ILs shows that ILs with shorter alkyl chain length on the imidazolium ring have the higher water sorption capacity, e.g., imidazolium-based ILs with anions $[Cl]^-$, $[BF_4]^-$, $[Br]^-$, $[Tf_2N]^-$, $[PF_6]^-$. Cao *et al.* [79] also compared ILs with different cations such as $[BMIM][Ac]$, $[BPy][Ac]$, $[BMIM][BF_4]$, $[BPy][BF_4]$, $[BMIM][PF_6]$, $[BPy][PF_6]$, $[BMIM][Br]$, $[BPy][Br]$, and $[P_{66614}][Br]$, and they found that ILs with an imidazolium cation $[BMIM]^+$ can absorb more water than those with a pyridinium cation $[BPy]^+$. Cao *et al.* [79] referred this behavior to the highest hydrophobicity of the pyridinium cation. Cao *et al.* [79] also studied the anion effect on water sorption for nine ILs with $[BMIM]^+$ cation and they found that ILs followed this trend $[Ac]^- > [Cl]^- > [Br]^- > [TFA]^- > [NO_3]^- > [TFO]^- > [BF_4]^- > [Tf_2N]^- > [CHO]^- > [PF_6]^-$. They stated that the largest difference in water sorption by changing the anion was found to be about 15% higher than that by cation and alkyl chain length. Binary systems $\{H_2O + IL\}$ found in the literature are listed in Annex I. We have correlated all experimental data with NRTL model. All NRTL parameters and the average relative deviation (ARD) on activity coefficients and pressure for each binary system are given in Table I.5. The average relative deviations on activity coefficient and pressure obtained with NRTL model range between 0.01 and 3.5 %. All deviations for the 35 investigated systems are listed in Table I.5. The slightly worse correlation may be due to the fact that these ILs show a miscibility gap in water which cannot be described by the NRTL model. With the exception of those systems all other correlation results are within $\pm 1\%$. Through the number of investigated systems one can see that NRTL-model can well represent $\{H_2O + ILs\}$ binary systems. The dataset show that all ILs studied decrease the vapor pressure of the related aqueous mixtures in different extents.

Passos *et al.* [68] have measured the VLE of 7 binary systems $\{H_2O + IL\}$ in which ILs studied have a common cation $[BMIM]^+$. Their experimental results indicate that the imidazolium-based ILs cause boiling-point elevations of different degrees according to the interaction strengths between water and the IL that mainly depends on the nature of the IL anion.

Table I.5: NRTL parameters of binary systems {H₂O + ILs}.

{Water (1) + ILs (2)}	a ₁₂	a ₂₁	b ₁₂	b ₂₁	α	(ΔP %)
{H ₂ O + [DMIM][DMP]}	-525.2989	-3700.8825	14.6673	-22.9459	0.3	1.41
{H ₂ O + [DMIM][Cl]}	-23638.0556	-2679.9360	45.8488	-17.5904	0.3	2.20
{H ₂ O + [DMIM][BF ₄]}	4775.9349	3876.5759	-2.9434	-23.6187	0.3	1.48
{H ₂ O + [EMIM][DMP]}	-962.1501	-7465.9491	23.9914	-14.6329	0.3	2.74
{H ₂ O + [EMIM][EtSO ₄]}	51456.5850	-44385.7299	-127.1046	100.0735	0.3	9.08
{H ₂ O + [EMIM][DEP]}	0.9000	0.3652	-33.6042	-28.0207	0.3	1.51
{H ₂ O + [EMIM][Ac]}	-34.7593	-7807.9223	-34.5694	-8.5813	0.3	7.49
{H ₂ O + [EMIM][I]}	0.9689	1.1548	-8.2621	47.1505	0.3	13.81
{H ₂ O + [EMIM][(CF ₃ SO ₂) ₂ N]}	-10481.0459	-1456.1633	63.3289	1.0287	0.3	1.27
{H ₂ O + [EMIM][TFA]}	47.0157	-2166.1843	40.2699	-19.5073	0.3	2.34
{H ₂ O + [EMIM][BF ₄]}	78.2628	248.7718	19.4310	-8.2595	0.3	1.35
{H ₂ O + [EMIM][Triflate]}	78.4993	242.7846	29.1640	-16.5453	0.3	0.69
{H ₂ O + [HOEtMIM][Cl]}	-168.5612	-905.4486	28.5594	-26.5397	0.3	1.01
{H ₂ O + [HOEtMIM][BF ₄]}	1999.1919	-602.1164	-0.8926	-13.4626	0.3	3.34
{H ₂ O + [BMIM][DBP]}	52.6389	-5571.6625	-34.0172	-5.0443	0.3	0.41
{H ₂ O + [BMIM][Br]}	-23175.1749	4229.7304	65.3736	-25.4916	0.3	1.52
{H ₂ O + [BMIM][BF ₄]}	1437.0274	-7894.3303	-9.8020	9.5830	0.3	3.99
{H ₂ O + [BMIM][MeSO ₄]}	8933.9651	223.1127	0.0003	1.6962	0.3	1.49
{H ₂ O + [BMIM][SCN]}	17958.0434	1.0407	-67.2928	795.7874	0.3	0.01
{H ₂ O + [BMIM][TOS]}	-318.8044	19270.2452	-38.6608	-65.6350	0.3	1.15
{H ₂ O + [BMIM][CF ₃ CO ₂]}	15872.5505	-9562.4848	-25.8048	5.8570	0.3	2.20
{H ₂ O + [BMIM][C ₁ SO ₃]}	9443.3815	-5721.7247	-1.4815	-13.2220	0.3	1.56
{H ₂ O + [BMIM][C ₁ CO ₂]}	0.8989	0.9340	-36.8681	-17.6819	0.3	13.94
{H ₂ O + [DEMA][OMs]}	3552.2300	-5223.2310	1.8642	-10.2724	0.3	4.24
{H ₂ O + [BMIM][MeSO ₄]}	8933.9651	223.1127	0.0003	1.6962	0.3	1.49
{H ₂ O + [BMIM][CF ₃ SO ₃]}	-3817.3847	-8923.7104	40.9752	9.2525	0.3	1.96
{H ₂ O + [BMIM][SCN]}	17958.0434	1.0407	-67.2928	795.7874	0.3	0.01
{H ₂ O + [BMIM][TOS]}	-318.8044	19270.2452	-38.6608	-65.6350	0.3	1.15
{H ₂ O + [BMIM][CF ₃ CO ₂]}	15872.5505	-9562.4848	-25.8048	5.8570	0.3	2.20
{H ₂ O + [BMIM][C ₁ SO ₃]}	9443.3815	-5721.7247	-1.4815	-13.2220	0.3	1.56
{H ₂ O + [BMIM][C ₁ CO ₂]}	0.8987	0.9279	-36.8867	-17.6110	0.3	13.94
{H ₂ O + [BMIM][(CF ₃ SO ₂) ₂ N]}	42050.3031	1.0407	-59.3941	795.7874	0.3	6.55
{H ₂ O + [BMIM][I]}	107632.0868	1.0407	-298.5630	795.7874	0.3	8.14
{H ₂ O + [BMIM][Cl]}	30802.2495	1.0407	-110.7024	795.7874	0.3	21.44
{H ₂ O + [BMPIP][DCA]}	4706.2445	2992.7192	20.6703	-25.9038	0.3	0.76
{H ₂ O + [BMPYR][DCA]}	26507.5279	-137.8009	-18.9712	-30.2341	0.3	0.32

The influence of ILs on the boiling temperatures follows the order: [CF₃SO₃]⁻ < [SCN]⁻ < [CF₃CO₂]⁻ < [TOS]⁻ < [Br]⁻ < [C₁SO₃]⁻ < [C₁CO₂]⁻. This work shows clearly that the observed trend is related to the anion and to its capacity to interact with water. Other research groups confirmed that anion has an essential role when aiming to lower the vapor pressure of water

H₂O. As an example, VLE of binary systems {H₂O + [EMIM] [X]} where the anion X is [DMP]⁻ or [EtSO₄]⁻ or [Ac]⁻ which are studied by Ren *et al.* [54] Zuo *et al.* [56] and Romich *et al.* [63] respectively. It is found that ethylsulfate anion [EtSO₄]⁻ corresponds to a moderate decrease in vapor pressure of H₂O while the dimethylphosphate anion [DMP]⁻ leads to a stronger attraction of the water molecules corresponding to a lower vapor pressure and hence lower activity coefficient. Then, with increasing compactness of the anion, the vapor pressure can be decreased more.

Zhao and his group [66] have shown that the effect of phosphoric based ILs on the vapor pressure lowering of water follows the order [MMIM][DMP] > [EMIM][DEP] > [BMIM][DBP]. It was noticed that ionic liquids with longer cation alkyl chain length cause a larger solubility but lower dependence of the solubility on temperature [46, 54]. Thus, ionic liquids with shorter cation alkyl chain are preferred ([DMIM]⁺ > [EMIM]⁺ > [BMIM]⁺ > [HMIM]⁺) due to more sensitive dependence of the solubility on temperature. The behavior of binary systems {H₂O + IL} strongly depends on the ionic sizes and to the ionic hydration ability of ILs [66].

It can be good to note that some ILs such as acetate or chloride-based ionic liquids are not suitable for absorptions cycles due to an insufficient stability and/or too high corrosion rates [80].

I.10.2.2. Heat capacity

Heat capacity is an important thermodynamic property since it is related to temperature derivatives of basic thermodynamic functions and, therefore, it is important for the calculation of differences in these functions between different temperatures. This property also indicates the ability of the substance to store heat; thus, it can be used to assess the efficiency of the substance as a thermal fluid [81].

Only one theoretical model is proposed in the literature to predict the heat capacity of binary systems containing ILs [80]. Lashkarbolooki *et al.* [82] evaluate the possible use of artificial neural network model to estimate the binary heat capacities of the ILs mixtures. The error analysis shows this approach leads to estimate the binary heat capacities of the ILs mixtures with an average absolute relative deviation of about 1.60%. In most cases, heat capacity is expressed using a temperature and composition dependent polynomial equation:

$$C_p = \sum_{i=0}^3 (A_i + B_i T) x m_2^i \quad (I.3)$$

where C_p is the mass heat capacity in $\text{kJ.kg}^{-1}.\text{K}^{-1}$, A_i and B_i are the regressive parameter, T is the absolute temperature in K , and $x m_2$ is the mass fraction of ILs. We have correlated all heat capacities data of $\{\text{H}_2\text{O} + \text{ILs}\}$ published in the literature using Eq. (I.3). The regressed parameters determined by a least-squares method are listed in Table I.6.

Table I.6: Mass heat capacity parameters of binary systems $\{\text{H}_2\text{O} (1) + \text{ILs} (2)\}$.

$\{\text{H}_2\text{O} (1) + \text{ILs} (2)\}$	A_0	A_1	A_2	A_3	B_0	B_1	B_2	B_3	$(\Delta C_p \%)$
$\{\text{H}_2\text{O} + [\text{DMIM}][\text{DMP}]\}$	3.7623	-1.7355	-5.5653	4.8733	0.0012	-0.0003	0.0147	-0.0142	0.23
$\{\text{H}_2\text{O} + [\text{EMIM}][\text{DMP}]\}$	-1.2394	-1.1119	-0.9982	-0.8977	0.0283	-0.0455	0.0545	-0.0185	2.11
$\{\text{H}_2\text{O} + [\text{EMIM}][\text{EtSO}_4]\}$	-5.0559	-13.9589	45.2418	-25.4069	0.0954	-0.2163	0.1738	-0.0504	1.05
$\{\text{H}_2\text{O} + [\text{EMIM}][\text{Ac}]\}$	4.1752	-1.9221	-7.7799	6.8077	0.0001	0.0027	0.0176	-0.0185	0.30
$\{\text{H}_2\text{O} + [\text{HOEtMIM}][\text{Cl}]\}$	3.1990	-6.1970	4.6065	-1.6142	0.0030	0.0106	-0.0132	0.0047	0.16
$\{\text{H}_2\text{O} + [\text{DEMA}][\text{OMS}]\}$	4.7283	-6.1401	-0.1972	3.0274	-0.0018	0.0161	-0.0081	-0.0047	0.55
$\{\text{H}_2\text{O} + [\text{EMIM}][\text{Triflate}]\}$	5.0135	-6.8405	2.6687	0.0509	-0.0027	0.0152	-0.0112	0.0004	0.21
$\{\text{H}_2\text{O} + [\text{BMIM}][\text{MeSO}_4]\}$	4.9273	-6.1129	0.3664	1.9235	-0.0028	0.0167	-0.0096	-0.0024	0.29
$\{\text{H}_2\text{O} + [\text{EMIM}][\text{TFA}]\}$	2.0195	12.2695	-32.6699	19.2440	0.0078	-0.0315	0.0639	-0.0381	5.72
$\{\text{H}_2\text{O} + [\text{BMIM}][\text{Triflate}]\}$	5.9515	-9.0845	4.5266	-0.5061	-0.0039	0.0152	-0.0057	-0.0037	0.27
$\{\text{H}_2\text{O} + [\text{BMIM}][\text{BF}_4]\}$	0.2292	0.2292	0.2292	0.2292	0.0006	0.0006	0.0006	0.0006	0.17
$\{\text{H}_2\text{O} + [\text{EMIM}][\text{DEP}]\}$	0.3292	0.3292	0.3292	0.3292	0.0006	0.0006	0.0006	0.0006	0.33

The mass excess molar heat capacity, C_p^E is the difference between the mixture heat capacity and the pure components:

$$C_p^E = C_p - \sum x m_i \cdot C_{p,i} \quad (I.4)$$

where C_p is the mass heat capacity $\text{kJ.kg}^{-1}.\text{K}^{-1}$ of the mixture; $C_{p,i}$ is the mass heat capacity of the pure compound; and $x m_i$ is its mass fraction. The values of C_p^E for the systems studied here are very small, on the same order of magnitude as the experimental uncertainty, so no significant analysis can be carried out. This means that an assumption of a linear decrease of C_p with the concentration of water (i.e., $C_p^E \approx 0$) is a very good estimate [83].

For each IL, there is a small increase in heat capacity with increasing temperature. Ficke [49] stated that the heat capacity should increase roughly linearly with increasing molar mass. This is because of the fact that heat capacity is dependent on the number of translational, vibrational, and rotational energy storage modes. Generally speaking, the mass heat capacity of the binary systems $\{\text{H}_2\text{O} + \text{ILs}\}$ is quite small, which leads to diminish power consumption, is beneficial to heat transfer and improves the COP in absorption cycle [46, 65]. While, C_p values for ILs are much lower than those for water. This means less energy will be required to produce a certain temperature increase in a given mass of IL than in the same mass of water [83].

I.10.2.3. Excess Enthalpy (H^E)

The search for ideal working pairs requires the knowledge of excess Gibbs free energies of binary mixtures of refrigerants and absorbents, which is thermodynamically related to the excess enthalpy (H^E). Excess enthalpy H^E is not only important for the calculation of the coefficient of performance but it also gives insight into the interactions between the molecules. Excess enthalpy describes the difference in the strength of molecular interactions between unlike species (water-IL interaction) and like species (IL-IL and water-water interaction). The excess enthalpies, H^E , can be determined directly by using calorimetry. Garcia-Miaja *et al.* [84] measured H^E for the binary systems $\{\text{H}_2\text{O} + [\text{BMPyr}][\text{BF}_4]\}$, $\{\text{H}_2\text{O} + [\text{EMIM}][\text{EtSO}_4]\}$, $\{\text{H}_2\text{O} + [\text{BMIM}][\text{MeSO}_4]\}$, $\{\text{H}_2\text{O} + [\text{BMIM}][\text{Triflate}]\}$ and $\{\text{H}_2\text{O} + [\text{EMIM}][\text{Triflate}]\}$. The H^E data of binary systems $\{\text{H}_2\text{O} + \text{ILs}\}$ measured by Garcia-Miaja *et al.* [84] as a function of the composition are represented in Figure I.12.

All systems studied have positive H^E values except for sulfate-based ILs systems. Very high H^E values (up to $2500 \text{ J} \cdot \text{mol}^{-1}$) were found for BF_4^- based systems and triflate-based ILs systems show moderate positive H^E values (about $1200 \text{ J} \cdot \text{mol}^{-1}$ at the maximum). Considering that negative excess enthalpy involves a net creation of interactions upon mixing, the authors stated that for tetrafluoroborate and triflate-based ILs the forces between the ions or molecules that form the dissimilar species, (IL–water interactions), are weaker than between those of similar ones (IL–IL and water–water interactions) [84].

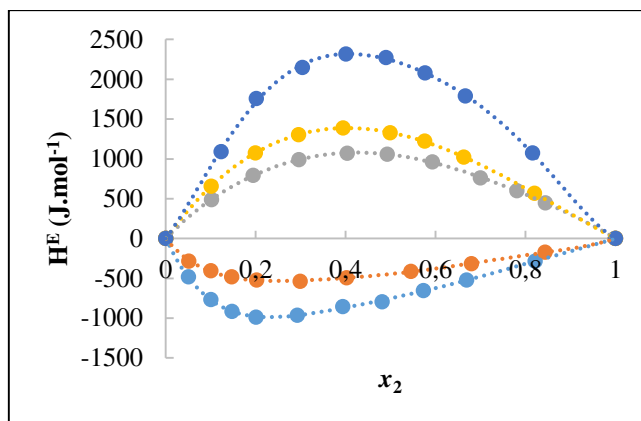


Figure I.12: Excess enthalpy, H^E for the binary mixtures { water (1) + ionic liquid (2)} at $T = 298.15$ K. Ionic liquids ● [EMIM][EtSO₄], ● [BMIM][MeSO₄], ● [EMIM][Triflate], ● [BMIM][Triflate], ● [BMPy][BF₄] [84].

H^E was fitted to Redlich Kister polynomials [57] of the form:

$$H^E = x m_1 x m_2 \sum_{i=1}^4 A_i (2x m_2 - 1)^{i-1} \quad (\text{I.5})$$

where H^E is the excess enthalpy in kJ.kg^{-1} , A_i is the regressive parameter, $x m_i$ is the mass fraction of species i ($i = 1, 2$). We have used Eq. (I.5) to correlate all systems found in the literature. The regressed parameters are listed in Table I.7.

It is noticeable that there is a lack of data of H^E for binary systems {H₂O + ILs} in the literature.

Table I.7: Excess enthalpy H^E parameters of binary systems {H₂O (1) + ILs (2)}.

{H ₂ O+ ILs}	A ₁	A ₂	A ₃	A ₄	(ΔH^E %)
{H ₂ O + [DMIM][DMP]}	-417.8554	-660.8119	1552.7531	-1418.4957	0.27
{H ₂ O + [EMIM][DEP]}	-969.0601	2058.2864	-1939.5085	1.0056	1.64
{H ₂ O + [EMIM][HSO ₄]}	-1315.2862	3532.7673	-2774.4377	0.9851	0.98
{H ₂ O + [EMIM][TFO]}	19.3366	184.7568	-331.6480	297.1489	0.52
{H ₂ O + [EMIM][DMP]}	743.5477	-5271.0368	7551.6799	-3914.4565	1.42
{H ₂ O + [EMIM][EtSO ₄]}	-74.1197	-32.2087	-3.9332	24.1222	1.41
{H ₂ O + [EMIM][TFA]}	-182.7499	110.6168	4.6321	-265.9890	2.60
{H ₂ O + [BMIM][BF ₄]}	113.3628	65.7448	47.2380	45.3341	4.66
{H ₂ O + [BMIM][MeSO ₄]}	-39.2160	-5.5123	-19.6878	9.3845	2.39
{H ₂ O + [BMIM][Triflate]}	41.4860	101.3003	-145.8678	201.9100	1.06

I.10.2.4. Density

The density is an important property due to the information obtained for moving a fluid around in a process.

In practice, the density of working pairs is closely related to temperature and composition, so the influence of the density change of a solution cannot be ignored when analyzing the absorption heat transformer cycle. The density of IL depends on the type of anion and cation, but the key parameter is the anion.

The most studied cation groups are those based on imidazolium and pyridinium. The density of most imidazolium based ILs roughly ranges within 1.1 and 1.6 g.cm⁻³. A wide range of imidazolium-based ILs has been studied including many different anions in an effort to demonstrate the potential to tailor specifically the properties of ILs for given applications. Halide salts are hydrophilic and miscible with water. Dong *et al.* [85] demonstrated that increasing the length of the alkyl chain for a series of 1-alkyl-3-methylimidazolium cations increases the hydrophobicity and then the densities of the ILs decrease. While the simple halide salts have significantly lower densities than the PF₆⁻ based ILs.

An increase of the water content or temperature causes a decrease of the density in most of the binary systems studied. Hence, physical properties of ILs can be adjusted to meet the needs of applications for hydrophilic ILs by adding water or changing the temperature [85].

By keeping the cation, Dong *et al.* [85] found that the densities of the {H₂O + [EMIM][Br]} substantially exceed those of the {H₂O + [EMIM][BF₄]} due to the greater mass of bromine atoms. Similarly, for the [BMIM]⁺ containing ILs aqueous solutions, the densities decrease as follows [BMIM][Br] > [BMIM][BF₄] > [BMIM][Cl].

The literature shows that structural variations such as alkyl chain length grafted on the cation and substituting the halides in the anion have a significant impact on the densities of the binary systems of {H₂O + ILs}. Adding CH₂ groups to the alkyl chain on the [C_nMIM]⁺ cation decreases the density, and the density increases as the mass of the anion increases [60,85]. Gong *et al.* [60] referred this behavior to the presence of electrostatic interaction among ionic species in the IL. Hence, by comparing [BMIM][DMP] and [EMIM][DMP], it was found that [EMIM][DMP] has a little higher density, which is likely due to the stronger electrostatic interaction between the smaller cation [EMIM]⁺ and the anion [DMP]⁻, though the cation [BMIM]⁺ has a higher dispersion energy due to its longer alkyl substitute [60].

The density data for the 19 investigated binary systems were regressed using Eq. (I.6) and listed in Table I.8.

$$\rho = \sum_{i=0}^3 (a_i + b_i T) x_2^i \quad (\text{I.6})$$

Where ρ is the density of the solution in $\text{g} \cdot \text{cm}^{-3}$, T is the absolute temperature in K, a_i and b_i are the regression parameters, and x_2^i is the molar fraction of the ILs.

Table I.8: Density parameters of binary systems {H₂O (1)+ ILs (2)}.

{H ₂ O (1) + ILs (2)}	a_0	a_1	a_2	a_3	b_0	b_1	b_2	b_3	(ρ %)
{H ₂ O + [DMIM][DMP]}	1.3609	0.2563	-0.0456	-0.1254	-0.0005	-0.0005	-0.0002	0.0005	0.05
{H ₂ O + [EMIM][DMP]}	1.4137	0.1774	-0.0962	-0.1587	-0.0008	-0.0008	0.0018	-0.0008	0.00
{H ₂ O + [EMIM][EtSO ₄]}	1.2936	0.4596	-0.2633	-0.0465	-0.0005	0.0000	-0.0010	0.0009	0.04
{H ₂ O + [EMIM][Ac]}	1249.5004	171.0933	-106.8954	-145.5366	-0.6473	0.4439	-1.6273	1.6784	0.05
{H ₂ O + [EMIM][Triflate]}	1.3060	0.6526	0.2328	-0.6067	-0.0008	0.0023	-0.0074	0.0053	0.92
{H ₂ O + [EMIM][DEP]}	0.3364	0.3364	0.3364	0.3364	-0.0002	-0.0002	-0.0002	-0.0002	0.01
{H ₂ O + [EMIM][TFA]}	1.1816	2.0379	-3.6392	1.9588	-0.0005	-0.0026	0.0052	-0.0029	0.97
{H ₂ O + [EMIM][BF ₄]}	1.2883	0.0032	-0.4303	-0.0065	-0.0009	0.0045	-0.0073	0.0052	0.50
{H ₂ O + [BMIM][BF ₄]}	1.4564	0.0025	-0.1654	-0.0107	-0.0010	-0.0004	0.0018	-0.0007	0.19
{H ₂ O + [BMIM][C(CN) ₃]}	1.2499	0.0027	0.0025	-0.0102	-0.0008	0.0002	-0.0002	0.0001	0.02
{H ₂ O + [BMIM][DMP]}	1.3660	0.0344	-0.0864	0.0457	-0.0009	0.0007	-0.0009	0.0004	0.11
{H ₂ O + [BMIM][C(CN) ₂]}	1.2511	0.0028	0.0026	-0.0113	-0.0008	0.0003	-0.0002	0.0001	0.02
{H ₂ O + [BMIM][HSO ₄]}	1.3503	0.0028	0.0004	-0.0132	-0.0014	0.0022	0.0021	-0.0037	0.96
{H ₂ O + [BMIM][MeSO ₄]}	1.2391	0.4936	-0.3432	0.0014	-0.0007	0.0009	-0.0027	0.0019	0.57
{H ₂ O + [BMIM][Triflate]}	1.3419	0.5432	-0.3695	0.0014	-0.0008	0.0009	-0.0027	0.0019	0.43
{H ₂ O + [BDMIM][BF ₄]}	0.9975	1.0038	0.9930	1.0105	0.0001	-0.0009	-0.0071	-0.0016	0.52
{H ₂ O + [HMIM][BF ₄]}	1.2365	0.0449	-0.1378	0.0750	-0.0008	0.0019	-0.0025	0.0012	0.18
{H ₂ O + [HOEtMIM][Cl]}	1.0828	0.9986	0.9965	0.9968	-0.0003	0.0027	-0.0318	0.0487	0.19
{H ₂ O + [DEMA][OMs]}	1359.9578	-444.5775	1306.9943	-1105.3731	-1.0054	2.6277	-6.2798	4.8167	0.02

Excess molar volume (V^E) is a crucial thermodynamic property to represent the non-ideality of a solution, which is defined as the difference of the molar volume between the real mixture and an ideal solution at the same temperature, pressure, and composition [60]. Excess volume V^E is a reflection of the compromising effects among molecular sizes and various interactions for a specific mixture and is dependent on the temperature and composition. It is obvious from literature that the molar volumes V_m of all mixtures increase linearly with the mole fractions of IL. Gong *et al.* [60] found that the binary mixtures $\{H_2O + [EMIM][DMP]\}$ and $\{H_2O + [BMIM][DMP]\}$ are close to the ideal solution behavior.

Gong *et al.* [60] referred negative excess volume to the stronger ion dipole interaction and charge transfer complication between IL and the solvent molecules, as well as the interstitial effect in molecular packing due to the differences in the size and shape of the component molecules, by which the volume of the liquid mixture is suitable to be contracted and reaches to the maximum at $x_{IL} \approx 0.3$ for all of the systems they studied [60]. Lehmann *et al.* [86] explained that, for aqueous systems, the increasing V^E with increasing temperature may result from the temperature dependence of the strength of hydrogen bonds. The excess molar volume V^E depends mainly on the intermolecular forces between components of the mixtures and on the packing due to the differences in size and shape of molecules. The negative excess volumes can be attributed to strong water-ionic liquid interactions and to an efficient packing of the components in the mixture.

Gonzalez *et al.* [87] studied excess properties included V^E for eight binary systems $\{H_2O + [BMIM][TFO], [BMPyr][TFO], [BMPy][TFO], [BMIM][DCA], [HMIM][DCA], [BMPyr][DCA], [MPy][MeSO_4], \text{ or } [EEPyr][EtSO_4]\}$ (Figure I.13 (a-c)).

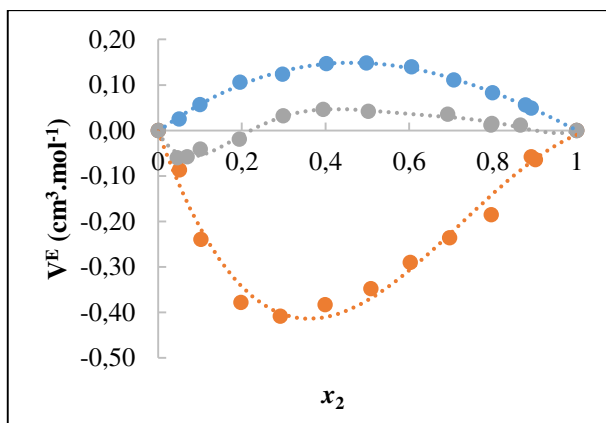
All of the binary systems studied in this work present asymmetrical curves. The binary systems containing $\{H_2O + \text{dicyanamide-based ILs}\}$ show a wavy behavior at low temperatures, with a minimum at high concentration of water that disappears when the temperature increases. The binary mixtures with trifluoromethanesulfonate-based ILs show the same wavy shape at the studied temperatures. This change from positive to negative in the V^E behavior was also observed in the literature (Garcia-Miaja *et al.* [84], Rodriguez and Brennecke [88], and Vercher *et al.* [89]) with aqueous mixtures containing trifluoromethane sulfonate-based ILs. Concerning pyridinium based ILs, Gonzalez *et al.* [87] found a wavy behavior with $\{H_2O + [MPy][MeSO_4]\}$ but negative V^E values were obtained, over the whole composition range for the system $\{H_2O + [EEPyr][EtSO_4]\}$. Negative V^E values were also found in literature for the aqueous system containing an imidazolium-based ionic liquid with the $[EtSO_4]^-$ as anion [90,

91, 92]. These results indicate that cation has a low influence on the behavior of V^E for the binary systems $\{H_2O + IL\}$. This observation is in good agreement with the results previously published [87, 88]. In the case of dicyanamide-based ILs, it was found that an increase of the alkyl chain length of the cation leads to smaller V^E values which can be attributed to differences in size and shape of the studied ILs and/or to different intermolecular interactions in the mixtures.

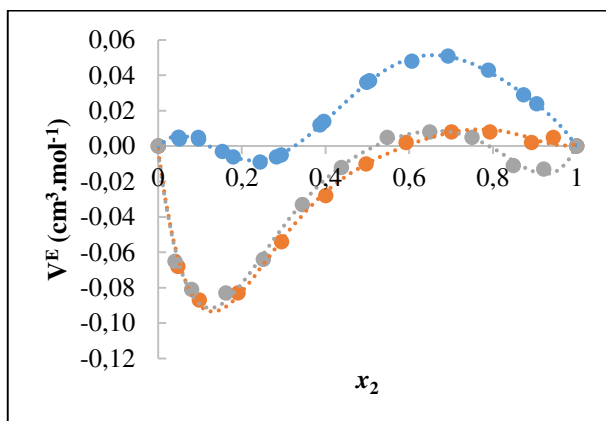
Several papers containing V^E data for binary mixtures containing water and other imidazolium, pyrrolidinium, and pyridinium-based ILs can be found in the literature [87] in which the shape of the V^E values is mainly related to the anion.

Gonzalez *et al.* [87] stated that, although these systems show similar V^E curves, since that all mixtures contain ILs with the same anion, the V^E values are different depending on the cation present. It is found that V^E for the ILs follow the trend:

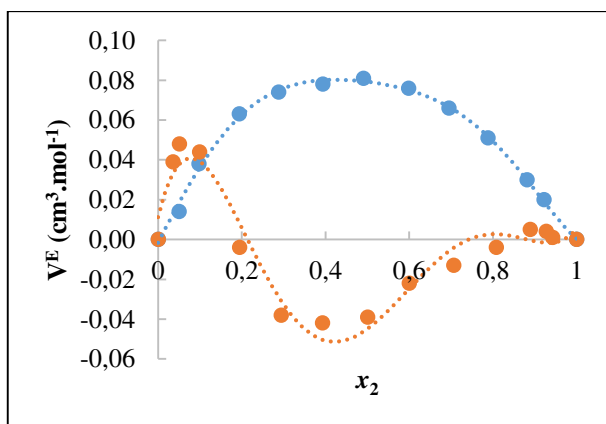
V^E (imidazolium) > V^E (pyridinium) \cong V^E (pyrrolidinium). This trend is in good agreement with the work of Garcia-Miaja *et al.* [84] on the binary systems $\{H_2O + [BMIM][BF_4]\}$ and $\{H_2O + [BMPy][BF_4]\}$.



(a)



(b)



(c)

Figure I.13: Excess molar volumes, V^E for the binary mixtures $\{\text{H}_2\text{O} (1) + \text{ILs} (2)\}$

at $T = 298.15 \text{ K}$. Ionic liquids: (a) ● [BMIM][DCA], ● [EETPy][EtSO₄], ●

[BMIM][TFO]; (b) ● [BMPy][DCA], ● [BMPyr][TFO], ● [BMPy][TFO]; (c) ●

[HMIM][DCA], ● [MPy][MeSO₄] [87].

I.10.2.5. Viscosity

Kim *et al.* [94] stated that higher viscosity ILs cause an increased pressure drop in the compression loop, which would result in larger pumping power or larger pipes and system volume. The viscosity increases with cation mass: EMIM << BMIM << HMIM. The viscosity is more dependent on the anion with the following order: Tf₂N << BF₄ << PF₆ [2]. However Rodriguez and Brennecke [88] stated that ILs including the fluorinated [OTF]⁻ and [TFA]⁻ anions lead to lower viscosities than the one with the non-fluorinated [EtSO₄]⁻ anion.

Gong *et al.* [60] mentioned that the viscosities of the ILs they studied are much higher, than that of water, ethanol and methanol, and follows the order of:

[BMIM][DMP] > [EMIM][DMP] >> ethanol > water > methanol at any temperatures. They referred the high viscosity of IL may be dominated by the “ionic” attributes of the liquid and the strong Coulombic interaction among different ions and ionic clusters. The migration of an IL entity, or an ionic pair, in the liquid will be strongly pulled by the surrounding ionic spheres with equal but opposite charge and thus shows a strong drag force for the movement, resulting in a high viscosity.

They also stated that the viscosity of the pure IL decreases drastically with the increasing temperature, for example, the viscosity of [EMIM][DMP] decreases by 87 %, that is, from 378.818 mPa.s at 293.15 K to 48.503 mPa.s at 333.15 K (Figure I.14), while the viscosity of methanol decreases less, only 34 %, for the same temperature range. Thus the viscosity of IL is more sensitive to temperature than the conventional molecular solvents. Ayou *et al.* [95] stated that viscosity of the ILs changes with alkyl chain length. The longer the alkyl chain length is the higher the viscosity of the IL.

They also attributed the cause of the drastic decrease of viscosity of the mixture when adding water to the following facts. **First**, since water has a much lower viscosity than the pure IL, which reduces the bulk viscosity of the binary mixture greatly due to the diluting effect. **Second**, when water is added to IL, the hydrogen bond between the anion and cation weakens, which increases the mobility of ions and decreases the viscosity of IL [47]. Nevertheless, He *et al.* [57] stated that since the absorber and generator temperatures of an absorption heat pump or absorption heat transformer are usually high, the viscosity of the working pairs is expected to be low. Thus, the high viscosity of the ionic liquid would not limit its use as a heat pump transformer absorbent [57].

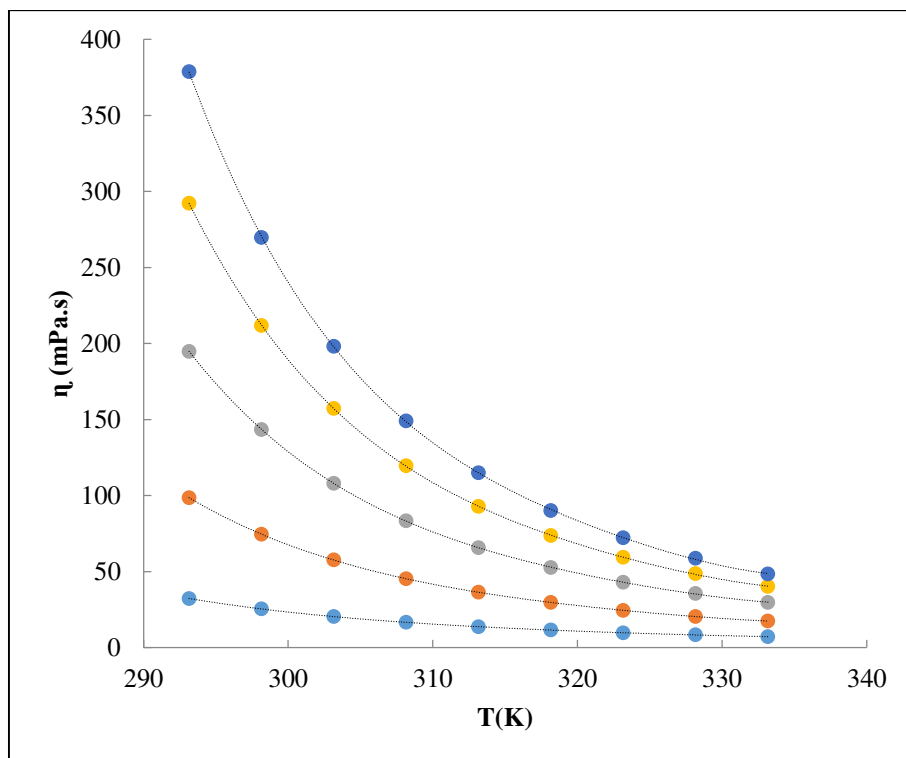


Figure I.14: Viscosity for the binary mixtures {water (1) + [EMIM][DMP] (2)} at different temperatures and mole fractions of IL ● $x_2 = 0.2$; ● $x_2 = 0.4$; ● $x_2 = 0.6$; ● $x_2 = 0.8$; ● $x_2 = 1$ with solid lines to guide the eye [60].

I.10.2.6. Thermal decomposition

It is well-known that the decomposition temperatures are highest for ionic liquids containing the $[\text{TF}_2\text{N}]$ anion [49]. Ficke [49] and Seiler *et al.* [80] declared that anion has an important influence on the decomposition temperature of ionic liquids. $[\text{EMIM}]^+$ based ILs span in temperature from 178 to 388 °C (Table I.9). An increasing alkyl chains has little effect. For example, $[\text{EMIM}][\text{EtSO}_4]$, $[\text{EMIM}][\text{MeSO}_4]$, and $[\text{EMIM}][\text{HSO}_4]$ the decomposition temperature is 355, 362, and 359 °C, respectively. $[\text{EMIM}][\text{TFA}]$ and $[\text{OHMIM}][\text{TFA}]$ show even lower decomposition temperatures [80]. Huangfu *et al.* [96] examined the thermal stability, of pure $[\text{BMIM}][\text{BF}_4]$ and $[\text{BMIM}]_2[\text{SO}_4]$. The temperature range of the respective liquid state was found to reach from −36 to 475 °C and from −93 to 263 °C, respectively. Ficke [49] stated that $[\text{EMIM}][\text{EtSO}_4]$ decomposes over time by reacting with water to form 1-ethyl-3-methylimidazolium hydrogen sulfate, $[\text{EMIM}][\text{HSO}_4]$, and ethanol.

Table I.9: Decomposition temperature for miscible ILs.

IL	Decomposition temperature (°C)	References
[EMIM][TFA]	178	49
[OHEMIM][TFA]	187	49
[EMIM][EtSO ₄]	355	49
[EMIM][HSO ₄]	359	49
[EMIM][MeSO ₄]	362	49
[EMIM][TFO]	388	49
[EMIM][MeSO ₃]	335	49
[EMIM][SCN]	281	49
[EMIM][DEP]	273	49
[P ₂₄₄₄][DEP]	314	49
[EMIM][Cl]	285	6
[EMIM][I]	303	6
[EMIM][PF ₆]	375	6
[EMIM][BF ₄]	412	6
[EMIM][Tf ₂ N]	455	6
[BMIM][I]	265	6
[BMIM][BF ₄]	403	6
[BMIM][PF ₆]	349	6
[BMIM][Cl]	253	6
[BMIM][Tf ₂ N]	439	6

Thermal decomposition could possibly be one of the most important properties to measure during the initial screening of an IL, especially for the operating temperatures of the processes related to this work.

Hence it is important to stress on the suitability of an ionic liquid in terms of stability cannot be judged only on the basis of analytical thermogravimetric analysis (TGA) measurements of the pure ionic liquid. Ideally, absorption cycle experiments are necessary to confirm the long-term stability (thermal and chemical stability) of an ionic liquid based working pair. If these absorption cycle trials cannot be accomplished due to complexity and/or cost reasons a method needs to be arranged where (i) the ionic liquid is mixed with a representative water concentration (i.e. 20 wt %), (ii) this mixture is reserved for a long period of time (several months) at similar generator conditions (for example temperature 100 °C), (iii) samples are finally taken from this mixture and analyzed for thermal and chemical stability using the reliable analytical methods. This technique also was suggested by Seiler *et al.* [80].

References

- [1] X. Zhang, D. Hu, Performance analysis of the single-stage absorption heat transformer using a new working pair composed of ionic liquid and water, *Applied Thermal Engineering*, 37 (2012) 129–135.
- [2] Kirk-Othmer, *Encyclopedia of Chemical Technology*. Vol. 26, Ionic Liquids (Stark, A.; K.R. Seddon), 836-920, John Wiley & Sons, Inc., Available Online. (May, 2008). <http://mrw.interscience.wiley.com/emrw/9780471238966/home>.
- [3] S.V. Dzyuba, R.A. Bartsch, Influence of structural variations in 1- alkyl (aralkyl)-3-methylimidazolium hexafluorophosphates and bis-(trifluoromethylsulfonyl) imides on physical properties of the ionic liquids, *Chem. Phys. Chem.*, 3 (2002) 161–166.
- [4] M. Freemantle, Designer solvents. Ionic liquids may boost clean technology development, *Chem. Eng. News*, 76 (1998) 13, 32–37.
- [5] P. Walden, Molecular weights and electrical conductivity of several fused salts, *Bull. Russ. Acad. Sci. (St. Petersburg)*, (1914) 405–422.
- [6] M.W. Arshad, CO₂ capture using ionic liquids. Master's thesis, Technical University of Denmark, Copenhagen; May 2009.
- [7] L.K. Chellappan, Synthesis of ionic liquids based on new cationic cores. PhD thesis, K.U. Faculty of Science, Heverlee (Leuven), Belgium; May 2012.
- [8] F.N. Hurley, T.P. Wier, The electrode position of aluminum from non-aqueous solutions at room temperature, *Journal of the Electrochemical Society*, 98 (1951) 207–212.
- [9] J. Robinson, R.A. Osteryoung, An electrochemical and spectroscopic study of some aromatic hydrocarbons in the room temperature molten salt system aluminum chloride-n-butylpyridinium chloride, *J. Am. Chem. Soc.*, 101 (1979) 323–327.
- [10] C.L. Hussey, Ionic liquids, *Adv. Molten Salt Chem.*, 5 (1983) 185–230.
- [11] D. Appleby, C.L. Hussey, K.R. Seddon, J.E. Turp, Room-temperature ionic liquids as solvents for electronic absorption spectroscopy of halide complexes, *Nature*, 323 (1986) 614–616.
- [12] T.B. Scheffler, C.L. Hussey, K.R. Seddon, C.M. Kear, P.D. Armitage, Molybdenum chloro-complexes in room-temperature chloroaluminate ionic liquids: stabilization of hexachloromolybdate (2-) and hexachloromolybdate (3-), *Inorg. Chem.*, 22 (1983) 2099–2100.

- [13] J.S. Wilkes, J.A. Levisky, R.A. Wilson, C.L. Hussey, Dialkylimidazolium chloroaluminate melts, a new class of room-temperature ionic liquids for electrochemistry, spectroscopy and synthesis, *Inorg. Chem.*, 21 (1982) 1263–1264.
- [14] J.S. Wilkes, A short history of ionic liquids—from molten salts to neoteric solvents, *Green Chem.*, 4 (2002) 73–80.
- [15] J.H. Davis, Jr., K.J. Forrester, T. Merrigan, Novel organic ionic liquids (OILs) incorporating cations derived from the antifungal drug miconazole, *Tetrahedron Lett.*, 39 (1998) 8955–58.
- [16] N.V. Plechkova, K.R. Seddon, Application of ionic liquids in the chemical industry, *Chemical Society Reviews*, 37 (2008) 123–150.
- [17] G.J. Kabo, A.V. Blokhin, A. Paulechka, U. Ya, A.G. Kabo, M.P. Shymanovich, J.V. Magee, Thermodynamic properties of 1-butyl-3-methylimidazolium hexafluorophosphate in the condensed state, *J. Chem. Eng. Data*, 49 (2004) 453–461.
- [18] R.M. Lynden-Bell, M.G. Del Pópolo, T.G.A. Youngs, J. Kohanoff, C.G. Hanke, J.B. Harper, C.C. Pinilla, Simulations of ionic liquids, solutions, and surfaces, *Acc. Chem. Res.*, 40 (2007) 1138–1145.
- [19] J. Pernak, A. Czepukowicz, R. Pozniak, New ionic liquids and their antielectrostatic properties, *Ind. Eng. Chem. Res.*, 40 (2001) 2379–2383.
- [20] U. Domanska, A. Marciniak, Activity coefficients at infinite dilution measurements for organic solutes and water in the 1-hexyloxymethyl-3-methylimidazolium and 1,3-dihexyloxymethyl-imidazolium bis(trifluoromethylsulfonyl)imide ionic liquids—The cation influence, *Fluid Phase Equilib.*, 286 (2009) 154–161.
- [21] A.L. Revelli, L.M. Sprunger, J. Gibbs, W.E. Acree Jr., G.A. Baker, F. Mutelet, Activity coefficients at infinite dilution of organic compounds in trihexyl (tetradecyl) phosphonium Bis(trifluoromethylsulfonyl)imide using inverse gas chromatography, *J. Chem. Eng. Data*, 54 (2009) 977–985.

- [22] U. Domanska, K. Paduszynski, Measurements of activity coefficients at infinite dilution of organic solutes and water in 1-propyl-1-methylpiperidinium bis{(trifluoromethyl)sulfonyl}imide ionic liquid using g.l.c, *J. Chem. Thermodyn.*, 42 (2010) 1361–66.
- [23] H. Tokuda, K. Hayamizu, K. Ishii, Md.A.B.H. Susan, M. Watanabe, Physicochemical properties and structures of room temperature ionic liquids. 1. Variation of anionic species, *J. Phys. Chem. B*, 108 (2004) 16593–16600.
- [24] K.R. Seddon, A. Stark, M.J. Torres, Influence of chloride, water, and organic solvents on the physical properties of ionic liquids, *Pure and App. Chem.*, 72 (2000) 2275–87.
- [25] M.G. Freire, P.J. Carvalho, A.M. Fernandes, I.M. Marrucho, A.J. Queimada, J.A.P. Coutinho, Surface tensions of imidazolium based ionic liquids: Anion, cation, temperature and water effect, *J. Colloid Interface Sci.*, 314 (2007) 621–630.
- [26] M. Smiglak, W.M. Reichert, J.D. Holbrey, J.S. Wilkes, J. Sun, J.S. Thrasher, K. Kirichenko, S. Singh, A.R. Katritzky, R.D. Rogers, Combustible ionic liquids by design: is laboratory safety another ionic liquid myth?, *Chem. Commun.*, 24 (2006) 2554–56.
- [27] M. Uerdingen, C. Treber, M. Balser, G. Schmitt, C. Werner, Corrosion behavior of ionic liquids, *Green Chem.*, 7 (2005) 321–325.
- [28] I. Perissi, U. Bardi, S. Caporali, A. Lavacchi, High temperature corrosion properties of ionic liquids, *Corros. Sci.*, 48 (2006) 2349–62.
- [29] R.A. Sheldon, R.M. Lau, M.J. Sogedra, F.V. Rantwijk, K.R. Seddon, Biocatalysis in ionic liquids, *Green Chem.*, 4 (2002) 147–151.
- [30] B. Jastorff, R. Stormann, J. Ranke, K. Molter, F. Stock, B. Oberheitmann, W. Hoffmann, J. Hoffmann, M. Nuchter, B. Ondruschka, J. Filser, How hazardous are ionic liquids? Structure activity relationships and biological testing as important elements for sustainability evaluation, *Green Chem.*, 5 (2003) 136–142.
- [31] S.A. Forsyth, J.M. Pringle, D.R. MacFarlane., Ionic liquids-An overview, *Aust. J. Chem.*, 57 (2004) 113–119.
- [32] H.C. Hodge, J.H. Sterner, Combined tabulation of toxicity classes, In: W.S. Spector (Ed.), *Handbook of toxicity*, W.B. Saunders Company, Philadelphia, 1956.

- [33] R.J. Bernot, E.E. Kennedy, G.A. Lamberti, Effects of ionic liquids on the survival, movement, and feeding behavior of the freshwater snail, *Physa acuta*. *Environ. Toxicol. Chem.*, 24 (2005) 1759–65.
- [34] E.J. Maginn, Research: Ionic Liquids: [//www.nd.edu/~ed/Research/IL_toxicology.html](http://www.nd.edu/~ed/Research/IL_toxicology.html) (May 23, 2008).
- [35] S.K. Mikkola, A. Robciuc, J. Lokajova, A.J. Holding, M. Lammerhofer, I. Kilpelainen, J.M. Holopainen, A.W.T King, S.K. Wiedmer, Impact of amphiphilic biomass-dissolving ionic liquids on biological cells and liposomes, *Environ. Sci. Technol.*, 49 (2015) 1870–1878.
- [36] D.J. Tempel, P.H. Henderson, J.R. Brzozowski, R.M. Pearlstein, J.J. Hart, D. Tavianini, First International Congress on Ionic Liquids (COIL-1), 19th–22nd June, Salzburg, Austria, 2005.
- [37] M. Khamooshi, K. Parham, U. Atikol, Overview of ionic liquids used as working fluids in absorption cycles, *Advances in Mechanical Engineering*, 620592 (2013) 1–7.
- [38] J. Sun, L. Fu, S. Zhang, A review of working fluids of absorption cycles, *Renewable and Sustainable Energy Reviews*, 16 (2012) 1899–1906.
- [39] I. Horuz, B. Kurt. Absorption heat transformers and an industrial application, *Renewable Energy*, 35 (2010) 2175–81.
- [40] F. Carre, Note sur de un appareil propre à produire du froid, *Comptes Rendus des Séances de L'Académie des Sciences*, Tome cinquante et unième, Paris, (1860) 1023–1027.
- [41] F. Carre, Rapport sur un appareil de M. Carré ayant pour objet la production du froid artificiel, *Comptes Rendus des Séances de L'Académie des Sciences*, Tome cinquante-quatrième, Paris, (1862) 827–840.
- [42] L.A. Schaefer, Single pressure absorption heat pump analysis. PhD thesis, Georgia Institute of Technology, Georgia, USA; May 2000.
- [43] P. Srihirin, S. Aphornratana, S. Chungpaibulpatana, A review of absorption refrigeration technologies, *Renewable and Sustainable Energy Reviews*, 5 (2001) 343–372.
- [44] W. Wu, B. Wang, W. Shi, X. Li, An overview of ammonia-based absorption chillers and heat pumps, *Renewable and Sustainable Energy Reviews* 31, (2014) 681–707.
- [45] A. De Lucas, M. Donate, C. Molero, J. Villasenor, J.F. Rodriguez, Performance evaluation and simulation of a new absorbent for an absorption refrigeration system, *Int. J. Refrig.*, 27 (2004) 324–330.

- [46] L. Dong, D. Zheng, N. Nie, Y. Li, Performance prediction of absorption refrigeration cycle based on the measurements of vapor pressure and heat capacity of $\{H_2O + [DMIM][DMP]\}$ system, *Applied Energy*, 98 (2012) 326–332.
- [47] D. Zheng, L. Dong, W. Huang, X. Wu, N. Nie, A review of imidazolium ionic liquids research and development towards working pair of absorption cycle, *Renewable and Sustainable Energy Reviews*, 37 (2014) 47–68.
- [48] S. Liang, W. Chen, K. Cheng, Y. Guo, X. Gui, The latent application of ionic liquids, In: *Absorption refrigeration, applications of ionic liquids in science and technology*, Prof. Scott Handy (Ed.), ISBN: 978-953-307-605-8, InTech, Available from: <http://www.intechopen.com/books/applications-of-ionic-liquids-in-science-and-technology/the-latent-application-of-ionic-liquids-in-absorption-refrigeration>, 2011.
- [49] L.E. Ficke, Thermodynamic properties of imidazolium and phosphonium based ionic liquid mixtures with water or carbon dioxide. PhD thesis, Chemical and Bio-molecular Engineering, University of Notre Dame, Notre Dame, Indiana; April 2010.
- [50] G. Grossman, Absorption heat transformer for process heat generation from solar ponds, *ASHRAE Trans.*, 97 (1991) 420–427.
- [51] M. Ikeuchi, T. Yumikura, E. Ozaki., G. Yamanaka, Design and performance of a high-temperature- boost absorption heat pump, *ASHRAE Trans.*, 90 (1985) 2081–94.
- [52] T. Nakanishi, T. Furukawa, N. Sato, Industrial high-temperature heat pump, *Hitachi zosen Tech. Rev.*, 42 (1981) 7–12.
- [53] W. Wu, B. Wang, W. Shi, X. Li, Absorption heating technologies: A review and perspective, *Appl. Energy*, 130 (2014) 51–71.
- [54] J. Ren, Z. Zhao, X. Zhang, Vapor pressures, excess enthalpies, and specific heat capacities of the binary working pairs containing the ionic liquid 1-ethyl-3-methylimidazolium dimethylphosphate, *J. Chem. Thermodynamics*, 43 (2011) 576–583.
- [55] X. Zhang, D. Hu, Performance simulation of the absorption chiller using water and ionic liquid 1-ethyl-3-methylimidazolium dimethylphosphate as the working pair, *Applied Thermal Engineering*, 31 (2011) 3316–21.
- [56] G. Zuo, Z. Zhao, S. Yan, X. Zhang, Thermodynamic properties of a new working pair: 1-ethyl-3-methylimidazolium ethylsulfate and water, *Chem. Eng. J.*, 156 (2010) 613–617.

- [57] Z. He, Z. Zhao, X. Zhang, H. Feng, Thermodynamic properties of new heat pump working pairs: 1,3-Dimethylimidazolium dimethylphosphate and water, ethanol and methanol, *Fluid Phase Equilibria*, 298 (2010) 83–91.
- [58] R. Kato, J. Gmehling, Measurement and correlation of vapor–liquid equilibria of binary systems containing the ionic liquids [EMIM][(CF₃SO₂)₂N], [BMIM][(CF₃SO₂)₂N], [MMIM][(CH₃)₂PO₄] and oxygenated organic compounds respectively water, *Fluid Phase Equilibria*, 231 (2005) 38–43.
- [59] J. Wang, D. Wang, Z. Li, F. Zhang, Vapor pressure measurement and correlation or prediction for water, 1-Propanol, 2-Propanol, and their binary mixtures with [MMIM][DMP] ionic liquid, *Chem. Eng. Data*, 55 (2010) 4872–4877.
- [60] Y. Gong, C. Shen, Y. Lu, H. Meng, C. Li, Viscosity and density measurements for six binary mixtures of water (methanol or ethanol) with an ionic liquid ([BMIM][DMP] or [EMIM][DMP]) at atmospheric pressure in the temperature range of (293.15 to 333.15), *J. Chem. Eng. Data*, 57 (2012) 33–39.
- [61] J.F. Wang, C.X. Li, Z.H. Wang, Z.J. Li, Y.B. Jiang, Vapor pressure measurement for water, methanol, ethanol, and their binary mixtures in the presence of an ionic liquid 1-ethyl-3-methylimidazolium dimethylphosphate, *Fluid Phase Equilibria*, 255 (2007) 186–192.
- [62] A. Yokozeki, M.B. Shiflett, Water solubility in ionic liquids and application to absorption cycles, *Ind. and Eng. Chem. Res.*, 49 (2010) 9496–9503.
- [63] C. Romich, N.C. Merkel, A. Valbonesi, K. Schaber, S. Sauer, T.J.S. Schubert, Thermodynamic properties of binary mixtures of water and room temperature ionic liquids: vapor pressure, heat capacities, densities and viscosities of water + 1-ethyl-3-methylimidazolium acetate and water + diethylmethylammonium methane sulfonate, *J. Chem. Eng. Data*, 57 (2012) 2258–64.
- [64] S. Fendt, S. Padmanabhan, H.W. Blanch, J.M. Prausnitz, Viscosities of acetate or chloride-based ionic liquids and some of their mixtures with water or other common solvents, *J. Chem. Eng. Data*, 56 (2011) 31–34.
- [65] N. Nie, D. Zheng, L. Dong, Y. Li, Thermodynamic properties of the water + 1- (2-hydroxyethyl)-3-methylimidazolium chloride system, *J. Chem. Eng. Data*, 57 (2012) 3598–3603.

- [66] J. Zhao, X.C. Jiang, C.X. Li, Z.H. Wang, Vapor pressure measurement for binary and ternary systems containing a phosphoric ionic liquid, *Fluid Phase Equilibria*, 247 (2006) 190–198.
- [67] E.I. Alevizou, G.D. Pappa, E.C. Voutsas, Prediction of phase equilibrium in mixtures containing ionic liquids using UNIFAC, *Fluid Phase Equilibria*, 284 (2009) 99–105.
- [68] H. Passos, I. Khan, F. Mutelet, M.B. Oliveira, P.J. Carvalho, L.M.N.B.F. Santos, C. Held, G. Sadowski, M.G. Freire, J.A.P. Coutinho, Vapor-liquid equilibria of water + alkylimidazolium-based ionic liquids: measurements and perturbed-chain statistical associating fluid theory modeling, *Ind. Eng. Chem. Res.*, 53 (2014) 3737–48.
- [69] Y. Chen, F. Mutelet, J.N. Jaubert, Experimental measurement and modeling of phase diagrams of binary systems encountered in the gasoline desulfurization process using ionic liquids, *J. of Chem. and Eng. Data*, 59 (2014) 603–612.
- [70] A. Nann, C. Held, G. Sadowski, Liquid-liquid equilibria of 1-butanol/water/IL systems, *Ind. and Eng. Chem. Res.*, 52 (2013) 18472–81.
- [71] F. Llorell, E. Valente, O. Vilaseca, L.F. Vega, Modeling complex associating mixtures with $[C_n\text{mim}][\text{Tf}_2\text{N}]$ ionic liquids: predictions from the Soft-SAFT equation, *J. of Phys. Chem. B*, 112 (2011) 4387–98.
- [72] A. Shariati, C.J. Peters, High-pressure phase behavior of systems with ionic liquids: measurements and modeling of the binary system fluoroform+1-ethyl-3-methylimidazolium hexafluorophosphate, *J. of Supercritical Fluids*, 25 (2003) 109–117.
- [73] P.J. Carvalho, V.H. Alvarez, J.J.B. Machado, J. Pauly, J.L. Daridon, I.M. Marrucho, M. Aznar, J.A.P. Coutinho, High pressure phase behavior of carbon dioxide in 1-alkyl-3-methylimidazolium bis(trifluoromethylsulfonyl) imide ionic liquids, *J. of Supercritical Fluids*, 48 (2009) 99–107.
- [74] P.J. Carvalho, V.H. Alvarez, I.M. Marrucho, M. Aznar, J.A.P. Coutinho, High carbon dioxide solubilities in trihexyl tetradecylphosphonium-based ionic liquids, *J. of Supercritical Fluids*, 52 (2010) 258–265.
- [75] P.J. Carvalho, V.H. Alvarez, I.M. Marrucho, M. Aznar, J.A.P. Coutinho, High pressure phase behavior of carbon dioxide in 1-butyl-3-methylimidazolium bis (trifluoromethylsulfonyl)

imide and 1-butyl-3-methylimidazolium dicyanamide ionic liquids, *J of Supercritical Fluids*, 50 (2009) 105–111.

[76] W. Ren, A.M. Scurto, Phase equilibria of imidazolium ionic liquids and the refrigerant gas, 1, 1, 1, 2-tetrafluoroethane (R-134a), *Fluid Phase Equilibria*, 286 (2009) 1–7.

[77] A.J. Morrissey, J.P. O'Donnell, Endothermic solutions and their application in absorption heat pumps, *Chem. Eng. Res. and Design*, 64 (1986) 404–406.

[78] R. Lungwitz, S. Spange, A hydrogen bond accepting (HBA) scale for anions, including room temperature ionic liquids, *New J. Chem.*, 32 (2008) 392–394.

[79] Y. Cao, Y. Chen, L. Lu, Z. Xue, T. Mu, Water sorption in functionalized ionic liquids: kinetics and intermolecular interactions, *Ind. Eng. Chem. Res.*, 52 (2013) 2073–83.

[80] M. Seiler, A. Kühn, F. Ziegler, X. Wang, Sustainable cooling strategies using new chemical system solutions, *Ind. Eng. Chem. Res.*, 52 (2013) 16519–46.

[81] H.C. Hu, A.N. Soriano, R.B. Leron, M.H. Li, Molar heat capacity of four aqueous ionic liquid mixtures, *Thermochimica Acta*, 519 (2011) 44–49.

[82] M. Lashkarbolooki, A.Z. Hezave, S. Ayatollahi, Artificial neural network as an applicable tool to predict the binary heat capacity of mixtures containing ionic liquids, *Fluid Phase Equilibria*, 324 (2012) 102–107.

[83] L.E. Ficke, H. Rodriguez, J.F. Brennecke, Heat capacities and excess enthalpies of 1-Ethyl-3-methylimidazolium-based ionic liquids and water, *J. Chem. Eng. Data*, 53 (2008) 2112–19.

[84] G. Garcia-Miaja, J. Troncoso, L. Romani, Excess enthalpy, density, and heat capacity for binary systems of alkyimidazolium-based ionic liquids + water, *J. Chem. Thermodyn.*, 41 (2009) 161–166.

[85] L. Dong, D.X. Zheng, Z. Wei, X.H. Wu, Synthesis of 1,3-dimethylimidazolium chloride and volumetric property investigations of its aqueous solution, *Int. J. Thermophys.*, 30 (2009) 1480–90.

[86] J. Lehmann, M.H. Rausch, A. Leipertz, A.P. Froba, Density and excess molar volumes for binary mixtures of ionic liquid 1-ethyl-3-methylimidazolium ethylsulfate with solvents, *J. Chem. Eng. Data*, 55 (2010) 4068–74.

- [87] E.J. Gonzalez, A. Dominguez, E.A. Macedo, Physical and excess properties of eight binary mixtures containing water and ionic liquids, *J. Chem. Eng. Data*, 57 (2012) 2165–76.
- [88] H. Rodriguez, J.F. Brennecke, Temperature and composition dependence of the density and viscosity of binary mixtures of water + ionic liquid, *J. Chem. Eng. Data*, 51(2006) 2145–55.
- [89] E. Vercher, A.V. Orchilles, P.J. Miguel, A. Martinez-Andreu, Volumetric and ultrasonic studies of 1-ethyl-3-methylimidazolium trifluoromethanesulfonate ionic liquid with methanol, ethanol, 1-propanol, and water at several temperatures, *J. Chem. Eng. Data*, 52 (2007) 1468–82.
- [90] D. Chakrabarty, A. Chakraborty, D. Seth, N. Sarkar, Effect of water, methanol, and acetonitrile on solvent relaxation and rotational relaxation of coumarin 153 in neat 1-hexyl-3-methylimidazolium hexafluorophosphate, *J. Phys. Chem. A*, 109 (2005) 1764–69.
- [91] S. Pandey, K.A. Fletcher, S.N. Baker, G.A. Baker, Correlation between the fluorescent response of microfluidity probes and the water content and viscosity of ionic liquid and water mixtures, *Analyst*, 129 (2004) 569–573.
- [92] L.P.N. Rebelo, V. Najdanovic-Visak, Z.P. Visak, M. Nunes da Ponte, J. Szydlowski, C.A. Cerdeirina, J. Troncoso, L. Romani, J.M.S.S. Esperanca, H.J.R. Guedes, H.C. de Sousa, A detailed thermodynamic analysis of [C₄mim][BF₄] + water as a case study to model ionic liquid aqueous solutions, *Green Chem.*, 6 (2004) 369–381.
- [93] K.R. Seddon, A. Stark, M.J. Torres, Influence of chloride, water, and organic solvents on the physical properties of ionic liquids, *Pure and Appl. Chem.*, 72 (2000) 2275–87.
- [94] Y.J. Kim, S. Kim, Y.K. Joshi, A.G. Fedorov, P.A. Kohl, Thermodynamic analysis of an absorption refrigeration system with ionic-liquid/refrigerant mixture as a working fluid, *Energy*, 44 (2012) 1005–1016.
- [95] D.S. Ayoub, M.R. Currás, D. Salavera, J. García, J.C. Bruno, A. Coronas, Performance analysis of absorption heat transformer cycles using ionic liquids based on imidazolium cation as absorbents with 2, 2, 2-trifluoroethanol as refrigerant, *Energy Conversion and Management*, 84 (2014) 512–523.
- [96] L. Huangfu, X. Wu, K. Guo, N. Ding, Heat characteristics research of a water-soluble ionic liquid as absorption workers, *Chinese Journal of Analytical Chemistry*, 50 (2011) 39–44.

CHAPTER TWO

THERMODYNAMIC OF BINARY SYSTEMS COMPOSED OF {WATER + IONIC LIQUID}

Thermodynamic and transport properties studies of binary systems provide information on the nature of interactions in the constituent binaries [1]. To design any process involving ionic liquids on an industrial scale, it is necessary to know a range of thermodynamic properties including vapor liquid equilibrium, heat capacity and excess enthalpy. Physical properties such as density are necessary for hydraulic calculations, fluid transport through pipes, mass and energy transfers. The aim of this chapter is to contribute to these efforts by establishment of various techniques as well as determination of thermodynamic and physico-chemical properties from a continuously growing portfolio of ionic liquids.

In this work, thermodynamic properties are determined for seven new binary systems composed of {H₂O + ILs}. This chapter covers in details all materials, experimental methods and equipment used during measurements. In addition, there is a brief discussion on thermodynamic theories and models including non-random two liquid (NRTL) model. The results obtained for each thermodynamic property are presented and discussed in detail.

II.1. Experimental section

II.1.1. Materials

The ILs used in this work can be classified as completely water miscible. The ILs were purchased commercially from Solvionic and Sigma-Aldrich. The physical properties of the studied ionic liquids are given in Table II.1. Chemicals such as n-hexane (purity > 99 %) and n-heptane (purity > 99 %) used for the validation of the vapor liquid equilibria apparatus were purchased from Sigma Aldrich. Tetrachloroethylene (purity > 99 %), n-undecane (purity > 99%) and n-dodecane (purity > 99 %) used as reference fluids for the densimeter were provided by Acros Organics and Sigma Aldrich, respectively. Ultrapure water was provided by Purelab

Ultra system ($> 18 \text{ M}\Omega\cdot\text{cm}$) (ELGA LabWater). Mercury with a purity of 99.99 % was purchased from Sigma Aldrich. To remove traces of water and volatile compounds, each ionic liquid was dried at moderate temperature (323.15 K) under vacuum during 24 h before all measurements. In addition, the structure of ILs was characterized with ^1H NMR (300 MHz, $(\text{CH}_3)_2\text{CO}$, ppm) prior to experimentation. Water content (Table II.1) was determined with a TIM550 Karl Fischer volumetric titration (Titralab) using the HYDRANAL-Solvent E as analyte (provided by Sigma-Aldrich).

II.1.2. Vapor Liquid Equilibrium (VLE)

While binary systems $\{\text{H}_2\text{O} + \text{IL}\}$ are asymmetric systems, the boiling-point method is more appropriate for VLE measurements of systems containing ILs [2-6]. In this work, two apparatus were used in order to have VLE data in large ranges of temperature, pressure and compositions.

Table II.1: Physical properties of studied ionic liquids.

Physical properties	[DMIM][MPh]	[DMIM][MeSO ₄]	[EMIM][MPh]	[EMIM][MeSO ₄]	[EMIM][EPh]	[BMIM][DCA]	[BMIM][Ac]
Structure							
Full name of IL	1,3-dimethylimidazolium methylphosphonate	1,3-dimethylimidazolium methyl sulfate	1-ethyl-3-methylimidazolium methyl phosphonate	1-ethyl-3-methylimidazolium methyl sulfate	1-ethyl-3-methylimidazolium ethyl phosphonate	1-butyl-3-methylimidazolium dicyanamide	1-butyl-3-methylimidazolium acetate
Color and shape (at 25 °C)	Yellow Liquid	Off-white Liquid	Yellow Liquid	Colorless Liquid	Colorless Liquid	Colorless Liquid	Yellow Liquid
Molecular formula	C ₆ H ₁₃ N ₂ PO ₃	C ₆ H ₁₂ N ₂ SO ₄	C ₇ H ₁₅ N ₂ PO ₃	C ₇ H ₁₄ N ₂ SO ₄	C ₈ H ₁₇ N ₂ PO ₃	C ₁₀ H ₁₅ N ₅	C ₁₀ H ₁₈ N ₂ O ₂
Purity (%)	> 98	99	> 98	99	> 98	99.5	> 98
Molecular weight (g.mol ⁻¹)	192.15	208.24	206.18	222.26	220.2	205.26	198.26
Melting point (°C)	n.d	n.d	n.d	n.d	n.d	-6	<-20
Density (g.cm ⁻³)	1.18 at 20°C	n.d	n.d	n.d	1.13 at 20°C	1.06 at 25°C	1.02 at 25°C
Viscosity (cP)	50.3 at 25°C	n.d	107 at 25°C	n.d	140 at 25°C	39.14 at 20°C	440 at 25°C
Decomposition temp. (°C)	> 200	n.d	n.d	n.d	n.d	300	220
Water content (ppm)	475.8	176.0	1161.3	133.0	704.4	1203.4	10056.4
Solubility in water	Miscible	Miscible	Miscible	Miscible	Miscible	Miscible	Miscible
Solubility in ethanol	Miscible	Miscible	Miscible	Miscible	Miscible	Miscible	Miscible
Solubility in acetone	Miscible	Miscible	Miscible	Miscible	Miscible	Miscible	Miscible
Source	Solvionic	Io-li-tec	Solvionic	Io-li-tec	Solvionic	Solvionic	Solvionic

II.1.2.1. Isobaric VLE apparatus

The apparatus for the VLE measurement is shown in Figure II.1. The apparatus mainly consists of an equilibrium vessel (250 cm^3), an oil bath, a condenser cooled by refrigerant (glycol aqueous solution), a temperature sensor (T900 series) thermocouple calibrated with high measuring accuracy ($T900 \pm 0.03\text{ }^\circ\text{C}$), a pressure transducer (Druck-PMP4010) with the accuracy of ($\pm 0.04\text{ \% FS BSL}$), a magnetic stirrer, and a vacuum pump.

The sample solution with an approximate volume of 50 cm^3 was loaded into the equilibrium vessel. The condenser is cooled with glycol solution to reach a sufficiently low temperature (267.15 K) necessary to minimize the amount of water vapor lost through the vacuum pump suction which could lead to variation of the initial composition of the sample solution.

In order to confirm the measuring accuracy, the seal fittings in the device should be kept in good connection to avoid air leakage. Vacuum is then established in the apparatus with the pump and the pressure set to the desired value with the valve. About 15 min. after the heating has been turned on, the temperature of the solution is generally stable and the vapor-liquid equilibrium is reached. By this means, a series of bubble point temperature and their corresponding vapor pressure were obtained. In order to check the reliability of the experimental apparatus, the bubble points of ultrapure water, n-hexane and n-heptane were measured. Measurements were in good agreement with the literature data.

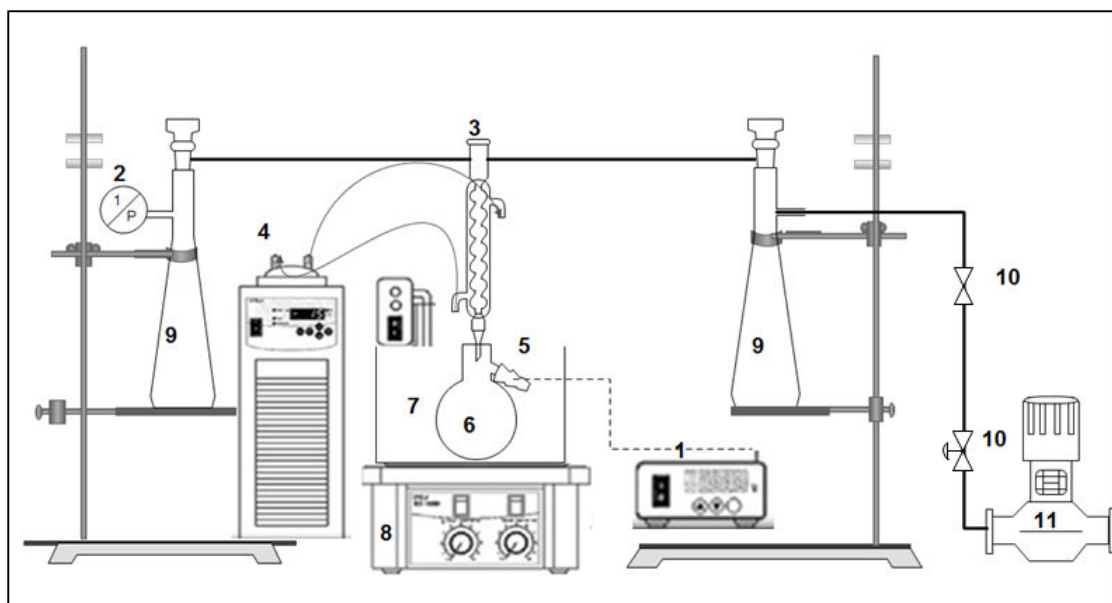


Figure II.1: Schematic diagram of isobaric VLE apparatus. 1. Temperature transmitter; 2. Pressure transducer (Druck-PMP4010); 3. Condenser; 4. Refrigerator; 5. Temperature sensor (T900 series); 6. Equilibrium vessel; 7. Thermostatic bath; 8. Magnetic stirrer; 9. Pressure buffer; 10. Vacuum control valve; 11. Vacuum pump.

This apparatus is not capable of measuring VLE in the IL rich composition range due to temperature instability at lower water mole fractions. Therefore, another method for VLE measurements adapted to the entire composition range is discussed in Section II.1.2.2.

II.1.2.2. Isothermal VLE measurement

The VLE measurements of binary mixtures have been performed in a glass cell by using a static method. The apparatus is shown schematically in Figure II.2. This apparatus can be applied for the measurement of reliable isothermal P-x data up to 323 K and 50 kPa. The experimental set up consists of a cell with an internal volume of about 15 cm³ kept at constant temperature using a thermostatic bath. The temperature inside the cell is measured by a platinum resistance thermometer PT-100 with an accuracy of ± 0.1 K.

The binary mixtures are weighted before introduction using an analytical balance with a resolution of $\pm 0.0003\text{g}$.

The homogeneity of the composition of each phase is attained with a teflon coated magnet in the cell during ten minutes before measurements. The vapor phase is exclusively composed of the solvent. The equilibrium in the cell is a rapid process. The pressure is monitored using a calibrated pressure sensor. The experiments were carried out in the temperature range $T = 298.15$ to 323.15 K . In order to avoid corrections on the liquid phase composition, the liquid volume of the binary mixture was much larger than the volume of the vapor phase. The experimental pressure is assessed to be reliable to within $\pm 1\%$ according to the test measurements. In order to calibrate the thermometer (T900) probe, a reference probe AVANTEC (Illkirch, France) was used. The (T900) instrument was supplied with a 5 points certificate of calibration. Uncertainty for pressure, temperature, weight readings and composition for VLE measurements are $\pm 0.4\text{ mbar}$, $\pm 0.06\text{ K}$, $\pm 0.0003\text{ g}$ and ± 0.005 , respectively.

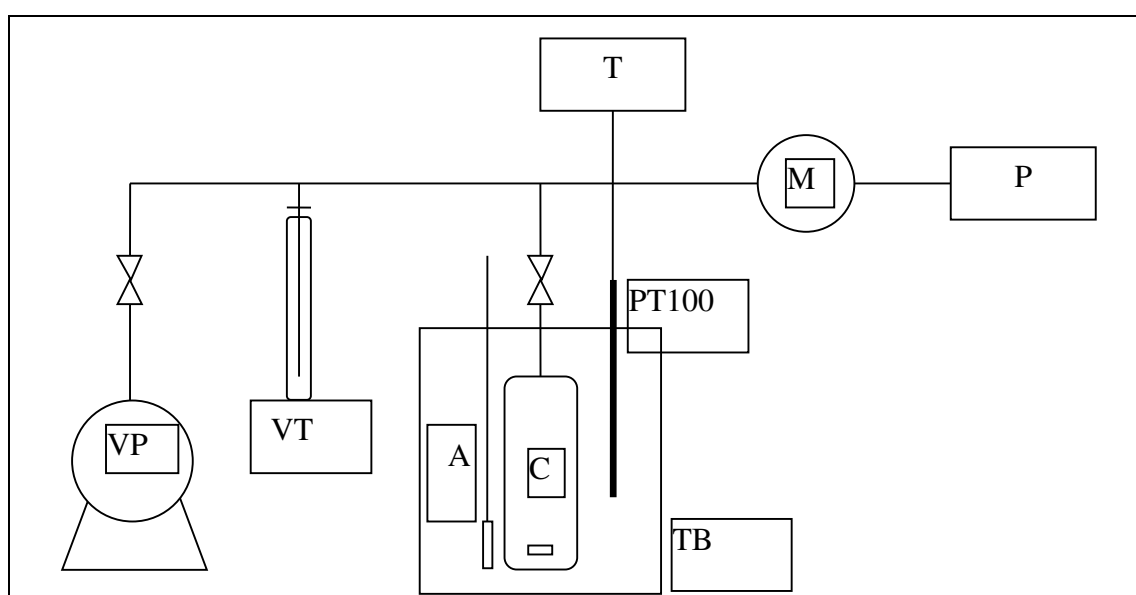


Figure II.2: Schematic representation of the VLE apparatus: VP: Vacuum Pump; VT: Vacuum Trap; A: Magnetic Stirrer; C: Equilibrium Cell; PT: Platinum resistance Thermometer (PT-100); T: Temperature Indicator; M: Calibrated Pressure Sensor, P: Digital Pressure Indicator and TB: Thermostatic Bath.

II.1.3. Heat capacity (C_p)

Measurements were performed using a Differential Scanning Calorimeter (microDSC III), manufactured by Setaram Co. (France), with Setsoft software data collection (Figure II.3). The heat capacity measurements were performed within temperatures ranging from 294.15 K to 338.15 K. The binary mixtures were prepared by weighing a precise amount of IL and water using a microbalance (Sartorius) with an uncertainty of $\pm 10^{-4}$ g. Good mixing was ensured by magnetic stirring. A sample of about (200-400 mg) was placed in a Hastelloy pan with a lid of the same material, and hermetically sealed (Figure II.4).



Figure II.3: Setaram microDSCIII Calorimeter.

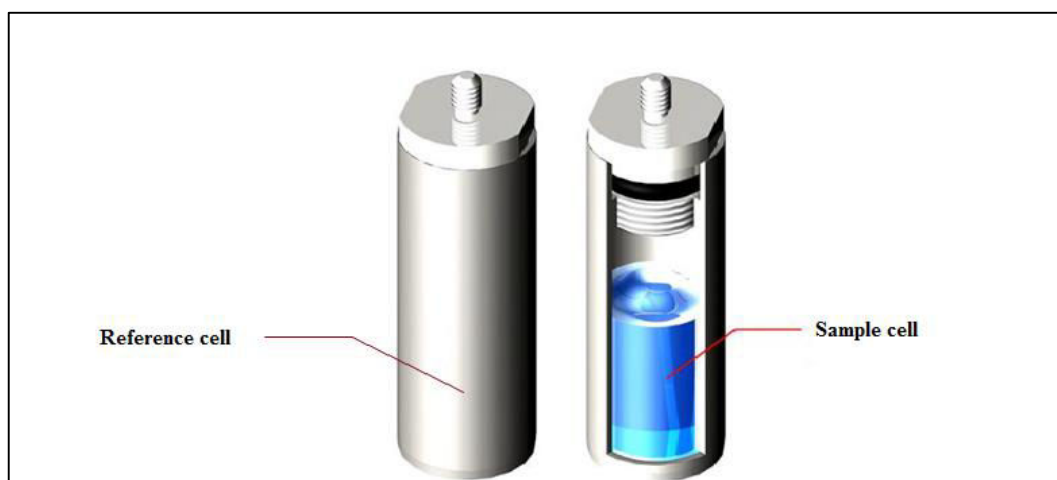


Figure II.4: MicroDSC III Hastelloy pans.

All the samples were prepared immediately prior to the measurements to avoid variations in composition due to evaporation or sorption of water. The heat capacity was determined by differential scanning method which is used extensively in literature. This method based on the comparison of the heat flow signal between the sample cell and the reference cell. The scanning rate is set at 0.3 K min^{-1} . The heat capacity of ultrapure water was measured in the temperature range from 294.15 K to 338.15 K in order to check the reliability of the experimental apparatus and experimental data were compared with the literature.

II.1.4. Density (ρ)

Experimental densities of the ILs were measured using an Anton Paar DMA 60 digital vibrating-tube densimeter, with a DMA 512P measuring cell at temperature range from 293.15 to 323.15 K at atmospheric pressure.

The working principle of an oscillation-type densimeter is based on the law of harmonic oscillation, in which a U tube is completely filled with the sample to be analyzed and subjected to an electromagnetic force. The measurement of the frequency and duration of vibration of the tube filled with the sample allows the determination of the density value of the sample.

The U tube oscillates at its fundamental frequency, which is a function of the system mass. If we suppose that the sample volume inside the cell is constant, it can be noticed that the oscillation frequency is therefore a function of the sample density. The oscillation period τ , is given by the following Eq.:

$$\tau = 2\pi \sqrt{\frac{\rho v + m}{c}} \quad (\text{II.1})$$

where ρ is the sample density, v the cell volume, m the cell mass and C the spring constant. Applying the square of Eq. (II.1) and substituting $A = \frac{4\pi^2 v}{c}$ and $B = \frac{4\pi^2 m}{c}$ we find:

$$\rho = \frac{(\tau^2 - B)}{A} \quad (\text{II.2})$$

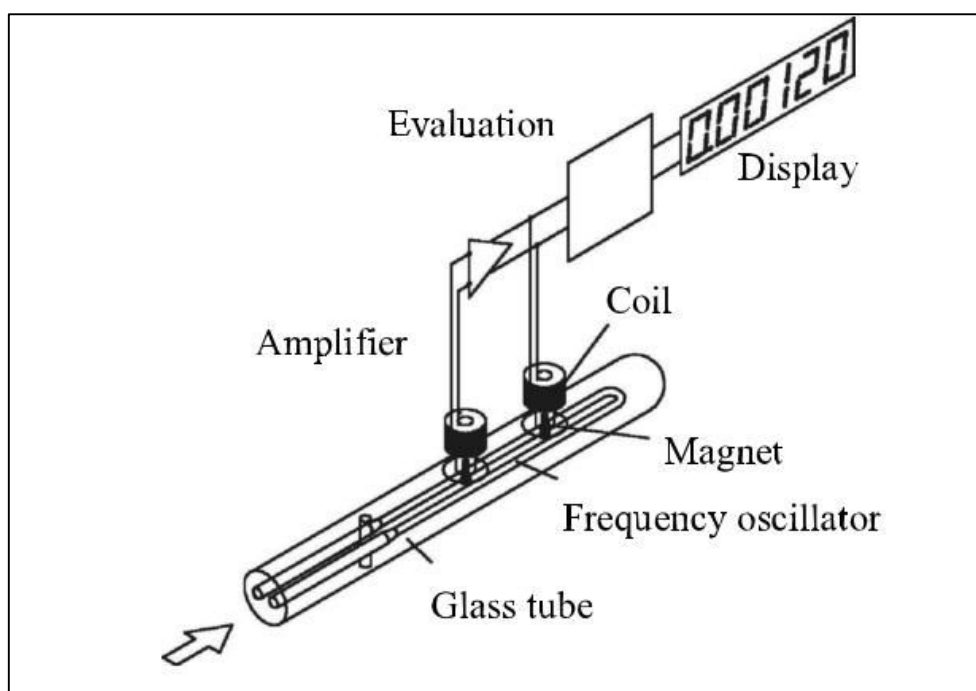


Figure II.5: DMA 512P measuring vibrating cell [7].

As shown in Figure II.5, the measuring cell consists of an oscillator U-shaped borosilicate glass tube that comprises about 0.7 ml of the sample. This tube has double walls and the space between them is filled with a gas with high coefficient of thermal conductivity. In that space is also placed a platinum resistance thermometer (PT-100) with an accuracy of ± 0.1 K that allows the temperature measurement of the fluid during the density measurement. Temperature of the cell is held constant to within ± 0.1 K by using a thermostatic bath with oil as the circulating fluid. The remaining instrumentation consists of a system of electronic excitement and electrical component that provide a signal transmission of the period for the processor unit, free of interferences. The vibrating U tube technology determines the density of a sample by:

$$\tau^2 = A \cdot \rho - B \quad (\text{II.3})$$

where ρ is density, τ is oscillation period, A and B are temperature-dependent coefficients determined by calibration using two substances of known densities. In this work, n-Dodecane, n-Undecane and tetrachloroethylene were used as reference fluids for the calibration of the vibrating-tube densimeter. The apparatus is precise to within 1×10^{-5} g·cm⁻³, and the uncertainty of the measurements was estimated to be better

than $\pm 1 \times 10^{-4} \text{ g} \cdot \text{cm}^{-3}$. The binary mixtures were prepared by weighing a precise amount of IL and water using a balance (Mettler TC-204) with an uncertainty of $\pm 10^{-4} \text{ g}$. Good mixing was ensured by using Teflon coated magnet stirring for 15 min. Charging of both pure compounds and mixtures into the vibrating tube is done carefully using a syringe to avoid occurrence of gas bubbles.

II.1.5. Excess enthalpy (H^E)

Excess enthalpy measurements of the ILs in water were obtained using the Calvet C80 calorimeter (Setaram Instrumentation). The apparatus operates between room temperature and 573 K. The calorimeter is based on the differential heat flux principle originally proposed by Tian and Calvet [8-10], which, under the correct setup, omits the need of knowing the heat capacity of the mixture.

The C80 calorimeter consists of a barrel-shaped, insulated enclosure attached to a base/console. The enclosure contains a large calorimetric block, within which two 12.5 cm^3 cylindrical wells are made for placement of the mixing cells. Highly sensitive heat flow detectors in the form of thermocouples surround the outer walls of the wells. These detectors send out signals upon detecting thermal exchanges between the cell and the calorimetric block, such as those occur during mixing processes. Within the calorimetric block, a Pt-100 platinum probe monitors the sample temperature, while a Pt-200 platinum probe is used to control the temperature. This setup forms a compact assembly heated by a peripheral resistor. A jacket surrounding the calorimetric block allows the circulation of cool air initiating from the interior fan, for the purpose of ventilation. The data signals are displayed in real time on a computer with the Setsoft software (version. 2000, from Setaram Instrumentation).

In this work, we used the reversal mixing cells made of stainless steel or hastelloy (Figure II.6). The cell is designed such that the assembled cell, prior mixing, consists of two liquid chambers, stacked on top of each other, with a button covering the top chamber. Upon rotation, the entire stacked structure within the cell collapses, and the two liquids contact. The higher density component (IL) is usually placed in the bottom chamber. In addition, mercury was used to completely separate the two liquids prior to mixing. The measurements were performed at atmospheric pressure for temperature

(312.92 K) and over the whole range of mole fraction. The mixing occurred using continuous reversal which consisted of rotating the entire cell 180°, the energy resulting from the rotation of the liquids has been verified to be negligible. The bottom section of the cell have a stainless steel lid that falls off with the 180° turn and serves as a “stirrer”.

The experimental method included three steps: a dynamic segment ramping up to the desired temperature; a one-hour isotherm prior to mixing followed by a two-hour isotherm after mixing. An integration of the heat flow peak produces the excess enthalpy, and each composition measured is repeated at least two times. The experimental uncertainty associated with this method is estimated to be $\pm 1\%$ considering the propagation of error and the ability to reproduce measurements with different samples over time.

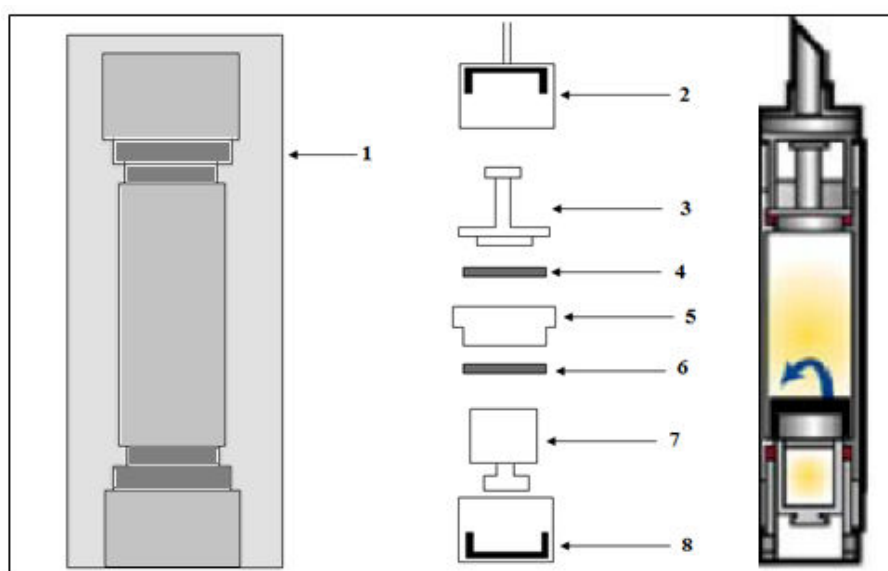


Figure II.6: Schematic diagram of C80 reversal mixing cell. 1. body of the stacked cell .2. vessel stopper .3. stainless steel stopper .4. Teflon O-ring .5. lid .6. Teflon O-ring .7. bottom chamber .8. bottom compartments of the cell.

II.2. Results and discussion

II.2.1. Vapor Liquid Equilibrium (VLE)

In order to check the reliability of the VLE measurement apparatuses, the vapor pressure of ultrapure water was measured. An average relative deviation (ARD) between the experimental data and those published in literature [11] were 0.35 %. These results confirm that these apparatuses are reliable and applicable for the experimental measurements (Table II.2).

Table II.2: Comparison of the saturated vapor pressure of pure water (P^{exp}) measured in this work and those published (P^{lit}) in the literature [11].

T (K)	P^{exp} (kPa)	P^{lit} (kPa)	ΔP (%)
319.15	10.00	10.01	0.05
333.33	19.99	19.94	0.23
333.35	20.00	19.96	0.19
342.45	30.01	30.04	0.10
349.31	40.09	40.23	0.36
354.65	49.97	50.07	0.20
354.66	50.00	50.09	0.18
358.88	60.10	59.23	1.45
ARD			0.35

All ILs studied in this work are completely miscible with water. Methods used and ranges of data at which the VLE of the 7 binary systems {H₂O + ILs} were measured are listed in Table II.3. All the experimental results are listed in Annex II. No VLE data for the seven binary systems studied in this work were found in the literature.

For methylsulfate based ionic liquids, isobaric method was used in the range of mole fractions of water from approximately 0.7 to 1 due to temperature instability of

temperature at lower water mole fractions, likely due to higher viscosity of the more concentrated IL and water mixtures [12, 13].

Table II.3: Summary of VLE measurements for the studied binary systems {H₂O (1) + ILs (2)}.

Binary system	Measuring method	Range of data		
		T(K)	P (kPa)	x ₂
{H ₂ O + [DMIM][MPh]}	Isobaric	322.42-396.25	11.84-91.60	0.06-0.40
{H ₂ O + [DMIM][MeSO ₄]}	Isobaric & Isothermal	298.35-382.11	0.58-90.30	0.10-0.80
{H ₂ O + [EMIM][MPh]}	Isobaric	329.37-396.49	11.92-91.18	0.10-0.41
{H ₂ O + [EMIM][MeSO ₄]}	Isobaric & Isothermal	293.15-379.40	0.87-90.11	0.10-0.80
{H ₂ O + [EMIM][EPh]}	Isobaric	326.28-392.51	10.69-73.01	0.10-0.40
{H ₂ O + [BMIM][Ac]}	Isobaric	324.16-389.62	10.48-79.60	0.11-0.30
{H ₂ O + [BMIM][DCA]}	Isobaric	319.44-381.57	11.12-90.39	0.10-0.31

The data set shows that the vapor pressure of the binary system decreases when the IL content increases in the mixture. The permanent ion–dipole interaction between the ionic liquid and water evokes a strong ability to absorb water, which is a very important property of a working pair for the absorption heat pump and absorption heat transformers.

Several studies have suggested that the water activity coefficient γ_1 may be related to the ionic liquids hydrophobicity [12, 14]. All the studied ILs are considered hydrophilic since they are fully soluble with water.

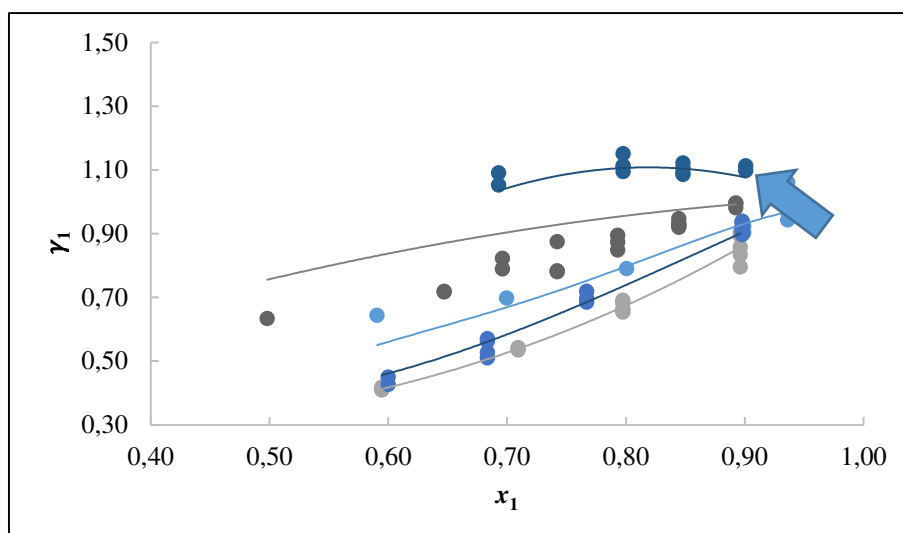


Figure II.7: Experimental γ_1 values for the binary systems $\{\text{H}_2\text{O} (1) + \text{ILs} (2)\}$ as a function of mole fraction of water (●) $\{\text{H}_2\text{O} + [\text{DMIM}][\text{MPh}]\}$; (●) $\{\text{H}_2\text{O} + [\text{EMIM}][\text{MPh}]\}$; (●) $\{\text{H}_2\text{O} + [\text{EMIM}][\text{EPh}]\}$; (●) $\{\text{H}_2\text{O} + [\text{DMIM}][\text{MeSO}_4]\}$; (●) $\{\text{H}_2\text{O} + [\text{BMIM}][\text{DCA}]\}$; —, calculated by NRTL equation.

In this study, most of activity coefficients of the investigated binary systems are lower than the unity indicating that these systems present a negative deviation from the ideal solution behavior. This behavior was also found for various families of ILs in the literature [3, 4]. The higher the content of IL is, the larger the deviation from the Raoult's law. The corresponding experimental activity coefficients of water as a function of mole fraction are shown in Annex II. for all the binary systems.

The {water + alkylphosphonates based ionic liquids} systems have activity coefficients of water smaller than unity over the entire composition range indicating stronger unlike interactions (IL/water) than like interactions (IL/IL and water/water).

On the other hand, [BMIM][DCA] shows less negative behavior than the rest of the investigated ILs (the maximum activity coefficient value is 1.17) (Figure II.7). There are two possible explanations for this behavior. The first reason may be the length of the alkyl chain. This elongation gives rise to the increase in the degree of ion association in the liquids, mainly caused by the van der Waals interactions between alkyl chains, hence increasing activity coefficient of the mixture [12]. The second explanation may be the presence of two cyanide groups $[\text{CN}]^-$ in the IL anion. Therefore, this does not enhance its ability to establish H-bonds with water but decreases its polarity [14].

Passos *et al.* [14] reported a similar behavior in the water activity coefficient of aqueous solutions of [BMIM][SCN]. They found that its activity coefficient is slightly positive reflecting the weaker IL–water interaction. Similar behavior was observed by Krolikowska *et al.* [15] for [BMPIP][DCA] IL and they referred this to increasing the alkyl chain length in an IL which causes the IL to become more hydrophobic thus increases the activity coefficient.

It was found that with respect to the anion, the activity coefficients and vapor pressure decrease as follows:

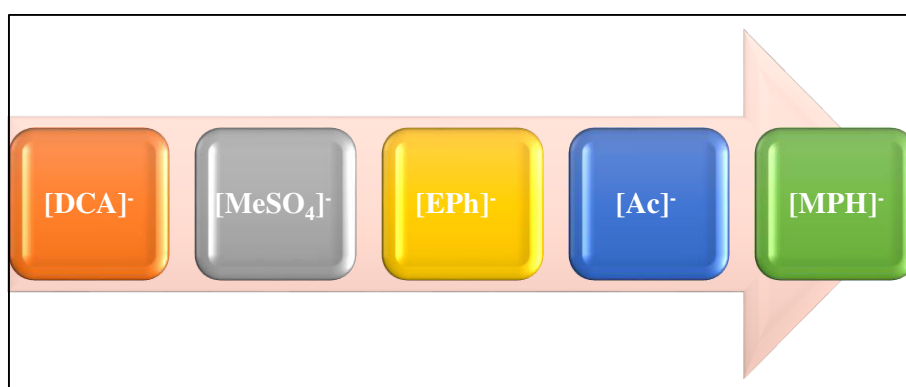


Figure II.8: The reduction trend of the activity coefficients and vapor pressure with respect to the anion type.

This means that methylphosphonate anion leads to a greater interaction with water molecules corresponding to a lower activity coefficient and lower vapor pressure. Methylsulfate anion $[\text{MeSO}_4]^-$ corresponds to a moderate decrease in vapor pressure of H_2O . Then, with increasing compactness of the anion (for example, $[\text{Ac}]^-$) the vapor pressure and activity coefficient can be lower. Furthermore, it was noticed that ionic liquids with shorter alkyl chain have a stronger ability to decrease the vapor pressure of water. This ability follows the order: $[\text{DMIM}]^+ > [\text{EMIM}]^+ > [\text{BMIM}]^+$. This is referred to the ability of ionic liquids with longer alkyl chain length to be soluble in water but this solubility has low dependence on temperature. Therefore, ionic liquids with shorter cation alkyl chain are more preferred due to their solubility dependence on temperature. Representative results for each system studied are shown in Figures II.9-II.12.

The bubble-point pressure of a binary mixture may be estimated using the classical Eq. (II.4):

$$P = \frac{P_1^{\text{sat}} \cdot x_1 \cdot \gamma_1}{C_1} + \frac{P_2^{\text{sat}} \cdot x_2 \cdot \gamma_2}{C_2} \quad (\text{II.4})$$

$$\text{with } C_i = \frac{\phi_i^{\text{vap}}(T, P, y_1, y_2)}{\phi_i^*(T, P_i^{\text{sat}})} \cdot \underbrace{\exp\left(\frac{1}{RT} \int_P^{P_i^{\text{sat}}} v_{\text{liq}}^* dP\right)}_{F_p} \quad i = 1, 2 \quad (\text{II.5})$$

where P_i^{sat} is the vapor pressure of the pure component i at system temperature, x_i represents mole fraction of component i in the liquid phase, ϕ_i^{vap} is the fugacity coefficient of component i in the gas phase, ϕ_i^* is the fugacity coefficient of pure component i at the saturation and F_p is the Poynting correction factor. Since the pressures are sufficiently low, the fugacity coefficients may be taken equal to 1 and the Poynting correction neglected.

Due to the low volatility of ionic liquids, we may assume that P_2^{sat} is zero for the ionic liquid and Eq (II.4) is then reduced to:

$$P = P_1^{\text{sat}} \cdot x_1 \cdot \gamma_1 \quad (\text{II.6})$$

The activity coefficient of the solute in the mixture was correlated using the NRTL model [16]:

$$\ln \gamma_1^{\text{NRTL}} = x_2^2 \left[\tau_{21} \left(\frac{G_{21}}{x_1 + x_2 G_{21}} \right)^2 + \frac{\tau_{12} G_{12}}{(x_2 + x_1 G_{12})^2} \right] \quad (\text{II.7})$$

$$\text{with } G_{ij} = \exp(-\alpha_{ij}\tau_{ij}), \tau_{ij} = \frac{g_{ij} - g_{jj}}{RT} = \frac{\Delta g_{ij}}{RT} \quad (\text{II.8})$$

The NRTL parameters (g_{12} - g_{22} , g_{21} - g_{11}) are those which minimize the following objective function:

$$OF = \sum_{i=1}^N (\gamma_i^{calc} - \gamma_i^{exp})^2 \quad (\text{II.9})$$

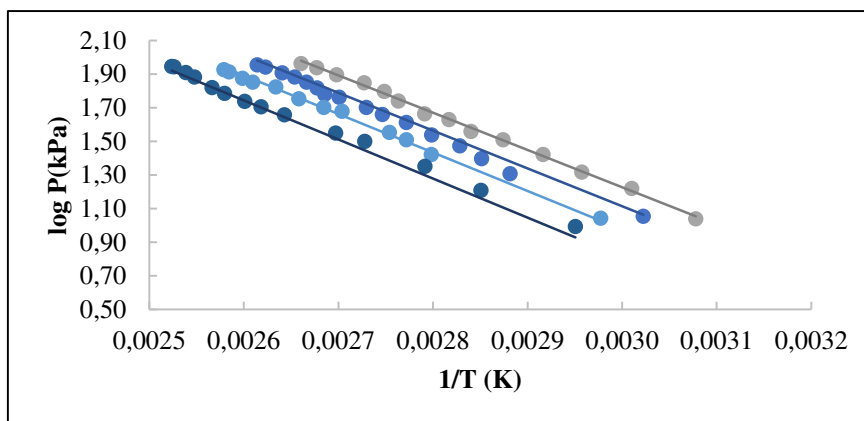
In order to consider temperature dependency, a linear temperature dependent relation for the interaction parameters Δg_{ij} was used:

$$\Delta g_{ij} = a_{ij} + b_{ij}T \quad (\text{II.10})$$

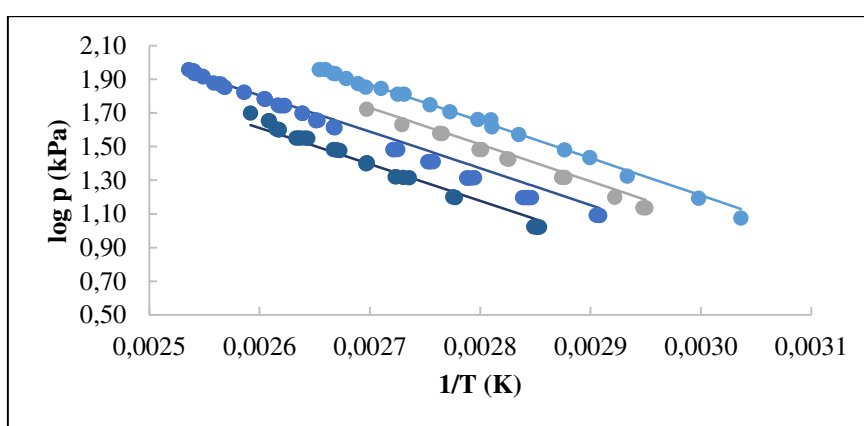
In this study, the non-randomness parameter α of the NRTL model was set equal to 0.3. This means that a total of four parameters per system have to be fitted. The regressed NRTL parameters (a_{12} , a_{21} , b_{12} , b_{21}) are given in Table (II.4) for each system. The predicted bubble-point curves are in good agreement with experimental data. The adjustable NRTL parameters were obtained by fitting the whole experimental vapor pressure data for all experimental temperatures and composition range using the least square method. The average relative deviations (ARD) for the 7 investigated systems given in Table II.4 indicate that NRTL model can be used to represent {H₂O + ILs} binary systems with a good accuracy.

Table II.4: NRTL parameters of the VLE data for {H₂O (1) + IL (2)}.

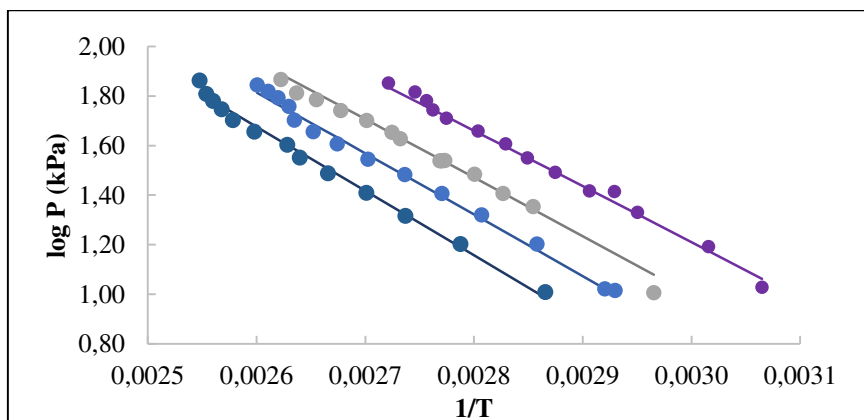
Binary system	$a_{12}/(\text{J.mol}^{-1})$	$a_{21}/(\text{J.mol}^{-1})$	$b_{12}/(\text{J.mol}^{-1})$	$b_{21}/(\text{J.mol}^{-1})$	α	(ΔP %)
{H ₂ O + [DMIM][MPh]}	-1442.2	-4996.0	20.6	-6.8	0.3	4.5
{H ₂ O + [DMIM][MeSO ₄]}	16520.4	-11074.1	-65.3	78.1	0.3	8.4
{H ₂ O + [EMIM][MPh]}	1.0	0.9	19.3	-24.8	0.3	9.3
{H ₂ O + [EMIM][MeSO ₄]}	100647.5	-15756.1	-319.8	47.0	0.3	9.6
{H ₂ O + [EMIM][EPh]}	-27575.3	-7654.0	74.0	1.8	0.3	4.0
{H ₂ O + [BMIM][AC]}	0.9	1.0	-39.0	-20.8	0.3	4.4
{H ₂ O + [BMIM][DCA]}	-12601.0	4341.8	85.1	-31.9	0.3	2.4



(a)

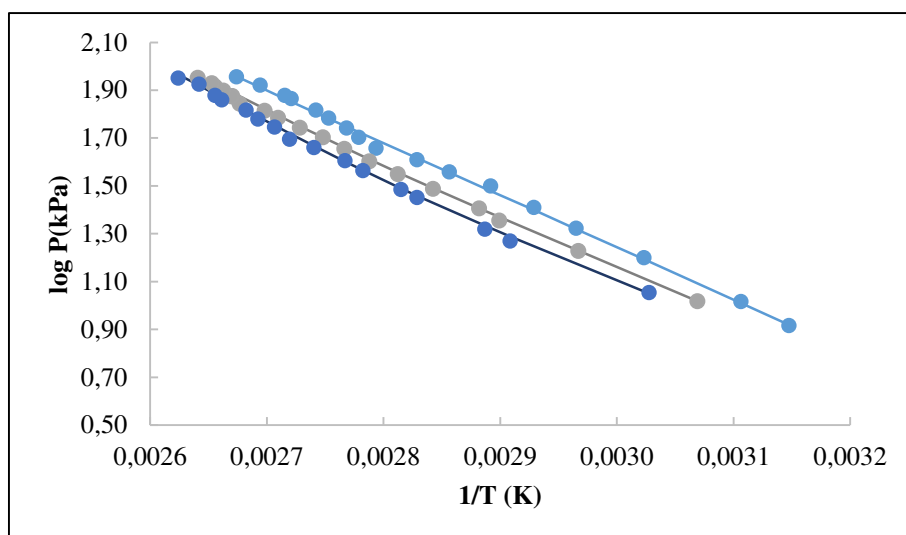


(b)

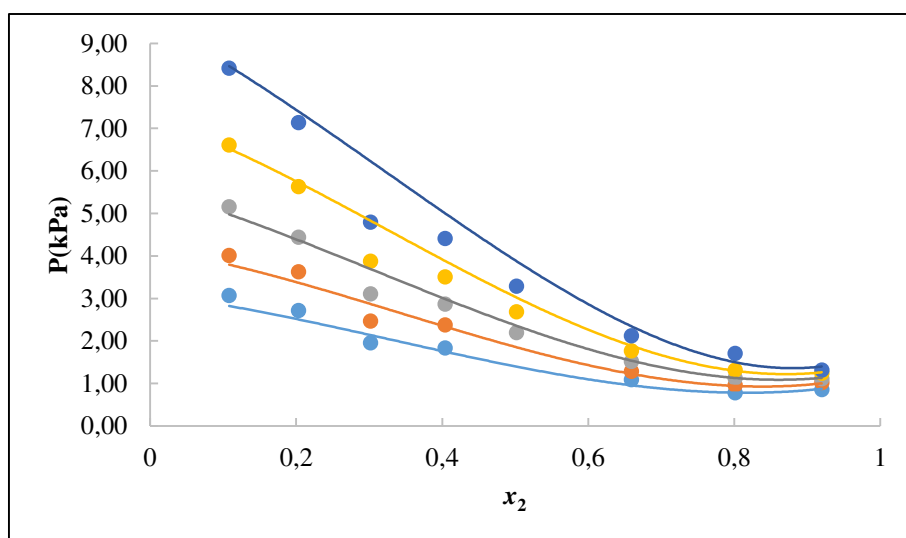


(c)

Figure II.9: Experimental VLE data for the investigated binary systems $\{\text{H}_2\text{O} (1) + \text{IL} (2)\}$ symbols are experimental data for different mole fractions of ILs and —, calculated by NRTL equation: (a) [DMIM][MPh] (●) $x_2 = 0.1$; (●) $x_2 = 0.19$; (●) $x_2 = 0.3$; (●) $x_2 = 0.4$, (b) [EMIM][MPh] (●) $x_2 = 0.1$; (●) $x_2 = 0.2$; (●) $x_2 = 0.29$; (●) $x_2 = 0.4$, (c) [EMIM][EPh] : (●) $x_2 = 0.1$; (●) $x_2 = 0.23$; (●) $x_2 = 0.31$; (●) $x_2 = 0.4$.

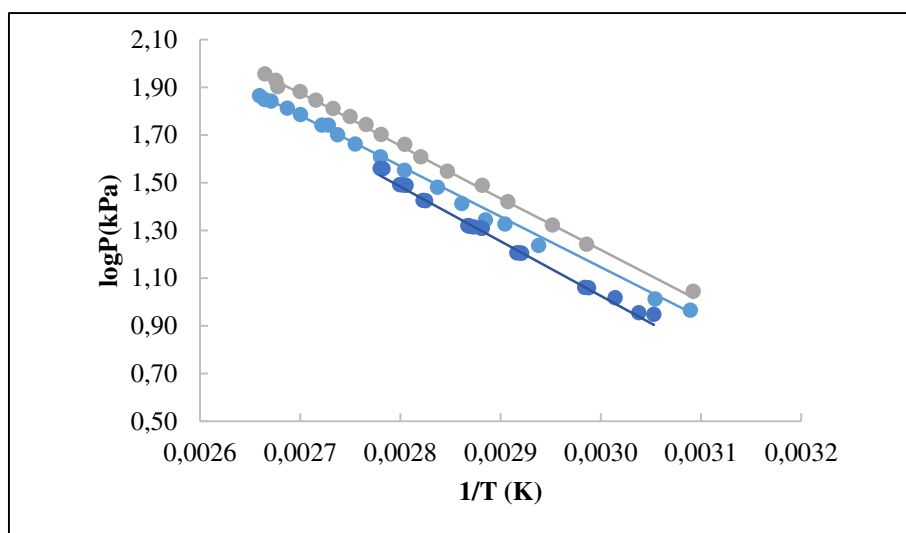


(a)

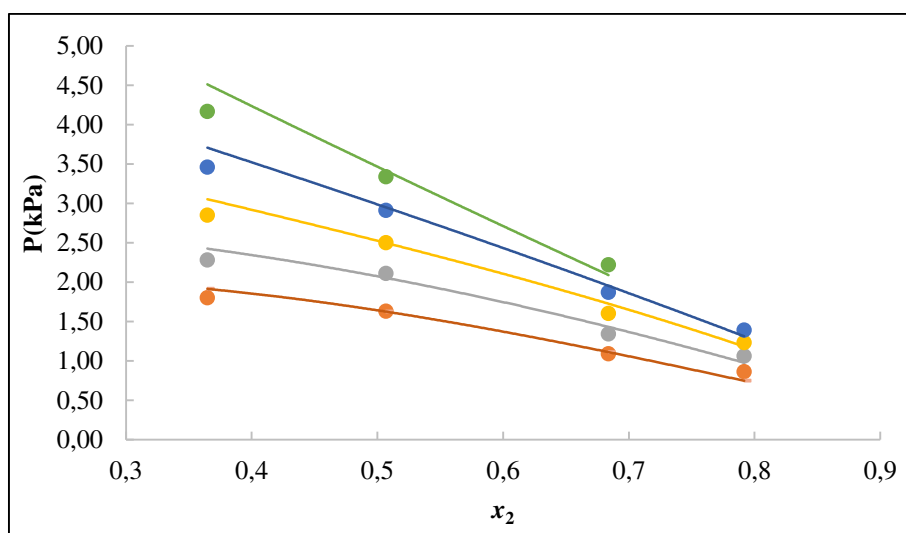


(b)

Figure II.10: Experimental VLE data for the investigated binary systems $\{\text{H}_2\text{O} (1) + [\text{DMIM}][\text{MeSO}_4] (2)\}$: (a) Isobaric VLE data symbols are experimental data at different mole fractions of $[\text{DMIM}][\text{MeSO}_4]$: (●) $x_2 = 0.1$; (●) $x_2 = 0.2$; (●) $x_2 = 0.25$; —, calculated by NRTL equation, (b) Isothermal VLE for: (●) $T = 298.15 \text{ K}$; (●) $T = 303.15 \text{ K}$; (●) $T = 308.15 \text{ K}$; (●) $T = 313.15 \text{ K}$; (●) $T = 318.15 \text{ K}$; —, calculated by NRTL.

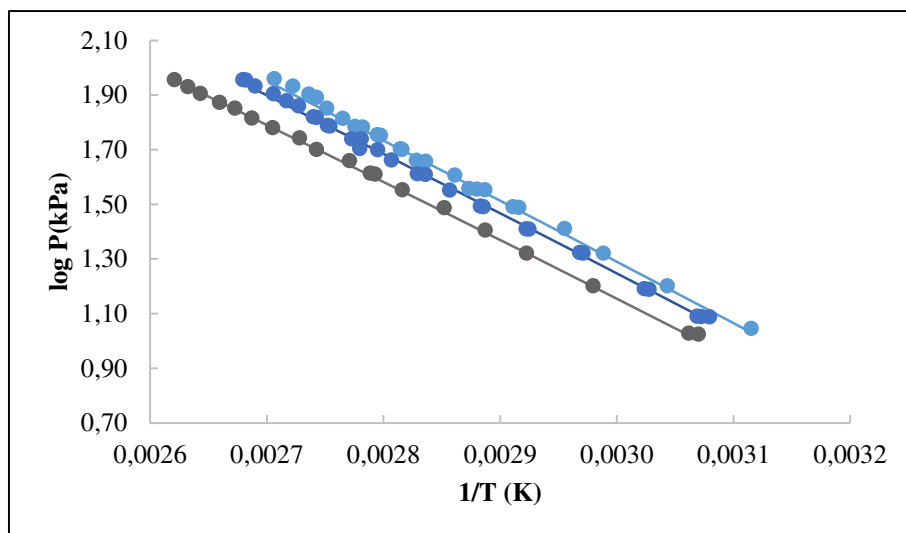


(a)

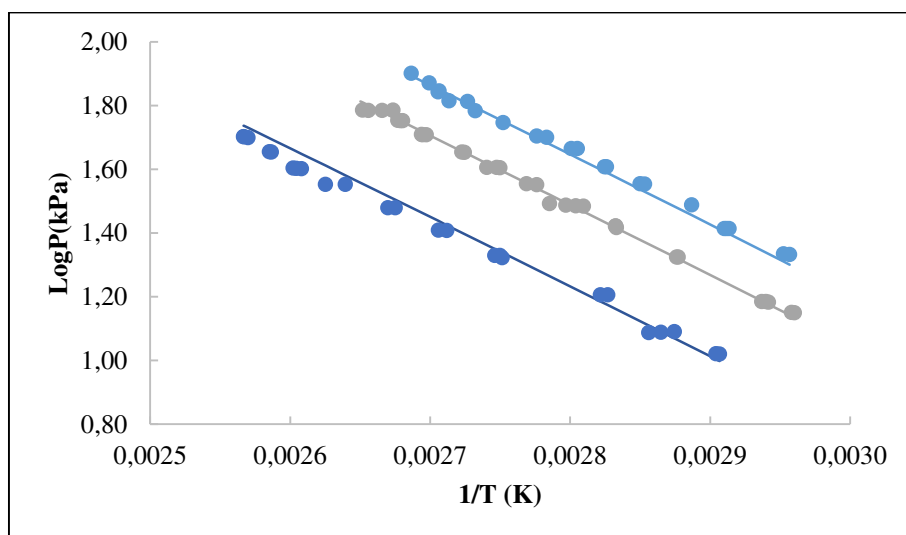


(b)

Figure II.11: Experimental VLE data for the investigated binary systems {H₂O (1) + [EMIM][MeSO₄] (2)}: (a) symbols are experimental data for different mole fractions of [EMIM][MeSO₄]: (●) $x_2=0.15$; (●) $x_2=0.25$; (●) $x_2=0.35$; —, calculated by NRTL equation, (b) Isothermal VLE for: (●) $T=293.15$ K; (●) $T=298.15$ K; (●) $T=303.15$; (●) $T=308.15$; (●) $T=313.15$ K; —, calculated by NRTL.



(a)



(b)

Figure II.12: Experimental VLE data for the investigated binary systems $\{\text{H}_2\text{O} (1) + \text{IL} (2)\}$ symbols are experimental data at different mole fractions of ILs and —, calculated by NRTL equation: (a) [BMIM][DCA]: (●) $x_2=0.1$; (●) $x_2=0.2$; (●) $x_2=0.3$, (b) [BMIM][Ac]: (●) $x_2=0.1$; (●) $x_2=0.2$; (●) $x_2=0.3$.

II.2.2. Heat capacity (C_p)

In order to check the reliability of the apparatus, heat capacity of ultrapure water was measured and compared to literature. Experimental results listed in Table II.5 are in good agreement with literature [4] within an ARD of 0.35%.

Table II.5: Mass heat capacity comparison of ultrapure water [4].

T(K)	C_p^{exp} (J.g ⁻¹ .K ⁻¹)	C_p^{lit} (J.g ⁻¹ .K ⁻¹)	$\Delta\%$
303.15	4.17	4.19	0.43
313.15	4.18	4.19	0.34
323.15	4.18	4.20	0.32
333.15	4.19	4.20	0.32
ARD			0.35

The molar heat capacities of the six investigated binary systems were measured at temperatures ranging from 294.15 K to 338.15 K, under atmospheric pressure and over the whole range of composition.

It can be observed from Annex II and Figures II.13-II.15 a slight increase of C_p with increasing temperature. It is clear that the value of C_p for pure ILs is much greater than that of water. This is expected since C_p is dependent on the number of translational, vibrational, and rotational energy storage modes in the molecule, and the molecular weight of the ILs is much greater than water. The heat capacity of the mixtures decreases with increasing water mole fraction. This trend agrees with those reported in the literature [12, 17, 18]. For the purpose of evaluating the molar heat capacity of pure ILs and their binary systems, the present C_p data were correlated as a function of temperature and composition using the following polynomial Eq. [4]:

$$C_p = \sum_{i=0}^3 (A_i + B_i T) x_2^i \quad (\text{II.11})$$

where C_p is the heat capacity in J.mol⁻¹.K⁻¹, A_i and B_i are the regression parameters, T is the absolute temperature in K, and x_2 is the mole fraction of IL. The regression parameters were determined by a least-square method and are listed in Table II.6. The

(ARD) between the experimental and calculated values ranges between 0.30 and 0.60 %. Based on the overall ARD% for the total data points, it can be said that polynomial function (II.11) successfully correlated the C_p of the binary system studied in this work.

If molar heat capacity is converted into mass heat capacity, we will find that the C_p values for ILs are lower than those for water [12]. This means less energy will be required to produce a certain temperature increase for a given mass of IL than for the same mass of water. Generally speaking, the heat capacities for all the binary systems studied are low, which is beneficial to heat transfer, reduce energy consumption and improves the coefficient of performance in absorption heat transformer cycle [12].

Table II.6: Parameters for the correlation of Eq. (II.11).

Binary system {H ₂ O (1) + IL (2)}	A ₀	A ₁	A ₂	A ₃	B ₀	B ₁	B ₂	B ₃	ΔC _p %
{H ₂ O + [DMIM][MeSO ₄]}	38.06	293.05	-6.40	-84.48	0.15	-0.38	0.63	-0.12	0.40
{H ₂ O + [EMIM][MeSO ₄]}	84.36	7.23	336.24	-78.13	-0.01	0.88	-1.15	0.35	0.93
{H ₂ O + [EMIM][EPH]}	213.10	-1324.07	3498.91	-2187.60	-0.48	5.53	-11.91	7.41	2.68
{H ₂ O + [BMIM][DCA]}	82.70	78.46	337.32	-223.31	0.00	0.68	-1.46	1.00	0.68

From heat capacity experimental data of pure IL and IL mixtures, the excess heat capacities C_p^E can be calculated by subtracting off the ideal mixture component:

$$C_p^E = C_p - \sum_i x_i * C_{p,i} \quad (\text{II.12})$$

C_p^E were fitted to Redlich–Kister polynomials of the form:

$$C_p^E = x_2 * (1 - x_2) * \sum_i^n B_i * (x_1 - x_2)^{(i-1)} \quad (\text{II.13})$$

$$\text{where } B_i = a_i + b_i * T(K) \quad (\text{II.14})$$

C_p^E is the excess heat capacity $\text{J.mol}^{-1}.\text{K}^{-1}$ of the mixture; x_i is the mole fraction of species i (where $i = 1, 2$), a_i and b_i are the regressive parameter, T is the absolute temperature in K. The number of terms (B_i), in Eq. (II.14), which should be used to represent C_p^E depends on the degree of complexity of the binary systems. In this work, five terms in Eq. (II.13) were found to satisfactory correlate the present measurements as indicated by a reasonable overall ARD C_p^E for the total data points (Table II.7) . As can be seen in Figures. II.16–II.18, Eq. (II.13) successfully represented the temperature and composition dependence of the excess molar heat capacity for the studied binary systems.

Table II.7: Parameters of Eq. (II.13).

Binary system	a ₁	a ₂	a ₃	a ₄	a ₅	b ₁	b ₂	b ₃	b ₄	b ₅	ΔC _p ^E %	
{H ₂ O (1)+ [DMIM][MeSO ₄] (2)}	53.18	146.60	-	-	1614.74	-0.13	-0.64	0.36	6.38	-4.79	34.39	
{H ₂ O (1) + [EMIM][MeSO ₄] (2)}	-	198.05	373.64	521.69	1334.91	1835.79	0.57	-1.15	2.26	4.43	-6.75	20.40
{H ₂ O (1) + [EMIM][EPh (2)]}	63.89	-249.93	585.71	1372.97	899.42	-0.12	0.65	-3.37	5.29	-1.11	41.02	
{H ₂ O (1) + [BMIM][DCA] (2)}	9.00	11.72	90.32	-383.40	212.95	-0.05	0.19	0.02	1.07	-0.88	16.53	

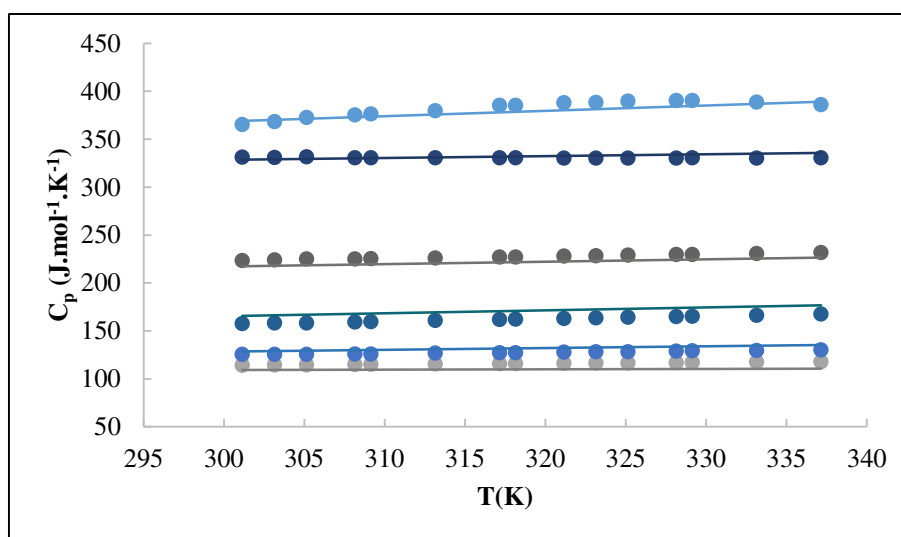
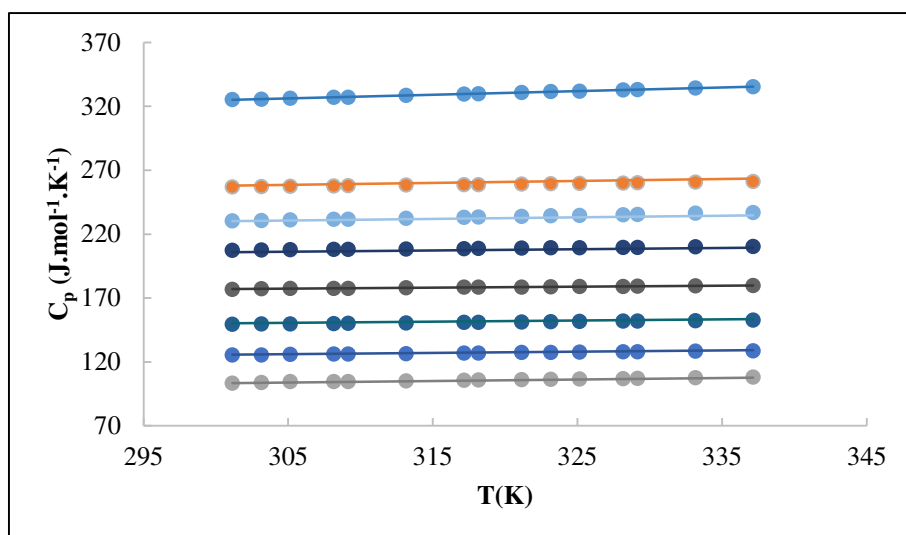
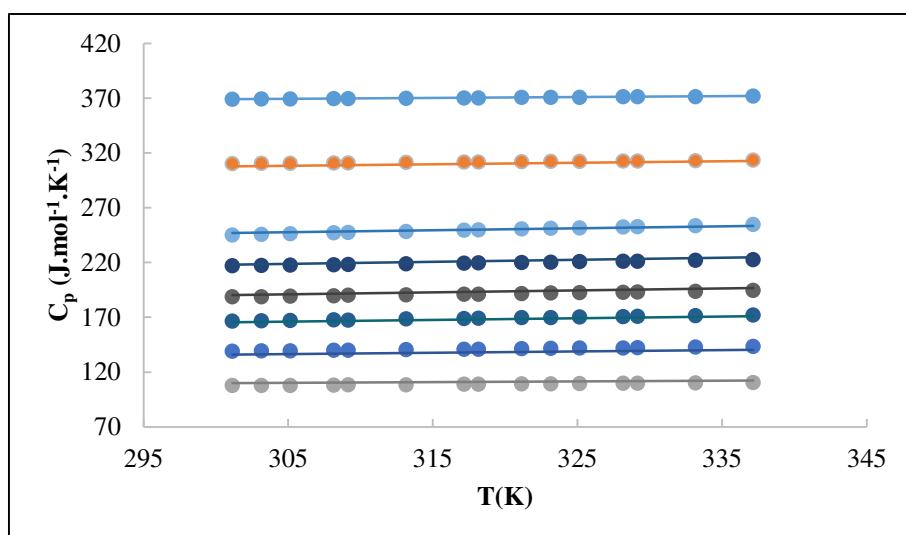


Figure II.13: Heat capacities of {H₂O (1) + ILs (2)} versus temperature at different mole fractions of IL: (a) {H₂O (1) + [EMIM][EPh] (2)} (●) $x_2=1$; (●) $x_2=0.1$; (●) $x_2=0.2$; (●) $x_2=0.3$; (●) $x_2=0.48$; (●) $x_2=0.87$; —, calculated by polynomial equation (II.11).



(a)



(b)

Figure II.14: Heat capacities of {H₂O (1) + ILs (2)} versus temperature at different mole fractions of IL: (a) {H₂O (1) + [DMIM][MeSO₄] (2)} (●) $x_2=1$; (●) $x_2=0.1$; (●) $x_2=0.2$; (●) $x_2=0.3$; (●) $x_2=0.4$; (●) $x_2=0.5$; (●) $x_2=0.6$; (●) $x_2=0.7$, (b) {H₂O (1) + [EMIM][MeSO₄] (2)} (●) $x_2=1$; (●) $x_2=0.1$; (●) $x_2=0.2$; (●) $x_2=0.3$; (●) $x_2=0.4$; (●) $x_2=0.5$; (●) $x_2=0.6$; (●) $x_2=0.8$; —, calculated by polynomial equation (II.11).

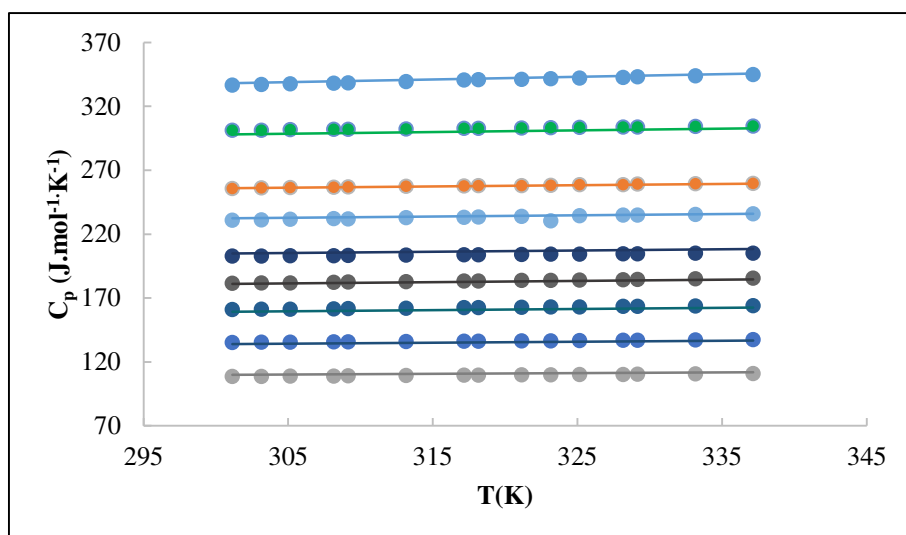


Figure II.15: Heat capacities of {H₂O (1) + [BMIM][DCA] (2)} versus temperature at different mole fractions of the IL: (●) $x_2=1$; (●) $x_2=0.1$; (●) $x_2=0.2$; (●) $x_2=0.3$; (●) $x_2=0.4$; (●) $x_2=0.5$; (●) $x_2=0.6$; (●) $x_2=0.7$; (●) $x_2=0.86$; —, calculated by polynomial equation (II.11).

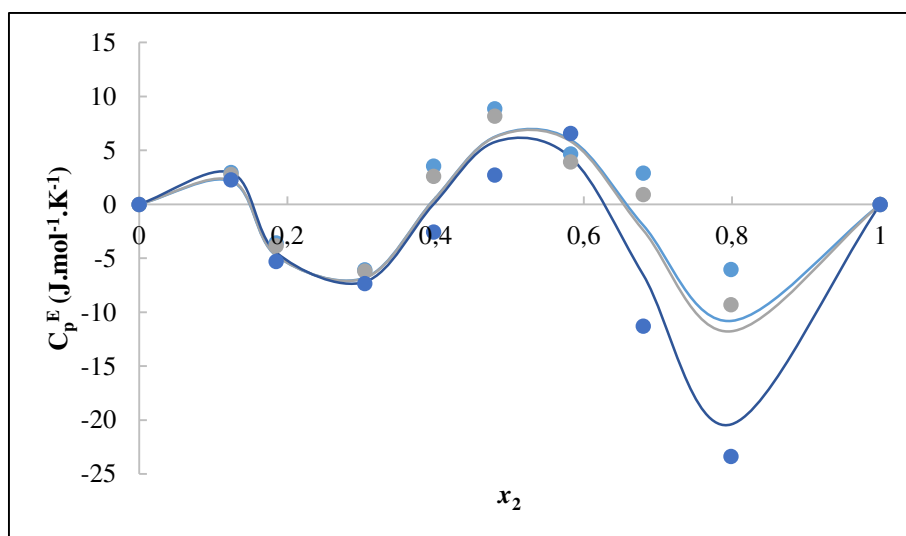
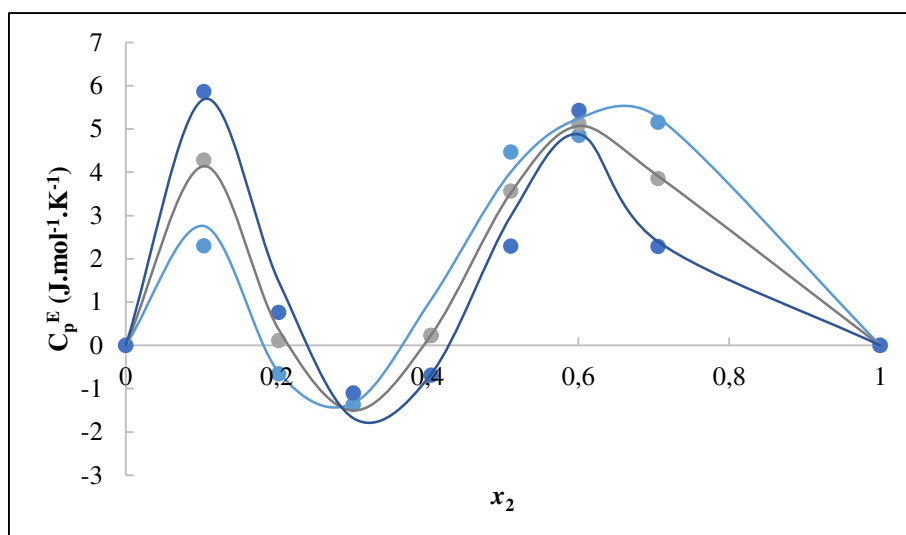
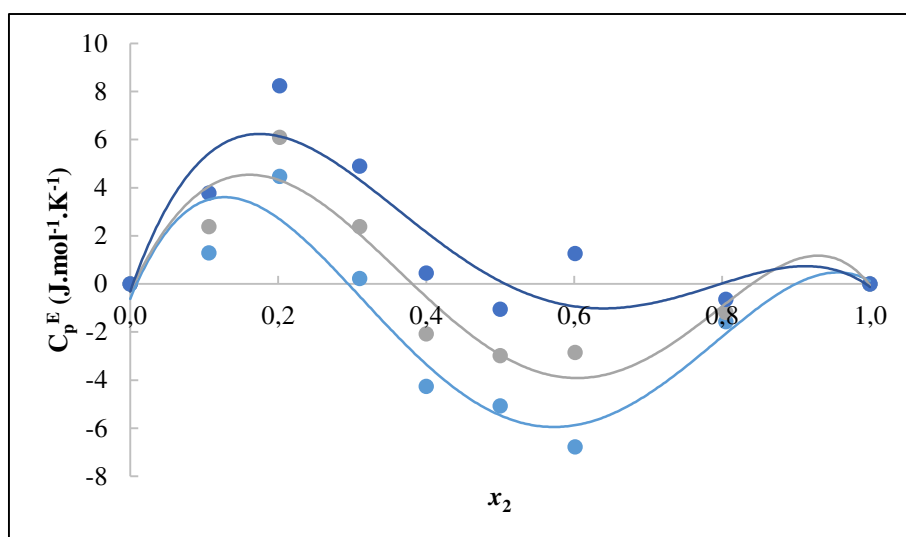


Figure II.16: Excess heat capacities of {H₂O (1) + ILs (2)} versus x_2 of the IL at different temperatures: {H₂O (1) + [EMIM][EPh] (2)} (●) $T=301.15\text{K}$; (●) $T=303.15\text{K}$; (●) $T=321.15\text{K}$; —, calculated by Redlich–Kister equation.



(a)



(b)

Figure II.17: Excess heat capacities of {H₂O (1) + ILs (2)} versus x_2 of the IL at different temperatures: (a) {H₂O (1) + [DMIM][MeSO₄] (2)} (●) T=301.15K; (●) T=318.15K; (●) T=337.15K, (b) {H₂O (1) + [EMIM][MeSO₄] (2)} (●) T=301.15K; (●) T=318.15K; (●) T=337.15K; —, calculated by Redlich–Kister equation.

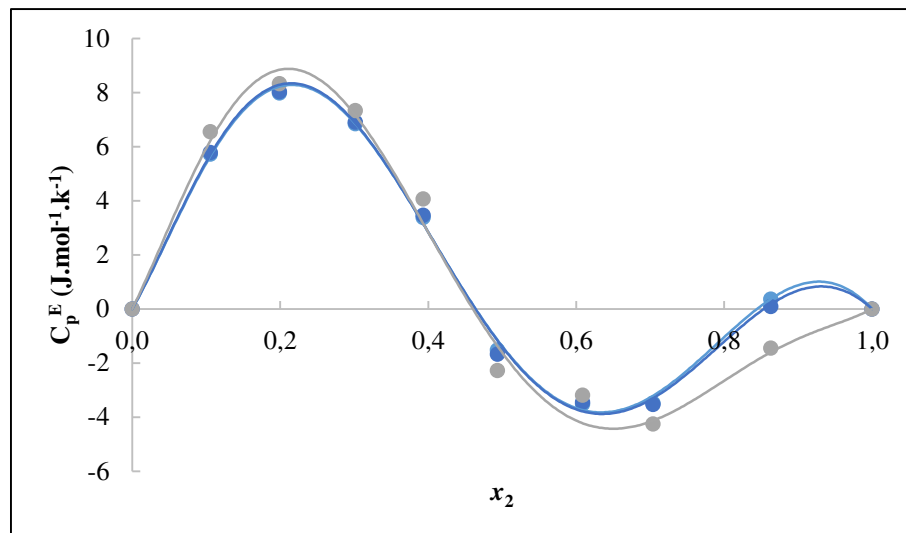


Figure II.18: Excess heat capacities of {H₂O (1) + [BMIM][DCA] (2)} versus x_2 of the IL at different temperatures: (●) T=301.15K; (●) T=303.15K; (●) T=321.15K;—, calculated by Redlich–Kister equation.

The excess molar heat capacities C_p^E obtained in this work are shown in Figures II.16–II.18. The C_p^E for all the studied {H₂O + ILs} binary systems have both positive and negative values with maxima at low and high ILs mole fractions and a minimum at intermediate composition and a positive temperature dependence. The C_p^E values for the {H₂O + [EMIM][EPh]} binary system have also positive and negative values with maxima at low (≈ 0.1) and intermediate IL mole fractions and a minimum at high IL concentration.

It can also be observed that at the lower composition of both {H₂O + [DMIM][MeSO₄]} and {H₂O + [BMIM][DCA]} binary systems the C_p^E values increase with increasing temperature while at the higher composition their values decrease with increasing temperature. This behavior is similar to that observed in literature [19]. The possible explanation for the negative values of the C_p^E may be due to the presence of IL/water interactions which are stronger than the corresponding IL/IL and water/water interactions in the aqueous mixtures while the positive values suggest the reverse.

II.2.3. Density (ρ)

The density of the six binary mixtures are measured in the whole range of molar concentration and in the range of temperature between 293.15 and 323.15K at the atmospheric pressure. The uncertainty in the experimental measurements was less than $\pm 0.0001 \text{ g.cm}^{-3}$ and the precision of the temperature was 0.1 K. Annex II presents the density values of the binary systems measured. All data were regressed by Eq. (II.15) [4].

$$\rho = \sum_{i=0}^3 (a_i + b_i T) x_2^i \quad (\text{II.15})$$

Where ρ is the density of the solution in g.cm^{-3} , T is the absolute temperature in K, a_i and b_i are the regression parameters, and x_2^i is the molar fraction of the ILs. The regression parameters are adjusted by a least-square method and are listed in Table II.8. The ARD between the experimental and calculated values range between 0.06 and 0.23 % (Figures II.20-II.22).

Table II.8: Parameters for the correlation of Eq. (II.15).

Binary system {H ₂ O (1) + IL (2)}	a ₀	a ₁	a ₂	a ₃	b ₀	b ₁	b ₂	b ₃	$\Delta\rho\%$
{H ₂ O + [DMIM][MPh]}	1.3682	0.1342	-0.0543	-0.0592	-0.0010	0.0018	-0.0031	0.0018	0.23
{H ₂ O + [DMIM][MeSO ₄]}	1.2556	0.8692	-1.0895	0.4893	-0.0005	-0.0002	0.0002	-0.0001	0.20
{H ₂ O + [EMIM][MPh]}	0.3401	0.3401	0.3401	0.3401	-0.0009	0.0014	-0.0021	0.0010	0.18
{H ₂ O + [EMIM][EPh]}	1.2843	0.0893	0.0046	-0.0586	-0.0007	0.0008	-0.0017	0.0010	0.16
{H ₂ O + [EMIM][MeSO ₄]}	1.2237	1.0775	-1.6129	0.7918	-0.0004	-0.0013	0.0023	-0.0012	0.22
{H ₂ O + [BMIM][DCA]}	1.2166	0.1235	-0.0526	-0.0499	-0.0007	0.0000	-0.0003	0.0004	0.06

The density values reported in the literature [20, 21, 22] for pure [DMIM][MeSO₄], [EMIM][MeSO₄] and [BMIM][DCA] are consistent with data obtained in this work (the difference between experimental data and those reported in literature are 0.06 %, 1.42%, 0.06, respectively). It is well known that impurities and water content of the ILs have a great influence upon density. It is possible to observe that the density decreases as the water content increases. Thus, the observed deviation between the results of this

study and Wang *et al.* [21] for [EMIM][MeSO₄] may be attributed to water contents of ILs which are significantly different (133.69 ppm in this study, higher than 200 ppm in Wang *et al.*).

Generally, the density values decrease with increasing temperature and decreasing ILs molar fraction. As a whole, the density of the studied imidazolium based ILs roughly ranges within 1.06 and 1.33 g.cm⁻³. It was noticed that increasing the length of the alkyl chain decreases the density of the IL. Hence, by comparing [DMIM][MPh] and [EMIM][MPh], it was found that [DMIM][MPh] has higher density. The same behavior is noticed for [DMIM][MeSO₄] and [EMIM][MeSO₄], [DMIM][MeSO₄] has higher density. A possible explanation for this can be the stronger electrostatic interaction between the smaller cation [DMIM]⁺ and the anions [MPh]⁻, [MeSO₄]⁻, though the cation [EMIM]⁺ has a higher dispersion energy due to its longer alkyl substitute [23]. Similarly, for the [BMIM]⁺ based ILs aqueous solutions, the density of [BMIM][DCA] found to be the lowest among the studied ionic liquids. The observed low density can be explained as follows, adding CH₂ groups to the alkyl chain on the [C_nMIM]⁺ cation decreases the density, and the density decrease as the mass of the anion decrease.

The density of the investigated binary systems decrease according to the following trend:

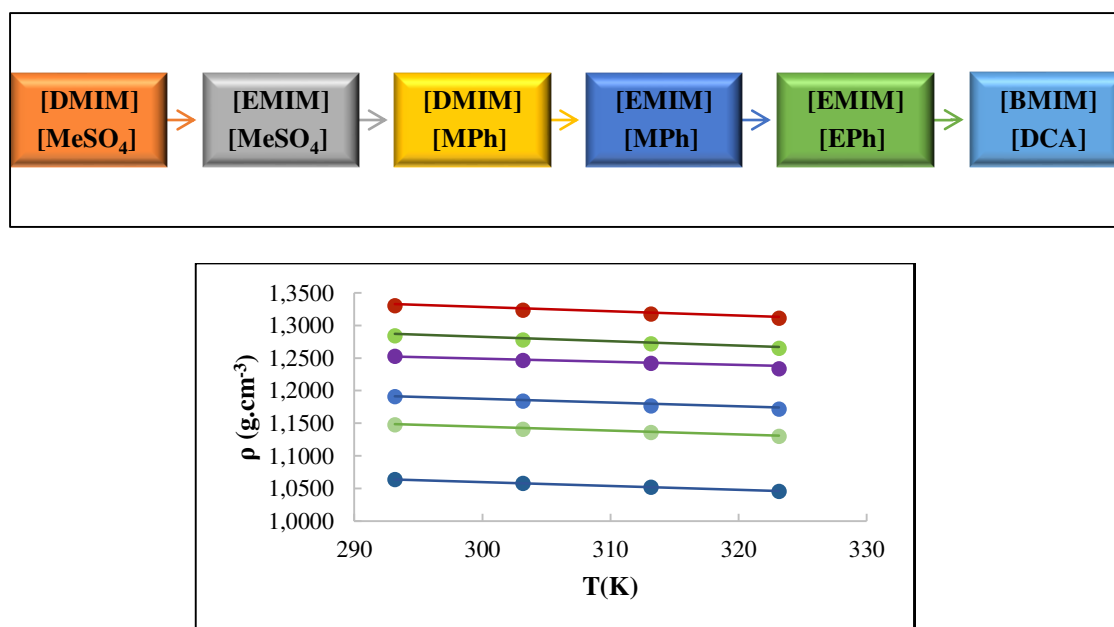
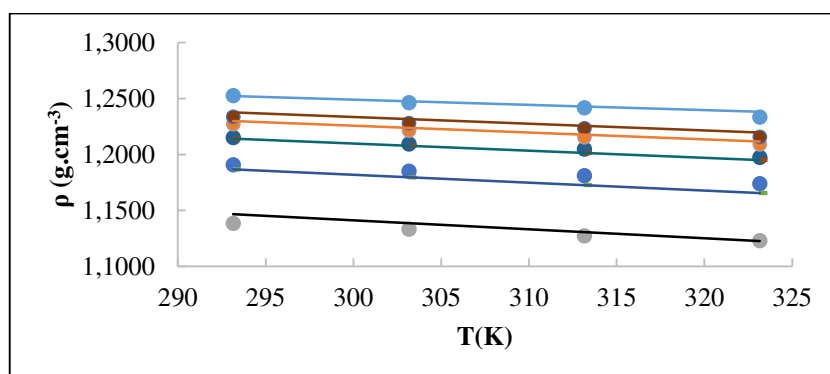
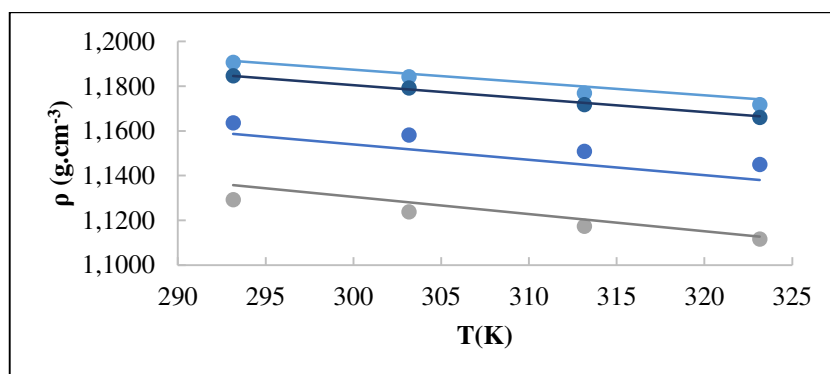


Figure II.19: Trend of density of the investigated pure ILs (●) [DMIM][MPh]; (●) [EMIM][MPh]; (●) [EMIM][EPh]; (●) [BMIM][DCA]; (●) [DMIM][MeSO₄]; (●) [EMIM][MeSO₄]; —, calculated by polynomial equation (II.15).

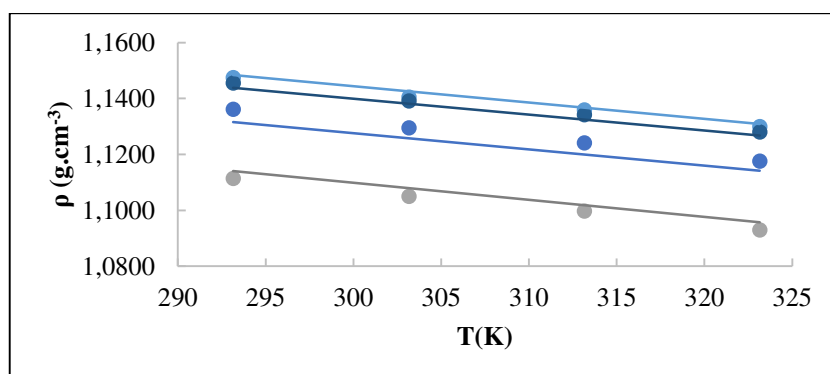
Alkylsulfates based ILs have the highest density because of the alkyl chain on the sulfate anion. [MeSO₄] increases the density due to decreasing negative charges on the oxygen atoms of the anions and increasing hydrophobicity [24].



(a)

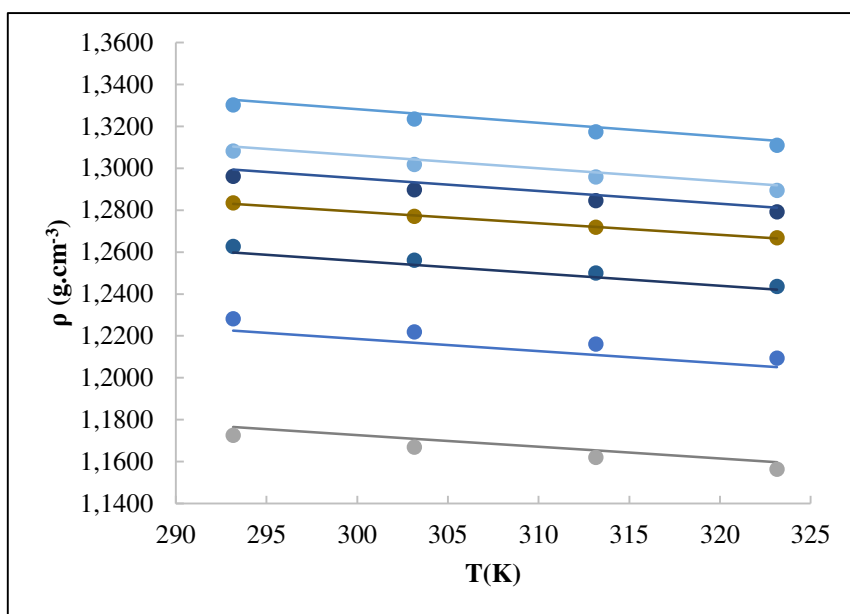


(b)

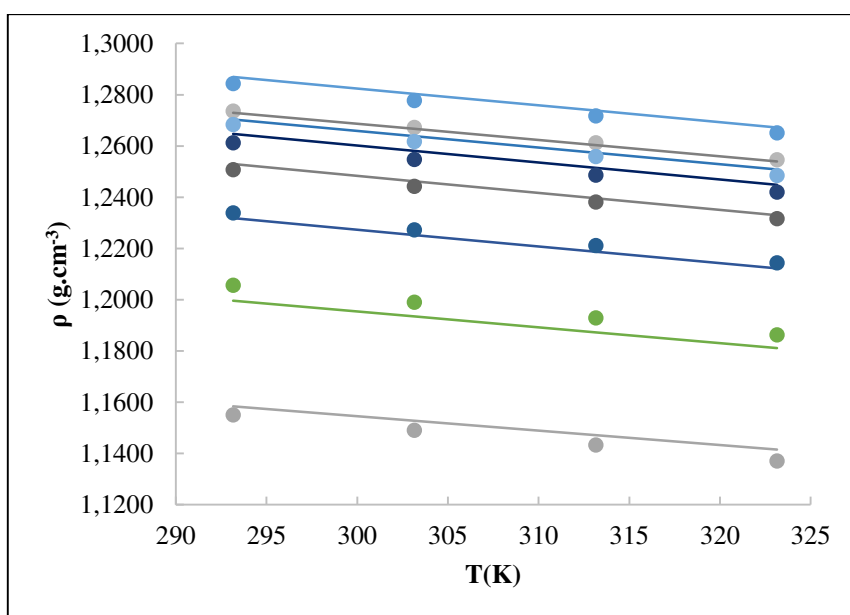


(c)

Figure II.20: Density of {H₂O (1) + IL (2)} versus temperature at different molar fractions of IL: (a) {H₂O (1) + [DMIM][MPh] (2)} (●) $x_2=1$; (●) $x_2=0.1$; (●) $x_2=0.2$; (●) $x_2=0.3$; (●) $x_2=0.4$; (●) $x_2=0.5$, (b) {H₂O (1) + [EMIM][MPh] (2)} (●) $x_2=1$; (●) $x_2=0.1$; (●) $x_2=0.2$; (●) $x_2=0.3$, (c) {H₂O (1) + [EMIM][EPh] (2)} (●) $x_2=1$; (●) $x_2=0.1$; (●) $x_2=0.2$; (●) $x_2=0.3$; —, calculated by polynomial equation (II.15).



(a)



(b)

Figure II.21: Density of {H₂O (1) + IL (2)} versus temperature at different molar fractions of IL: (a) {H₂O (1) + [DMIM][MeSO₄] (2)} (●) $x_2=1$; (●) $x_2=0.1$; (●) $x_2=0.2$; (●) $x_2=0.3$; (●) $x_2=0.4$; (●) $x_2=0.5$; (●) $x_2=0.6$, (b) {H₂O (1) + [EMIM][MeSO₄] (2)} (●) $x_2=1$; (●) $x_2=0.1$; (●) $x_2=0.2$; (●) $x_2=0.3$; (●) $x_2=0.4$; (●) $x_2=0.5$; (●) $x_2=0.6$; (●) $x_2=0.7$;—, calculated by polynomial equation (II.15).

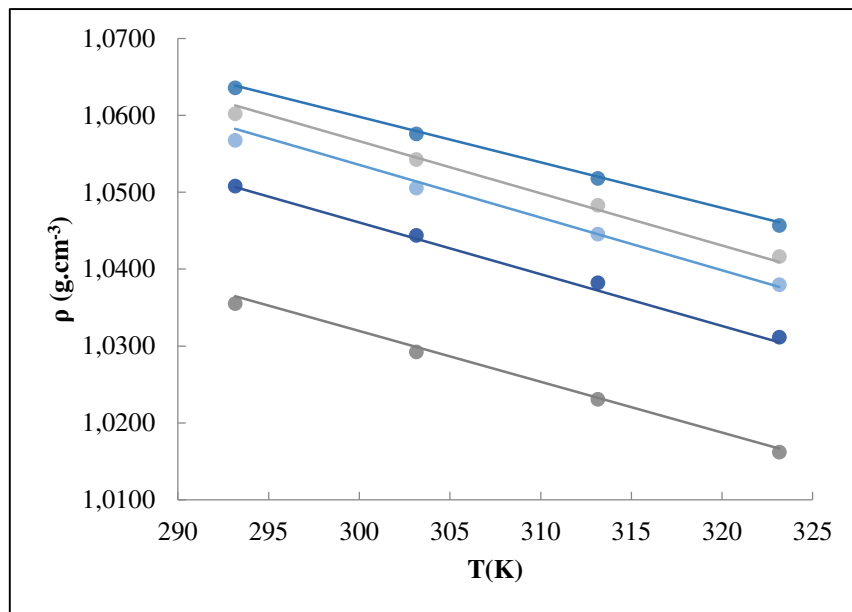


Figure II.22: Density of {H₂O (1) + [BMIM][DCA] (2)} versus temperature at different molar fractions of [BMIM][DCA]: (●) $x_2=1$; (●) $x_2=0.1$; (●) $x_2=0.3$; (●) $x_2=0.5$; (●) $x_2=0.7$; —, calculated by polynomial equation (II.15).

II.2.3.1. Excess molar volume V^E

Volumetric properties of binary mixtures depend not only on size, shape, and chemical nature of the components of a mixture [23], but also on the (solute + solute, solvent + solvent, solute + solvent) interactions and on structural effects occurring from interstitial accommodation due to differences in molar volume and free volume between solution components [25].

The experimental density data were used to calculate the excess molar volume V^E by using Eq. (II.16). These data are presented in Figures (II.23-II.25).

$$V^E = V_m - \sum_i x_i V_i^* \quad (\text{II.16})$$

Where V_m is the molar volume of the mixture, and x_i, V_i^* represent the mole fraction and the molar volume of component i , respectively.

As it can be observed from the data, the six studied binary systems present asymmetrical curves. This behavior is quite common with mixtures containing two components with a large molar volume difference [25, 26]. The studied binary systems showed a wavy V^E shape with a minimum level at moderate (≈ 0.4) mole fraction of ILs. Negative V^E values are obtained for five studied binary systems with phosphonate based ionic liquids and methylsulfates based ILs. Negative V^E values were also found in literature for the binary systems containing imidazolium-based ionic liquid [27]. The change from negative to positive in the V^E behavior was observed for four binary systems [DMIM][MPh], [EMIM][EPh], [DMIM][MeSO₄] and [EMIM][MeSO₄]. These results agree well with the behavior observed by Garcia-Miaja *et al.* [18], Rodriguez and Brennecke [28], and Vercher *et al.* [29].

It is well known that the excess molar volume V^E depends mainly on the intermolecular forces between components of the mixtures and on the packing due to the differences in size and shape of molecules. According to this, the dominant negative effect is due to the association of the polar water molecules with the anions, either through H bonding or through attraction of the polar water to a highly charged small ion. Competition between these effects gives rise to the wavy curves and even in one case a double humped curve [26].

Experimental measurements show that an increase of the alkyl chain length of the cation leads to smaller V^E values. This behavior was also observed by Garcia-Miaja *et al.*, [18].

In contrast, the behavior of the system {H₂O + [BMIM][DCA]} exhibits positive values of the V^E in the whole composition range. This trend is in accordance with results published by Gonzalez *et al* [25]. A possible explanation for the dominant positive effect might be due to the weakening of the (IL + IL) association in the rich IL region and the dissociation of the H-bonded water network in the dilute IL concentration region. Furthermore, V^E depends mainly on the intermolecular forces between components of the mixtures, and on the packing due to the differences in size and shape of molecules. According to this, the positive V^E values can be attributed to weak water-ionic liquid interactions and to feeble packing of the components in the mixture.

Some authors [25, 26] stated that anions have great effect on V^E . The anion can influence the magnitude, shape and sign of the V^E curves of binary mixtures {H₂O + IL}. We found that the anions containing oxygen atoms ([MPh], [MeSO₄]) result in

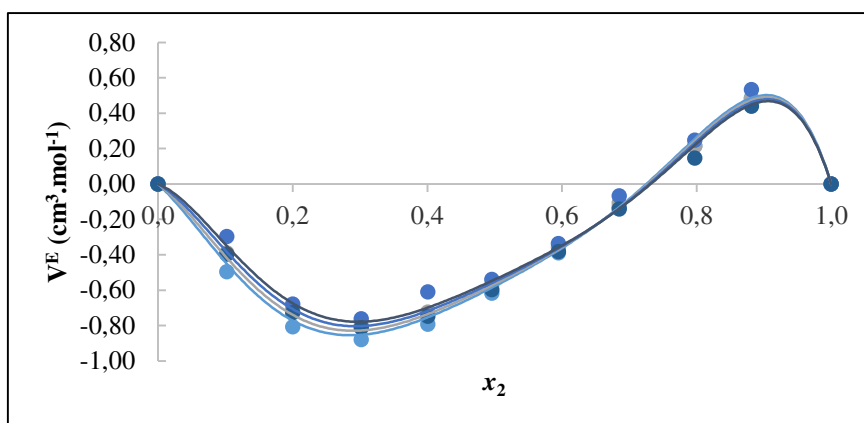
negative V^E values especially at the lower temperatures while the more hydrophobic anion [DCA] tend to result in positive V^E values especially at high temperatures.

The decrease in the magnitude of the negative V^E values and the increase in the magnitude of the positive V^E values with increasing temperature might be attributed to the decreasing importance of hydrogen bonding with increasing temperature. Furthermore, this behavior can indicate the occurrence of two very different processes. At low IL concentrations, the negative V^E values mean that there is an association between IL and a large number of H_2O molecules. This effect becomes weaker as the temperature increases and as the concentration of the IL increases. At the other end of the composition scale (x_2 tending toward 1), the V^E values are positive and probably due to the disruption of both or either of the self-association effects. This disturbance is the principal feature in this region and is clearly more important than the (IL + H_2O) association. Because of the difference of size between IL molecules and water and the IL rich phase concentration, it suggests that this positive effect is due to the disruption of the (IL + IL) association because any disruption of the water self-association would hardly be noticed. At high and very dilute IL concentration ends, the V^E data is not temperature dependent [26].

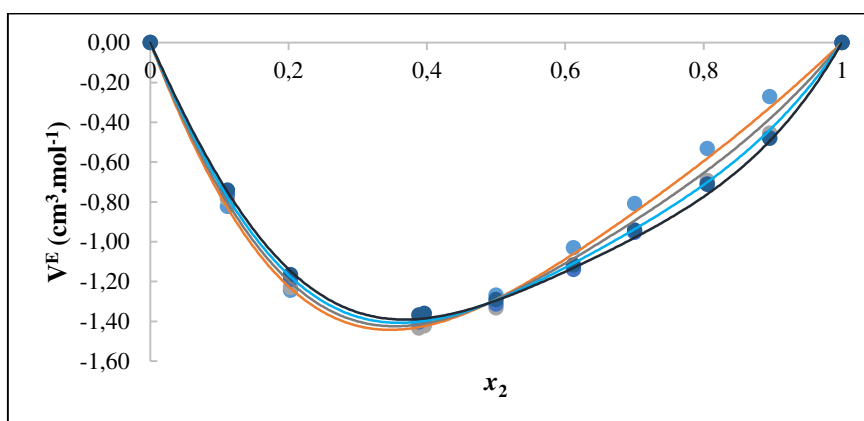
All V^E experimental data are correlated using the Redlich-Kister equation and regression parameters are listed in Table II.9. It is found that the calculated values are significantly consistent with the experimental data (Figures II.23-II.25).

Table II.9: Redlich Kister parameters for the representation of V^E of binary systems
 $\{H_2O (1) + ILs (2)\}$

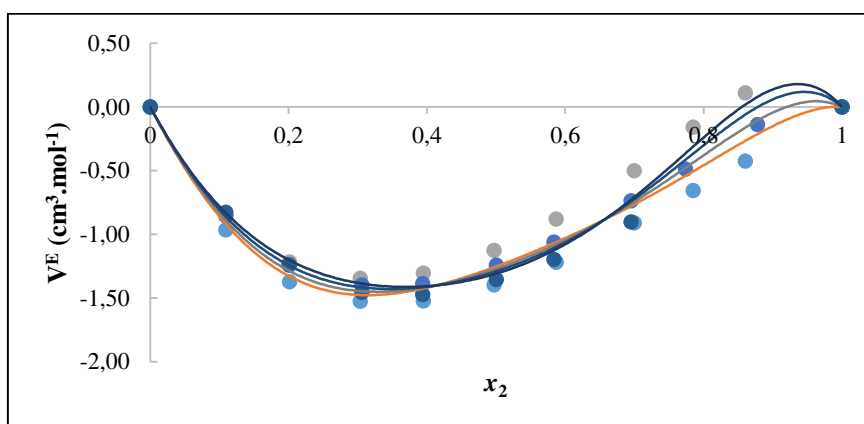
Binary system	a ₁	a ₂	a ₃	a ₄	a ₅	b ₁	b ₂	b ₃	b ₄	b ₅	ΔV^E %
{H ₂ O + [DMIM][MPh]}	-3.79	-7.64	0.88	-12.72	1.20	0.00	0.01	0.02	0.03	2.10	12.12
{H ₂ O + [DMIM][MeSO ₄]}	-1.96	-4.08	-7.09	4.76	1.01	0.00	0.01	0.03	-0.01	0.27	26.41
{H ₂ O + [EMIM][MPh]}	-4.93	-13.27	5.71	-9.75	1.15	0.00	0.03	-0.02	0.04	0.20	3.58
{H ₂ O + [EMIM][EPh]}	-2.81	-12.02	-38.25	36.29	1.03	-0.01	0.03	0.13	-0.13	0.59	24.19
{H ₂ O + [EMIM][MeSO ₄]}	-3.67	-6.74	-2.73	2.73	0.98	0.01	0.02	0.01	-0.01	0.16	31.40
{H ₂ O + [BMIM][DCA]}	-7.44	-4.22	-2.27	-1.98	664.54	0.03	0.01	0.01	0.01	-2.12	7.83



(a)

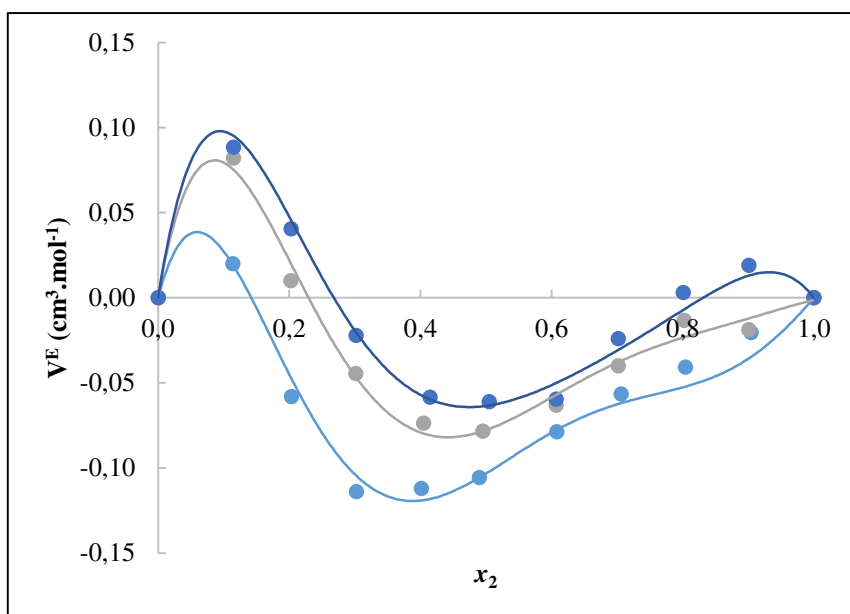


(b)

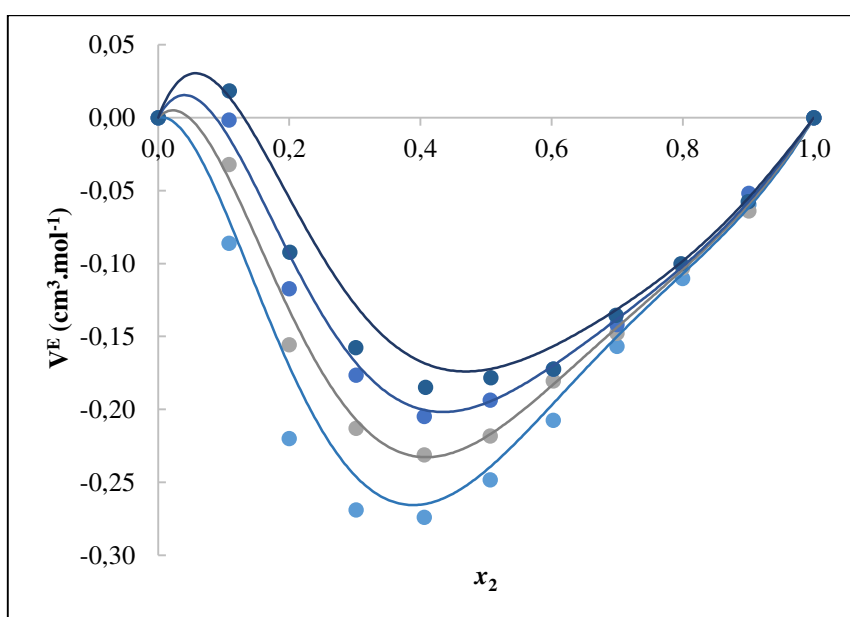


(c)

Figure II.23: Experimental excess molar volume, V^E against mole fraction of IL at different temperatures, (a) $\{\text{H}_2\text{O} + [\text{DMIM}][\text{MPh}]\}$: (●) $T=293.15\text{ K}$; (●) $T = 303.15\text{ K}$; (●) $T = 313.15\text{ K}$; (●) $T = 323.15\text{ K}$, (b) $\{\text{H}_2\text{O} + [\text{EMIM}][\text{MPh}]\}$: T : (●) $T=293.15\text{ K}$; (●) $T = 303.15\text{ K}$; (●) $T = 313.15\text{ K}$; (●) $T = 323.15\text{ K}$, (c) $\{\text{H}_2\text{O} + [\text{EMIM}][\text{EPh}]\}$: T : (●) $T=293.15\text{ K}$; (●) $T = 303.15\text{ K}$; (●) $T = 313.15\text{ K}$; (●) $T = 323.15\text{ K}$; —, correlated by Redlich-kister equation.



(a)



(b)

Figure II.24: Experimental excess molar volume, V^E against mole fraction of IL at different temperatures, (a) $\{\text{H}_2\text{O} + [\text{DMIM}][\text{MeSO}_4]\}$: T: (●) $T=293.15\text{ K}$; (●) $T = 313.15\text{ K}$; (●) $T = 323.15\text{ K}$, (b) $\{\text{H}_2\text{O} + [\text{EMIM}][\text{MeSO}_4]\}$: T: (●) $T=293.15\text{ K}$; (●) $T = 303.15\text{ K}$; (●) $T = 313.15\text{ K}$; (●) $T = 323.15\text{ K}$; —, correlated by Redlich-kister equation.

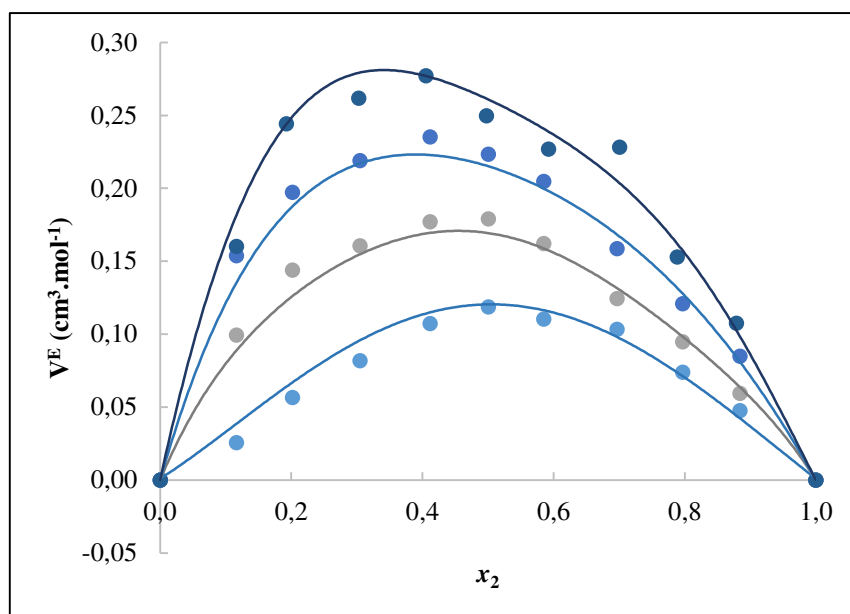


Figure II.25: Experimental excess molar volume, V^E against mole fraction of $\{H_2O + [BMIM][DCA]\}$ at different temperature T : (●) $T=293.15$ K; (●) $T = 303.15$ K; (●) $T = 313.15$ K; (●) $T = 323.15$ K; —, correlated by Redlich-kister equation.

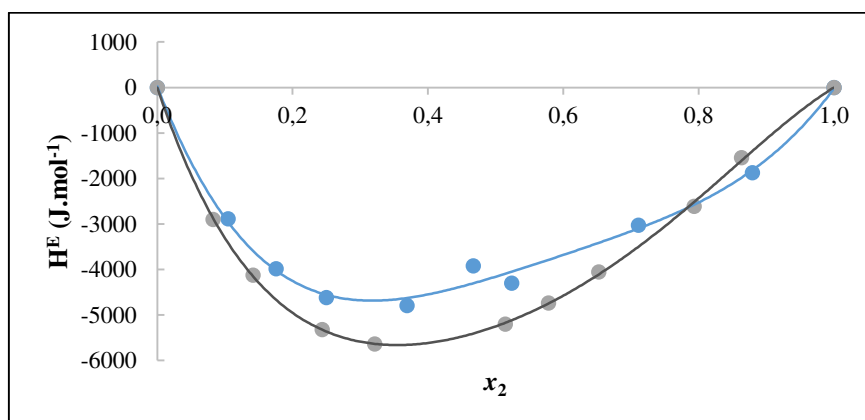
II.2.4. Excess molar Enthalpy (H^E)

In this work, the excess molar enthalpies, H^E , of five binary systems are presented (Figures II.26-II.28) and are listed in Annex II. Although extensive research has been carried out on ionic liquids binary systems with water, there is a lack of discussion about excess enthalpy in literature. Negative enthalpies were found for all systems at $T = 312.92$ K. Therefore, negative values of the excess enthalpy suggest that the water/IL interactions are stronger than the corresponding IL/IL and water/water interactions.

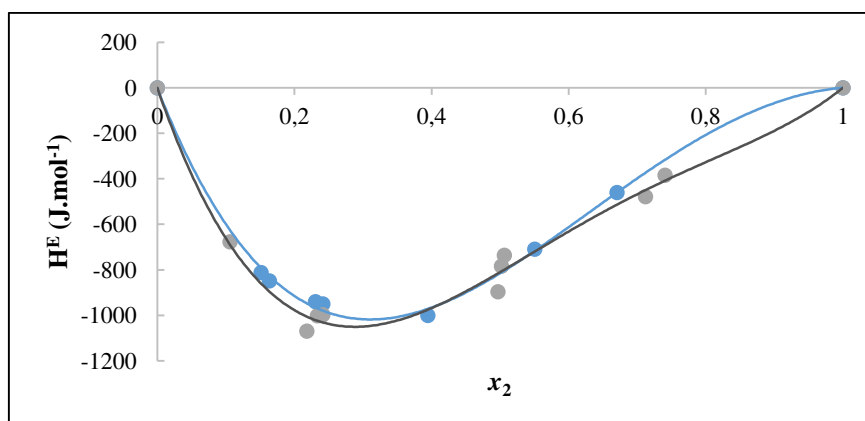
Effect of ILs cation: The effect of cation is less significant than the anion effect which suggests that the major interactions between the water and the ILs takes place, at the anions. It is interesting to note that both $[DMIM]^+$ based ILs show a slightly lower negative excess enthalpy than $[EMIM]^+$ based ILs. It seems possible that these results are due to the longer alkyl chain length in $[EMIM]^+$ which leads to a stronger hydrophobic effect than the hydration effect. The increased repulsion of the water molecules in such cations results in an increase in the energy of the system, hence

leading the process to be more exothermic [30]. Thus, the magnitude of H^E follows the order: $[\text{EMIM}]^+ < [\text{DMIM}]^+$ (Figure II.26).

It should be highlighted that similar phenomena was already discussed by Kurnia and Coutinho [31], they observed the same behavior with $[\text{C}_6\text{iQuin}][\text{SCN}]$ and $[\text{C}_8\text{iQuin}][\text{SCN}]$. The authors suggested that this behavior may be due to the enhancement of the favorable interaction between IL and water which leads to increasing exothermic behavior with increasing the alkyl chain length. Nevertheless, it is difficult to find if this is an unusual behavior related with the imidazolium and quinolinium-based ILs or is just a problem associated with the limited experimental data available. More data on these systems are required to establish the reason behind this particular trend.



(a)



(b)

Figure II.26: Experimental excess molar enthalpy, H^E against different mole fraction x_2 of: (●) $[\text{DMIM}][\text{MPh}]$, (●) $[\text{EMIM}][\text{MPh}]$, (b) (●) $[\text{DMIM}][\text{MeSO}_4]$, (●) $[\text{EMIM}][\text{MeSO}_4]$ at 312.92 K (b) ; —, correlated by Redlich-kister equation.

Effect of ILs anion: The experimental data available allow a comparison of the effect of three ILs anions on the excess enthalpies of $\{H_2O + IL\}$ binary systems. For $[EMIM]^+$ based ILs, the exothermic behavior of $\{H_2O + IL\}$ increases in the following order: $[MeSO_4]^- < [EPh]^- < [MPh]^-$. The same behavior was noticed for $[DMIM]^+$ based ILs (Figure II.27). The excess enthalpies decrease (become more negative) with the increasing hydrophilicity of the anions or the hydrogen bonding acceptor ability. The same trend is also observed with molecular simulation by Ficke and Brennecke [32] and Kurnia and Coutinho.[31] Methyl sulfate anion $[MeSO_4]^-$ decreases the exothermic effect due to decreasing negative charges on the oxygen atoms of the anions and increasing hydrophobicity. All H^E experimental data are correlated using the Redlich-Kister equation and regression parameters are listed in Table II.10. It is found that the calculated values are significantly consistent with the experimental data (Figures II.27-II.28).

Table II.10: Redlich-Kister parameters for H^E for $\{H_2O (1) + ILs (2)\}$.

Binary system	A ₁	A ₂	A ₃	A ₄	$\Delta\%$
$\{H_2O + [DMIM][MPh]\}$	-16582.69	10105.69	-12835.62	-3168.39	2.72
$\{H_2O + [DMIM][MeSO_4]\}$	-3304.76	3475.58	65.52	1591.83	2.20
$\{H_2O + [EMIM][MPh]\}$	-20996.20	10554.39	-5769.54	7132.76	1.28
$\{H_2O + [EMIM][EPh]\}$	-19034.15	10205.39	-4611.32	6153.53	1.22
$\{H_2O + [EMIM][MeSO_4]\}$	-3240.60	3522.29	-2319.36	-373.28	5.11

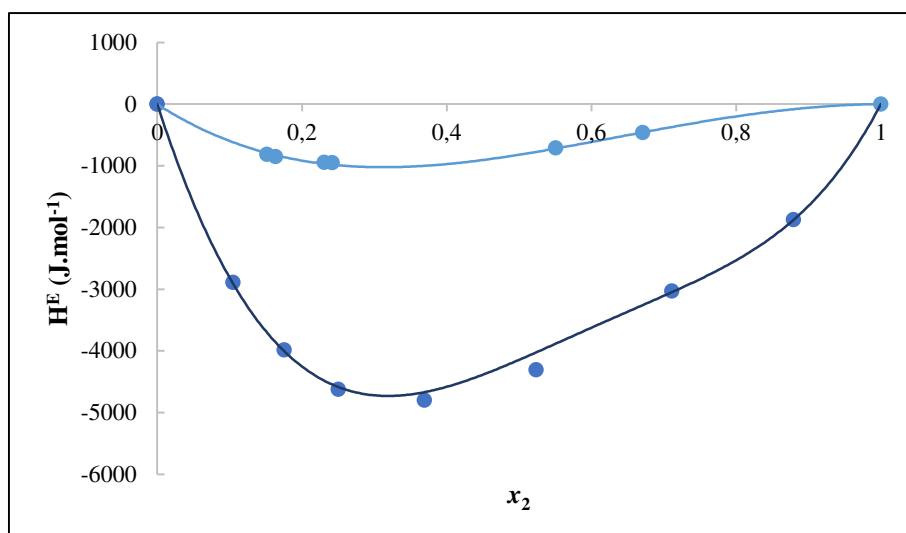


Figure II.27: Experimental excess molar enthalpy, H^E against different mole fraction x_2 of: (●) $\{H_2O + [DMIM][MeSO_4]\}$, (●) $\{H_2O + [DMIM][MPh]\}$ at 312.92 K; —, correlated by Redlich-kister equation.

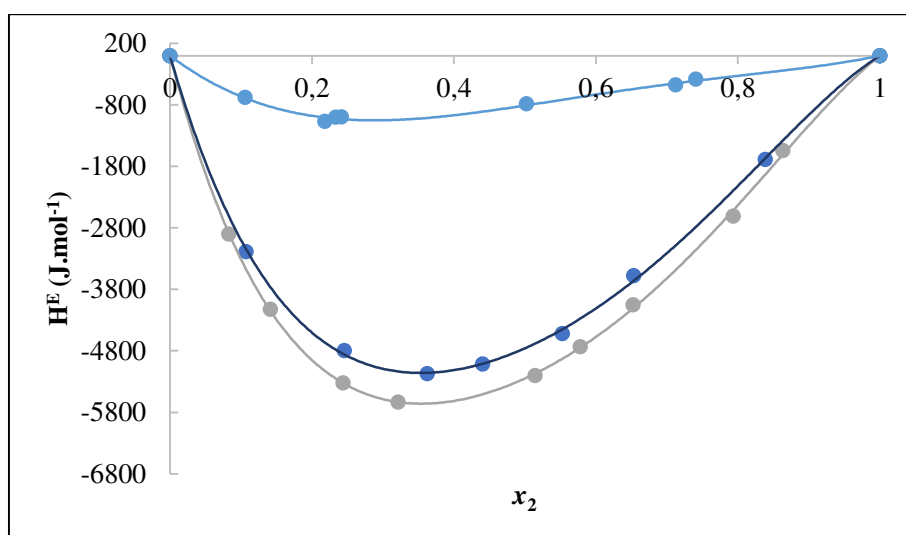


Figure II.28: Experimental excess molar enthalpy, H^E against different mole fraction x_2 of: (●) $\{H_2O + [EMIM][MPh]\}$, (●) $\{H_2O + [EMIM][EPh]\}$, (●) $\{H_2O + [EMIM][MeSO_4]\}$ at 312.92 K (b) ; —, correlated by Redlich-kister equation.

References

- [1] M. Hasan, A.P. Hiray, U.B. Kadam, D.F. Shirude, K.J. Kurhe, A.B. Sawant, Densities, sound speed, and IR studies of (methanol + 1-acetoxybutane) and (methanol + 1,1-dimethylethyl ester) at (298.15, 303.15, 308.15, and 313.15) K, *J. Chem. Eng. Data*, 55 (2010) 535–538.
- [2] L. Dong, D. Zheng, N. Nie, Y. Li, Performance prediction of absorption refrigeration cycle based on the measurements of vapor pressure and heat capacity of {H₂O + [DMIM][DMP]} system, *Applied Energy*, 98 (2012) 326–332.
- [3] Z. He, Z. Zhao, X. Zhang, H. Feng, Thermodynamic properties of new heat pump working pairs: 1,3-dimethylimidazolium dimethylphosphate and water, ethanol and methanol, *Fluid Phase Equilibria*, 298 (2010) 83–91.
- [4] N. Nie, D. Zheng, L. Dong, Y. Li, Thermodynamic properties of the water + 1- (2-hydroxyethyl)-3-methylimidazolium chloride system, *J. Chem. Eng. Data*, 57 (2012) 3598–3603.
- [5] A.L. Revelli, F. Mutelet, J.N. Jaubert, (Vapor + liquid) equilibria of binary mixtures containing light alcohols and ionic liquids, *J. Chem. Thermodynamics*, 42 (2010) 177–181.
- [6] G. Zuo, Z. Zhao, S. Yan, X. Zhang, Thermodynamic properties of a new working pair: 1-ethyl-3-methylimidazolium ethylsulfate and water, *Chem. Eng. J.*, 156 (2010) 613–617.
- [7] A. Furtado, E. Batista, I. Spohr, E. Filipe, Measurement of density using oscillation-type density meters calibration, traceability and uncertainties, Instituto Portugues da Qualidade (IPQ).
- [8] E. Calvet, H. Prat, *Microcalorimétrie. Applications Physico-chimiques et Biologiques* Masson et Cie, Paris (1956).
- [9] E. Calvet, H. Prat, *Recent progress in microcalorimetry*, Pergamon Press, Oxford (1963).
- [10] A. Tian, Microcalorimètre à compensation par effets Peltier et Joule, *Bulletin de la Societe de Chimique*, 33 (1924) 427.

- [11] J.W. Zondlo, Vapor pressure, liquid density, and the latent heat of vaporization as functions of temperature for four dipolar aprotic solvents, *J. Chem. Eng. Data*, 32 (1987) 11-13.
- [12] L.E. Ficke, Thermodynamic properties of imidazolium and phosphonium based ionic liquid mixtures with water or carbon dioxide. PhD thesis, Chemical and Biomolecular Engineering, University of Notre Dame, Notre Dame, Indiana; April 2010.
- [13] L.D. Simoni, L.E. Ficke, C.A. Lambert, M.A. Stadtherr, J.F. Brennecke, Measurement and prediction of vapor - liquid equilibrium of aqueous 1-ethyl-3-methylimidazolium-based ionic liquid systems, *Ind. Eng. Chem. Res.*, 49 (2010) 3893–3901.
- [14] H. Passos, I. Khan, F. Mutelet, M.B. Oliveira, P.J. Carvalho, L.M.N.B.F. Santos, C. Held, G. Sadowski, M.G. Freire, J.A.P. Coutinho, Vapor-liquid equilibria of water + alkylimidazolium-based ionic liquids: measurements and perturbed-chain statistical associating fluid theory modeling, *Ind. Eng. Chem. Res.*, 53 (2014) 3737–48.
- [15] M. Krolikowska, M. Zawadzki, M. Królikowski, Physicochemical and thermodynamic study on aqueous solutions of dicyanamide – based ionic liquids, *J. Chem. Thermodynamics*, 70 (2014) 127–137.
- [16] H. Renon, J. M. Prausnitz, Local compositions in thermodynamic excess functions for liquid mixtures, *AIChE J.*, 14 (1968) 135-144.
- [17] L.E. Ficke, H. Rodriguez, J.F. Brennecke, Heat capacities and excess enthalpies of 1-ethyl-3-methylimidazolium-based ionic liquids and water, *J. Chem. Eng. Data*, 53 (2008) 2112–2119.
- [18] G. Garcia-Miaja, J. Troncoso, L. Romani, Excess enthalpy, density, and heat capacity for binary systems of alkylimidazolium-based ionic liquids + water, *J. Chem. Thermodynamics*, 41 (2009) 161–166.
- [19] H.C. Hu, A.N. Soriano, R.B. Leron, M.H. Li, Molar heat capacity of four aqueous ionic liquid mixtures, *Thermochimica Acta*, 519 (2011), 44–49.

- [20] A.B. Pereiro, F. Santamarta, E. Tojo, A. Rodriguez, J. Tojo, Temperature dependence of physical properties of ionic liquid 1,3-dimethylimidazolium methyl sulfate, *J. Chem. Eng. Data*, 51 (2006) 952–954.
- [21] J.Y. Wang, F.Y. Zhao, Y.M. Liu, X.L. Wang, Y.Q. Hu, Thermophysical properties of pure 1-ethyl-3-methylimidazolium methylsulphate and its binary mixtures with alcohols, *Fluid Phase Equilibria*, 305 (2011) 114–120.
- [22] J.M.P. França, F. Reis, S.I.C. Vieira, M.J.V. Lourenço, F.J.V. Santos, C.A. Nieto de Castro, A.A.H. Padua, Thermophysical properties of ionic liquid dicyanamide (DCA) nanosystems, *J. of Chem. Thermodynamics*, 79 (2014) 248–257.
- [23] Y. Gong, C. Shen, Y. Lu, H. Meng, C. Li, Viscosity and density measurements for six binary mixtures of water (methanol or ethanol) with an ionic liquid ([BMIM][DMP] or [EMIM][DMP]) at atmospheric pressure in the temperature range of (293.15 to 333.15), *J. Chem. Eng. Data*, 57 (2012) 33–39.
- [24] M. Seiler, A. Kuhn, F. Ziegler, X. Wang, Sustainable cooling strategies using new chemical system solutions, *Ind. Eng. Chem. Res.*, 52 (2013) 16519–46.
- [25] E.J. Gonzalez, A. Dominguez, E.A. Macedo, Physical and excess properties of eight binary mixtures containing water and ionic liquids, *J. Chem. Eng. Data*, 57 (2012) 2165–76.
- [26] I. Bahadur, T. Letcher, S. Singh, G.G. Redhi, P. Venkatesu, D. Ramjugernath, Excess molar volumes of binary mixtures (an ionic liquid + water): A review, *J. Chem. Thermodynamics*, 82 (2015) 34–46.
- [27] A. Bhattacharjee, C. Varanda, M.G. Freire, S. Matted, L.M.N.B.F. Santos, I.M. Marrucho, J.A.P. Coutinho, Density and viscosity data for binary mixtures of 1-alkyl-3-methylimidazolium alkylsulfates + water, *J. Chem. Eng. Data*, 57 (2012) 3473–3482.
- [28] H. Rodriguez, J.F. Brennecke, Temperature and composition dependence of the density and viscosity of binary mixtures of water + ionic liquid, *J. Chem. Eng. Data*, 51(2006) 2145–55.

- [29] E. Vercher, A.V. Orchilles, P.J. Miguel, A. Martinez-Andreu, Volumetric and ultrasonic studies of 1-ethyl-3-methylimidazolium trifluoromethanesulfonate ionic liquid with methanol, ethanol, 1-propanol, and water at several temperatures, *J. Chem. Eng. Data*, 52 (2007) 1468–82.
- [30] G. Rai, A. Kumar, A reversal from endothermic to exothermic behavior of imidazolium-based ionic liquids in molecular solvents, *Chemical Physics Letters*, 496 (2010) 143–147.
- [31] K.A. Kurnia, J.A.P. Coutinho, Overview of the excess enthalpies of the binary mixtures composed of molecular solvents and ionic liquids and their modeling using COSMO-RS, *Ind. Eng. Chem. Res.*, 52 (2013) 13862–74.
- [32] L.E. Ficke, J.F. Brennecke, Interactions of ionic liquids and water, *J. of Phys. Chem. B*, 114 (2010) 10496–501.

CHAPTER THREE

PERFORMANCE SIMULATION (COP)

The aim of this chapter is to simulate the performance of absorption heat transformers using the new seven working pairs {H₂O + ILs} based on the experimentally measured thermodynamic properties mentioned in chapter two and on the mass and energy balance for each component of the system. In order to evaluate the new working pairs the simulation results are compared with those of the already used {H₂O + LiBr} working fluid and the simulation results for 11 binary systems found in the literature.

For sake of simplicity, the investigated binary systems are divided into 3 groups (Table III.1). The first group (Group I) includes the seven binary systems investigated by our research group. The second group (Group II) contains the binary systems for which a complete set of properties was published in the literature. Group III gathers a series of {H₂O + ILs} binary systems for which thermodynamic properties data are mainly limited to VLE data.

Table III.1: Thermodynamic properties of binary systems investigated in this work.

Groups	Binary system	Thermodynamic properties			
		VLE	H ^E	C _p	ρ
I	{H ₂ O + [DMIM][MPh]}	Boiling P. method	Calvet C80	MicroDSCIII	Anton Paar DMA60
	{H ₂ O + [DMIM][MeSO ₄]}	Boiling P. method	Calvet C80	MicroDSCIII	Anton Paar DMA60
	{H ₂ O + [EMIM][MPh]}	Boiling P. method	Calvet C80	MicroDSCIII	Anton Paar DMA60
	{H ₂ O + [EMIM][MeSO ₄]}	Boiling P. method	Calvet C80	MicroDSCIII	Anton Paar DMA60
	{H ₂ O + [EMIM][EPh]}	Boiling P. method	Calvet C80	MicroDSCIII	Anton Paar DMA60
	{H ₂ O + [BMIM][Ac]}	Boiling P. method			
	{H ₂ O + [BMIM][DCA]}	Boiling P. method		MicroDSC	Anton Paar
II	{H ₂ O+DMIMDMP}	Boiling P. method	Adiabatic solution calorimeter	Calvet BT2.15	Gravity balance
	{H ₂ O+EMIMDMP}	Boiling P. method	Adiabatic solution calorimeter	Adiabatic solution calorimeter	Anton Paar
	{H ₂ O+EMIMDEP}	Dual circulation	Setaram C80	Mettler Toledo DSC	Anton Paar DMA4500
	{H ₂ O+ [EMIM][AC]}	(FTIR) spectroscopy	n.d.	DSC	Pycnometer
	{H ₂ O+[HOEtMIM][Cl]}	Boiling P. method	n.d.	Calvet BT2.15	Anton Paar DMA4500M
	{H ₂ O+[EMIM][EtSO ₄]}	Boiling P. method	Calvet microcalorimeter	Isoperibol solution calorimeter	specific gravity balance
	{H ₂ O+ [EMIM][Triflate]}	Fischer Labodest apparatus	Calvet microcalorimeter	MicroDSCIII	Anton Paar DMA5000
	{H ₂ O+ [EMIM][TFA]}	Fischer Labodest apparatus	Setaram C80	Mettler Toledo DSC	Anton Paar DMA4500
	{H ₂ O+[DEMA][OMs]}	(FTIR) spectroscopy	n.d.	DSC	Pycnometer
	{H ₂ O+ [BMIM][Triflate]}	isobaric microebulliometer	Calvet microcalorimeter	MicroDSCIII	Anton Paar DMA5000
	{H ₂ O+ [BMIM][BF ₄]}	Boiling P. method	Calvet microcalorimeter	DSC	Anton Paar DMA 5000

Groups	Binary system	Thermodynamic properties			
		VLE	H ^E	C _p	ρ
III	{H ₂ O+ [DMIM][BF ₄]}	Boiling P. method	n.d.	n.d.	n.d.
	{H ₂ O+ [HOEtMIM][BF ₄]}	Boiling P. method	n.d.	n.d.	n.d.
	{H ₂ O+ [HOEtMIM][TFA]}	Fischer Labodest apparatus	n.d.	n.d.	n.d.
	{H ₂ O+ [EMIM][BF ₄]}	Static method	n.d.	n.d.	n.d.
	{H ₂ O+ [EMIM][I]}	Static method	n.d.	n.d.	n.d.
	{H ₂ O + [EMIM][Tf ₂ N]}	Static method	n.d.	n.d.	n.d.
	{H ₂ O+ [EMIM][SCN]}	Ebulliometric method	n.d.	n.d.	n.d.
	{H ₂ O + [EMIM][TOS]}	Ebulliometric method	n.d.	n.d.	n.d.
	{H ₂ O + [BMIM][C ₁ SO ₃]}	Isobaric microebulliometer	n.d.	n.d.	n.d.
	{H ₂ O + [BMIM][Cl]}	Labodest apparatus	n.d.	n.d.	n.d.
	{H ₂ O + [BMIM][Br]}	Boiling P. method	n.d.	n.d.	n.d.
	{H ₂ O + [BMIM][Ac]}	Static method	n.d.	n.d.	n.d.
	{H ₂ O + [BMIM][CF ₃ CO ₂]}	Isobaric microebulliometer	n.d.	n.d.	n.d.
	{H ₂ O + [BMIM][I]}	Static method	n.d.	n.d.	n.d.
	{H ₂ O + [BMIM][SCN]}	Static method	n.d.	n.d.	n.d.
	{H ₂ O + [BMIM][TOS]}	Isobaric microebulliometer	n.d.	n.d.	n.d.
	{H ₂ O + [BMIM][Tf ₂ N]}	Static method	n.d.	n.d.	n.d.
	{H ₂ O + [BMIM][MeSO ₄]}	Labosdest app.	n.d.	n.d.	n.d.
	{H ₂ O + [BMIM][DBP]}	Ebulliometric method	n.d.	n.d.	n.d.
	{H ₂ O + [BMPYR][DCA]}	Dynamic method	n.d.	n.d.	n.d.
	{H ₂ O + [BMPIP][DCA]}	Ebulliometric method	n.d.	n.d.	n.d.
	{H ₂ O + [HMIM][BF ₄]}	Ebulliometric method	n.d.	n.d.	n.d.

III.1. Simulation of the AHT cycle performance

In order to determine the suitability of a working pair for an AHP cycle, performance of such a cycle using this mixture has to be assessed by simulation or experiment. Some researchers have carried out such works, but the main method is still limited to simulation and analysis on the basis of thermo-physical properties of the IL working pairs. The published works mainly focus on single-effect absorption cooling cycle. This work focuses on single effect absorption heat transformers (AHT) (Figure III.1). To simplify simulation of the thermodynamic cycle performance of AHT using $\{H_2O + ILs\}$ as working pairs, the following assumptions are made [1, 2, 3]:

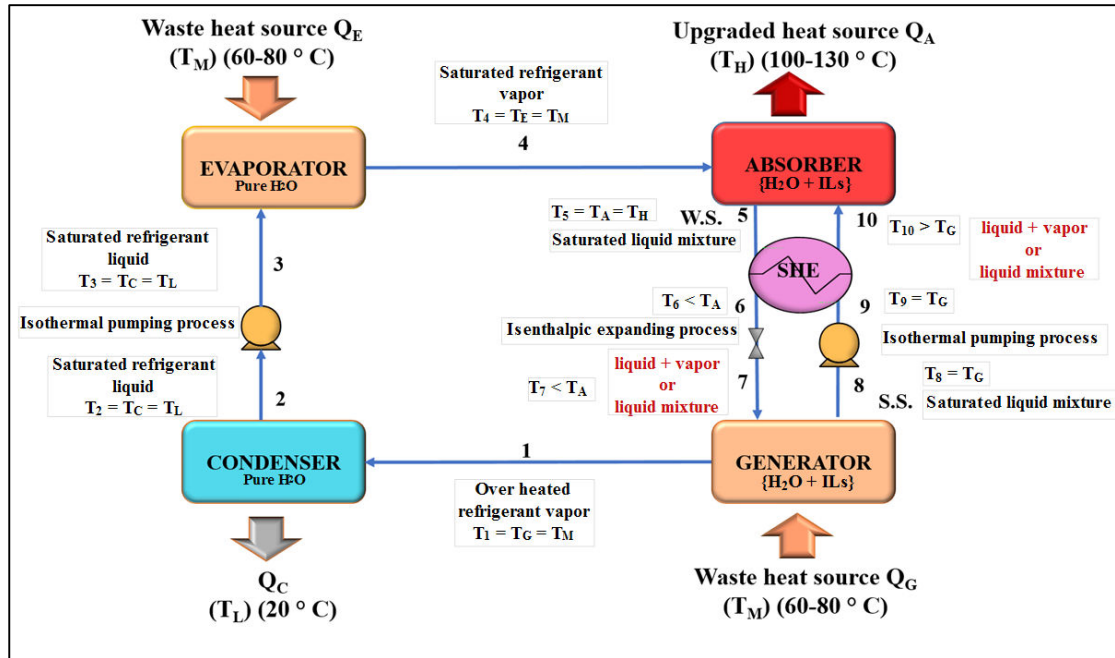


Figure III.1: Schematic diagram of an absorption heat transformer; T_M -medium temperature, T_L -low temperature, T_H -high temperature, SHE-solution heat exchanger.

- (1) The analysis is carried out under steady state conditions;
- (2) The solutions leaving the generator and the absorber are saturated liquids;
- (3) Liquid and vapor at the outlet of the condenser and the evaporator are saturated;
- (4) Thermal and pressure losses during the whole cyclic process are neglected;
- (5) The expanding process in the throttling valves is isenthalpic;

(6) The minimum temperature difference between cold and hot streams in the solution heat exchanger (SHE) is 5 K. The proposed value ensures a not too large SHE size and the prevention of excessive energy loss.

(7) The mechanical energy consumed by the pumps is neglected;

(8) The pressures of the condenser and the generator are equal ($p_G = p_C$), and the pressures of the absorber and evaporator are equal ($p_A = p_E$);

It is essential to establish the mass and energy balance equations for each component and get characteristics of the main state points in the cycle as follows:

The generator can be described by the overall and ionic liquid mass balances and heat balance equations:

$$\dot{m}_7 - \dot{m}_1 - \dot{m}_8 = 0 \quad (\text{III.1})$$

$$\dot{m}_7 x_7^m = \dot{m}_8 x_8^m \quad (\text{III.2})$$

$$Q_G + \dot{m}_7 h_7 - \dot{m}_8 h_8 - \dot{m}_1 h_1 = 0 \quad (\text{III.3})$$

The strong solution at the outlet of the generator is a saturated liquid, so the pressure at this point is the bubble pressure:

$$p_8 = p(T_8, x_8^m) \quad (\text{III.4})$$

Where $T_8 = T_G$ and $p_8 = p_c$

The condenser can be described by:

$$\dot{m}_1 = \dot{m}_2 = \dot{m}_3 = 1 \text{ kg.s}^{-1} \quad (\text{III.5})$$

$$\dot{m}_1 h_1 - \dot{m}_2 h_2 - Q_c = 0 \quad (\text{III.6})$$

For state point 2 (saturated liquid water at the condenser outlet), we have:

$$p_2 = p_c = p^s(T_c) \quad (\text{III.7})$$

In the case of the evaporator:

$$\dot{m}_3 = \dot{m}_4 \quad (\text{III.8})$$

$$\dot{m}_4 h_4 - \dot{m}_3 h_3 - Q_E = 0 \quad (\text{III.9})$$

Vapor is saturated at the outlet of the evaporator, so for point 4, we have:

$$p_4 = p_E = p^s(T_E) \quad (\text{III.10})$$

Balance equations for the absorber give:

$$\dot{m}_4 + \dot{m}_{10} - \dot{m}_5 = 0 \quad (\text{III.11})$$

$$\dot{m}_5 x_5^m = \dot{m}_{10} x_{10}^m \quad (\text{III.12})$$

$$\dot{m}_4 h_4 + \dot{m}_{10} h_{10} - \dot{m}_5 h_5 - Q_A = 0 \quad (\text{III.13})$$

State point 5 is described by equation (III.14)

$$p_5 = p(T_5, x_5^m) \quad (\text{III.14})$$

Where $T_5 = T_A$ and $p_5 = p_E$

In the solution heat exchanger (SHE), the hot stream is the weak solution (point 5) coming from the absorber and the cold stream is the strong solution (point 9) coming from the generator. Since weak solution flowrate is higher than strong solution flowrate and heat capacity of weak solution is higher than the one of rich solution (weak solution contains more water than rich solution and water heat capacity is higher than IL's), it appears that:

$$\dot{m}_{ws} \cdot C_{p\ ws} > \dot{m}_{ss} \cdot C_{p\ ss}$$

Then, the minimal temperature approach is between hot inlet (point 5) and cold outlet (point 10) streams:

$$T_5(\text{hot inlet}) - T_{10}(\text{hot outlet}) = 5K \quad (\text{III.15})$$

Heat balance on the solution heat exchanger can be written:

$$\dot{m}_5 h_5 + \dot{m}_9 h_9 - \dot{m}_6 h_6 - \dot{m}_{10} h_{10} = 0 \quad (\text{III.16})$$

Where \dot{m}_i , h_i , x_i^m ($i=1,2,3,\dots,10$) are respectively the mass flow rate (kg.s^{-1}), specific enthalpy (kJ.kg^{-1}) and mass fraction of absorbent (IL) of each stream. $p^s(T)$ is the saturated vapor pressure of refrigerant H_2O and $p(T, x)$ the saturated pressure of the working mixture $\{\text{H}_2\text{O} + \text{ILs}\}$. They are obtained by the following relations:

$$p(T, x) = x_1 \gamma_1 p_1^s(T) \quad (\text{III.17})$$

$$p^s(T) = (\text{Exp}(73.649 - 7258.2 / T - 7.3037 * \ln(T) + 4.1653 * 10^{-6} * (T^2))) / 1000 \quad (\text{III.18})$$

Where p is the total pressure, x_1 , γ_1 and p_1^s are the water mole fraction in the liquid phase, water activity coefficient for the liquid phase, and saturated vapor pressure of water, respectively.

Usually the temperature of the waste heat used to drive an absorption heat transformer as well as the output temperatures are known for a given application, so the generator, evaporator, condenser and absorber temperatures T_G , T_E , T_C and T_A are known and taken as independent variables in the present research.

The coefficient of performance, COP, is defined as the ratio of available heat output at the absorber to the total heat input to the system Eq. (III.19) [2].

$$COP = \frac{Q_A}{Q_G + Q_E} \quad (III.19)$$

Generally, the enthalpy of liquid mixtures can be expressed as follows:

$$h = x_1^m h_1 + x_2^m h_2 + \Delta_{mix} h \quad (III.20)$$

where

$$h_1 = h_{ref} + \frac{1}{\rho_{1,liq,T_{ref}}} * (p - p_{ref}) + \int_{T_{ref}}^T C_{p,1} dT \quad (III.21)$$

$$h_2 = h_{ref} + \frac{1}{\rho_{2,liq,T_{ref}}} * (p - p_{ref}) + \int_{T_{ref}}^T C_{p,2} dT \quad (III.22)$$

Where, h_1 and h_2 are the enthalpies of pure liquids H₂O and IL, x_1^m and x_2^m are the mass fractions of H₂O and IL, respectively, $\Delta_{mix} h$ is the mixing enthalpy of the system (it can sometimes be neglected). $C_{p,1}$ and $C_{p,2}$ are the heat capacities of H₂O and IL respectively. The reference state for enthalpy calculations is defined T_{ref} , h_{ref} and p_{ref} respectively its temperature, enthalpy and pressure. This parameters are chosen arbitrarily as being:

$$h_{ref} = 0$$

$$T_{ref} = 273.15K$$

$$p_{ref} = 101.325kPa$$

$\rho_{1,liq,T_{ref}}$ and $\rho_{2,liq,T_{ref}}$ are the densities of pure liquid water and pure IL at reference temperature and pressure.

The concentration difference between strong and weak solutions Δx , and gross temperature lift Δt are defined as follows;

$$\Delta x^m = x_8^m - x_5^m = x_s^m - x_w^m \quad (III.23)$$

$$\Delta t = T_A - T_E \quad (III.24)$$

The solution circulation ratio f is defined as the ratio of the mass flow rate of the strong solution, produced in generator, per unit mass of refrigerant vapor formed in the generator:

$$f = \frac{\dot{m}_7}{\dot{m}_1} = \frac{x_s^m}{(x_s^m - x_w^m)} \quad (III.25)$$

Meanwhile the available heat outputs q (kJ/kg) per unit mass of refrigerant can be expressed as:

$$q = \frac{Q_A}{\dot{m}_1} \quad (III.26)$$

One of the most important criteria for evaluating the absorption cycle is the circulation ratio f . Through high f , the equipment costs, operating expenses and the energy requirements of heating and pumping processes will increase accordingly. Circulation

ratios in $\{\text{H}_2\text{O} + \text{LiBr}\}$ and $\{\text{H}_2\text{O} + \text{NH}_3\}$ systems usually are small, with typical values being around $f = 10$ [4, 5].

III.2. COP definition for an Absorption refrigeration cycle

Up to now, the performance of $\{\text{H}_2\text{O} + \text{ILs}\}$ as working fluids was evaluated for absorption refrigeration cycle. Zhang and Hu [6] estimated the COP of $\{\text{water} + [\text{EMIM}][\text{DMP}]\}$ and $\{\text{H}_2\text{O} + \text{LiBr}\}$ mixtures under the same operating conditions. The COP of the absorption chiller for $\{\text{H}_2\text{O} + [\text{EMIM}][\text{DMP}]\}$ was lower than that of $\{\text{H}_2\text{O} + \text{LiBr}\}$ by 7% but still higher than 0.7. They observed that the generation temperature for $\{\text{H}_2\text{O} + [\text{EMIM}][\text{DMP}]\}$ was lower than $\{\text{H}_2\text{O} + \text{LiBr}\}$. Hence, this indicated that absorption chiller using $\{\text{H}_2\text{O} + [\text{EMIM}][\text{DMP}]\}$ as working fluid can be operated by lower temperature level waste heat under the same operation conditions. Therefore, they concluded that the $\{\text{H}_2\text{O} + [\text{EMIM}][\text{DMP}]\}$ binary system has a potential to be a new working pair for the absorption chiller driven by low-grade waste heat or hot water generated by common solar collector.

Kim *et al.* [7] estimated the COP for binary system consisting of $\{\text{H}_2\text{O} + [\text{EMIM}][\text{BF}_4]\}$ with evaporator and condenser temperatures being 25°C and 50°C , respectively. Its value reaches 0.91. The authors stated that their studied binary system leads to high COP because of the suitable compatibility of water with $[\text{EMIM}][\text{BF}_4]$ and the superior properties of water as a heat transfer fluid, such as large latent heat of evaporation, followed by extremely small refrigerant (water) flow rate.

Dong *et al.* [1] (Table III.2) evaluated the cycle performance of a single-effect absorption refrigeration cycle using $\{\text{H}_2\text{O} + [\text{DMIM}][\text{DMP}]\}$ system. The simulation results show that the cycle performance of $\{\text{H}_2\text{O} + [\text{DMIM}][\text{DMP}]\}$ is close to that of conventional working pair $\{\text{H}_2\text{O} + \text{LiBr}\}$. However, the use of the $\{\text{H}_2\text{O} + [\text{DMIM}][\text{DMP}]\}$ system, allows to extend the operating temperature range and to overcome the disadvantages of crystallization and corrosion caused by $\{\text{H}_2\text{O} + \text{LiBr}\}$.

Table III.2: COP of {H₂O + absorbent} binary systems for absorption refrigeration cycle found in literature.

T(K)	T _C	T _E	T _G	T _A
	313.15	283.15	373.15	303.15
Refrigerant	Absorbent	COP	<i>f</i>	Reference
H ₂ O	LiBr	0.78	4.08	8
H ₂ O	[DMIM][DMP]	0.66	5.32	8
H ₂ O	[EMIM][DMP]	0.69	8.66	8
H ₂ O	[EMIM][BF ₄]	0.53	18.20	8
H ₂ O	[EMIM][EtSO ₄]	0.57	13.57	8
H ₂ O	[EMIM][DEP]	0.59	7.75	8
H ₂ O	[BMIM][BF ₄]	0.54	13.00	8
H ₂ O	[BMIM][I]	0.53	23.70	8
H ₂ O	[BMIM][DBP]	0.53	11.17	8
H ₂ O	[EEIM][DEP]	0.57	12.38	8
H ₂ O	[Choline][Gly]	0.45	4.79	8
H ₂ O	[Choline][MeSO ₃]	0.64	7.32	8
H ₂ O	[Choline][Lac]	0.66	7.79	8
T(K)	T _C	T _E	T _G	T _A
	313.15	283.15	373.15	303.15
Refrigerant	Absorbent	COP	<i>f</i>	Reference
H ₂ O	LiBr	0.84	6.59	1
H ₂ O	[DMIM][DMP]	0.83	8.77	1
H ₂ O	[DMIM][Cl]	0.83	9.54	3

III.3.Absorption heat transformer

In this section, the thermodynamic performance of an absorption heat transformer system using the new binary systems (Group I) as working fluids is numerically evaluated.

To evaluate the performance of an AHT a VBA dedicated calculation code has been developed (Figures III.2 and III.3). The simulation results for AHT using the new working binary systems are compared to each other and to the data found in literature for the classical working fluid {H₂O +LiBr}. Results are also compared to simulation results for binary systems of group II (see Table III.3). Deviations among the calculated and literature results exist because different calculations are based on different property

data, thermodynamic models, and operating conditions, e.g., heat source temperature. In this work, evaporating temperature T_E , condensing temperature T_C , absorbing temperature T_A and generator temperature T_G are set to 80 °C, 20 °C, 130 °C, and 80 °C, respectively. These values were modified in order to study the influence of each component temperature (T_G , T_E , T_A , T_C) on the performance of the AHT.

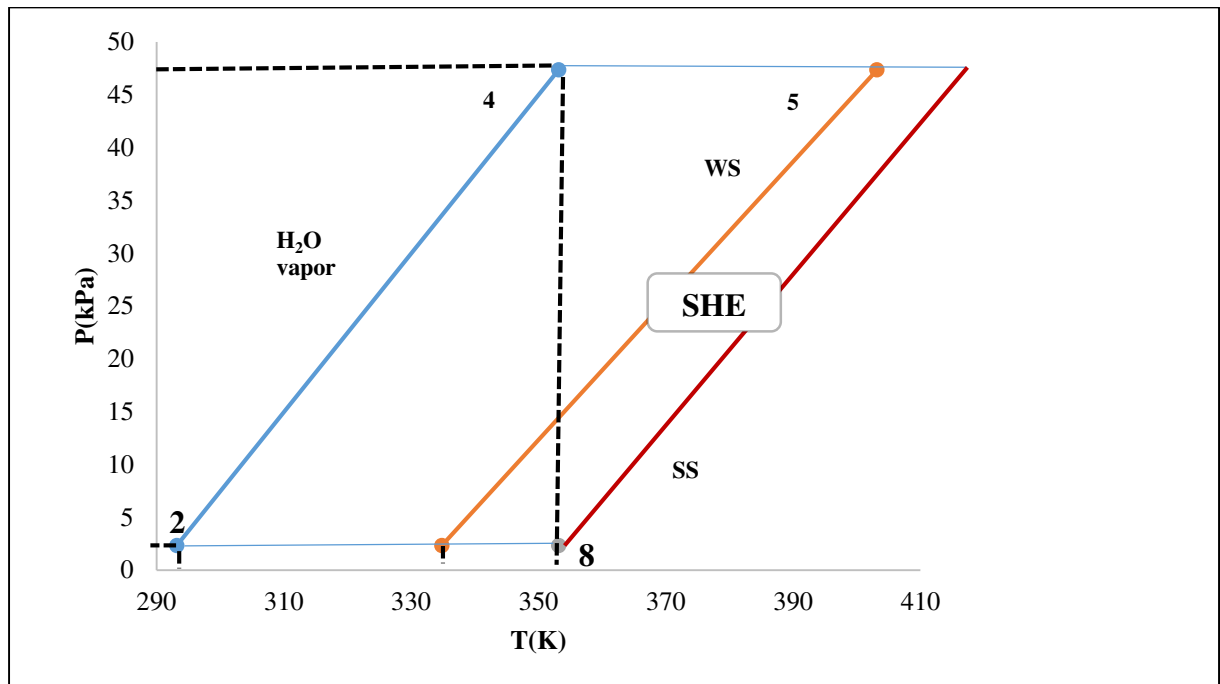


Figure III.2: Thermodynamic cycle in absorption heat transformer (AHT).

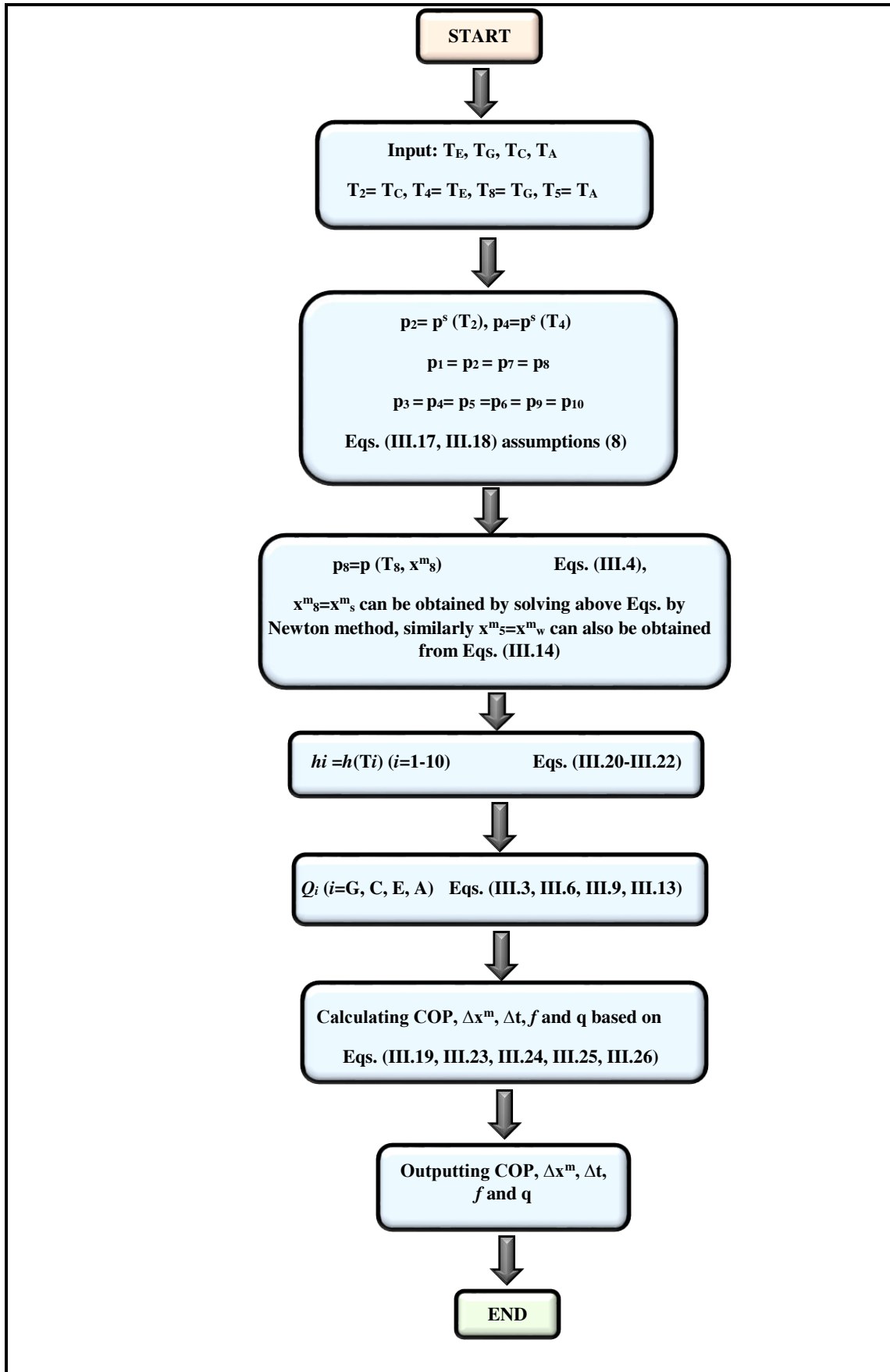


Figure III.3: Flow chart for COP simulation.

Table III.3: Calculated COP of {H₂O + ILs} binary systems for absorption heat transformer cycle compared to data found in literature^{*,**}.

Groups	T (K)		T _C	T _E	T _G	T _A
			308.15	363.15	363.15	403.15
	Refrigerant	Absorbent	COP	x ^m _s	Δx ^m	f
I	Water	[DMIM][MPh]	0.44	0.97	0.05	19.73
	Water	[DMIM][MeSO ₄]	0.44	0.97	0.05	21.81
	Water	[EMIM][MPh]	0.44	0.96	0.07	13.55
	Water	[EMIM][EPh]	0.43	0.96	0.04	27.04
	Water	[EMIM][MeSO ₄]	0.43	0.97	0.04	22.76
	Water	[BMIM][DCA]	0.44	0.98	0.05	21.18
Ref.	Water	LiBr*	0.5	0.64	0.07	11
	TFE	E181*	0.42	0.9	0.1	9
II	Water	[EMIM][DMP]*	0.48	n.d	n.d	n.d
	Water	[DMIM][DMP]	0.45	0.92	0.09	10.01
	Water	[EMIM][DMP]	0.44	0.92	0.08	11.26
	Water	[EMIM][DEP]	0.44	0.92	0.07	13.54
	Water	[EMIM][AC]	0.44	0.87	0.08	10.54
	Water	[HOEtMIM][Cl]	0.45	0.94	0.1	9.88
	Water	[EMIM][EtSO ₄]	0.41	0.97	0.03	38.21
	Water	[EMIM][Triflate]	0.42	0.99	0.02	41.34
	Water	[EMIM][TFA]	0.44	0.97	0.05	19.7
	Water	[DEMA][Oms]	0.44	0.95	0.08	12.63
	Water	[BMIM][Triflate]	0.36	0.99	0.01	71.56
	Water	[BMIM][BF ₄]	0.43	0.97	0.04	25.01
Groups	T (K)		T _C	T _E	T _G	T _A
			298.15	353.15	353.15	403.15
	Refrigerant	Absorbent	COP	x ^m _s	Δx ^m	f
I	Water	[DMIM][MPh]	0.41	0.98	0.03	35.68
	Water	[DMIM][MeSO ₄]	0.42	0.98	0.04	27.09
	Water	[EMIM][MPh]	0.43	0.97	0.05	21.8
	Water	[EMIM][EPh]	0.34	0.96	0.01	85.02
	Water	[EMIM][MeSO ₄]	0.42	0.98	0.04	27.42
	Water	[BMIM][DCA]	0.42	0.98	0.03	31.22
Ref.	Water	LiBr**	0.48	n.d	n.d	9.51
II	Water	[DMIM][DMP]	0.43	0.93	0.06	15.92
	Water	[EMIM][DMP]	0.41	0.93	0.05	19.52
	Water	[EMIM][DEP]	0.42	0.92	0.04	21.06
	Water	[EMIM][AC]	0.43	0.87	0.05	17.98
	Water	[HOEtMIM][Cl]	0.43	0.95	0.06	15.58
	Water	[EMIM][EtSO ₄]	0.14	0.97	0.01	172.47

Groups	T (K)		T _C	T _E	T _G	T _A
			298.15	353.15	353.15	403.15
	Refrigerant	Absorbent	COP	x ^m _s	Δx ^m	f
II	Water	[EMIM][Triflate]	0.38	0.99	0.01	69.49
	Water	[EMIM][TFA]	0.42	0.97	0.03	31.99
	Water	[DEMA][Oms]	0.43	0.96	0.05	21.07
	Water	[BMIM][Triflate]	0.27	0.99	0.01	140.5
	Water	[BMIM][BF ₄]	0.4	0.97	0.02	43.6
Groups	T (K)		T _C	T _E	T _G	T _A
			293.15	353.15	353.15	403.15
	Refrigerant	Absorbent	COP	x ^m _s	Δx ^m	f
I	Water	[DMIM][MPh]	0.42	0.98	0.03	29.26
	Water	[DMIM][MeSO ₄]	0.43	0.99	0.04	22.7
	Water	[EMIM][MPh]	0.43	0.98	0.05	18.68
	Water	[EMIM][EPH]	0.39	0.96	0.02	49.89
	Water	[EMIM][MeSO ₄]	0.43	0.98	0.04	24.16
	Water	[BMIM][DCA]	0.42	0.99	0.04	27.48
II	Water	[DMIM][DMP]	0.44	0.94	0.07	12.9
	Water	[EMIM][DMP]	0.42	0.94	0.06	15.09
	Water	[EMIM][AC]	0.43	0.89	0.06	14.16
	Water	[EMIM][DEP]	0.43	0.88	0.93	17.71
	Water	[HOEtMIM][Cl]	0.43	0.96	0.07	13.14
	Water	[EMIM][EtSO ₄]	0.35	0.98	0.01	74.48
	Water	[EMIM][Triflate]	0.39	0.99	0.02	60.08
	Water	[EMIM][TFA]	0.42	0.98	0.04	26.58
	Water	[DEMA][Oms]	0.43	0.97	0.06	17.3
	Water	[BMIM][Triflate]	0.32	0.99	0.01	108.71
	Water	[BMIM][BF ₄]	0.41	0.98	0.03	34.96

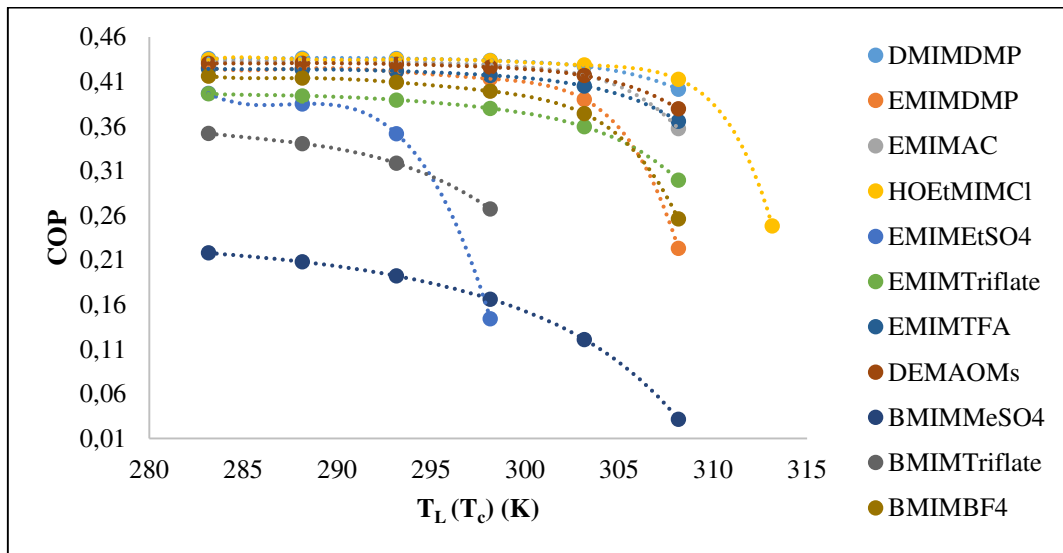
*Data found in literature [2]

**Data found in literature [9]

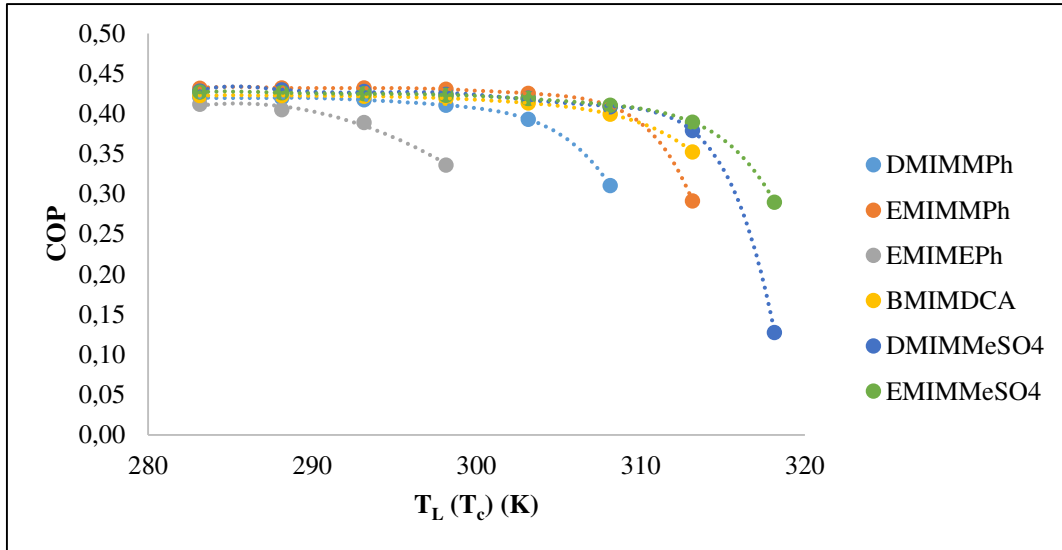
To illustrate how the AHT system main components temperatures affect the system performance, the results are shown in Figures (III.4, III.5, and III.6). As can be seen from Figure III.4 (a,b), while the condenser temperature ($T_c = T_L$) increases at constant generator (T_G), evaporator (T_E) and absorber (T_A) temperatures, the COP decreases. Figure III.4 shows a relatively high COP up to about 303.15 K followed by a sharp decrease as the condenser temperature rises above 303.15 K. The variation of the condenser temperature affects the concentration of refrigerant in the strong solution, which can be approximated by the following Eq.

$$x_8^{ss} = \frac{p_c}{\gamma_w p^{sat}(T_8)} \quad (\text{III.27})$$

where p_c is the vapor pressure at the condenser and $p^{sat}(T_8)$ is the saturation vapor pressure at T_8 , x_8^{ss} and γ_w are the mole fraction of ILs at point 8 (strong solution) and activity coefficient of the refrigerant, respectively. As the temperature increases, the system low pressure will increase and the ILs mole fraction in the strong solution will decrease. Hence, the strong solution concentration will decrease, resulting in an increase of the circulation ratio. It is found that the lower the condensing temperature is, the higher the COP or available temperature lift will be. This is why the AHT is more efficient during winter [2]. The variation of the condenser temperature affects as well the heat input of the evaporator Q_E . From Eq. (III.9) we can see that as T_c increase h_3 increase, hence, Q_E will decrease as well as COP.



(a) Group II binary systems



(b) Group I binary systems

Figure III.4: COP of binary systems {water + ILs} versus $T_L (T_c)$ for single effect absorption heat transformer cycle.

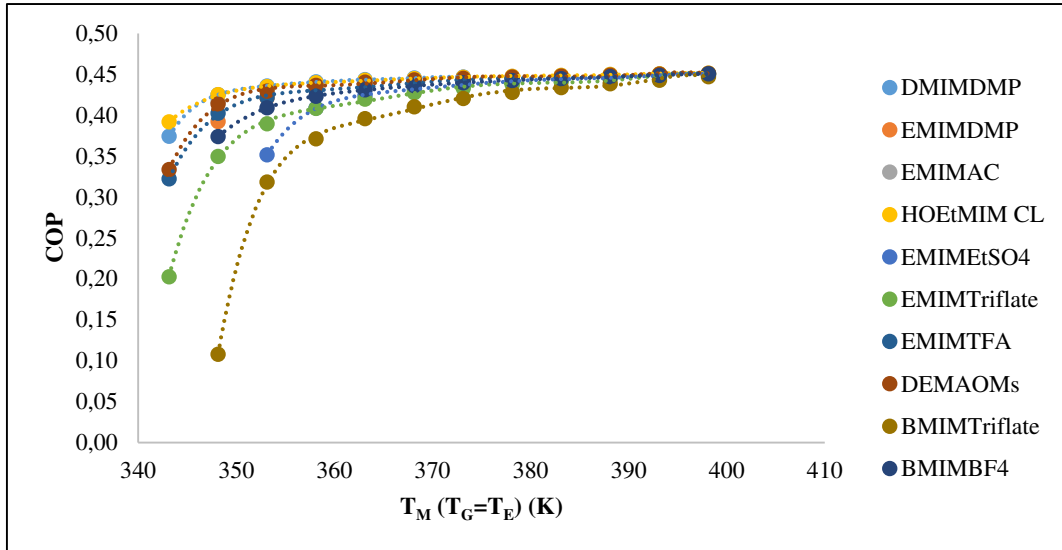
On the other hand, when the evaporator and the generator temperatures increase ($T_E = T_G = T_M$) at constant absorber and condenser temperatures, the COP of various binary systems have the same behavior: COP sharply increases initially, then becomes stable, and slightly declines finally as presented in Figure III.5. This is because when the evaporator temperature increases, the system high pressure will increase and the weak solution concentration will decrease.

The variation of the generator directly affects the concentration of refrigerant in the weak solution, which can be approximated by Eq. (III.28) [7].

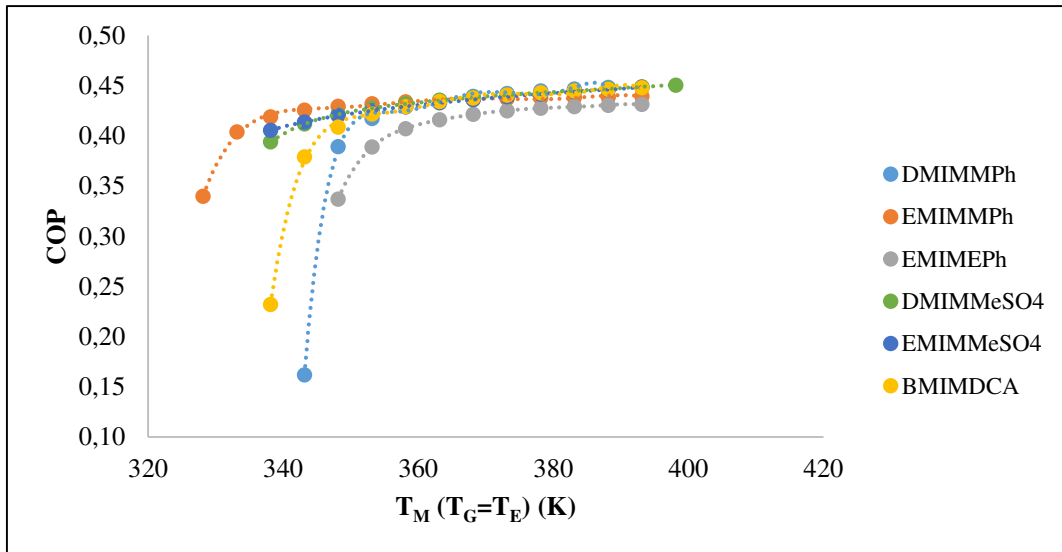
$$x_5^{ws} = \frac{p_E}{\gamma_w p^{sat}(T_5)} \quad (III.28)$$

where p_E is the vapor pressure at the evaporator and $p^{sat}(T_5)$ is the saturation vapor pressure at T_5 , x_5^{ws} and γ_w are the mole fraction of ILs at point 5 (weak solution) and activity coefficient of the refrigerant, respectively. As the temperature increases, the refrigerant mole fraction also increases which leads to decrease the concentration of the weak solution. The circulation ratio of the solution will then vary accordingly.

Consequently, the effect of the reduced circulation ratio and the increased enthalpy on the heat input to the generator leads to an increase of the COP in Figure III.5.



(a) Group II binary systems



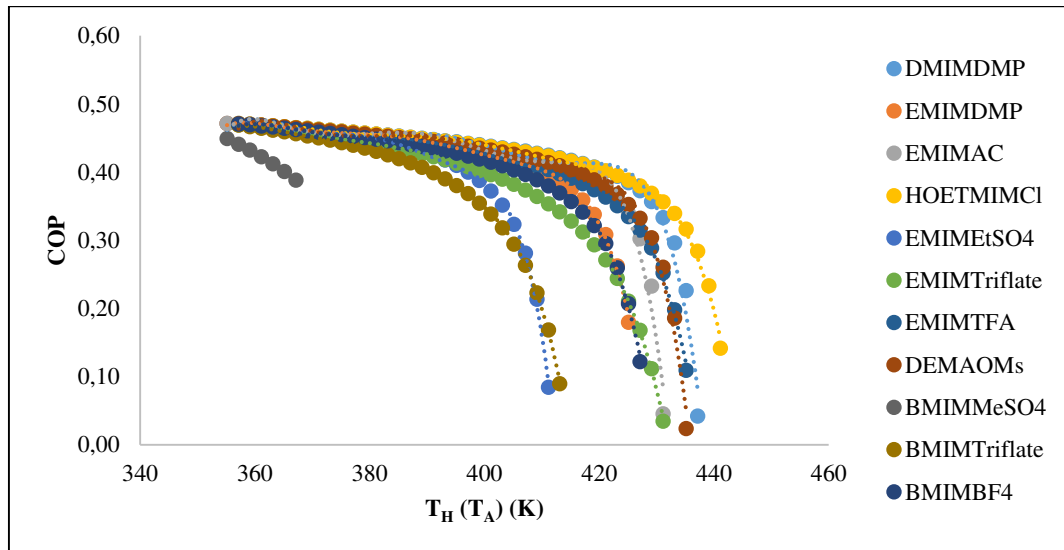
(b) Group I binary systems

Figure III.5: COP of binary systems {water + ILs} versus T_M ($T_G=T_E$) for single effect absorption heat transformer cycle.

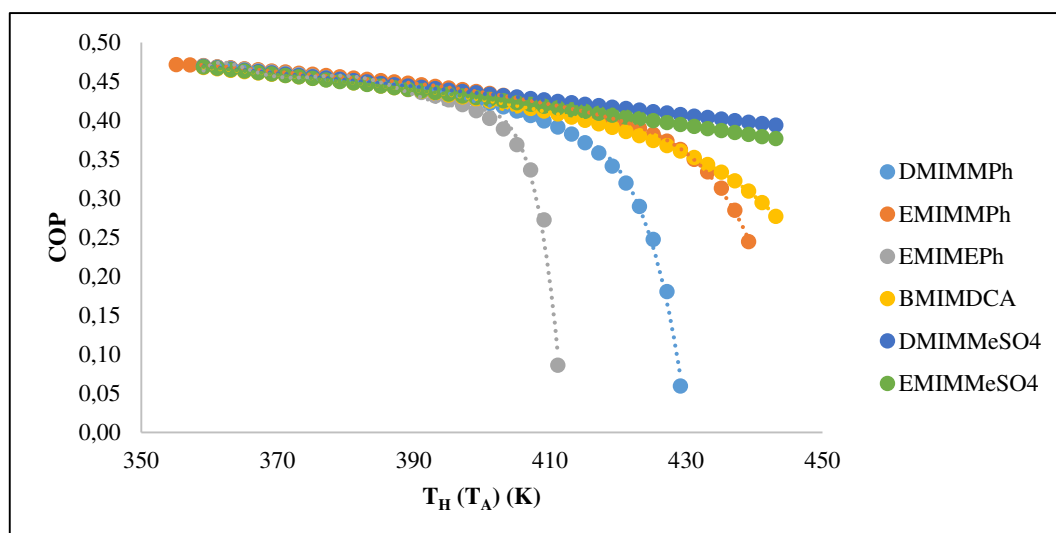
As the generator temperature reaches its minimum f tends toward infinity and so is the required heat for the generator. Consequently, the COP of the cycle tends toward zero.

With the increase of generator temperature f decreases, COP sharply increases and then smoothens.

From Figure III.6 (a,b), it can be seen that the COP of AHT for the working pairs will decrease at different rate with the increase of the absorber temperature ($T_A = T_H$). This behavior can be explained using Figure III.7 (a,b) that illustrates the concentration variation of weak solutions with absorbing temperature T_A . The strong solution leaving the generator has a concentration x_s^m , which is rich in absorbent more than the weak solution, hence it can absorb refrigerant vapor easier. For given generator and condenser temperatures, x_s^m does not vary with T_A , but x_w^m increases with T_A . The higher the absorber temperature T_A or gross temperature lift Δt is, the higher the content of IL in the weak solution is. This leads to the decrease of concentration difference $\Delta x^m = x_s^m - x_w^m$ or to the increase of flow rate ratio f and mechanical power losses which is the same behavior observed by Zhang and Hu. [2].

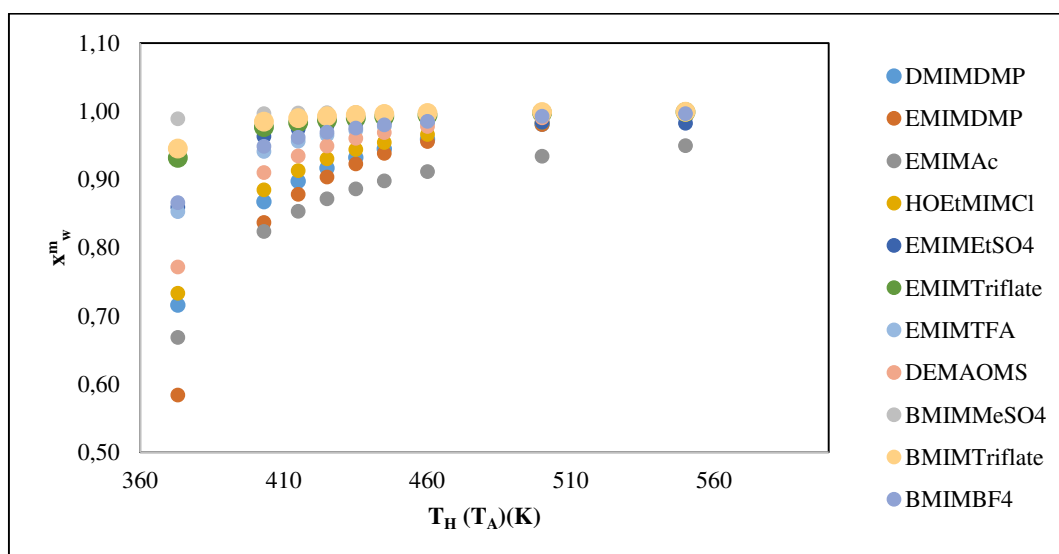


(a) Group II binary systems

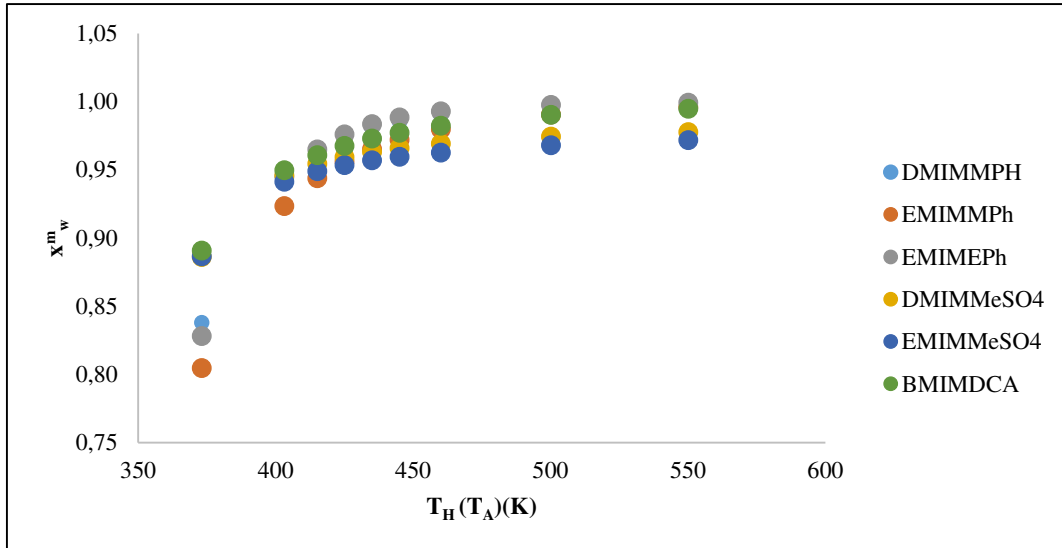


(b) Group I binary systems

Figure III.6: COP of binary systems {water + ILs} versus T_H (T_A) for single effect absorption heat transformer cycle.



(a) Group II binary systems



(b) Group I binary systems

Figure III.7: Effect of T_H on (x^m_w) weak solution concentration.**Table III.4:** The available heat output per unit mass of refrigerant (q) for AHT cycle.

T_C	T_G	T_E	T_A
293.15	353.15	353.15	403.15
Binary system (Group I)	q (kJ.kg ⁻¹)	Binary system (Group II)	q (kJ.kg ⁻¹)
{H ₂ O+[DMIM][MPh]}	1836.87	{H ₂ O+[DMIM][DMP]}	1982.31
{H ₂ O+[EMIM][MPh]}	1951.65	{H ₂ O+[EMIM][DMP]}	1867.90
{H ₂ O+[EMIM][EPh]}	1633.61	{H ₂ O+[EMIM][AC]}	1953.77
{H ₂ O+[DMIM][MeSO ₄]}	1915.92	{H ₂ O+[EMIM][TFA]}	1871.63
{H ₂ O+[EMIM][MeSO ₄]}	1896.56	{H ₂ O+[HOEtMIM][Cl]}	1974.05
{H ₂ O+[BMIM][DCA]}	1871.11	{H ₂ O+[DEMA][OMs]}	1932.00
T_C	T_G	T_E	T_A
308.15	363.15	363.15	403.15
Binary system (Group I)	q (kJ.kg ⁻¹)	Binary system (Group II)	q (kJ.kg ⁻¹)
{H ₂ O+[DMIM][MPh]}	1944.11	{H ₂ O+[DMIM][DMP]}	2028.68
{H ₂ O+[EMIM][MPh]}	2012.93	{H ₂ O+[EMIM][DMP]}	1950.12
{H ₂ O+[EMIM][EPh]}	1868.75	{H ₂ O+[EMIM][DEP]}	1971.25
{H ₂ O+[DMIM][MeSO ₄]}	1938.79	{H ₂ O+[EMIM][AC]}	2012.03
{H ₂ O+[EMIM][MeSO ₄]}	1924.76	{H ₂ O+[EMIM][TFA]}	1950.71
{H ₂ O+[BMIM][DCA]}	1943.32	{H ₂ O+[HOEtMIM][Cl]}	2026.24

The available heat output per unit mass of refrigerant (q) for the studied binary systems was calculated and compared with Zhang and Hu.data [2] under the same conditions: generation, evaporation, condensing and absorption temperatures are 363.15, 363.15, 308.15 and 403.15 K (Table III.4).

It is found that $\{H_2O + [EMIM][MPh]\}$ has the highest q value, 2012.93 kJ.kg^{-1} , in the investigated binary systems (Group I). Meanwhile, q value for $\{H_2O + [DMIM][DMP]\}$ is 2028.68 kJ.kg^{-1} and $\{H_2O + [HOEtMIM][Cl]\}$ is slightly less 2026 kJ.kg^{-1} . For the other binary systems q ranges between 1971 and 1527 kJ.kg^{-1} (Table III.4). This is less than 2466 kJ.kg^{-1} for $\{H_2O + LiBr\}$, but it is much larger than 311 kJ.kg^{-1} for $\{TFE + TEGDME\}$. So under the same available heat output conditions, the amount of water cycled in the AHT will be much less than that of TFE. This will decrease the mechanical power losses and the size of pipes and pumps.

The mass fraction of IL in the strong solution is exceeding 0.9 for most of the binary systems studied, while it is only 0.64 for $\{H_2O + LiBr\}$ (Table III.3). Under the same circulation ratio f condition the concentration difference for most of the binary systems and $\{TFE + TEGDME\}$ is larger than that of $\{H_2O + LiBr\}$, which will enhance the absorbing process in the absorber.

The simulation results show that the COP of the investigated binary systems are close to that of conventional working pair $\{H_2O + LiBr\}$. On the other hand, for the cycle using $\{H_2O + ILs\}$ pairs, the operating temperature range can be extended and the disadvantages of crystallization and corrosion caused by $\{H_2O + LiBr\}$ can be avoided.

Simulations for evaporating temperature T_E , condensing temperature T_C , absorbing temperature T_A and generator temperature T_G set to 80°C, 20°C, 130°C, and 80 °C respectively, showed that the COP values for the studied binary systems have the following trend:

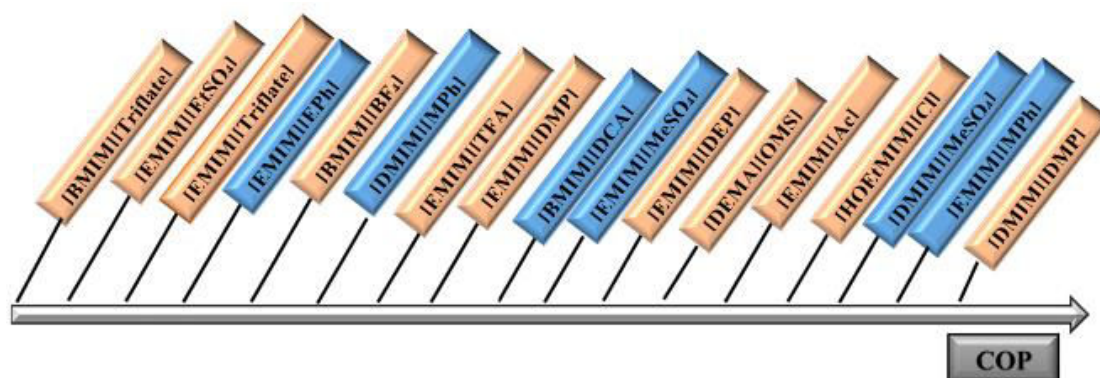


Figure III.8: Simulation trend for the investigated binary systems

Group I (■) and II (■).

Cations with shorter alkyl chains are preferred ($[DMIM] > [EMIM] > [BMIM]$) due to more sensitive dependence of the solubility on temperature. Hence, we can conclude that ionic liquids with short alkyl chains lead to higher COP values and lower circulation ratio f .

Binary systems containing ionic liquids with small and compact anions such as acetate or chloride based ionic liquids lead to high COP. Nie *et al.* [10] stated that $[HOEtMIM][Cl]$ is a suitable alternative working pair for absorption heat pump. Furthermore, Romich *et al.* [11] stated that $[EMIM][Ac]$ and $[DEMA][OMS]$ are applicable in absorption cycles. However, Seiler *et al.* [12] stated that neither acetate nor chloride-based ionic liquids are suitable for AHT due to an insufficient stability and/or too high corrosion rates.

It was noticed that binary system composed of $\{H_2O + [BMIM][MeSO_4]\}$ exhibits smaller Δt than the other investigated 17 systems. Its largest observed Δt is about 40 K and the lowest is 30K. Simulation of binary system consisting of $\{H_2O + [BMIM][MeSO_4]\}$ is not promising maybe due to low solubility of IL in water or to stability of the IL [13]. In contrast to the earlier findings, the two based sulfates ionic liquids investigated by the authors (Group I) have high COP values and low circulation ratio. A possible explanation for this might be the short alkyl chain length which results in better affinity of IL with H_2O .

In this work, only binary system VLE was measured for the $\{H_2O + [BMIM][Ac]\}$ mixture. These data were correlated using NRTL and circulation ratio f has been calculated. Simulation for this binary system was done for the same temperature

conditions than for the rest of simulations. Results showed that this binary system allows to reach a low f value of 19.14. In the light of these results, it would be highly recommended to further investigate this binary system. Twenty three binary systems are found to have only VLE data in literature (Group III) lacking other thermodynamic properties. Using NRTL the VLE data of these 23 binary systems were correlated, and f were determined. Simulation for these binary systems were done for the same conditions. Simulation results showed that there are promising binary systems exhibiting low f values such as [BMIM][C₁SO₃], [BMIM][I], [BMPyr][DCA] which are 19.89, 16.96 and 17.25 respectively. In the light of these results, it would as well be highly recommended to further investigate these binary systems.

In brief, seventeen binary systems consisting of {H₂O + ILs} were studied as working fluids for absorption heat transformers. Their basic thermodynamic properties including vapor pressure, heat capacity, excess enthalpy, viscosity and density were analyzed. The VLE values of these 17 binary solutions showed a considerable negative deviation from Raoult's law, which is an important characteristic for absorption working fluids. The excess enthalpies data measured and found in literature for number of the binary systems at different IL concentrations and at different temperatures were negative and were correlated by Redlich–Kister-type equation. These results provided an insight into the interactions of the absorbent and refrigerant, which is key information needed for evaluating the performance of the new working pairs. Although viscosity of pure ILs were high, but it would decrease sharply when the ILs were heated or mixed with water. Since the absorption and generation temperatures of an absorption transformer are usually high, the viscosity of the {H₂O + ILs} pairs is expected to be low. Consequently, the high viscosity of the ionic liquid would not limit its use as a heat pump absorbent. Eventually, the simulation results show that the performance of the new binary systems is close to that of conventional working pair {H₂O + LiBr}. Nevertheless, for the cycle using {H₂O + ILs} systems, the operating temperature range has been extended and the disadvantages of crystallization and corrosion caused by {H₂O + LiBr} can be relieved.

References

- [1] L. Dong , D. Zheng, N. Nie, Y. Li, Performance prediction of absorption refrigeration cycle based on the measurements of vapor pressure and heat capacity of {H₂O + [DMIM][DMP]} system, *Applied Energy*, 98 (2012) 326–332.
- [2] X. Zhang, D. Hu, Performance analysis of the single-stage absorption heat transformer using a new working pair composed of ionic liquid and water, *Applied Thermal Engineering*, 37 (2012) 129–135.
- [3] D. Zheng, L. Dong, W. Huang, X. Wu, N. Nie, A review of imidazolium ionic liquids research and development towards working pair of absorption cycle, *Renewable and Sustainable Energy Reviews*, 37 (2014) 47–68.
- [4] M. Khamooshi, K. Parham, U. Atikol, Overview of ionic liquids used as working fluids in absorption cycles, *Advances in Mechanical Engineering*, 620592 (2013) 1–7.
- [5] T. Nakanishi, T. Furukawa, N. Sato, Industrial high-temperature heat pump, *Hitachi zosen Tech Rev*, 42 (1981) 7–12.
- [6] X. Zhang, D. Hu, Performance simulation of the absorption chiller using water and ionic liquid 1-ethyl-3-methylimidazolium dimethylphosphate as the working pair, *Applied Thermal Engineering*, 31 (2011) 3316–21.
- [7] Y.J. Kim, S. Kim, Y.K. Joshi, A.G. Fedorov, P.A. Kohl, Thermodynamic analysis of an absorption refrigeration system with ionic-liquid/refrigerant mixture as a working fluid, *Energy*, 44 (2012) 1005–1016.
- [8] A. Yokozeki, M.B. Shiflett, Water solubility in ionic liquids and application to absorption cycles, *Ind. Eng. Chem. Res.*, 49 (2010) 9496–9503.
- [9] K. Parham, M. Khamooshi, D.B.K. Tematio, M. Yari, U. Atikol, Absorption heat transformers – A comprehensive review, *Renewable and Sustainable Energy Reviews*, 34 (2014) 430–452.

- [10] N. Nie, D. Zheng, L. Dong, Y. Li, Thermodynamic properties of the water + 1- (2-hydroxyethyl)-3-methylimidazolium chloride system, *J. Chem. Eng. Data*, 57 (2012) 3598–3603.
- [11] C. Romich, N.C. Merkel, A. Valbonesi, K. Schaber, S. Sauer, T.J.S. Schubert, Thermodynamic properties of binary mixtures of water and room-temperature ionic liquids: vapor pressure, heat capacities, densities and viscosities of water + 1-ethyl-3-methylimidazolium acetate and water + Diethylmethylammonium methane sulfonate, *J. Chem. Eng. Data*, 57 (2012) 2258–2264.
- [12] M. Seiler, A. Kuhn, F. Ziegler, X. Wang, Sustainable cooling strategies using new chemical system solutions, *Ind. Eng. Chem. Res.*, 52 (2013) 16519–46.
- [13] L.E. Ficke, Thermodynamic properties of imidazolium and phosphonium based ionic liquid mixtures with water or carbon dioxide. PhD thesis, Chemical and Biomolecular Engineering, University of Notre Dame, Notre Dame, Indiana; April 2010.

CONCLUSIONS AND PERSPECTIVES

This dissertation has proposed binary systems consisting of {water + ILs} as alternative working fluids in absorption heat transformers in order to overcome the drawbacks of the commonly used working pair {H₂O + LiBr}.

In the present work, an extensive investigation of thermodynamic properties of binary systems {H₂O + ILs} was accomplished. Simulation of the performance of absorption heat transformers using the new working pairs {H₂O + ILs} was performed using experimental thermodynamic properties and by solving the mass and energy balance for each component of the system.

Experimental measurements of vapor-liquid equilibrium, heat capacity, density and excess enthalpy were measured. The results of these investigation show that most of the binary systems studied have activity coefficients lower than unity, results from the stronger IL-water interactions than the water-water. The higher the content of IL is, the larger the deviation from the Raoult's law. This means that there is strong affinity between ILs and water which is a very important property of a working pair for absorption heat transformers. Generally, the heat capacities of {H₂O + ILs} binary systems are low, which is suitable for heat transfer, decreases energy consumption and increases the coefficient of performance in absorption heat transformers. Excess enthalpy for the investigated binary systems are negative. These results provide an insight into the interactions of the absorbent (ILs) and refrigerant (water) which is a key information for evaluation the potential of the new working pairs. Viscosity of pure ILs are high, but it would reduce sharply when ILs are heated or water is added. As the absorber and generator temperatures of an absorption heat transformers are usually high, the viscosity of the {H₂O + ILs} working pairs is expected to be low. Accordingly, the high viscosity of the ionic liquid would not limit its use as an absorbent.

The simulation results of working fluids {H₂O + ILs} show that the performance (in term of coefficient of performance COP) of the new binary systems is close to that of conventional working pair {H₂O + LiBr}. Nevertheless, for the cycle using {H₂O + ILs} systems, the operating temperature range has been extended and the disadvantages of crystallization and corrosion caused by {H₂O + LiBr} can be relieved.

Finally, a number of important limitations need to be considered. Although many ionic liquids became commercially available from companies such as Sigma-Aldrich, BASF,

Fluka, Solchemar, Scionix, Solvent Innovation, Acros, etc., but still a lot of ionic liquids are made primarily in laboratory scale quantities and sell for around €1-€10/g.

Additionally, impurities that may result from the synthesis process affects the transport properties of the IL and IL mixtures. It has been shown that water impurities decrease density and halide impurities affect the density values [1]. Thus, any known impurities for an IL should be reported. The isobaric VLE experimental method was limited by temperature instability which occurred at the ILs high composition range. This is due to the elevated viscosity for this range of composition. Future research should therefore concentrate on the investigation of VLE under higher temperatures in order to simulate the conditions of the working fluids in absorption heat transformer. Moreover, both isobaric and isothermal methods consume a long time to reach equilibrium. A reasonable approach to tackle the VLE issue could be the implementation of static headspace gas chromatography (GC). This method is faster and can be applied for the entire range of composition [2].

In view of the promising simulation results of the investigated binary systems, it is recommended that further research be undertaken in the following areas:

Our work shows that there are promising ILs, future research should therefore concentrate on the investigation of corrosion of these ILs and their mixture with water. Corrosion can be examined by electrochemical and weight loss methods through exposing different metals and alloys (copper, nickel, etc.) to ILs for a definite time and temperature.

One of the major areas that needs to be studied for the IL and water binary system is the long term stability. Each IL of interest should be saturated with water and studied at elevated temperatures for long periods of time. This will provide insights for the behavior of the binary mixture and the probability of decomposition of ILs and the result byproduct. Clearly, decomposition period must be taken into account when trying to use ILs as absorbents in AHT.

There is a definite need for investigating the viscosity because this parameter affects other transport properties such as diffusion and thermal conductivity as it affects heat

and mass transfer. Full knowledge about the viscosity provide an insight into stirring, mixing and pumping processes.

The questions of how ionic liquids are to be disposed and their effect on environment should be fully discussed. Further research might explore toxicology and ecotoxicology of the ILs of interest and their mixtures with water. Aqueous toxicology investigations are the most important topic of interest concerning ionic liquids environmental safety. Toxicity of the investigated ILs can be determined for *Daphnia magna*. Its response to ionic liquids is, essential for evaluating how these new solvents will impact an environmental ecosystem.

Furthermore, flammability of the investigated ILs and their mixture with water should be examined.

Then, a predictive thermodynamic model based on group contribution could be a useful tool to predict the performance of working fluids containing ionic liquids in AHT.

This work has focused only on single effect absorption heat transformers (AHT) and completely miscible ionic liquids in water, it would be interesting to study partially miscible ILs and different configuration of AHT such as absorption-demixing heat transformer (ADHT) cycle, double stage and double effect absorption heat transformers (DAHTs), or triple absorption heat transformer (TAHTs) [3, 4, 5].

In this dissertation, we studied binary systems {H₂O + ILs} as alternative working fluids for AHT cycle. The obtained results are promising but further studies on the interaction between ionic liquids and other refrigerants such as R134a/ethanol/methanol/HFO (HFO-YF1234) /CO₂ could be performed. A future study investigating thermodynamic properties of imidazolium, piperidinium and pyrrolidinium based ionic liquids with different anions such as alkylphosphonates, dialkylphosphates, dicyanamide and acetate would be interesting. As a final step, a pilot unit could be instructed in order to evaluate the performance of the investigated binary systems and to improve the process.

References

- [1] K.R. Seddon, A. Stark, M.J. Torres, Influence of chloride, water, and organic solvents on the physical properties of ionic liquids, *Pure and Applied Chemistry*, 72 (2000), 2275–2287.
- [2] L.E. Ficke, Thermodynamic properties of imidazolium and phosphonium based ionic liquid mixtures with water or carbon dioxide. PhD thesis, Chemical and Biomolecular Engineering, University of Notre Dame, Notre Dame, Indiana; April 2010.
- [3] D. Alonso, T. Cachot, J.M. Hornut, Experimental study of an innovative absorption heat transformer using partially miscible working mixtures, *International Journal of Thermal Sciences*, 42 (2003) 631–638.
- [4] D. Alonso, T. Cachot, J.M. Hornut, Performance simulation of an absorption heat transformer operating with partially miscible mixtures, *Applied Energy*, 72 (2002) 583–597.
- [5] K. Parham, M. Khamooshi, D.B.K. Tematio, M. Yari, U. Atikol, Absorption heat transformers – A comprehensive review, *Renewable and Sustainable Energy Reviews*, 34 (2014) 430–452.

I.9.1. Annex

I.9.1. {H₂O + Ionic liquids} binary systems in literature**Table 1.1.:** Binary systems composed of {water + ILs} were used in AH cycle.

ILs	Refrigerant	VLE methods	Therm. Prop.	Ref.
1,3-dimethylimidazolium Chloride [DMIM][Cl]	H ₂ O	B. P. method	ρ	1, 2
1,3-dimethylimidazolium Tetrafluoroborate [DMIM][BF ₄]	H ₂ O	B. P. method		3
1,3-dimethylimidazolium dimethylphosphate [DMIM][DMP]	H ₂ O	B. P. method	C_p , ρ , H^E , Viscosity	4,5,6
1-(2-hydroxyethyl)-3-methylimidazolium chloride [HOEtMIM][Cl]	H ₂ O	B. P. method	C_p , ρ	7
1-(2-hydroxyethyl)-3-methylimidazolium Tetrafluoroborate [HOEtMIM][BF ₄]	H ₂ O	B. P. method		8
1-(2-hydroxyethyl)-3-methylimidazolium trifluoroacetate [HOEtMIM][TFA]	H ₂ O	Fischer Labodest apparatus	H^E	9
1-ethyl-3-methylimidazolium tetrafluoroborate [EMIM][BF ₄]	H ₂ O	Static method	ρ	10, 11
1-ethyl-3-methylimidazolium iodide [EMIM][I]	H ₂ O	Static method		10
1-ethyl-3-methylimidazolium dimethylphosphate [EMIM][DMP]	H ₂ O	B. P. method	C_p , ρ , H^E , Viscosity	12, 13, 14
1-ethyl-3-methylimidazolium bis-(trifluoromethylsulfonyl)imide [EMIM][Tf ₂ N] or [(CF ₃ SO ₂) ₂ N]	H ₂ O	Static method		5, 15, 16
1-ethyl-3-methylimidazolium acetate [EMIM][Ac]	H ₂ O	Dynamic method	C_p , ρ , Viscosity	17, 18
1-ethyl-3-methylimidazolium hydrogen sulfate [EMIM][HSO ₄]	H ₂ O		H^E	19
1-ethyl-3-methylimidazolium ethyl sulfate [EMIM][EtSO ₄]	H ₂ O	B. p. method & static method & Fischer Labodest apparatus	C_p , ρ , H^E , Viscosity	20, 21
1-ethyl-3-methylimidazolium diethyl phosphate [EMIM][DEP]	H ₂ O	Circulation still.	H^E	9, 22
1-ethyl-3-methylimidazolium trifluoromethanesulfonate [EMIM][TFO] [Triflate]	H ₂ O	Static method & Fischer Labodest apparatus	C_p , ρ , H^E	23, 24
1-ethyl-3-methylimidazolium trifluoroacetat [EMIM][TFA]	H ₂ O	Fischer Labodest apparatus	C_p , ρ , H^E	20
1-ethyl-3-methylimidazolium thiocyanate [EMIM][SCN]	H ₂ O	Ebulliometric method		19, 25, 26
1-ethyl-3-methylimidazolium methanesulfonate [EMIM][MeSO ₃]	H ₂ O		H^E	9
1-ethyl-3-methylimidazolium tosylate [EMIM][TOS]	H ₂ O	Ebulliometric method		27
1-butyl-3-methylimidazolium tetrafluoroborate [BMIM][BF ₄]	H ₂ O	B.P. method & Static method	C_p , ρ , H^E , Viscosity	8, 25
1-butyl-3-methylimidazolium trifluoromethanesulfonate [BMIM][CF ₃ SO ₃][TFO][triflate]	H ₂ O	Isobaric microebulliometer	C_p , ρ , H^E	28

ILs	Refrigerant	VLE methods	Therm. Prop.	Ref.
1-butyl-3-methylimidazolium methanesulfonate [BMIM][C ₁ SO ₃]	H ₂ O	Isobaric microebulliometer		28
1-butyl-3-methylimidazolium chloride [BMIM][Cl]	H ₂ O	Labodest apparatus		28
1-butyl-3-methylimidazolium bromide [BMIM][Br]	H ₂ O	B. p. method & Isobaric microebulliometer		28
1-butyl-3-methylimidazolium acetate [BMIM][Ac]	H ₂ O	Isobaric microebulliometer, Static method		28
1-butyl-3-methylimidazolium trifluoroacetate [BMIM][CF ₃ CO ₂]	H ₂ O	Isobaric microebulliometer		28
1-butyl-3-methylimidazolium iodide [BMIM][I]	H ₂ O	Static method		29
1-butyl-3-methylimidazolium thiocyanate [BMIM][SCN]	H ₂ O	Isobaric microebulliometer, Static method		28, 29
1-butyl-3-methylimidazolium tosylate [BMIM][TOS]	H ₂ O	Isobaric microebulliometer		28
1-butyl-3-methylimidazolium dicyanamide [BMIM][N(CN) ₂]	H ₂ O		ρ, viscosity	30
1-butyl-3-methylimidazolium tricyanomethane [BMIM][C(CN) ₃]	H ₂ O		ρ, viscosity	30
1-butyl-3-methylimidazolium bis(trifluoromethylsulfonyl)imide [BMIM][Tf ₂ N]	H ₂ O	Static method	VLE data	15, 31
1-butyl-3-methylimidazolium Methylsulfate [BMIM][MeSO ₄]	H ₂ O	Labosdest app.	C _p , ρ, H ^E	23
1-butyl-3-methylimidazolium dibutyl phosphate [BMIM][DBP]	H ₂ O	Ebulliometric method		22
diethylmethylammonium Methane Sulfonate [DEMA][Oms]	H ₂ O	Dynamic method		17
1-butyl-1-methylpyrrolidinium dicyanamide [BMPYR][DCA]	H ₂ O	Ebulliometric method		32
1-butyl-1-methylpiperidinium dicyanamide [BMPIP][DCA]	H ₂ O	Ebulliometric method		32
1-hexyl-3-methylimidazolium tetrafluoroborate [HMIM][BF ₄]	H ₂ O		ρ	11
1-butyl-2,3-dimethylimidazolium tetrafluoroborat [BDMIM][BF ₄]	H ₂ O		ρ, viscosity	33

References

- [1] J.Wang, D. Zheng, L. Fan , L. Dong, Vapor pressure measurement for the water + 1,3-dimethylimidazolium chloride system and 2, 2, 2-trifluoroethanol + 1-ethyl-3-methylimidazolium tetrafluoroborate system, *J. Chem. Eng. Data*, 55 (2010) 2128–32.
- [2] L. Dong, D.X. Zheng, Z. Wei, X.H. Wu, Synthesis of 1,3-dimethylimidazolium chloride and volumetric property investigations of its aqueous solution, *Int. J. Thermophys*, 30 (2009) 1480–90.
- [3] W. Xianghong, L. Jing, F. Lihua, Z. Danxing, D. Li, Vapor pressure measurement of water + 1,3 dimethylimidazolium system, *Chinese Journal of Chemical Engineering*, 19 (2011) 473-477.
- [4] L. Dong, D. Zheng, N. Nie, Y. Li, Performance prediction of absorption refrigeration cycle based on the measurements of vapor pressure and heat capacity of {H₂O + [DMIM][DMP]} system, *Applied Energy*, 98 (2012) 326–332.
- [5] R. Kato, J. Gmehling, Measurement and correlation of vapor–liquid equilibria of binary systems containing the ionic liquids [EMIM][(CF₃SO₂)₂N], [BMIM][(CF₃SO₂)₂N], [MMIM][(CH₃)₂PO₄] and oxygenated organic compounds respectively water, *Fluid Phase Equilibria*, 231 (2005) 38–43.
- [6] Z. He, Z. Zhao, X. Zhang, H. Feng, Thermodynamic properties of new heat pump working pairs: 1,3-dimethylimidazolium dimethylphosphate and water, ethanol and methanol, *Fluid Phase Equilibria*, 298 (2010) 83–91.
- [7] N. Nie, D. Zheng, L. Dong, Y. Li, Thermodynamic properties of the water + 1- (2-hydroxyethyl)-3-methylimidazolium chloride system, *J. Chem. Eng. Data*, 57 (2012) 3598–3603.
- [8] K. Kim, S. Park, S. Choi, H. Lee, Vapor pressures of the 1-butyl-3-methylimidazolium bromide + water, 1-butyl-3-methylimidazolium tetrafluoroborate + water, and 1-(2-hydroxyethyl)-3-methylimidazolium tetrafluoroborate + water systems, *J. Chem. Eng. Data*, 49 (2004) 1550-53.
- [9] L.E. Ficke, Thermodynamic properties of imidazolium and phosphonium based ionic liquid mixtures with water or carbon dioxide. PhD thesis, Chemical and Biomolecular Engineering, University of Notre Dame, Notre Dame, Indiana; April 2010.
- [10] H. Kato, K. Nishikawa, H. Murai, T. Morita, Y. Koga, Chemical potentials in aqueous solutions of some ionic liquids with the 1-ethyl-3-methylimidazolium cation, *J. Phys. Chem. B*, 112 (2008) 13344–48.
- [11] A. Stoppa, J. Hunger, R. Buchner, Conductivities of binary mixtures of ionic liquids with polar solvents, *J. Chem. Eng. Data*, 54 (2009) 472–479.

- [12] J. Ren, Z. Zhao, X. Zhang, Vapor pressures, excess enthalpies, and specific heat capacities of the binary working pairs containing the ionic liquid 1-ethyl-3-methylimidazolium dimethylphosphate, *J. Chem. Thermodynamics*, 43 (2011) 576–583.
- [13] J.F. Wang, C.X. Li, Z.H. Wang, Z.J. Li, Y.B. Jiang, Vapor pressure measurement for water, methanol, ethanol, and their binary mixtures in the presence of an ionic liquid 1-ethyl-3-methylimidazolium dimethylphosphate, *Fluid Phase Equilibria*, 255 (2007) 186–192.
- [14] X. Zhang, D. Hu, Performance simulation of the absorption chiller using water and ionic liquid 1-ethyl-3-methylimidazolium dimethylphosphate as the working pair, *Applied Thermal Engineering*, 31 (2011) 3316–21.
- [15] C.P. Fredlake, J.M. Crosthwaite, D.G. Hert, S.N.V.K. ki, J.F. Brennecke, Thermophysical properties of imidazolium-based ionic liquids, *Chem. Eng. Data*, 49 (2004) 954-964.
- [16] M. Doker, J. Gmehling, Measurement and prediction of vapor–liquid equilibria of ternary systems containing ionic liquids, *Fluid Phase Equilibria*, 227 (2005) 255–266.
- [17] C. Romich, N.C. Merkel, A. Valbonesi, K. Schaber, S. Sauer, T.J.S. Schubert, Thermodynamic properties of binary mixtures of water and room temperature ionic liquids: vapor pressure, heat capacities, densities and viscosities of water + 1-ethyl-3-methylimidazolium acetate and water + diethylmethylanmonium methane sulfonate, *J. Chem. Eng. Data*, 57 (2012) 2258–64.
- [18] S. Fendt, S. Padmanabhan, H.W. Blanch, J.M. Prausnitz, Viscosities of acetate or chloride-based ionic liquids and some of their mixtures with water or other common solvents, *J. Chem. Eng. Data*, 56 (2011) 31–34.
- [19] L.E. Ficke, R.R. Novak, J.F. Brennecke, Thermodynamic and thermophysical properties of ionic liquid + water systems, *J. Chem. Eng. Data*, 55 (2010) 4946–50.
- [20] L.E. Ficke, H. Rodriguez, J.F. Brennecke, Heat capacities and excess enthalpies of 1-Ethyl-3-methylimidazolium-based ionic liquids and water, *J. Chem. Eng. Data*, 53 (2008) 2112–19.
- [21] G. Zuo, Z. Zhao, S. Yan, X. Zhang, Thermodynamic properties of a new working pair: 1-ethyl-3-methylimidazolium ethylsulfate and water, *Chem. Eng. J.*, 156 (2010) 613–617.
- [22] J. Zhao, X.C. Jiang, C.X. Li, Z.H. Wang, Vapor pressure measurement for binary and ternary systems containing a phosphoric ionic liquid, *Fluid Phase Equilibria*, 247 (2006) 190–198.
- [23] G. Garcia-Miaja, J. Troncoso, L. Romani, Excess enthalpy, density, and heat capacity for binary systems of alkylimidazolium-based ionic liquids + water, *J. Chem. Thermodyn.*, 41 (2009) 161–166.

- [24] L.D. Simoni, L.E. Ficke, C.A. Lambert, M.A. Stadtherr, J.F. Brennecke, Measurement and prediction of vapor-liquid equilibrium of aqueous 1-ethyl-3-methylimidazolium-based ionic liquid systems, *Ind. Eng. Chem. Res.*, 49 (2010) 3893–3901.
- [25] P. Navarro, M. Larriba, E. Rojo, J. Garcia, F. Rodriguez, Thermal properties of cyano-based ionic liquids, *J. Chem. Eng. Data*, 58 (2013) 2187–93.
- [26] M. Krolikowska, T. Hofman, Densities, isobaric expansivities and isothermal compressibilities of the thiocyanate-based ionic liquids at temperatures (298.15–338.15 K) and pressures up to 10 MPa, *Thermochimica Acta*, 530 (2012) 1-6.
- [27] U. Domanska, M. Krolikowska, M. Krolikowski, Phase behaviour and physico-chemical properties of the binary systems {1-ethyl-3-methylimidazolium thiocyanate, or 1-ethyl-3-methylimidazolium tosylate + water, or + an alcohol}, *Fluid Phase Equilibria*, 294 (2010) 72–83.
- [28] H. Passos, I. Khan, F. Mutelet, M.B. Oliveira, P.J. Carvalho, L.M.N.B.F. Santos, C. Held, G. Sadowski, M.G. Freire, J.A.P. Coutinho, Vapor-liquid equilibria of water + alkylimidazolium-based ionic liquids: measurements and perturbed-chain statistical associating fluid theory modeling, *Ind. Eng. Chem. Res.*, 53 (2014) 3737–48.
- [29] Y. Nakata, K. Kohara, K. Matsumoto, R. Hagiwara, Thermal properties of ionic liquid and water binary systems applied to heat pipes, *J. Chem. Eng. Data*, 56 (2011) 1840-46.
- [30] P.J. Carvalh, T. Regueira, L.M.N.B.F. Santos, J. Fernandez, J.A.P. Coutinho, Effect of water on the viscosities and densities of 1-butyl-3-methylimidazolium dicyanamide and 1-butyl-3-methylimidazolium tricyanomethane at atmospheric pressure, *J. Chem. Eng. Data*, 55 (2010) 645–652.
- [31] M. Doker, J. Gmehling, Measurement and prediction of vapor–liquid equilibria of ternary systems containing ionic liquids, *Fluid Phase Equilibria*, 227 (2005) 255–266.
- [32] M. Krolikowska, M. Zawadzki, M. Krolikowski, Physicochemical and thermodynamic study on aqueous solutions of dicyanamide – based ionic liquids, *J. Chem. Thermodynamics*, 70 (2014) 127-137.
- [33] I. Bou Malham, M. Turmine, Viscosities and refractive indices of binary mixtures of 1-butyl-3-methylimidazolium tetrafluoroborate and 1-butyl-2,3-dimethylimidazolium tetrafluoroborate with water at 298 K, *J. Chem. Thermodynamics*, 40 (2008) 718–723.

II. Annex

II.2.1. Vapor Liquid Equilibrium (VLE)

Table II.1: Vapor-liquid equilibrium data of binary system {H₂O (1) + [DMIM][MPh] (2)}.

T(K)	P ^{exp} (kPa)	P ^{NRTL} (kPa)	γ_1^{exp}	γ_1^{NRTL}
$x_1 = 0.94$				
322.42	11.84	10.78	1.06	0.98
329.68	15.36	15.37	0.97	0.98
336.91	20.90	21.50	0.94	0.97
340.75	25.74	25.53	0.98	0.97
346.42	31.19	32.63	0.93	0.97
350.24	36.68	38.30	0.93	0.97
353.45	42.05	43.69	0.94	0.96
356.48	46.88	49.35	0.93	0.96
358.50	50.21	53.45	0.92	0.96
360.85	55.67	58.57	0.93	0.96
364.64	66.70	67.71	0.96	0.96
366.03	71.38	71.34	0.98	0.96
366.87	77.70	73.61	1.03	0.96
$x_1 = 0.90$				
324.89	10.93	11.22	0.90	0.92
332.22	16.59	15.99	0.97	0.92
338.14	20.76	21.01	0.92	0.92
342.90	26.36	25.96	0.95	0.92
347.95	32.31	32.26	0.94	0.92
352.09	36.15	38.35	0.89	0.91
355.00	42.54	43.18	0.93	0.91
358.25	46.16	49.17	0.88	0.91
361.89	54.84	56.69	0.91	0.91
363.81	62.51	61.03	0.97	0.91
366.66	70.60	67.98	0.98	0.91
370.64	78.64	78.78	0.95	0.91
373.52	86.78	87.45	0.94	0.91
375.84	91.60	95.00	0.91	0.91
$x_1 = 0.80$				
330.88	11.36	11.46	0.79	0.79
347.03	20.27	24.05	0.69	0.80
350.70	24.90	28.15	0.73	0.80
353.54	29.71	31.71	0.77	0.80

T(K)	P ^{exp} (kPa)	P ^{NRTL} (kPa)	γ_1^{exp}	γ_1^{NRTL}
357.33	34.58	37.05	0.77	0.80
360.78	40.87	42.55	0.80	0.80
364.11	45.62	48.50	0.78	0.80
366.37	50.25	52.92	0.79	0.80
370.28	57.77	61.36	0.79	0.81
372.37	60.14	66.31	0.76	0.81
373.48	65.66	69.07	0.80	0.81
375.06	71.13	73.17	0.82	0.81
376.82	76.20	77.97	0.83	0.81
378.72	80.81	83.44	0.82	0.81
381.27	87.36	91.28	0.81	0.81
382.55	90.25	95.44	0.80	0.81
$x_1 = 0.70$				
335.89	11.04	10.58	0.70	0.69
357.37	26.39	27.53	0.67	0.71
360.75	32.30	31.62	0.72	0.71
363.13	35.80	34.80	0.73	0.71
369.82	47.76	45.20	0.76	0.72
372.48	50.33	50.00	0.73	0.72
376.22	56.68	57.47	0.72	0.72
379.67	66.70	65.16	0.75	0.72
383.21	71.27	73.93	0.71	0.73
384.80	75.11	78.17	0.71	0.73
386.93	81.84	84.17	0.72	0.73
387.73	84.22	86.52	0.72	0.73
$x_1 = 0.59$				
338.90	9.84	8.41	0.64	0.60
350.80	16.18	14.51	0.64	0.62
358.23	22.48	19.99	0.66	0.62
366.59	31.56	28.14	0.67	0.63
370.76	35.40	33.15	0.65	0.64
378.35	45.51	44.22	0.63	0.64
381.93	50.70	50.42	0.63	0.65
384.49	54.60	55.28	0.62	0.65
387.65	61.11	61.82	0.62	0.65
389.63	66.12	66.24	0.63	0.65
392.49	76.33	73.07	0.67	0.66
393.89	81.13	76.63	0.68	0.66
395.87	87.71	81.90	0.69	0.66
396.25	88.19	82.94	0.68	0.66
			ARD	4.45

Uncertainty x_1 , T and γ_1 are 0.005, 0.06 and 0.001, respectively.

Table II.2: Vapor-liquid equilibrium data of binary system {H₂O (1) + [EMIM][MPh] (2)}.

T(K)	P ^{exp} (kPa)	P ^{NRTL} (kPa)	γ_1^{exp}	γ_1^{NRTL}
$x_1 = 0.90$				
329.37	11.92	13.49	0.80	0.90
333.55	15.63	16.40	0.86	0.90
340.92	21.16	22.85	0.83	0.90
344.90	27.26	27.14	0.90	0.90
347.66	30.25	30.50	0.89	0.90
352.74	37.47	37.61	0.90	0.90
355.80	41.56	42.53	0.88	0.90
355.93	45.78	42.75	0.96	0.90
357.43	45.92	45.37	0.91	0.90
360.69	50.97	51.51	0.89	0.90
$x_1 = 0.80$				
338.98	13.70	15.22	0.66	0.73
339.28	13.73	15.42	0.65	0.73
342.25	15.85	17.57	0.66	0.73
347.61	20.78	22.09	0.69	0.73
347.97	20.83	22.42	0.68	0.73
353.88	26.69	28.58	0.69	0.73
354.10	26.80	28.84	0.68	0.73
356.99	30.50	32.35	0.69	0.73
357.29	30.49	32.74	0.68	0.73
361.59	37.99	38.69	0.72	0.73
$x_1 = 0.71$				
343.84	12.37	13.61	0.54	0.60
344.08	12.39	13.75	0.54	0.60
344.22	12.40	13.83	0.54	0.60
351.32	15.76	18.63	0.51	0.60
351.58	15.76	18.83	0.50	0.60
351.81	15.77	19.01	0.50	0.60
352.11	15.79	19.24	0.49	0.60
352.32	15.80	19.41	0.49	0.60
357.79	20.69	24.15	0.51	0.60
358.18	20.64	24.52	0.50	0.60
$x_1 = 0.60$				
350.43	10.53	11.50	0.42	0.46
350.64	10.52	11.60	0.41	0.46
350.91	10.58	11.73	0.41	0.46
350.98	10.59	11.77	0.41	0.46
351.07	10.60	11.81	0.41	0.46
360.04	15.81	16.88	0.43	0.46
360.33	15.92	17.07	0.43	0.46
360.24	15.93	17.01	0.43	0.46
365.55	20.70	20.82	0.45	0.46
366.27	20.77	21.39	0.44	0.46
			ARD	9.34

Uncertainty x_1 , T and γ_1 are 0.005, 0.06 and 0.001, respectively.

Table II.3: Vapor-liquid equilibrium data of binary system {H₂O (1) + [EMIM][EPh] (2)}.

T(K)	P ^{exp} (kPa)	P ^{NRTL} (kPa)	γ_1^{exp}	γ_1^{NRTL}
$x_1 = 0.90$				
326.28	10.69	11.55	0.83	0.89
331.59	15.60	14.95	0.94	0.90
338.94	21.44	21.04	0.92	0.90
341.41	26.02	23.50	1.00	0.91
344.09	26.17	26.46	0.90	0.91
347.86	31.03	31.14	0.91	0.91
351.00	35.55	35.56	0.91	0.91
353.46	40.44	39.38	0.94	0.91
356.65	45.58	44.85	0.93	0.92
360.43	51.38	52.14	0.91	0.92
362.02	55.48	55.49	0.92	0.92
362.78	60.55	57.15	0.98	0.92
364.21	65.62	60.39	1.00	0.92
367.47	71.18	68.37	0.96	0.92
$x_1 = 0.77$				
337.22	10.16	11.98	0.55	0.65
350.33	22.58	22.02	0.70	0.68
353.76	25.50	25.61	0.68	0.69
357.08	30.56	29.55	0.72	0.70
360.59	34.65	34.27	0.71	0.70
360.96	34.63	34.80	0.70	0.70
361.16	34.61	35.09	0.69	0.70
365.99	42.53	42.77	0.71	0.71
367.03	45.03	44.60	0.72	0.72
370.18	50.25	50.55	0.72	0.72
373.50	55.15	57.53	0.70	0.73
376.64	60.98	64.86	0.69	0.74
379.23	65.03	71.49	0.68	0.74
381.33	73.63	77.28	0.71	0.75
$x_1 = 0.68$				
341.32	10.37	9.98	0.53	0.51
342.41	10.53	10.53	0.51	0.51
349.91	15.96	15.08	0.56	0.53
356.27	20.92	20.19	0.57	0.55
360.96	25.54	24.85	0.58	0.56
365.47	30.43	30.18	0.58	0.58
370.02	35.11	36.53	0.57	0.59
373.96	40.47	42.92	0.57	0.60
377.07	45.36	48.61	0.57	0.61
379.53	50.50	53.56	0.58	0.62
380.26	57.32	55.11	0.65	0.62
381.70	62.16	58.28	0.67	0.63

T(K)	P ^{exp} (kPa)	P ^{NRTL} (kPa)	γ_1^{exp}	γ_1^{NRTL}
383.06	65.94	61.41	0.68	0.63
384.51	70.05	64.91	0.68	0.63
$x_1 = 0.60$				
348.97	10.22	9.67	0.43	0.40
358.73	15.97	15.47	0.45	0.44
365.37	20.72	20.96	0.45	0.46
370.22	25.65	25.98	0.47	0.48
375.12	30.76	32.07	0.47	0.49
378.83	35.64	37.46	0.48	0.51
380.46	40.19	40.07	0.51	0.51
384.91	45.38	47.99	0.50	0.53
387.88	50.50	53.98	0.50	0.54
389.41	55.83	57.31	0.53	0.54
390.63	60.39	60.09	0.55	0.55
391.56	64.49	62.29	0.57	0.55
392.51	73.01	64.60	0.63	0.55
			ARD	3.98

Uncertainty x_1 , T and γ_1 are 0.005, 0.06 and 0.001, respectively.

Table II.4: Vapor-liquid equilibrium data of binary system {H₂O (1) + [DMIM][MeSO₄] (2)}.

T(K)	P ^{exp} (kPa)	P ^{NRTL} (kPa)	γ_1^{exp}	γ_1^{NRTL}
$x_1 = 0.20$				
293.15	0.63	0.64	1.36	1.37
298.15	0.78	0.77	1.24	1.22
303.75	0.96	0.94	1.10	1.08
313.25	1.32	1.29	0.90	0.88
318.65	1.71	1.53	0.88	0.78
323.45	2.20	1.75	0.88	0.71
328.55	3.05	2.02	0.96	0.63
$x_1 = 0.34$				
295.65	1.04	0.87	1.12	0.93
298.15	1.09	0.97	1.01	0.90
303.25	1.29	1.23	0.89	0.85
308.15	1.52	1.53	0.79	0.80
313.15	1.77	1.89	0.70	0.75
318.15	2.12	2.33	0.65	0.71
323.15	2.70	2.83	0.64	0.67
328.05	3.48	3.42	0.65	0.64
328.15	3.49	3.43	0.65	0.64
$x_1 = 0.50$				
306.25	1.85	2.14	0.73	0.85

T(K)	P ^{exp} (kPa)	P ^{NRTL} (kPa)	γ_1^{exp}	γ_1^{NRTL}
308.15	2.20	2.35	0.78	0.84
313.15	2.69	3.01	0.73	0.82
318.15	3.29	3.81	0.69	0.80
323.55	4.09	4.88	0.65	0.78
328.75	5.12	6.14	0.63	0.76
$x_1 = 0.60$				
293.75	1.44	1.34	1.00	0.93
298.15	1.84	1.73	0.97	0.92
303.65	2.38	2.34	0.91	0.90
308.15	2.87	2.98	0.86	0.89
313.25	3.51	3.87	0.79	0.87
318.85	4.41	5.11	0.74	0.86
323.85	5.40	6.48	0.71	0.85
323.95	5.41	6.51	0.71	0.85
$x_1 = 0.65$				
342.88	14.30	17.20	0.72	0.86
346.59	16.82	20.06	0.72	0.86
351.51	20.75	24.47	0.72	0.85
355.65	26.11	28.79	0.77	0.85
358.91	30.43	32.63	0.79	0.85
362.41	35.65	37.21	0.81	0.84
365.51	41.79	41.71	0.84	0.84
368.22	45.18	46.00	0.82	0.84
369.37	51.00	47.93	0.89	0.84
370.88	56.86	50.56	0.94	0.84
370.28	60.74	49.50	1.03	0.84
372.31	66.34	53.17	1.04	0.84
$x_1 = 0.70$				
331.75	10.70	11.82	0.82	0.91
343.20	17.17	19.56	0.79	0.90
349.81	21.86	25.73	0.76	0.89
353.75	25.69	30.13	0.76	0.89
360.33	33.88	38.89	0.77	0.89
360.79	35.34	39.57	0.79	0.89
363.74	39.87	44.21	0.80	0.89
366.62	45.62	49.16	0.82	0.88
369.92	49.66	55.39	0.79	0.88
370.96	55.40	57.49	0.85	0.88
373.04	61.22	61.87	0.87	0.88
373.40	64.51	62.66	0.91	0.88
376.02	71.97	68.64	0.92	0.88
377.56	75.20	72.37	0.91	0.88
379.22	78.60	76.58	0.90	0.88
380.23	83.12	79.23	0.92	0.88

T(K)	P ^{exp} (kPa)	P ^{NRTL} (kPa)	γ_1^{exp}	γ_1^{NRTL}
382.11	87.66	84.38	0.91	0.88
$x_1 = 0.70$				
293.15	1.49	1.56	0.91	0.96
298.35	1.96	2.12	0.88	0.95
303.15	2.47	2.79	0.83	0.94
308.35	3.11	3.71	0.78	0.93
313.45	3.88	4.86	0.74	0.93
318.15	4.80	6.18	0.72	0.92
323.15	6.01	7.91	0.70	0.92
$x_1 = 0.74$				
330.28	11.33	12.12	0.88	0.94
343.82	18.60	22.12	0.78	0.93
346.40	20.85	24.66	0.78	0.93
353.50	28.29	32.95	0.79	0.92
355.23	30.57	35.29	0.80	0.92
359.42	36.60	41.55	0.81	0.92
361.40	40.39	44.82	0.83	0.92
364.91	45.75	51.13	0.82	0.92
367.70	49.57	56.66	0.80	0.92
369.45	55.80	60.38	0.85	0.92
371.43	60.19	64.83	0.85	0.92
372.82	65.61	68.11	0.88	0.92
375.76	72.52	75.51	0.88	0.92
376.55	75.64	77.61	0.89	0.92
378.53	84.31	83.08	0.93	0.92
381.11	89.40	90.68	0.90	0.91
$x_1 = 0.79$				
325.82	10.43	10.74	0.93	0.96
337.04	16.91	18.08	0.90	0.96
344.91	22.64	25.47	0.85	0.95
346.98	25.45	27.79	0.87	0.95
351.80	30.74	33.89	0.86	0.95
355.58	35.44	39.43	0.86	0.95
358.70	40.11	44.56	0.86	0.95
361.48	45.17	49.59	0.87	0.95
363.90	50.45	54.34	0.88	0.95
366.51	55.43	59.89	0.88	0.95
369.04	60.98	65.71	0.88	0.95
370.61	65.17	69.55	0.89	0.95
373.58	69.70	77.33	0.85	0.95
374.46	75.10	79.77	0.89	0.95
374.59	75.00	80.14	0.89	0.95
375.54	79.10	82.85	0.91	0.95
376.58	82.40	85.91	0.91	0.95

T(K)	P ^{exp} (kPa)	P ^{NRTL} (kPa)	γ_1^{exp}	γ_1^{NRTL}
376.94	85.11	86.99	0.93	0.95
378.66	89.62	92.31	0.92	0.95
$x_1 = 0.80$				
293.15	1.99	1.82	1.07	0.98
298.65	2.72	2.54	1.05	0.98
302.45	3.34	3.16	1.03	0.97
308.15	4.44	4.35	0.99	0.97
313.15	5.63	5.70	0.96	0.97
318.15	7.14	7.38	0.93	0.97
323.15	8.96	9.48	0.91	0.96
$x_1 = 0.84$				
329.78	13.43	14.07	0.93	0.98
332.70	15.62	16.12	0.95	0.98
339.83	20.96	22.23	0.92	0.98
345.11	26.63	27.94	0.93	0.98
348.77	30.91	32.58	0.92	0.97
353.98	35.70	40.30	0.86	0.97
355.47	40.47	42.77	0.92	0.97
358.42	44.85	48.03	0.91	0.97
360.57	50.19	52.20	0.94	0.97
363.17	58.88	57.64	0.99	0.97
366.75	64.13	65.91	0.95	0.97
367.94	69.26	68.86	0.98	0.97
368.91	69.95	71.35	0.95	0.97
370.23	74.26	74.86	0.96	0.97
371.90	79.01	79.50	0.97	0.97
373.99	82.79	85.65	0.94	0.97
$x_1 = 0.89$				
293.25	2.32	2.09	1.11	0.99
298.15	3.07	2.81	1.09	0.99
303.15	4.01	3.76	1.06	0.99
308.15	5.16	4.98	1.03	0.99
313.15	6.61	6.53	1.00	0.99
318.15	8.42	8.48	0.98	0.99
323.15	10.59	10.91	0.96	0.99
323.15	10.60	10.91	0.96	0.99
317.70	8.24	8.29	0.98	0.99
321.91	10.40	10.27	1.00	0.99
330.78	15.85	15.77	0.99	0.99
337.24	21.06	21.21	0.98	0.99
341.44	25.74	25.55	1.00	0.99
345.80	31.60	30.82	1.01	0.99
350.10	36.17	36.89	0.97	0.99
353.51	40.65	42.39	0.95	0.99

T(K)	P ^{exp} (kPa)	P ^{NRTL} (kPa)	γ_1^{exp}	γ_1^{NRTL}
357.95	45.49	50.57	0.89	0.99
359.87	50.43	54.49	0.91	0.99
361.23	55.21	57.43	0.95	0.99
363.25	60.79	62.02	0.97	0.99
364.68	65.69	65.46	0.99	0.99
367.52	73.30	72.76	0.99	0.99
368.26	75.56	74.77	1.00	0.99
371.16	83.47	83.09	0.99	0.99
373.98	90.30	91.90	0.97	0.99
			ARD	8.42

Uncertainty x_1 , T and γ_1 are 0.005, 0.1 and 0.06, respectively.

Table II.5: Vapor-liquid equilibrium data of binary system {H₂O (1) + [EMIM][MeSO₄] (2)}.

T(K)	P ^{exp} (kPa)	P ^{NRTL} (kPa)	γ_1^{exp}	γ_1^{NRTL}
$x_1 = 0.21$				
293.25	0.86	0.75	1.75	1.52
298.15	1.06	0.98	1.60	1.48
303.15	1.23	1.18	1.39	1.34
308.15	1.39	1.31	1.19	1.12
$x_1 = 0.32$				
293.15	1.09	1.11	1.47	1.50
298.15	1.34	1.43	1.34	1.43
303.15	1.60	1.73	1.19	1.28
308.15	1.87	1.95	1.05	1.10
313.25	2.23	2.09	0.95	0.89
$x_1 = 0.49$				
293.15	1.63	1.63	1.41	1.41
298.15	2.11	2.05	1.35	1.31
303.15	2.50	2.50	1.19	1.19
308.15	2.91	2.95	1.05	1.06
313.15	3.34	3.41	0.92	0.94
$x_1 = 0.64$				
293.15	1.80	1.91	1.21	1.29
298.15	2.28	2.43	1.13	1.20
303.45	2.85	3.05	1.04	1.11
308.15	3.46	3.71	0.97	1.04
313.05	4.17	4.51	0.89	0.97
327.55	8.89	8.23	0.90	0.84
329.15	9.02	8.80	0.85	0.83
331.75	10.43	9.79	0.87	0.82
346.99	20.37	18.52	0.86	0.78

T(K)	P ^{exp} (kPa)	P ^{NRTL} (kPa)	γ_1^{exp}	γ_1^{NRTL}
347.08	20.40	18.59	0.86	0.78
347.22	20.45	18.69	0.86	0.78
334.68	11.49	11.06	0.84	0.80
335.11	11.52	11.26	0.82	0.80
342.33	16.02	15.23	0.83	0.79
342.58	16.06	15.39	0.82	0.79
342.91	16.09	15.61	0.81	0.79
348.07	20.67	19.37	0.84	0.78
348.48	20.75	19.71	0.83	0.78
348.66	20.89	19.85	0.82	0.78
348.74	20.91	19.92	0.82	0.78
353.95	26.64	24.74	0.85	0.79
354.27	26.69	25.07	0.84	0.79
356.40	30.87	27.37	0.89	0.79
356.81	30.95	27.83	0.88	0.79
357.21	31.04	28.29	0.87	0.79
359.38	36.22	30.92	0.93	0.79
359.55	36.25	31.13	0.92	0.79
359.63	36.28	31.23	0.92	0.79
359.74	36.31	31.37	0.92	0.79
$x_1 = 0.69$				
329.29	10.72	10.02	0.93	0.87
342.64	16.72	17.83	0.79	0.85
341.13	16.25	16.72	0.82	0.85
346.59	21.49	21.10	0.86	0.85
350.26	26.32	24.62	0.91	0.85
355.76	30.61	30.93	0.84	0.85
357.51	35.60	33.23	0.91	0.85
361.52	40.82	39.07	0.90	0.86
365.57	47.47	45.89	0.90	0.87
368.43	50.80	51.31	0.86	0.87
$x_1 = 0.74$				
323.67	9.24	8.71	0.98	0.93
327.41	10.31	10.33	0.91	0.92
340.35	17.26	18.36	0.84	0.90
346.63	22.10	24.07	0.82	0.90
356.61	35.75	36.46	0.89	0.90
359.70	40.63	41.29	0.89	0.91
366.57	55.28	54.08	0.94	0.92
372.14	65.00	66.80	0.90	0.92
374.43	69.56	72.72	0.89	0.93
376.02	73.39	77.09	0.88	0.93
344.30	21.22	21.79	0.87	0.90
349.47	25.91	27.14	0.86	0.90
352.48	30.29	30.77	0.89	0.90
362.98	46.04	47.03	0.89	0.91
365.31	50.33	51.50	0.89	0.91

T(K)	P ^{exp} (kPa)	P ^{NRTL} (kPa)	γ_1^{exp}	γ_1^{NRTL}
367.40	55.28	55.83	0.91	0.92
370.35	61.10	62.46	0.90	0.92
375.29	70.60	75.06	0.87	0.93
$x_1 = 0.79$				
336.66	15.80	17.23	0.86	0.94
344.60	22.01	24.40	0.84	0.93
348.84	26.41	29.23	0.85	0.94
352.29	30.77	33.75	0.85	0.94
355.63	35.48	38.69	0.86	0.94
358.67	41.20	43.72	0.89	0.94
361.78	45.80	49.43	0.87	0.94
363.76	50.61	53.40	0.90	0.95
366.22	56.09	58.69	0.91	0.95
368.55	60.76	64.11	0.90	0.95
370.98	64.87	70.20	0.88	0.95
372.93	68.97	75.44	0.87	0.95
373.37	70.80	76.66	0.88	0.95
374.20	73.40	79.02	0.89	0.96
375.66	78.16	83.31	0.90	0.96
377.59	81.60	89.29	0.88	0.96
379.40	87.20	95.21	0.88	0.96
$x_1 = 0.84$				
323.39	11.08	10.24	1.05	0.97
334.90	17.49	17.56	0.96	0.97
338.78	21.01	20.91	0.97	0.97
343.94	26.38	26.21	0.97	0.97
346.99	30.87	29.86	1.00	0.97
351.25	35.39	35.69	0.96	0.97
354.56	40.59	40.87	0.96	0.97
356.57	45.89	44.31	1.00	0.97
359.60	50.41	49.97	0.98	0.97
361.58	55.52	53.98	1.00	0.97
363.68	60.09	58.54	1.00	0.97
365.91	64.83	63.72	0.99	0.97
368.26	70.30	69.60	0.99	0.98
370.37	76.35	75.26	0.99	0.98
373.49	80.00	84.32	0.93	0.98
373.73	85.09	85.05	0.98	0.98
375.25	90.58	89.82	0.99	0.98
$x_1 = 0.84$				
293.15	2.85	2.14	1.44	1.08
298.15	4.22	2.82	1.58	1.05
303.15	5.12	3.69	1.43	1.03
308.15	6.14	4.79	1.29	1.01
313.15	7.38	6.19	1.18	0.99
$x_1 = 0.90$				
322.69	12.79	10.69	1.18	0.99

T(K)	P ^{exp} (kPa)	P ^{NRTL} (kPa)	γ_1^{exp}	γ_1^{NRTL}
323.89	13.07	11.34	1.14	0.99
330.25	16.25	15.38	1.04	0.99
333.73	21.24	18.08	1.16	0.99
340.20	28.78	24.20	1.17	0.99
344.08	31.62	28.66	1.09	0.99
346.78	37.34	32.16	1.15	0.99
348.67	40.63	34.82	1.15	0.99
352.02	46.06	40.00	1.14	0.99
354.20	50.10	43.70	1.13	0.99
359.64	55.08	54.23	1.00	0.99
360.44	59.81	55.95	1.06	0.99
361.89	65.28	59.17	1.09	0.99
364.18	70.20	64.58	1.08	0.99
366.39	75.33	70.18	1.06	0.99
367.70	80.41	73.69	1.08	0.99
369.20	84.16	77.89	1.07	0.99
370.28	88.97	81.03	1.09	0.99
371.55	90.11	84.87	1.05	0.99
			ARD	9.57

Uncertainty x_1 , T and γ_1 are 0.005, 0.06 and 0.001, respectively.

Table II.6: Vapor-liquid equilibrium data of binary system {H₂O (1) + [BMIM][DCA] (2)}.

T(K)	P ^{exp} (kPa)	P ^{NRTL} (kPa)	γ_1^{exp}	γ_1^{NRTL}
$x_1 = 0.90$				
321.00	11.12	10.74	1.11	1.07
328.58	15.91	15.60	1.10	1.08
334.61	20.96	20.71	1.09	1.08
338.38	25.81	24.57	1.13	1.08
342.93	30.86	30.03	1.11	1.08
343.52	31.03	30.81	1.09	1.08
346.40	35.74	34.86	1.11	1.08
347.23	36.01	36.10	1.08	1.08
348.03	36.15	37.34	1.05	1.08
349.50	40.46	39.70	1.10	1.08
352.60	45.44	45.11	1.09	1.08
353.60	45.91	46.98	1.06	1.08
355.13	50.31	49.96	1.09	1.08
355.29	50.49	50.29	1.09	1.08
357.46	56.62	54.82	1.12	1.08
357.83	56.84	55.62	1.11	1.08
359.43	60.77	59.22	1.11	1.08
360.31	61.11	61.28	1.08	1.08

T(K)	P ^{exp} (kPa)	P ^{NRTL} (kPa)	γ_1^{exp}	γ_1^{NRTL}
361.67	65.35	64.58	1.09	1.08
363.46	71.20	69.16	1.11	1.08
364.63	78.04	72.29	1.17	1.08
365.48	80.25	74.64	1.16	1.08
367.33	85.72	79.97	1.16	1.08
369.50	91.28	86.62	1.14	1.08
$x_1 = 0.85$				
319.44	9.44	9.60	1.09	1.10
322.46	11.36	11.18	1.12	1.10
323.15	11.43	11.57	1.09	1.10
329.52	15.80	15.76	1.11	1.10
335.23	20.79	20.56	1.12	1.10
335.56	20.85	20.87	1.10	1.10
341.02	26.53	26.62	1.10	1.10
344.13	30.61	30.46	1.11	1.10
344.42	30.65	30.84	1.10	1.10
347.69	35.54	35.42	1.11	1.10
348.96	35.64	37.34	1.05	1.10
351.85	40.66	42.05	1.07	1.10
352.35	40.74	42.92	1.05	1.10
355.14	45.28	48.01	1.04	1.10
357.91	49.88	53.56	1.03	1.10
360.99	55.26	60.35	1.01	1.10
362.71	61.36	64.44	1.05	1.10
364.72	65.48	69.51	1.04	1.10
366.41	72.61	74.03	1.08	1.10
367.19	75.14	76.20	1.09	1.10
369.60	81.07	83.22	1.07	1.10
370.07	86.93	84.65	1.13	1.10
373.01	91.25	94.07	1.07	1.10
$x_1 = 0.80$				
324.72	12.26	11.78	1.15	1.11
325.49	12.29	12.23	1.11	1.11
325.86	12.32	12.45	1.09	1.11
330.30	15.48	15.37	1.11	1.10
330.74	15.55	15.69	1.09	1.10
336.56	20.98	20.47	1.13	1.10
336.90	21.10	20.79	1.12	1.10
341.91	25.67	25.90	1.09	1.10
342.18	25.74	26.20	1.08	1.10
346.54	31.05	31.53	1.08	1.10
346.84	31.16	31.92	1.07	1.10
350.05	35.72	36.45	1.07	1.09
352.61	40.67	40.43	1.10	1.09
353.47	40.91	41.84	1.07	1.09
356.29	45.96	46.78	1.07	1.09
357.77	50.16	49.56	1.10	1.09

T(K)	P ^{exp} (kPa)	P ^{NRTL} (kPa)	γ_1^{exp}	γ_1^{NRTL}
359.77	50.69	53.53	1.03	1.09
359.59	54.92	53.16	1.13	1.09
360.65	54.99	55.36	1.08	1.09
363.11	61.21	60.75	1.10	1.09
363.40	61.49	61.41	1.09	1.09
364.62	65.78	64.26	1.11	1.09
364.98	66.16	65.13	1.10	1.09
366.66	72.51	69.28	1.14	1.09
368.09	75.69	72.99	1.13	1.09
369.61	80.45	77.11	1.13	1.08
371.77	85.70	83.29	1.11	1.08
372.87	90.35	86.60	1.13	1.08
373.22	90.46	87.67	1.12	1.08
$x_1 = 0.75$				
333.91	15.84	16.60	1.03	1.08
340.07	21.13	21.80	1.04	1.07
345.36	25.66	27.29	1.00	1.06
350.26	30.92	33.36	0.98	1.06
353.12	35.21	37.39	1.00	1.06
356.07	40.78	41.97	1.02	1.05
358.13	45.48	45.44	1.05	1.05
362.25	52.46	53.09	1.04	1.05
363.48	55.71	55.57	1.05	1.05
365.03	61.28	58.83	1.09	1.05
365.98	61.41	60.90	1.05	1.04
368.05	65.78	65.63	1.05	1.04
371.50	71.86	74.18	1.01	1.04
373.38	75.20	79.20	0.99	1.04
374.79	80.50	83.16	1.00	1.04
375.88	86.18	86.32	1.03	1.04
377.05	90.04	89.82	1.04	1.03
$x_1 = 0.70$				
326.61	10.68	10.49	1.05	1.03
325.73	10.60	10.07	1.09	1.04
335.60	15.94	15.80	1.03	1.02
342.15	20.96	20.95	1.01	1.01
346.37	25.49	24.95	1.03	1.01
350.64	30.72	29.63	1.04	1.00
355.11	35.77	35.30	1.01	0.99
358.07	40.81	39.51	1.02	0.99
358.59	41.12	40.30	1.01	0.99
360.90	45.74	43.93	1.03	0.99
364.63	50.29	50.36	0.98	0.98
366.55	55.32	53.96	1.00	0.98
369.67	60.46	60.25	0.98	0.97
372.16	65.43	65.70	0.97	0.97
374.15	71.17	70.33	0.98	0.97

T(K)	P ^{exp} (kPa)	P ^{NRTL} (kPa)	γ_1^{exp}	γ_1^{NRTL}
376.01	74.68	74.90	0.96	0.96
378.36	80.49	81.02	0.96	0.96
379.90	85.30	85.24	0.96	0.96
381.57	90.39	90.02	0.96	0.96
			ARD	2.42

Uncertainty x_1 , T and γ_1 are 0.005, 0.06 and 0.001, respectively.

Table II.7: Vapor-liquid equilibrium data of binary system {H₂O (1) + [BMIM][AC] (2)}.

T(K)	P ^{exp} (kPa)	P ^{NRTL} (kPa)	γ_1^{exp}	γ_1^{NRTL}
$x_1 = 0.90$				
324.16	12.81	10.33	1.11	0.89
326.89	12.86	11.81	0.97	0.89
327.47	12.88	12.14	0.95	0.89
327.67	12.90	12.26	0.94	0.89
330.02	15.45	13.72	1.00	0.89
330.76	15.48	14.20	0.97	0.89
331.41	15.50	14.64	0.94	0.89
338.21	21.52	19.99	0.96	0.89
338.71	21.62	20.45	0.94	0.89
343.22	25.92	24.92	0.93	0.89
343.45	25.92	25.17	0.92	0.89
343.63	25.93	25.37	0.91	0.89
346.41	30.81	28.57	0.96	0.89
350.48	35.75	33.86	0.94	0.89
350.87	35.87	34.41	0.93	0.89
353.86	40.51	38.86	0.93	0.89
354.03	40.55	39.13	0.92	0.89
356.48	46.26	43.15	0.96	0.89
357.04	46.30	44.12	0.94	0.89
359.30	50.19	48.20	0.93	0.89
360.20	50.67	49.92	0.90	0.89
363.37	55.83	56.36	0.88	0.89
365.99	60.80	62.20	0.87	0.89
366.74	64.94	63.96	0.91	0.89
368.53	65.25	68.33	0.85	0.89
369.48	70.08	70.74	0.88	0.89
369.59	69.70	71.03	0.87	0.89
370.45	74.27	73.29	0.90	0.89
372.23	79.60	78.15	0.91	0.89
$x_1 = 0.79$				
337.82	14.12	13.65	0.72	0.69
338.06	14.15	13.80	0.71	0.69
339.93	15.24	15.00	0.70	0.69
340.15	15.31	15.14	0.70	0.69
340.50	15.31	15.38	0.69	0.69

T(K)	P ^{exp} (kPa)	P ^{NRTL} (kPa)	γ_1^{exp}	γ_1^{NRTL}
347.57	21.10	20.84	0.70	0.69
347.71	21.14	20.97	0.70	0.69
352.96	26.11	26.04	0.70	0.69
353.04	26.43	26.12	0.70	0.69
353.06	26.41	26.14	0.70	0.69
355.92	30.53	29.32	0.72	0.69
356.64	30.61	30.17	0.70	0.69
357.52	30.71	31.24	0.68	0.69
359.02	31.08	33.13	0.65	0.69
360.20	35.66	34.68	0.71	0.69
361.17	35.90	36.00	0.69	0.69
363.65	40.25	39.58	0.71	0.69
363.97	40.32	40.06	0.70	0.69
364.89	40.40	41.47	0.68	0.69
367.05	45.03	44.95	0.69	0.69
367.28	45.05	45.33	0.69	0.69
370.76	51.12	51.49	0.69	0.69
371.13	51.05	52.19	0.68	0.69
371.23	51.20	52.38	0.68	0.69
373.09	56.52	55.99	0.70	0.69
373.30	56.58	56.41	0.70	0.69
374.04	60.99	57.92	0.73	0.69
375.13	60.97	60.20	0.70	0.69
376.51	60.92	63.18	0.67	0.69
377.11	61.02	64.52	0.66	0.69
377.33	61.02	65.02	0.65	0.69
$x_1 = 0.68$				
344.04	10.48	9.97	0.47	0.45
344.33	10.51	10.09	0.47	0.45
347.90	12.31	11.74	0.47	0.45
349.07	12.26	12.33	0.45	0.45
350.12	12.24	12.88	0.43	0.45
353.75	16.09	14.94	0.48	0.45
354.39	16.09	15.33	0.47	0.45
363.46	21.03	21.83	0.43	0.45
363.65	21.39	21.99	0.44	0.45
364.13	21.39	22.39	0.43	0.45
368.74	25.61	26.58	0.43	0.45
369.57	25.63	27.40	0.42	0.45
373.82	30.19	31.93	0.42	0.45
374.56	30.19	32.78	0.41	0.45
378.88	35.69	38.12	0.42	0.45
380.93	35.74	40.90	0.39	0.45
383.41	40.02	44.47	0.40	0.45
384.29	40.13	45.80	0.39	0.45
386.61	45.12	49.46	0.41	0.45
386.80	45.15	49.77	0.41	0.45
389.14	50.01	53.72	0.42	0.45
389.57	50.36	54.48	0.42	0.45
389.62	50.35	54.57	0.41	0.45
			ARD	4.44

Uncertainty x_1 , T and γ_1 are 0.005, 0.06 and 0.001, respectively.

$$\Delta P \% = 100 * \frac{|p^{exp} - p^{NRTL}|}{p^{exp}}$$

$$ARD = 1/n * \sum_{i=1}^n \frac{|p^{exp} - p^{NRTL}|}{p^{exp}}$$

II.2.2. Heat capacity (C_p)

Table II.8: Experimental molar heat capacity and excess molar heat capacity of the binary system {H₂O (1) + [EMIM][EPh] (2)}.

x_2	0	0.12	0.19	0.3	0.4	0.48	0.58	0.68	0.8	0.87	1
T(K)	C_p (J.mol ⁻¹ .K ⁻¹)										
301.15	75.34	114.37	125.5	157.62	194.16	223.45	249.00	275.60	301.10	331.34	365.43
303.15	75.31	114.53	125.77	158.38	194.39	224.20	250.00	275.64	300.23	330.95	368.43
305.15	75.29	114.71	125.58	158.45	195.27	225.22	250.40	275.73	300.29	331.79	372.63
308.15	75.27	115.01	125.98	159.47	194.91	225.26	257.02	276.30	300.52	330.62	375.46
309.15	75.26	115.11	126.12	159.74	195.24	225.47	258.00	275.76	301.24	330.59	376.41
313.15	75.24	115.56	126.91	160.91	195.90	226.21	260.37	276.36	300.93	330.62	379.75
317.15	75.24	115.90	127.21	161.94	196.29	227.21	261.81	276.84	301.40	330.82	385.35
318.15	75.24	116.07	127.43	162.22	196.54	227.18	262.50	276.77	301.52	330.65	385.45
321.15	75.24	116.40	127.89	163.17	197.01	228.15	264.06	276.80	301.88	330.42	388.11
323.15	75.25	116.60	128.22	163.66	197.35	228.40	264.67	277.01	302.18	330.49	388.56
325.15	75.25	116.77	128.45	164.29	197.66	229.01	265.22	277.16	302.42	330.49	389.65
328.15	75.27	117.08	128.99	165.07	198.12	229.92	265.98	277.39	303.04	330.50	390.49
329.15	75.28	117.19	129.14	165.35	198.21	229.97	266.53	277.47	303.01	330.61	390.48
333.15	75.31	117.62	129.74	166.5	198.86	230.97	266.79	277.81	303.44	330.43	388.79
337.15	75.35	118.01	130.39	167.62	199.48	231.93	266.46	278.12	303.86	330.58	386.23
T(K)	C_p^E (J.mol ⁻¹ .K ⁻¹)										
301.15	0	2.97	-3.56	-6.05	3.54	8.86	4.68	2.91	-6.03	5.08	0
303.15	0	2.78	-3.83	-6.18	2.59	8.19	3.95	0.92	-9.29	2.09	0
305.15	0	2.46	-4.78	-7.38	1.82	7.21	1.91	-1.83	-12.57	-0.69	0
308.15	0	2.43	-4.88	-7.21	0.35	5.90	6.89	-3.19	-14.6	-4.32	0
309.15	0	2.42	-4.91	-7.22	0.30	5.66	7.32	-4.37	-14.64	-5.17	0
313.15	0	2.46	-4.73	-7.06	-0.36	4.81	7.75	-6.04	-17.61	-8.02	0
317.15	0	2.12	-5.46	-7.73	-2.18	3.12	5.94	-9.36	-21.62	-12.66	0
318.15	0	2.27	-5.26	-7.48	-1.97	3.04	6.56	-9.50	-21.58	-12.93	0
321.15	0	2.27	-5.30	-7.34	-2.57	2.73	6.57	-11.28	-23.35	-15.46	0
323.15	0	2.41	-5.05	-6.99	-2.4	2.77	6.91	-11.38	-23.40	-15.78	0
325.15	0	2.43	-5.03	-6.70	-2.53	2.85	6.83	-11.97	-24.03	-16.71	0
328.15	0	2.63	-4.66	-6.19	-2.42	3.34	7.09	-12.33	-24.10	-17.44	0
329.15	0	2.73	-4.51	-5.91	-2.33	3.40	7.64	-12.24	-24.12	-17.32	0
333.15	0	3.35	-3.63	-4.27	-1.03	5.19	8.88	-10.76	-22.34	-16.04	0
337.15	0	4.01	-2.54	-2.39	0.58	7.36	10.02	-8.72	-19.88	-13.68	0

Table II.9: Experimental molar heat capacity and excess molar heat capacity of the binary system {H₂O (1) + [DMIM][MeSO₄] (2)}.

x_2	0.00	0.10	0.20	0.30	0.40	0.51	0.60	0.71	1.00
T(K)	C_p (J.mol ⁻¹ .K ⁻¹)								
301.15	75.34	103.50	125.39	149.47	176.77	207.44	230.45	256.98	325.39
303.15	75.31	103.90	125.57	149.65	177.38	207.58	230.65	257.21	325.70
305.15	75.29	104.68	125.90	149.83	177.44	207.75	231.08	257.44	326.34
308.15	75.27	104.63	126.13	150.10	177.54	208.00	231.58	257.82	327.12
309.15	75.26	104.77	126.21	150.19	177.54	208.00	231.65	257.91	327.14
313.15	75.24	105.30	126.52	150.56	178.01	208.41	232.48	258.56	328.54
317.15	75.24	105.78	126.89	150.92	178.44	208.68	233.18	258.69	329.58
318.15	75.24	105.85	126.99	151.01	178.51	208.76	233.36	258.81	329.87
321.15	75.24	106.23	127.35	151.28	178.58	209.14	233.88	259.16	330.73
323.15	75.25	106.51	127.48	151.47	178.74	209.29	234.50	259.54	331.63
325.15	75.25	106.71	127.67	151.65	178.97	209.41	234.73	259.68	331.94
328.15	75.27	107.02	127.96	151.92	179.09	209.66	235.25	260.03	332.79
329.15	75.28	107.18	128.05	152.01	179.23	209.70	235.45	260.15	333.08
333.15	75.31	107.66	128.45	152.37	179.59	210.12	236.31	260.80	334.36
337.15	75.35	108.10	128.83	152.74	179.88	210.34	237.00	261.13	335.33
T(K)	C_p^E (J.mol ⁻¹ .K ⁻¹)								
301.15	0.00	2.30	-0.66	-1.36	0.23	4.47	4.86	5.16	0.00
303.15	0.00	2.70	-0.52	-1.26	0.73	4.47	4.88	5.17	0.00
305.15	0.00	3.43	-0.31	-1.25	0.55	4.32	4.94	4.96	0.00
308.15	0.00	3.32	-0.22	-1.20	0.35	4.19	4.97	4.79	0.00
309.15	0.00	3.46	-0.13	-1.11	0.35	4.18	5.03	4.87	0.00
313.15	0.00	3.87	-0.09	-1.16	0.26	3.89	5.03	4.55	0.00
317.15	0.00	4.25	0.07	-1.10	0.28	3.63	5.11	3.94	0.00
318.15	0.00	4.29	0.11	-1.10	0.23	3.56	5.12	3.85	0.00
321.15	0.00	4.58	0.30	-1.09	-0.05	3.50	5.12	3.59	0.00
323.15	0.00	4.76	0.24	-1.18	-0.26	3.19	5.19	3.35	0.00
325.15	0.00	4.91	0.36	-1.10	-0.16	3.15	5.23	3.26	0.00
328.15	0.00	5.12	0.46	-1.10	-0.40	2.95	5.23	3.00	0.00
329.15	0.00	5.24	0.49	-1.10	-0.37	2.84	5.26	2.91	0.00
333.15	0.00	5.56	0.61	-1.15	-0.56	2.59	5.33	2.65	0.00
337.15	0.00	5.86	0.76	-1.10	-0.69	2.30	5.43	2.29	0.00

Table II.10: Experimental molar heat capacity and excess molar heat capacity of the binary system {H₂O (1) + [EMIM][MeSO₄] (2)}.

x_2	0.00	0.11	0.20	0.31	0.40	0.50	0.60	0.81	1.00
T(K)	C_p (J.mol ⁻¹ .K ⁻¹)								
301.15	75.34	107.87	139.23	166.68	188.70	217.21	245.22	310.39	369.17
303.15	75.31	107.87	139.32	167.04	188.89	217.57	245.85	310.57	369.33
305.15	75.29	107.98	139.56	167.27	189.43	217.86	246.45	310.75	369.49
308.15	75.27	108.34	139.93	167.90	189.83	218.02	247.20	311.06	369.73
309.15	75.26	108.50	140.12	167.53	190.22	218.36	247.46	311.13	369.78
313.15	75.24	108.63	140.56	168.58	190.52	219.00	248.58	311.45	370.11
317.15	75.24	108.96	140.89	169.00	191.26	219.46	249.59	311.84	370.37
318.15	75.24	108.99	141.02	169.16	191.33	219.89	249.86	311.78	370.44
321.15	75.24	109.37	141.56	169.75	191.82	220.08	250.72	312.06	370.88
323.15	75.25	109.49	141.70	170.00	192.26	220.44	251.24	312.43	370.89
325.15	75.25	109.57	141.95	170.32	192.51	220.91	251.73	312.51	371.01
328.15	75.27	109.96	142.22	170.75	193.00	221.21	252.46	312.78	371.36
329.15	75.28	109.98	142.52	170.91	193.22	221.30	252.73	312.87	371.43
333.15	75.31	110.30	143.02	171.69	193.79	222.09	253.79	313.16	371.57
337.15	75.35	110.67	143.57	172.24	194.55	222.65	254.95	313.60	371.98
T(K)	C_p^E (J.mol ⁻¹ .K ⁻¹)								
301.15	0.00	1.30	4.47	0.22	-4.26	-5.07	-6.77	-1.57	0.00
303.15	0.00	1.30	4.55	0.55	-4.11	-4.78	-6.22	-1.52	0.00
305.15	0.00	1.42	4.78	0.74	-3.63	-4.56	-5.72	-1.46	0.00
308.15	0.00	1.77	5.12	1.32	-3.31	-4.51	-5.10	-1.34	0.00
309.15	0.00	1.93	5.30	0.94	-2.94	-4.19	-4.86	-1.31	0.00
313.15	0.00	2.04	5.69	1.90	-2.76	-3.71	-3.94	-1.25	0.00
317.15	0.00	2.35	5.98	2.25	-2.11	-3.37	-3.08	-1.06	0.00
318.15	0.00	2.38	6.09	2.38	-2.08	-2.97	-2.85	-1.18	0.00
321.15	0.00	2.70	6.54	2.83	-1.77	-3.01	-2.26	-1.26	0.00
323.15	0.00	2.82	6.67	3.07	-1.34	-2.66	-1.75	-0.90	0.00
325.15	0.00	2.87	6.90	3.35	-1.14	-2.25	-1.34	-0.92	0.00
328.15	0.00	3.21	7.09	3.66	-0.80	-2.13	-0.81	-0.93	0.00
329.15	0.00	3.22	7.36	3.80	-0.60	-2.08	-0.60	-0.90	0.00
333.15	0.00	3.49	7.80	4.51	-0.11	-1.38	0.37	-0.72	0.00
337.15	0.00	3.78	8.24	4.90	0.46	-1.04	1.27	-0.63	0.00

Table II.11: Experimental molar heat capacity and excess molar heat capacity of the binary system {H₂O (1) + [BMIM][DCA] (2)}.

x_2	0.00	0.11	0.20	0.30	0.39	0.49	0.61	0.70	0.86	1.00
T(K)	C_p (J.mol ⁻¹ .K ⁻¹)									
301.15	75.34	108.67	135.32	160.99	181.53	202.88	230.92	255.83	301.26	336.73
303.15	75.31	108.75	135.44	161.17	181.77	202.94	231.26	256.09	301.37	337.18
305.15	75.29	108.86	135.55	161.34	181.84	203.00	231.61	256.38	301.74	337.63
308.15	75.27	109.04	135.69	161.66	182.37	203.22	232.21	256.75	301.97	338.16
309.15	75.26	109.10	135.85	161.74	182.49	203.28	232.03	256.87	302.05	338.38
313.15	75.24	109.38	136.00	161.99	182.79	203.62	232.87	257.36	302.31	339.38
317.15	75.24	109.65	136.22	162.43	183.26	203.78	233.28	257.64	302.68	340.54
318.15	75.24	109.69	136.30	162.52	183.38	203.95	233.53	257.87	302.78	340.75
321.15	75.24	109.85	136.45	162.70	183.85	204.19	233.83	258.05	303.15	341.04
323.15	75.25	109.98	136.59	162.91	183.93	204.25	230.32	258.31	303.31	341.71
325.15	75.25	110.11	136.70	163.09	184.16	204.39	234.41	258.69	303.49	342.04
328.15	75.27	110.30	136.87	163.48	184.45	204.60	234.80	258.79	303.77	342.62
329.15	75.28	110.33	137.03	163.49	184.62	204.67	234.86	259.10	303.87	343.13
333.15	75.31	110.64	137.17	163.81	185.16	205.05	235.49	259.46	304.37	343.80
337.15	75.35	110.87	137.40	164.16	185.56	205.22	236.02	259.63	304.65	344.78
T(K)	C_p^E (J.mol ⁻¹ .K ⁻¹)									
301.15	0.00	5.73	7.98	6.85	3.39	-1.52	-3.52	-3.48	0.37	0.00
303.15	0.00	5.79	8.03	6.91	3.46	-1.67	-3.44	-3.53	0.09	0.00
305.15	0.00	5.87	8.07	6.96	3.36	-1.82	-3.35	-3.55	0.07	0.00
308.15	0.00	6.01	8.12	7.13	3.70	-1.84	-3.07	-3.54	-0.15	0.00
309.15	0.00	6.05	8.25	7.15	3.74	-1.88	-3.38	-3.58	-0.25	0.00
313.15	0.00	6.25	8.21	7.11	3.65	-2.04	-3.14	-3.79	-0.87	0.00
317.15	0.00	6.41	8.21	7.21	3.68	-2.44	-3.43	-4.31	-1.48	0.00
318.15	0.00	6.42	8.25	7.23	3.72	-2.38	-3.31	-4.23	-1.57	0.00
321.15	0.00	6.55	8.33	7.33	4.07	-2.28	-3.19	-4.26	-1.45	0.00
323.15	0.00	6.60	8.33	7.33	3.88	-2.55	-7.11	-4.48	-1.87	0.00
325.15	0.00	6.69	8.37	7.40	3.98	-2.58	-3.22	-4.33	-1.97	0.00
328.15	0.00	6.81	8.41	7.61	4.03	-2.66	-3.19	-4.64	-2.20	0.00
329.15	0.00	6.77	8.47	7.46	4.00	-2.85	-3.45	-4.70	-2.54	0.00
333.15	0.00	6.98	8.45	7.56	4.25	-2.82	-3.23	-4.81	-2.62	0.00
337.15	0.00	7.07	8.45	7.58	4.24	-3.15	-3.32	-5.35	-3.19	0.00

II.2.3. Density (ρ)**Table II.12:** Experimental densities ($\text{g}\cdot\text{cm}^{-3}$) and excess molar volume of the binary system $\{\text{H}_2\text{O} (1) + [\text{DMIM}][\text{MPh}] (2)\}$.

x_2	0.00	0.10	0.20	0.30	0.40	0.50	0.60	0.70	0.80	0.90	1.00
T(k)	$\rho (\text{g}\cdot\text{cm}^{-3})$										
293.15	0.9987	1.1383	1.1908	1.2151	1.2271	1.2337	1.2381	1.2407	1.2428	1.2440	1.2525
303.15	0.9956	1.1332	1.1850	1.2094	1.2213	1.2280	1.2324	1.2348	1.2371	1.2382	1.2464
313.15	0.9925	1.1273	1.1810	1.2048	1.2153	1.2233	1.2277	1.2299	1.2322	1.2331	1.2417
323.15	0.9880	1.1229	1.1740	1.1975	1.2092	1.2157	1.2199	1.2224	1.2249	1.2257	1.2334
T(k)	$V^E (\text{cm}^3\cdot\text{mol}^{-1})$										
293.15	0.00	-0.50	-0.81	-0.88	-0.79	-0.62	-0.39	-0.13	0.21	0.49	0.00
303.15	0.00	-0.39	-0.70	-0.80	-0.72	-0.57	-0.36	-0.11	0.21	0.48	0.00
313.15	0.00	-0.30	-0.68	-0.76	-0.61	-0.54	-0.34	-0.07	0.25	0.53	0.00
323.15	0.00	-0.40	-0.73	-0.81	-0.75	-0.60	-0.38	-0.14	0.15	0.44	0.00
										ARD%	12.12

Table II.13: Experimental densities ($\text{g}\cdot\text{cm}^{-3}$) and excess molar volume of the binary system $\{\text{H}_2\text{O} (1) + [\text{EMIM}][\text{MPh}] (2)\}$.

x_2	0.00	0.11	0.20	0.39	0.40	0.50	0.61	0.70	0.81	0.90	1.00
T(K)	$\rho (\text{g}\cdot\text{cm}^{-3})$										
293.15	0.9973	1.1292	1.1636	1.1845	1.1850	1.1881	1.1895	1.1899	1.1903	1.1904	1.1906
303.15	0.9959	1.1238	1.1582	1.1792	1.1794	1.1828	1.1843	1.1850	1.1852	1.1853	1.1841
313.15	0.9922	1.1173	1.1508	1.1717	1.1718	1.1754	1.1772	1.1778	1.1781	1.1782	1.1768
323.15	0.9879	1.1116	1.1450	1.1659	1.1662	1.1699	1.1717	1.1724	1.1729	1.1730	1.1717
T(k)	$V^E (\text{cm}^3\cdot\text{mol}^{-1})$										
293.15	0.00	-0.82	-1.24	-1.40	-1.40	-1.27	-1.03	-0.81	-0.53	-0.27	0.00
303.15	0.00	-0.78	-1.23	-1.43	-1.42	-1.33	-1.13	-0.95	-0.69	-0.45	0.00
313.15	0.00	-0.76	-1.19	-1.40	-1.39	-1.31	-1.14	-0.95	-0.71	-0.48	0.00
323.15	0.00	-0.74	-1.17	-1.37	-1.36	-1.29	-1.12	-0.94	-0.71	-0.48	0.00
										ARD%	3.58

Table II.14: Experimental densities ($\text{g}\cdot\text{cm}^{-3}$) and excess molar volume of the binary system $\{\text{H}_2\text{O} (1) + [\text{EMIM}][\text{EPH}] (2)\}$.

x_2	0.00	0.10	0.20	0.30	0.40	0.50	0.60	0.70	0.80	0.90	1.00
T(k)	$\rho (\text{g}\cdot\text{cm}^{-3})$										
293.15	0.9976	1.1114	1.1362	1.1455	1.1487	1.1498	1.1498	1.1491	1.1485	1.1481	1.1503
303.15	0.9958	1.1050	1.1295	1.1392	1.1424	1.1433	1.1431	1.1423	1.1414	1.1410	1.1439
313.15	0.9922	1.0998	1.1241	1.1342	1.1373	1.1385	1.1385	1.1379	1.1373	1.1367	1.1376
323.15	0.9888	1.0930	1.1176	1.1280	1.1312	1.1323	1.1323	1.1317			1.1300
T(k)	$V^E (\text{cm}^3\cdot\text{mol}^{-1})$										
293.15	0.00	-0.97	-1.37	-1.53	-1.52	-1.40	-1.22	-0.91	-0.66	-0.42	0.00
303.15	0.00	-0.86	-1.22	-1.34	-1.30	-1.13	-0.88	-0.50	-0.16	0.11	0.00
313.15	0.00	-0.86	-1.24	-1.40	-1.39	-1.24	-1.06	-0.74	-0.49	-0.14	0.00
323.15	0.00	-0.83	-1.24	-1.45	-1.47	-1.36	-1.20	-0.90			0.00
										ARD%	24.19

Table II.15: Experimental densities ($\text{g}\cdot\text{cm}^{-3}$) and excess molar volume of the binary system $\{\text{H}_2\text{O} (1) + [\text{DMIM}][\text{MeSO}_4] (2)\}$.

x_2	0.00	0.11	0.20	0.30	0.40	0.49	0.61	0.71	0.80	0.90	1.00
T(k)	$\rho (\text{g}\cdot\text{cm}^{-3})$										
293.15	0.9987	1.1725	1.2282	1.2627	1.2834	1.2961	1.3082	1.3156	1.3215	1.3264	1.3302
303.15	0.9956	1.1669	1.2220	1.2561	1.2770	1.2898	1.3018	1.3092	1.3150	1.3199	1.3235
313.15	0.9925	1.1614	1.2161	1.2500	1.2718	1.2845	1.2958	1.3028	1.3087	1.3136	1.3174
323.15	0.9880	1.1563	1.2093	1.2436	1.2668	1.2791	1.2893	1.2962	1.3019	1.3067	1.3109
T(k)	$V^E (\text{cm}^3\cdot\text{mol}^{-1})$										
293.15	0.00	0.02	-0.06	-0.11	-0.11	-0.11	-0.08	-0.06	-0.04	-0.02	0.00
303.15	0.00	0.06	-0.02	-0.07	-0.09	-0.09	-0.08	-0.06	-0.05	-0.04	0.00
313.15	0.00	0.08	0.01	-0.04	-0.07	-0.08	-0.06	-0.04	-0.01	-0.02	0.00
323.15	0.00	0.09	0.04	-0.02	-0.06	-0.06	-0.06	-0.02	0.00	0.02	0.00
										ARD%	26.41

Table II.16: Experimental densities ($\text{g}\cdot\text{cm}^{-3}$) and excess molar volume of the binary system $\{\text{H}_2\text{O} (1) + [\text{EMIM}][\text{MeSO}_4] (2)\}$.

x_2	0.00	0.11	0.20	0.30	0.41	0.51	0.60	0.70	0.80	0.90	1.00
T (K)	$\rho (\text{g}\cdot\text{cm}^{-3})$										
293.15	0.9987	1.1550	1.2056	1.2339	1.2507	1.2612	1.2683	1.2736	1.2780	1.2815	1.2843
303.15	0.9956	1.1490	1.1990	1.2273	1.2442	1.2547	1.2618	1.2672	1.2715	1.2751	1.2777
313.15	0.9925	1.1433	1.1929	1.2211	1.2381	1.2486	1.2558	1.2612	1.2629	1.2690	1.2717
323.15	0.9880	1.1369	1.1862	1.2143	1.2316	1.2420	1.2484	1.2546	1.2589	1.2619	1.2651
T (K)	$V^E (\text{cm}^3\cdot\text{mol}^{-1})$										
293.15	0.00	-0.09	-0.22	-0.27	-0.27	-0.25	-0.21	-0.16	-0.11	-0.06	0.00
303.15	0.00	-0.03	-0.16	-0.21	-0.23	-0.22	-0.18	-0.15	-0.10	-0.06	0.00
313.15	0.00	0.00	-0.12	-0.18	-0.20	-0.19	-0.17	-0.14		-0.05	0.00
323.15	0.00	0.02	-0.09	-0.16	-0.18	-0.18	-0.17	-0.14	-0.10	-0.06	0.00
										ARD%	31.40

Table II.17: Experimental densities ($\text{g}\cdot\text{cm}^{-3}$) and excess molar volume of the binary system $\{\text{H}_2\text{O} (1) + [\text{BMIM}][\text{DCA}] (2)\}$.

x_2	0.00	0.10	0.20	0.30	0.40	0.50	0.60	0.70	0.80	0.90	1.00
T(K)	$\rho (\text{g}\cdot\text{cm}^{-3})$										
293.15	0.9987	1.0355	1.0446	1.0508	1.0545	1.0568	1.0585	1.0602	1.0615	1.0625	1.0636
303.15	0.9956	1.0293	1.0381	1.0444	1.0483	1.0505	1.0523	1.0542	1.0555	1.0565	1.0576
313.15	0.9925	1.0231	1.0320	1.0382	1.0421	1.0446	1.0464	1.0483	1.0496	1.0506	1.0518
323.15	0.9880	1.0162	1.0237	1.0311	1.0351	1.0380	1.0401	1.0417	1.0432	1.0442	1.0457
T(K)	$V^E (\text{cm}^3\cdot\text{mol}^{-1})$										
293.15	0.00	0.03	0.06	0.08	0.11	0.12	0.11	0.10	0.07	0.05	0.00
303.15	0.00	0.10	0.14	0.16	0.18	0.18	0.16	0.12	0.09	0.06	0.00
313.15	0.00	0.15	0.20	0.22	0.24	0.22	0.20	0.16	0.12	0.08	0.00
323.15	0.00	0.16	0.24	0.26	0.28	0.25	0.23	0.23	0.15	0.11	0.00
										ARD%	7.83

$$\Delta V^E \% = 100 * \frac{|V^{E,exp} - V^{E,RK}|}{V^{E,exp}}$$

$$ARD = 1/n * \sum_{i=1}^n \frac{|V^{E,exp} - V^{E,RK}|}{V^{E,exp}}$$

II.2.4. Excess molar Enthalpy (H^E)**Table II.18:** Excess molar enthalpies at $T = 312.92$ K for binary system $\{H_2O (1) + ILs (2)\}$.

[DMIM][MPH]		[EMIM][MPH]		[EMIM][EPH]		[DMIM][MeSO4]		[EMIM][MeSO4]		
H ^E (J.mol ⁻¹)										
x ₂	H ^E	x ₂	H ^E	x ₂	H ^E	x ₂	H ^E	x ₂	H ^E	
0.10	-2888.97	0.08	-2902.62	0.11	-3189.53	0.15	-812.44	0.11	-677.13	
0.18	-3983.14	0.14	-4123.91	0.25	-4798.76	0.16	-848.65	0.24	-997.57	
0.25	-4620.02	0.24	-5324.67	0.36	-5171.67	0.24	-949.84	0.23	-1002.30	
0.37	-4794.79	0.32	-5637.40	0.44	-5016.65	0.23	-940.29	0.22	-1069.72	
0.52	-4302.44	0.51	-5201.96	0.55	-4521.59	0.55	-708.44	0.50	-784.19	
0.71	-3026.86	0.58	-4733.74	0.65	-3578.77	0.67	-459.77	0.74	-384.21	
0.88	-1873.35	0.79	-2610.43	0.84	-1691.62				0.71	-478.27
		0.65	-4051.51							
		0.86	-1542.90							

Abstract

Recently, the cost and use of energy continually rise. Hence, humans are close to face serious environmental problems such as increasing CO₂ discharges. In this regard, global community is to achieve the ambitious objective of reducing carbon footprint and to ensure that the heating demand is covered in a sustainable manner. Since, enormous amounts of low-temperature waste heat are released on daily bases from many industrial plants to the atmosphere at temperatures between 60 - 100°C. Absorption heat transformers (AHT) are interesting because they can recover low temperature waste heat from different industrial activities and renewable energy sources such as solar and geothermal. AHT can be used to upgrade waste heat to produce useful heat for heating and hot water supplies. Nowadays, the standard working pairs used for AHTs are {ammonia + water} and {water + lithium bromide}. However, both of the working pairs show questionable behavior such as toxicity, crystallization and corrosiveness. Therefore, exploring new working pairs which do not exhibit limitations become of great importance. This work includes an investigation to analyze the AHT systems using {water + ionic liquids} binary systems as working fluids. First, basic thermodynamic properties including vapor pressure, density, heat capacity as well as excess enthalpy of these binary systems were measured at various temperatures with different ionic liquid concentrations. The thermodynamic properties data were correlated by different equations, respectively. The correlated values were significantly consistent with the experimental data. Next, simulation of the AHT performance based on the thermodynamic properties of the new working pairs and on the mass and energy balance for each component of the system were performed. Results show that the {H₂O + ILs} binary systems are promising alternatives to replace the already used {H₂O + LiBr} working pairs.

Résumé

Ces dernières années, les coûts et la demande en énergie n'ont cessé d'augmenter. Par conséquent, l'humanité fait face à de graves menaces environnementales telles que l'augmentation des rejets de CO₂. À cet égard, la communauté internationale doit parvenir à réduire de son empreinte carbone et à veiller à ce que les besoins en énergie thermique soient couverts de manière durable. D'importantes quantités de chaleur résiduaire à basse température (60 - 100°C) sont libérées quotidiennement dans l'atmosphère par de nombreuses installations industrielles. Les thermo-transformateurs de chaleur à absorption constituent un outil intéressant car ils peuvent revaloriser des chaleurs résiduaire pour produire de la chaleur utile pour le chauffage et la production d'eau chaude. Actuellement, les mélanges de travail utilisés dans les pompes à absorption sont les systèmes {ammoniac + eau} et {eau + bromure de lithium}. Cependant, ces deux fluides de travail présentent certains inconvénients tels que la toxicité, la cristallisation et la corrosivité. Par conséquent, il est important de rechercher de nouveaux mélanges de travail. Cette étude a pour objectif d'évaluer l'intérêt d'utiliser des mélanges constitués de liquides ioniques et d'eau au sein de thermo-transformateurs à absorption. Tout d'abord, les propriétés thermodynamiques de ces systèmes binaires (pression de vapeur, densité, capacité thermique et enthalpie d'excès) ont été mesurées dans un large domaine de température et de composition. Ces données expérimentales ont été corrélées à l'aide de modèles thermodynamiques adéquats. Ensuite, les performances de ces fluides de travail ont été évaluées. Les résultats montrent que les systèmes binaires {H₂O + ILs} sont une alternative prometteuse aux fluides de travail traditionnels tels que {H₂O + LiBr}.